UNIVERSITY OF GENOA

Department of Civil, Chemical and Environmental Engineering (DICCA)

PhD Program in Civil, Chemical and Environmental Engineering

Curriculum in Structural and Geotechnical Engineering,
Mechanics and Materials – Cycle XXXIII

Doctoral Dissertation

Ambient vibration tools supporting the model-based seismic assessment of existing buildings

Daniele Sivori

May 2021

AMBIENT VIBRATION TOOLS SUPPORTING THE MODEL-BASED SEISMIC ASSESSMENT OF EXISTING BUILDINGS

BY

DANIELE SIVORI

*Dissertation discussed in partial fulfillment of
the requirements for the Degree of*

DOCTOR OF PHILOSOPHY

*in Civil, Chemical and Environmental Engineering
Curriculum in Structural and Geotechnical Engineering, Mechanics and Materials
Department of Civil, Chemical and Environmental Engineering (DICCA)
University of Genoa, Italy*

May 2021

Scientific Supervisors

Serena Cattari, Associate Professor
    Department of Civil, Chemical and Environmental Engineering (DICCA),
    University of Genoa, Italy

Marco Lepidi, Associate Professor
    Department of Civil, Chemical and Environmental Engineering (DICCA),
    University of Genoa, Italy

External Reviewers

Giovanni Fabbrocino, Full Professor
    Department of Biosciences and Territory (DIBT),
    University of Molise, Italy

Guéguen Philippe, Research Director
    Institute of Earth Science (ISTerre),
    Université Grenoble Alpes/CNRS Université Gustave Eiffel, France

Examination Committee

Luigi Gambarotta, Full Professor
    Department of Civil, Chemical and Environmental Engineering (DICCA),
    University of Genoa, Italy

Filippo Ubertini, Full Professor
    Department of Civil and Environmental Engineering (DICA),
    University of Perugia, Italy

Francesca da Porto, Full Professor
    Department of Geosciences,
    University of Padua, Italy

Acknowledgements

Abstract

The technological advancements of the last decades are making dynamic monitoring an efficient and widespread resource to investigate the safety and health of engineering structures. In the wake of these developments, the thesis proposes methodological tools supporting the seismic assessment of existing buildings through the use of *ambient vibration tests*. In this context, the literature highlights considerable room to broaden the ongoing research, especially regarding masonry buildings. The recent earthquakes, once again, highlighted the significant vulnerability of this structural typology as an important part of our built heritage, remarking the importance of risk mitigation strategies for the territorial scale. The thesis builds upon a simplified methodology recently proposed in the literature, conceived to assess the post-seismic serviceability of strategic buildings based on their operational modal parameters. The original contributions of the work pursue the theoretical and numerical validation of its basic simplifying assumptions, in structural modelling – such as the in-plane rigid behaving floor diaphragms – and seismic analysis – related to the nonlinear fundamental frequency variations induced by earthquakes. These strategies are commonly employed in the seismic assessment of existing buildings, but require further developments for masonry buildings. The novel proposal of the thesis takes advantage of ambient vibration data to establish direct and inverse mechanical problems in the frequency domain targeted at, first, qualitatively distinguishing between rigid and nonrigid behaving diaphragms and, second, quantitatively identifying their *in-plane shear stiffness*, mechanical feature playing a primary role in the seismic behaviour of masonry buildings. The application of these tools to real case studies points out their relevance in the updating and validation of structural models for seismic assessment purposes. In the light of these achievements, a model-based computational framework is proposed to develop *frequency decay-damage control charts* for masonry buildings, which exploit ambient vibration measurements for quick damage evaluations in post-earthquake scenarios. The results of the simulations, finally, highlight the generally conservative nature of ambient vibration-based simplified methodologies, confirming their suitability for the serviceability assessment of existing masonry buildings.

Contents

List of Tables

9

List of Figures

11

14

Chapter 1

Introduction

The dynamic monitoring of existing structures is flourishing in civil engineering, thanks to increasing computational power, advancements in data processing and technological improvements in sensors. Nevertheless, its actual employment is mostly limited to scientifically relevant, strategic or monumental architectures. In this context, recent proposals in the literature pursue the use of ambient vibration measurements to support seismic mitigation strategies at the urban and territorial scale. The systematic availability of monitoring data from existing buildings, expected in the very next future, motivates the research conducted in this thesis, pursuing the integration of dynamic measurements in seismic assessment procedures. Particular attention will be addressed to masonry buildings which, for their peculiar mechanical characteristics and intrinsic seismic vulnerability, pose some challenges of theoretical and applied interest.

1.1 State of the art

In the past three decades, the use of experimental dynamic measurements has gained widespread diffusion in civil and structural engineering as a fundamental tool to investigate the dynamic behaviour of existing structures (De Roeck et al., 2000; Cunha & Caetano, 2006; Brownjohn, 2007). This new and growing success is primarily due to the improvement in performance and reduction in the cost of sensors, increasing computational capability of computers matched with extraordinary developments in the fields of data processing and system identification (Reynders & De Roeck, 2008; Rainieri & Fabbrocino, 2010; Sun et al., 2014).

The study of the experimental dynamics of existing structures plays a key role in several theoretical and technical problems of engineering. Among the others, this knowledge is valuable to reduce the uncertainties in linear and nonlinear structural modelling (Capecchi & Vestroni, 1993; Friswell et al., 2001; De Sortis et al., 2005; Jaishi & Ren, 2005; Ren & Chen, 2010; Reynders et al., 2010; Pierdicca et al., 2016; García-Macías et al., 2019), to investigate previously unknown dynamic interactions (Gattulli et al., 2005; Lepidi et al., 2009), to detect, localize and quantify structural damage (Salawu, 1997; Doebling et al., 1998; Capecchi & Vestroni, 1999; Vestroni & Capecchi, 2000; C. R. Farrar et al., 2001; Peeters et al., 2001; Carden & Fanning, 2004; Morassi & Vestroni, 2008; Nagarajaiah &

Basu, 2009; Gattulli et al., 2016; Tsogka et al., 2017), to support the design and assess the efficacy of interventions for retrofitting, isolation and control (Yi et al., 2001; Gattulli et al., 2009; Lepidi et al., 2009; Brownjohn et al., 2011; Foti et al., 2014; Amezquita-Sanchez & Adeli, 2016; Ierimonti et al., 2020). The importance of dynamic testing is growing in the complementary field of earthquake engineering as well, in particular, to support the seismic assessment of existing structures (Michel et al., 2008; Snoj et al., 2013).

In this framework, Ambient Vibration Tests (AVTs) hold a significant relevance compared to more traditional non-destructive techniques employing forced vibrations, requiring no artificial excitation but exploiting available natural (i.e. ground micro-tremors, wind, ocean waves) or human (pedestrian and vehicle traffic) input sources (C. Farrar & James Iii, 1997; Giraldo et al., 2009). Identifying the dynamic modal properties from measurements of ambient response is known as *operational modal analysis* (Brincker et al., 2001b; Rainieri & Fabbrocino, 2014), which refers to the serviceability conditions of structures in which the measurements are commonly acquired. The first civil engineering-related applications of the literature appear in the early '30s, with relevant studies on bridges. It is from the mid-70s that this research field undergoes a large growth, thanks to a renewed interest in the study of ambient, wind and earthquake-induced vibrations involving buildings, dams, chimneys (Ivanovic et al., 2000).

Alongside the technological advancements in measurement instrumentation, the field of system identification saw huge signs of progress from the '90s, both from the theoretical and computational point of view. In these decades, several *output-only* techniques – in the time and frequency domain, with nonparametric and parametric models, for single and multiple inputs and outputs, based on deterministic and probabilistic approaches (Peeters & De Roeck, 2001; Reynders, 2012; Au et al., 2013) – were studied and developed in the form of computer algorithms, continuously improving the accuracy and efficiency of modal identification. More recently, with the increasing availability of *structural health monitoring* systems (Federici et al., 2012; Federici et al., 2015; Ewins, 2016), huge efforts are being spent towards the processing, modelling and interpretation of real-time fluxes of data (Brownjohn, 2007; C. R. Farrar & Worden, 2007), especially for the assessment and conservation of strategic infrastructures, historic (Lorenzoni et al., 2018; Clementi et al., 2021) and monumental heritage (Gentile & Saisi, 2007; Bocca et al., 2011; Potenza et al., 2015; Ubertini et al., 2016).

Ambient vibrations for the seismic assessment of existing buildings

For what concerns ambient vibration testing of existing buildings, one of the very first articles in the literature dates back to 1936 and deals with the estimation of their fundamental period (Carder, 1936). In this respect, the employment of ambient vibrations measurements in the study of the dynamic behaviour of existing buildings is originally tied to earthquake engineering purposes, with the general aim of improving the prediction of the seismic response. The literature addresses, to name few topics, changes in the structural behaviour prior, during and after the earthquake, the variability of the seismic response to different soils and excitation conditions, site amplification effects and soil-structure interaction, model definition, calibration and validation through parameter estimation and structural identification, health monitoring and retrofitting and, not least, seismic vulnerability assessment (Guéguen et al., 2014).

Most of the contributions in the field involve the study of the fundamental frequencies, shape deformations and damping properties (Ivanovic et al., 2000). In particular, vibration tests have been widely used to improve the definition of empirical relationships between the fundamental frequencies of buildings and one or more structural characteristics – mainly the height, the so-called *period-height relationships* (Navarro & Oliveira, 2005; Gallipoli et al., 2010; Michel et al., 2010a) – to be implemented in simplified assessment methods according to code provisions (e.g. EN1998-1).

It is worth mentioning a second broad field of research, which has grown in importance alongside the advent of monitoring networks, dealing with the assessment of structural damage from vibration measurements. The founding idea is to consider the natural frequencies of vibration as diagnostic parameters regarding the structural integrity (Salawu, 1997), given that the occurrence of damage causes a permanent loss in structural stiffness and the consequent elongation of fundamental periods. Such effect has been extensively studied through laboratory experiments, seismic observations and numerical simulations (Calvi et al., 2006b; Masi & Vona, 2010; Katsanos et al., 2014; Vidal et al., 2014).

As highlighted by the literature, the variation in the fundamental frequencies of vibration of buildings can be observed both during and after earthquakes (Bodin et al., 2012), in presence but also in absence of structural damage (Çelebi, 2007). To briefly sum up these recent findings, such variation is an amplitude-dependent phenomenon, composed of a transient – reversible – contribution and a permanent – irreversible – contribution. For what concerns the first, which is observed during the seismic event and will be referred to as *co-seismic shift*, it can be related to reversible material and geometrical nonlinearities, pertaining both to the soil the structure and generally caused by their mutual dynamic interaction (Todorovska, 2009). The structural nonlinearities can be traced back to, among other reasons, temporary micro-cracking and sliding effects in the building materials. The frequency *wander* (Clinton et al., 2006) is observed not only in the case of strong earthquakes but also in weak forced vibrations and seismic motions (Spina & Lamonaca, 1998; Ceravolo et al., 2017), in which case it may be influenced by the characteristic of the input (Michel & Gueguen, 2010). Indeed, if no structural damage occurs, the frequency shift gradually vanishes with time, so that the pre-seismic values of the fundamental frequencies are completely recovered.

The variations in fundamental frequencies observed after the seismic event – referred to in the thesis as *post-seismic decay* – conversely, reflects a permanent stiffness degradation due to structural damage. This is the relationship that underlies modern health-monitoring applications. Based on these principles, starting from damage detection up to its quantification, the research community undertook the development of non-destructive evaluation techniques (Picozzi et al., 2010; Ponzo et al., 2010) to be employed in structural health monitoring applications and post-earthquake assessments. It has been recently remarked, moreover, that a quasi-permanent part of the post-seismic decay – linked to material strain (A. Astorga et al., 2018; A. Astorga & Guéguen, 2020a, 2020b) – can be slowly recovered over time, and how such a recovery can be employed as a proxy for the structural health assessment (A. L. Astorga et al., 2019; Guéguen et al., 2020).

Another relevant research subject that, figuratively speaking, prioritize *prevention* rather than *treatment*, is of particular interest for this thesis. The vulnerability assessment of buildings is today a crucial task for seismic risk mitigation in hazardous areas. In the last two decades, this topic saw the rise of analytical methods over empirical ones (Calvi et al.,

2006a; Gueguen, 2013). If, on the one hand, mechanical-based approaches provide accurate predictions on the basis of a robust physical foundation, on the other hand, they surely require greater efforts in model formulation and validation. Moreover, a balance between model fidelity and simplicity has to be found, based on the scale – structural, urban, territorial – at which the assessment is intended. Indeed, the seismic assessment of buildings is generally a difficult task due to the complexity of existing structures, whose *a priori* knowledge is commonly affected by several uncertainties – including but not limited to the properties of materials and elements, the effectiveness of structural details, the boundary conditions, the soil-structure interaction, the presence of pre-existing damage, structural ageing and deterioration.

The reliability of the assessment relies on the possibility to fortify such knowledge, narrowing the influence of uncertainties on the analysis results. This requirement calls for a major effort in experimental testing and diagnostic investigations. In this respect, experimental data coming from in situ ambient vibration measurements are suited for the task, providing some insights into the dynamic behaviour of the structure which, although related to operational conditions, are still extremely valuable for seismic assessment purposes (Boutin et al., 2005; Hans et al., 2005). For what concerns the small scale, i.e. the assessment of a single structure, ambient vibration testing is useful to define, calibrate and validate structural formulations (Skolnik et al., 2006; Michel et al., 2010b; Caprili et al., 2012) usually consisting in high-fidelity computational models, by reducing the uncertainties related to mechanical properties, structural configuration, external and internal constraints, dynamic interactions, modelling assumptions.

Nevertheless, ambient vibration measurements are suited to support mitigation strategies of the seismic risk at the urban and territorial scales. In such cases, since a vast built environment is involved, the employment of synthetic but representative models is essential to avoid unaffordable costs in computation and time. To this end, some authors propose the direct use of experimental modal parameters to reproduce the dynamic behaviour of the structure, employing monodimensional lumped-mass shear beams models to estimate the response to weak earthquakes (Michel et al., 2008; Michel et al., 2010b). Other contributions employed AVTs to calibrate the fragility curves of buildings up to low levels of structural damage (Michel et al., 2009; Michel et al., 2012; Perrault et al., 2013).

In the wake of these developments, the Italian Department of Civil Protection (DPC) has recently proposed a simplified methodology to assess the seismic serviceability of strategic buildings based on experimental modal parameters identified from AVTs, called *Seismic Model from Ambient Vibrations* (SMAV, Mori et al., 2015; Mori & Spina, 2015). SMAV has been conceived as a *spetidive* (i.e. quick) tool for large-scale assessments, as part of a more comprehensive framework to assess the efficiency of the urban emergency systems during earthquakes (Dolce, 2012; Dolce et al., 2018). For this reason, the procedure relies on simplifying modelling assumptions – in-plane rigid behaviour of floor diaphragms (Acunzo et al., 2018) – as well as a straightforward analysis technique – linear analysis with response spectrum – to achieve time-saving evaluations. A more recent extension of the method pursued the application to masonry buildings (Spina et al., 2019), introducing the use of *frequency shift curves* to take into account their nonlinear behaviour during earthquakes. The peculiarities of this structural typology, such as the presence of deformable floors (i.e. timber floors, vaults) and the pronounced nonlinear behaviour of masonry, could violate one or more of the SMAV assumptions and undermine the reliability of its predictions.

These issues, which will be further explored in the following, suggest an in-depth validation of the methodology, employing high-fidelity mechanical models and refined analysis techniques.

1.2 Motivations and objectives

The literature state of the art highlights an evolving panorama in the use of ambient vibration measurements for earthquake engineering purposes, in particular regarding the seismic assessment of existing buildings (Section 1.1). The abundance of studies lays down a fertile ground for developments, nevertheless, some knowledge gaps in the research are still to be addressed. The first and most relevant weakness of the literature appears to be the relatively limited number of contributions involving masonry buildings, if compared to those related to concrete buildings – or other built typologies, such as masonry monumental structures, in which the use of AVTs is more frequent. The applications exploiting vibration data to support the seismic assessment of masonry buildings are quite a few, especially those facing large-scale evaluations beyond research purposes (Michel et al., 2010a; Reuland et al., 2019; Simões et al., 2020).

It should be pointed out that, among other construction techniques, unreinforced masonry (URM) is a widespread solution in the long-standing building tradition of urban areas, which is still widely diffused in seismic-prone regions. To make a practical example for what concerns Italy, according to a national census carried out in 2011 by the Italian National Statistical Institute (ISTAT), around 80 % of over 21000 residential buildings surveyed in Central Italy – specifically, in the areas hit by the Central Italy earthquake sequence in 2016/2017 (https://www.istat.it/en/archivio/190374) – are built with masonry, compared to the national average of 57.2 %. Moreover, 70.8 % of the total was built before 1971, year in which important regulations ruling the seismic design of concrete structures were established.

The wide diffusion of masonry buildings in a moderate-to-high seismic hazard territory, their consistent age, their significant vulnerability – remarked by the recent Italian earthquakes that hit Umbria and Marche in 1997, Abruzzo in 2009, Emilia-Romagna in 2012, Central Italy in 2016/2017 (Ceci et al., 2010; Cattari et al., 2012; Sisti et al., 2019; Sorrentino et al., 2019) – demands for the development and actuation of prevention strategies, to contain the potentially huge life and economic losses (Dolce & Di Bucci, 2017). These issues are even more concerning for strategic masonry buildings, such as town halls, which hold a primary role in the management of seismic emergency (Di Ludovico et al., 2019).

Identification, modelling and analysis issues in the AV-based seismic assessment of masonry buildings

Due to the large number of masonry structures exposed to the risk, simple and reliable seismic assessment techniques are mandatory to put in action risk-mitigation strategies at a large scale, guaranteeing both the safety and the preservation of the built heritage. In this regard, the recent proposal of SMAV to quickly assess the seismic response of buildings through AVTs is appealing from an engineering perspective, thanks to its efficiency and wide range of applicability. However, some of the simplifying assumptions regarding the

modelling – in-plane rigid behaviour of floor diaphragms – as well as the assessment phase – linear analysis with response spectrum and frequency shift – pose some question regarding the reliability of simplified assessment procedures for masonry building. Among the other possibilities and open issues, the developments of the thesis take inspiration from these topics, which are better identified in the following paragraphs.

The first topic regards the modelling hypotheses related to the in-plane behaviour of the floor diaphragms (Kunnath et al., 1991), which are commonly diffused in seismic engineering applications. They are aimed, in most cases, at the employment of synthetic models and simplified formulations, avoiding high computational costs during seismic analysis. This is especially true for large-scale assessment strategies, in which such requirements are forced by the large number of structures involved. That is the case of SMAV, which exploits a simplified rigid-diaphragm model of the building to first, quickly estimate the modal mass ratios from ambient vibration data – essential to the prediction of the seismic response in the assessment stage (Acunzo et al., 2018; Spina et al., 2018) – and, second, to deduce the seismic response of unmeasured points of the structure.

Although some structural typologies, such as reinforced concrete or steel buildings, can be reasonably associated with the hypothesis of perfectly rigid diaphragms (Greco et al., 2020), this assumption is much more problematic for existing masonry buildings, which constitute the principal application field of the present thesis. The difficulties arise, on the one hand, from the great variety of diaphragm typologies (timber floors, vaults, steel beams and hollow clay blocks, concrete slabs, etc.) and, on the other hand, from the role played by the connection with the vertical walls in the dynamic response of the structure. Within this framework, the likely occurrence of moderate to severe seismic damage may add a source of structural uncertainties, in post-earthquake scenarios.

The recent observations of the seismic damage caused by L'Aquila earthquake in 2009 – made available by the Italian Department of Civil Protection through the Da.D.O platform (Dolce et al., 2019) – pointed out the importance of the in-plane deformability of floor diaphragms in the seismic response of masonry buildings (Del Gaudio et al., 2019; Rosti et al., 2020). These research contributions highlight the greater seismic vulnerability of buildings characterized by vaults (aggravated by out-of-plane actions, often in absence of retaining steel tie rods) and, in general, deformable floors, potentially not able to guarantee an efficient redistribution of the horizontal actions among the vertical walls, i.e. to produce a "box-like" behaviour preventing local mechanisms of collapse. On the contrary, it is well established that the in-plane stiffness of floor diaphragms positively influences the global dynamic behaviour of the structure, ensuring the lateral load redistribution and reducing the level of potential damage.

The empirical fragility curves proposed by Rosti et al., 2020 show a clear example of these effects, highlighting how deformable floor diaphragms – alongside other important factors, such as the masonry quality and the presence of co-seismic devices such as tie rods – have a nonnegligible influence on the seismic vulnerability of existing buildings (Figure 1.1a). Nevertheless, it is not a straightforward task to discriminate *a priori* rigid-behaving diaphragms from nonrigid-behaving ones, without further experimental evidence. National and international codes have recently acknowledged these issues, posing the attention on the modelling of deformable diaphragms in the seismic assessment of existing building and ruling, accordingly, the analysis strategies and the definition of performance levels (see, for example, the recent proposals included in the Italian NTC 2018, Circular 21/1/19 No. 7).
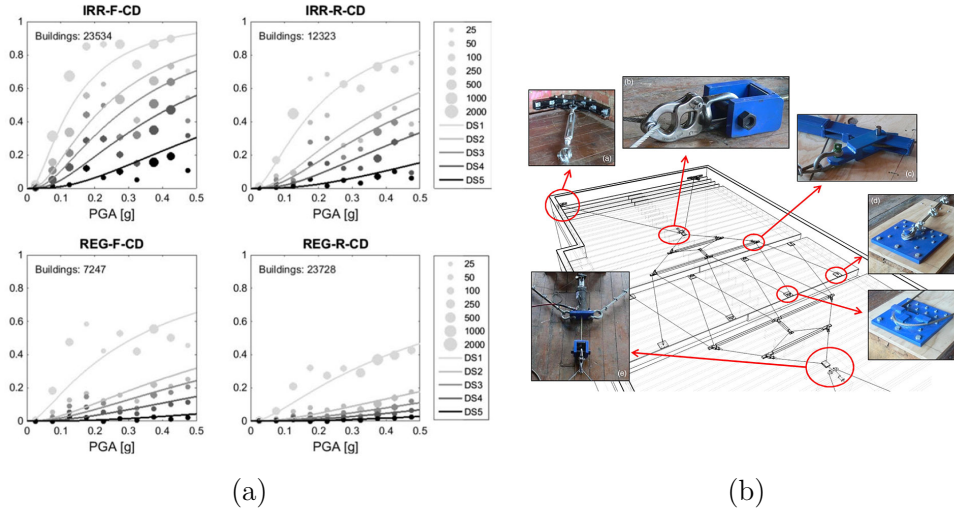
Figure 1.1: (a) Empirical fragility curves of masonry buildings with regular (REG) and irregular (IRR) masonry typology, deformable (F) and rigid (R) floor diaphragms, with co-seismic devices (DC) (adapted from Rosti et al., 2020). (b) Testing device proposed for the estimation of the in-plane stiffness of timber floor diaphragms in existing buildings (from Giongo et al., 2015).

Thus, deepening the knowledge on this topic is of great interest for purpose of formulating or updating consistent analytical, computational and experimental models. To this end, the support of structural diagnostic investigations is fundamental. If several in situ tests are available to investigate the material properties (for the masonry see Kržan et al., 2015; Boschi et al., 2019), much less are the experimental techniques proposed to evaluate the stiffness of floor diaphragms. Some solutions have been proposed to investigate the stiffness of timber floors and the effectiveness of their connections to the vertical walls (Giongo et al., 2015; Dizhur et al., 2020; Rizzi et al., 2020). Nevertheless, these field tests commonly involve complex mechanical systems and invasive interventions (Figure 1.1b). For other floor typologies, such as vaults, these studies are usually carried out in a laboratory environment (Rossi et al., 2016; Rossi et al., 2017) or through numerical simulations (Cattari et al., 2008). Within this context, the use of ambient vibration measurements to identify unknown mechanical parameters, validate modelling assumptions and update structural models seems an attractive choice.

The second topic, more closely related to the employment of vibration measurements in seismic engineering, deals with the fundamental frequency variations exhibited by masonry buildings during and after earthquakes. Several authors have looked into the so-called seismic *wander* of fundamental frequencies of buildings, through experimental observations of their seismic response. However, most of the investigations dealt with reinforced concrete structures. For what concerns masonry, this effect has been recently reproduced in a laboratory environment on two scaled building prototypes (Michel et al., 2011) and identified on a real monitored building (Spina et al., 2019). As previously highlighted, this phenomenon is of primary interest in structural health monitoring and is likewise relevant for seismic assessment purposes. It is determinant, in particular, in simplified formulations

23

addressed to large-scale predictions and relying on experimental results acquired under ambient excitation.

This is the case of the SMAV assessment strategy, in which the employment of the *frequency shifts curves* (Spina et al., 2019) in a linear approach is required – already for low seismic intensity and slight structural damage – to correctly describe the nonstationary and nonlinear behaviour of buildings during the earthquake, thus ensuring reliable evaluations. Nevertheless, the frequency drops employed by SMAV – although consistent with the seismic behaviour exhibited by an actual building – have been developed at the scale of the masonry panel, but are employed to govern the global dynamics of the structure.

These motivations suggest the need for in-depth validations of the SMAV simplified approach, in particular for what concerns its application to masonry buildings. As pointed out by the several contributions of the literature, the concept of seismic-induced frequency variations goes way beyond the application just mentioned. This knowledge plays a primary role in the post-earthquake scenario as well, where quick evaluations regarding the damage, performance and safety level of structures are required. Due to their diffusion, reducing the knowledge gaps regarding masonry buildings has strong implications in the mitigation of the earthquake effects perceived by the structures and, more importantly, suffered by human society.

In this respect, the main objective of the thesis is to propose methodological AVTs-based tools to guide, validate and update structural models for the seismic analysis of buildings, paving the ground for the systematic integration of vibration measurements in seismic assessment procedures. The thesis will address the theoretical and numerical validation of the rigid diaphragm assumption as well as the structural identification of diaphragm shear stiffness by ambient vibration data. In the wake of these achievements, a vibration-based procedure – exploiting pre-seismic measurements for model calibration and post-seismic measurements for damage estimation – will be proposed to build a statistical *frequency-variation control chart* for monitored buildings, to support the quick decision-making process in the post-earthquake scenario.

Hopefully, the cost reduction of experimental instruments and the continuous development of smart and powerful algorithms of data processing, accompanied by the growing competencies of the technicians, will make economically and operationally feasible the rapid diffusion in the current engineering practice of evaluation procedures previously confined to strategic or monumental structures. In this sense, the number of existing buildings for which instrumental data and experimental modal information are available is rapidly growing, thanks also to monitoring projects at the national scale (Dolce et al., 2017a; A. Astorga et al., 2020). It is not utopian to expect that, in the next future, the availability of such information will be extended to cover the entire stock of buildings exposed to seismic risk.

1.3 Organization of the thesis

Chapter 1 has provided a general overview of the background that motivates the thesis, identifying some knowledge gaps in the state-of-the-art literature and proposing possible developments of the research.

Chapter 2 presents the theoretical tools adopted in the research, referred to as direct methods – employed in structural modelling and analysis – and inverse methods – to solve modal and structural identification problems. Among the direct methods, particular attention is given to Equivalent Frame Models (EFMs) of masonry buildings, employed as a high-fidelity approach in the seismic simulations presented in the thesis. The Multi Rigid Polygon (MRP) technique and its simplifying assumptions are briefly examined, pointing out drawbacks as well as advantages when combined with experimental modal parameters. In this respect, the Frequency Domain Decomposition (FDD) is employed as the reference technique for output-only modal identification, given its physically meaningful relationship with the spectral density functions. Finally, the discussion addresses the Seismic Model From Ambient Vibration (SMAV) methodology for the quick serviceability assessment of masonry buildings, highlighting its vibration-based nature and the peculiar approach in addressing the problem of seismic-induced variations of fundamental frequencies.

Chapter 3 presents a cross-section of sample buildings - belonging to different structural typologies - analysed through ambient vibration tests. From this database, a couple of significant structures are selected as case studies, constituting the prototype models in the simulations and experimental validations of the thesis proposals. The discussion involves a detailed description of the mechanical characteristic, the ambient vibration measurements, the results of modal identification. The JetPACS steel frame is selected for validation purposes, being a simple laboratory structure built in a controlled environment. Conversely, the Pizzoli town hall – a monitored masonry building hit by recent earthquakes – is oriented to test the practical application of the thesis.

Chapter 4 collects the original contributions of the thesis, involving the development of ambient vibration-based tools supporting the seismic assessment of existing buildings. In particular, the discussion addresses modelling and identification problems related to the deformability of floor diaphragms.

First, exploiting the frequency representation of the rigid and deformable variables of motions, ambient vibrations data are employed to discriminate between rigid and nonrigid-behaving diaphragms, achieving a qualitative validation of the *rigid-diaphragm assumption* (Sivori et al., 2020b). The further investigation of a low-fidelity dynamic model of the diaphragm allows deriving inverse analytical relationships which, starting from the experimental frequencies of rigid and shear-deformable modes, provide a quantitative estimate of its *in-plane shear stiffness* (Sivori et al., 2021b). The proposals are validated through analytical methods, numerical simulations and experimental applications, highlighting their relevance in the updating and validation of structural models for seismic assessment purposes.

Taking advantage of the developed tools, the dynamically calibrated equivalent frame model of the Pizzoli town hall – a monitored masonry building – is employed to simulate the seismic-induced variations of the fundamental frequencies of the building to earthquakes of increasing intensity. A time-frequency analysis provides the identification of the building

25

co-seismic frequency shifts, in good accordance with experimental evidence. The post-seismic frequency decay, identified from the pseudo-experimental ambient vibrations of the building after the earthquake, are employed to propose the novel *frequency decay-damage control chart* of the building, which associates an expected level of structural damage to a measured decay in the fundamental frequencies, conceived as a quick assessment tool in post-earthquake scenarios (Sivori et al., 2021a).

Chapter 5 presents the seismic computational framework – relying on multiple stripe analysis – established to assess the reliability of SMAV for masonry buildings. The Pizzoli town hall is employed as a *benchmark* case to compare the predictions of SMAV with the results of nonlinear dynamic analyses on the equivalent frame model of the building. The simulation results highlight the conservative nature of the SMAV methodology, nevertheless outlining its range of applicability.

Chapter 6, finally, concludes the research of the thesis, summarizing its achievements and suggesting possible further developments.

Chapter 2

Methodological framework

The study of the seismic response of structures and the field of random vibrations are closely related in earthquake engineering. They involve, naturally, the statement and solution of direct and inverse problems. To the first pertain the structural models, mathematical formulations to predict the system response from knowledge of the model parameters and excitation. To the second, conversely, pertain the inverse techniques to identify unknown modal and structural quantities, starting from the observation of the system response.

2.1 Direct methods

2.1.1 Equivalent frame models

Several modelling techniques have been proposed in the literature for the analysis of masonry structures (Lourenço, 2002; Roca et al., 2010; D'Altri et al., 2019). Among various possibilities, they can be synthetically classified following two criteria (Calderini et al., 2010), the scale of analysis, material or structural element, and description of the masonry continuum, continuous or discrete (Figure 2.1). In seismic engineering, in particular, the class of the Structural Element Models (SEM) – sometimes referred to as *macroelement* models – holds a relevant position thanks to its simplicity and effectiveness. The peculiarity of this class lies in the identification of macroscopic elements, allowing an exhaustive description of the structure with a limited number of static and kinematic variables. The leading idea is to identify portions of the masonry continuum subjected to recurrent damage modes, for example from observation of structural damage in the post-earthquake scenario.

The SEM class discretizes the masonry into macroelements, which can exhibit damage, cracking, sliding on the basis of the assumed mechanical properties and nonlinear constitutive laws. Being characterized by a small number of mechanical parameters and degrees of freedom, these methods guarantee a reduced computational effort in the modelling and the analysis phases. The choice of the modelling strategy to be employed should depend on the structure geometrical and mechanical characteristic and its expected seismic response (Calderini et al., 2012; Lagomarsino & Cattari, 2015a). Generally, continuous models of structural elements are suitable to simulate the global seismic response of the buildings (Figure 2.2a), which is mainly associated with the *box-like* behaviour and in-plane response of walls, as long as the effects of the local response of single parts – usually characterized

27
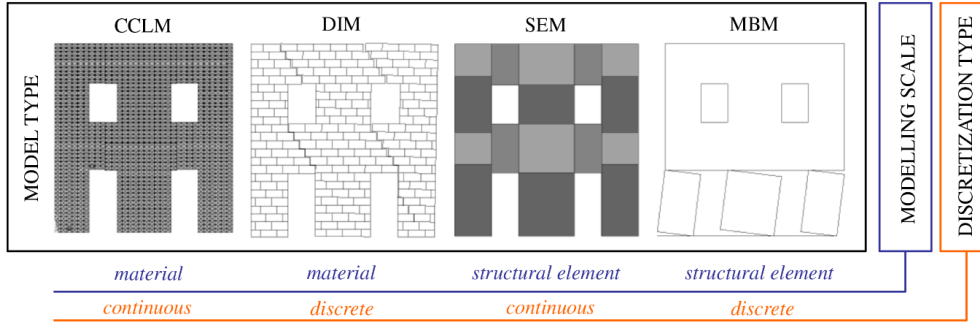
Figure 2.1: Modelling strategies for masonry buildings (from Lagomarsino and Cattari, 2015a).

by the activation of out-of-plane mechanisms, Figure 2.2b – can be neglected or analysed separately.

The thesis is oriented to the investigation of the global seismic response of existing buildings, with particular attention to unreinforced masonry buildings. For these reasons, the following paragraphs present a brief description of the *equivalent frame method* belonging to the SEM class. In the thesis, this high-fidelity modelling technique is adopted as a reference for the simulation of the seismic behaviour of masonry buildings. In Chapter 5, in particular, the equivalent-frame approach is employed to assess the reliability of simplified rigid-polygon models for large-scale seismic assessments (Section 2.1.2).

In this respect, continuum-constitutive law models (CCLM in Figure 2.1) – commonly referred to as *finite element models*, even though this term is more general – can simulate the seismic response of masonry structures with a higher degree of accuracy, if compared to SEM. Nevertheless, their practical employment reveals some issues, primary the large computational burden required even with modern computing power. The use of structural element models is often preferred, not only in the engineering practice but also in the research field, allowing to perform both static and dynamic nonlinear analyses more efficiently, thanks to the limited number of structural elements involved in the simulations. As previously introduced, this technique is based on the identification of macroscopic structural elements, masonry portions defined as piers and spandrels, described geometrically and kinematically through finite elements (shells or frames) and statically through their internal forces. The static equilibrium of the elements, indeed, can be formulated by referring to the internal force resultants instead of the continuum stress. *Piers*, the portions of the wall between two adjacent horizontally aligned openings, are the main vertical resisting elements to gravitational and seismic loads. *Spandrels*, the portions of the wall between two vertically aligned openings, are considered as secondary horizontal elements for what concerns gravitational loads, whereas they play a primary load in coupling the response of adjacent piers during seismic loads.

The so-called *Equivalent Frame Models* (EFM) are probably the most diffused in the SEM class. They idealize the masonry walls as a frame in which deformable elements (piers and spandrels) provide the nonlinear response, whereas the rigid nodes – portions that usually do not exhibit seismic damage in existing buildings – provide the connection among elements (Figure 2.4). The whole structure is assembled from the bi-dimensional

(a)   (b)
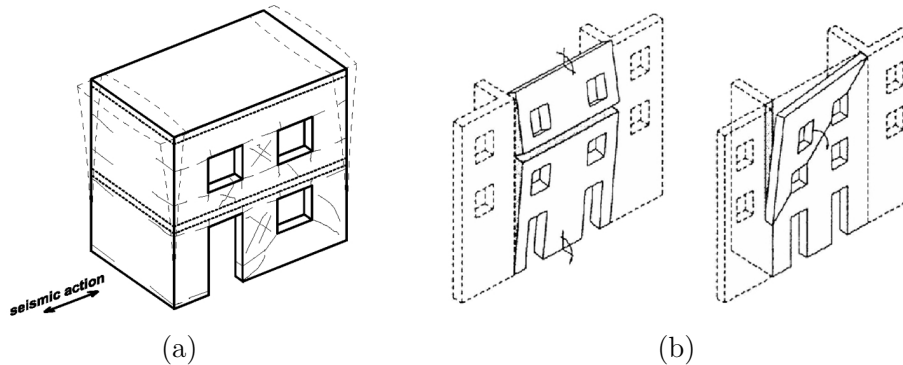
Figure 2.2: (a) Global and (b) local response of a masonry building (adapted from Magenes, 2006; D'Ayala and Speranza, 2003).

frames representing masonry walls – taking into account, in most cases, only the walls in-plane response – and from horizontal diaphragms, which may be representative of perfectly rigid or deformable floors. The EFM overcomes with little effort, from a computational point of view, the limitations of more simplified models relying on stronger assumptions – to cite two extreme cases, assuming the spandrels as perfectly stiff leading to a shear-type idealization (strong spandrel-weak pier, SSWP) or, on the contrary, assuming the spandrels with null strength and stiffness leading to a cantilever scheme for the piers (weak spandrel-strong pier, WSSP), Figure 2.3. Being both pier and spandrel elements modelled, the transition through different boundary conditions are obtained from the progressive damage of elements, rather than from a priori considerations. The equivalent-frame idealization of the structure, thus, is commonly considered the most suitable for the seismic analysis of masonry buildings, thanks to the simplicity of its implementation and the efficiency in solving nonlinear analyses.

In the last decades, the EFM met great success in the professional engineering field, as highlighted by the recommendations of national and international codes (e.g. NTC 2018 and EN1998-3 for Italy and Europe, respectively). In this respect, very recently, the Italian Network of University Laboratories in Earthquake Engineering (ReLUIS, http://www.reluis.it/index.php?lang=en) – initially, in the framework of the ReLUIS Project 2019-2021, Topic "Masonry Structures" and, currently, in the ReLUIS Project 2014-2018, Working Package 10 - "Code contributions relating to existing masonry structures" funded by DPC – has proposed some guidelines regarding the use of software codes for the seismic assessment of masonry buildings. The specific activity of Task 10.3, named "URM nonlinear modelling - Benchmark project" published the downloadable document "Use of software packages for the seismic assessment of URM buildings, Release v1.0 (in Italian)". A large part of the discussion, which is mainly addressed to the practice field, is dedicated to the EF technique, which is compared to other modelling strategies through the employment of real existing buildings as *benchmark* case studies (Cattari et al., 2017; Cattari et al., 2018a).

Despite the large use of the EFM, however, several drawbacks of this approach have been recently highlighted and critically reviewed (Quagliarini et al., 2017). The reliability and the correct use of these models represent today research topics of great concern, as
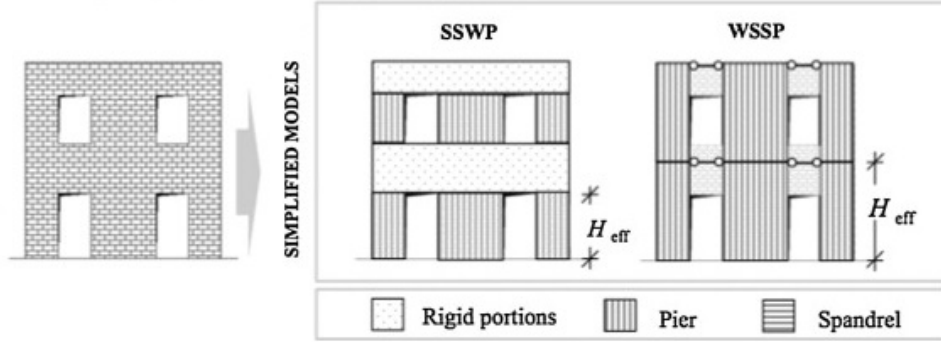
Figure 2.3: Masonry wall idealization according to simplified models, in which the behaviour of spandrels leads to the shear-type idealization (strong spandrel-weak pier, SSWP) or the cantilever scheme for the piers (weak spandrel-strong pier, WSSP). Adapted from Lagomarsino et al., 2013.
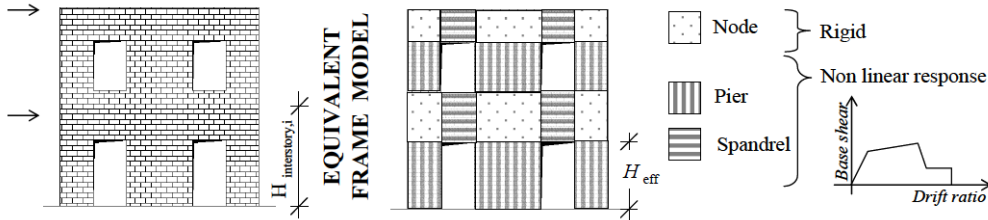
Figure 2.4: Masonry wall idealization according to the Equivalent Frame Model (adapted from Cattari and Lagomarsino, 2009).

discussed in literature by several authors (Marques & Lourenço, 2011; De Falco et al., 2017; Cattari et al., 2018a). Common issues and uncertainties involve the identification of the geometry of the structural elements, the mesh definition, the modelling of the out-of-plane response of the wall. The critical analysis of these aspects is out of the scope of the thesis, which makes use of the most recent research advancements achieved in this field (Camilletti, 2019). However, in the following, some remarks are given regarding the modelling of floor diaphragms in EF models, given the importance of this topic in seismic simulations regarding masonry buildings. The implications of deformable diaphragms on the seismic behaviour of existing buildings have been already discussed (Section 1.2) and motivate some of the analytical and experimental contributions of the thesis (Chapter 4).

Modelling of floor diaphragms

In three-dimensional structural models of buildings, the floor diaphragms have a serious influence on the static and, more importantly, the dynamic behaviour of the structure. The floor mechanical role, focusing on masonry buildings, is to guarantee the vertical and horizontal loads redistribution between the bearing walls. For what concerns EF models, the modelling of floors diaphragms is usually pursued through strong simplified hypotheses. In general, the linear elastic behaviour of diaphragms is assumed. Nevertheless, during

earthquakes, the floor diaphragms could exhibit nonlinearity (such as significant angular deformation) and be involved by damage that may affect its capacity to transfer loads. Still, no sufficient data are present in the literature to avoid the linear approximation (as highlighted in CNR-DT 212/2013). A further simplification regards the diaphragm stiffness's, which are considered negligible if acting out of its plane.

From the seismic engineering point of view, the in-plane stiffnesses – in particular the one governing the shear deformation – are the ones ensuring the joint response of bearing walls. Rigid-behaving diaphragms, thus, are able to redistribute the seismic actions between the walls so that a "box-like" global behaviour is developed, avoiding the activations of local mechanisms. In this respect, different assumptions regarding the diaphragm in-plane stiffness may significantly affect its predicted response, as recently highlighted by some research contributions (Nakamura et al., 2017; Marino, 2018; Marino et al., 2019). Many of the available structural codes, above all those addressed to engineering practice, assume the floors as infinitely rigid in their plane. However, this assumption cannot be always considered as fulfilled, especially for existing masonry building, where traditional construction techniques – such as timber floors – are still present.

For these reasons, some EFM implementations allow modelling the floors diaphragms as orthotropic membranes of finite in-plane stiffness. This is the case of the TREMURI program developed at the University of Genoa, employing 3- or 4-nodes finite plane-stress elements (Lagomarsino et al., 2013). Thus, apart from sharing vertical loads to the walls, the floors are considered as planar stiffening elements governing the distribution of horizontal actions among the walls, whereas their local flexural behaviour in the global building response is neglected. Indeed, the evaluation of the stiffness properties of existing floors may be rather simple in some typologies, such as reinforced concrete floors, where they can be ascribed to a single structural element (in this case, the slab). In other cases, such as vaults, the actual structural stiffness has a stronger geometrical dependence, requiring further caution in the definition of the equivalent plane diaphragm (Cattari et al., 2008). For timber floors, specific indications are given by codes (such as NZSEE 2017) as well as scientific contributions (Piazza et al., 2008; Brignola et al., 2012). Recently, the mechanical behaviour of timber floors has been investigated through both numerical methods and in situ campaigns (Giongo et al., 2015; Casagrande et al., 2018). Such experimental investigations, as proposed in Chapter 4, can be conducted employing *ambient vibration tests* as well, to discriminate between rigid and nonrigid behaving floor diaphragms with modal identification (Section 4.3.1) and, furthermore, to estimate their in-plane shear stiffness through model-based structural identification (Section 4.3.2).

Nonlinear response and constitutive laws of masonry panels

The prediction of the building – global – behaviour, once the masonry walls have been idealized as a three-dimensional assembly of structural elements, naturally depends on the – local – behaviour of its constitutive elements, the masonry panels. In this regard, several formulations have been proposed in the literature to describe their nonlinear response (Calderini et al., 2010; Marques & Lourenço, 2011).

The fundamental prerequisite is the proper simulation of the main in-plane failures of the masonry panel, due to the actions of vertical and horizontal loads. Observations of seismic and artificially induced damage on masonry panels show two emerging behaviours – shear
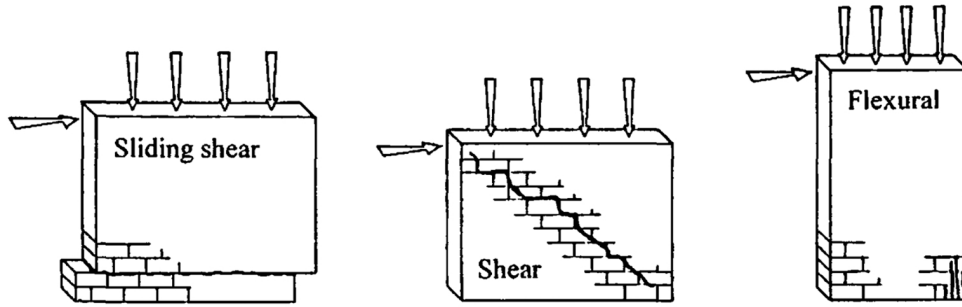
Figure 2.5: In-plane failure modes of masonry panels subjected to seismic loads (from Tomaževič, 1999). From left to right, shear failure with sliding, shear failure with diagonal cracking, flexural failure with rocking and crushing.
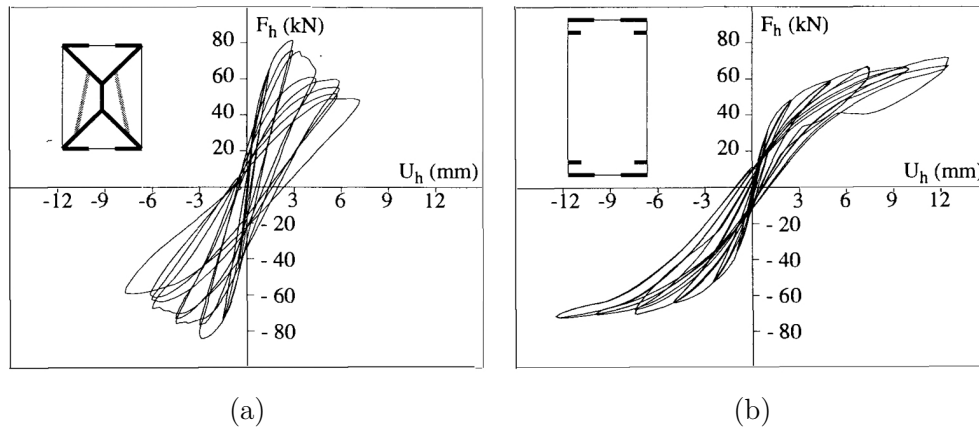
Figure 2.6: Hysteretic response of (a) a low (squat) panel exhibiting flexural behaviour and (b) a high (slender) panel exhibiting shear behaviour (from Anthoine et al., 1995).

and flexural – leading to different failure modes – sliding shear failure or diagonal cracking for the first, rocking and crushing for the second (Figure 2.5). The occurrence of different (or mixed failures) generally depends on several parameters, among others, the geometry of the panel, its compression state and boundary conditions, the mechanical and geometrical properties of the masonry constituents. Each failure type, indeed, is described by a different capacity-displacement relationship and exhibits a peculiar hysteretic response (Figures 2.6a,b). A first-order classification, among the several models available in the literature, may consist of the use of one-dimensional or two-dimensional structural description of the masonry panels.

Regarding the class of one-dimensional models – referred to as frame elements – one of the options is the use of nonlinear beam models, which describe the masonry panels as shear-deformable beams. Their nonlinear behaviour can be defined in terms of global stiffness, strength and ultimate displacement capacity by a proper shear-drift relationship. The simplified nonlinear beam elements implemented in TREMURI program follow this
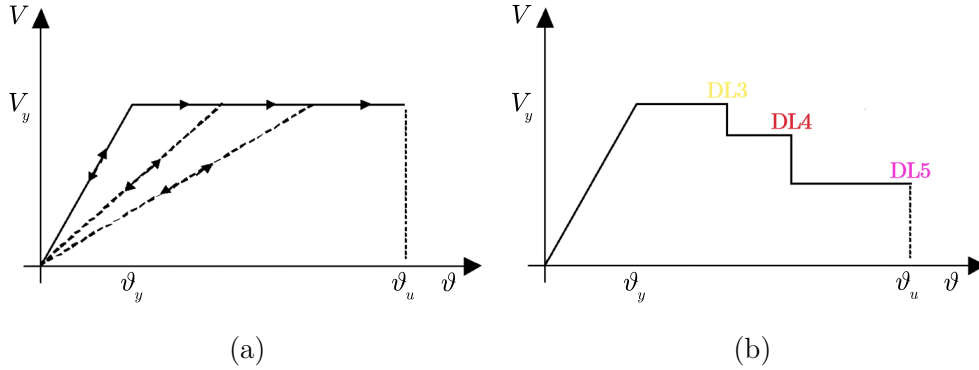
Figure 2.7: Masonry panel shear-drift $(V - \vartheta)$ relationships according to (a) the elastic-plastic law, (b) the piecewise linear law with strength degradation corresponding to increasing damage levels (adapted from Cattari et al., 2005; CNR-DT 212/2013).

approach, describing the behaviour of masonry panels with a bilinear relationship with strength cut-off and, for nonmonotonic actions, stiffness decay in the nonlinear regime. In particular, the inelastic behaviour of the structural elements is governed by a lumped-plasticity approach, in which inelasticity occurs in defined portions of the structural elements. The linear shear-deformable beams, thus, are connected by inelastic links – plastic hinges – in which damage, cracking, sliding and rotations are concentrated.

The constitutive laws governing the behaviour of the masonry panels, in the general case, are expressed in terms of shear-drift relationships, according to more or less detailed approaches. The simplest possibility, as suggested by the Italian Building Code NTC 2018, is to assume an elastic-plastic law (Figure 2.7a). The stiffness is evaluated according to the beam theory, accounting for both the shear and flexural contributions, the strength is provided by simplified resistance criteria associated with the different failure modes, and the ultimate displacement capacity is derived by experimental results or literature data. However, more refined constitutive laws can be adopted as well (as suggested by the Italian CNR-DT 212/2013). In such a case, the post-peak behaviour is described with a progressive strength degradation for fixed drift thresholds and corresponding to increasing Damage Levels (DLs), thus representing a more realistic description of the actual behaviour of masonry panels during experimental tests (Figure 2.7b). It is possible to identify, along the shear-drift $(V - \vartheta)$ curve, five different damage levels, which correspond to as many *performance* conditions. The first two damage levels pertain to the elastic branch, the second being commonly associated with the peak resistance. The drift thresholds correspond to the third and fourth levels of damage (DL3 and DL4), conversely, belong to the plastic branch and are usually recommended by national and international standards. The fifth damage level (DL5) corresponds to a complete loss of capacity to horizontal loads.

For what concerns the stiffness reduction, this effect can be considered in a simplified way, adopting reduced stiffness properties representing damaged conditions of the material – 50 % is the percentage commonly suggested by codes – or, following a more refined alternative, through empirical formulations correlating the stiffness value with the actual compressive state during the analysis (Lagomarsino et al., 2013).

Finally, regarding the ultimate capacity, the strength is assessed according to simplified criteria related to the most probable failure mechanisms. The most diffused simplified models present in the literature and codes are based on the approximate evaluation of the local – i.e. mean – stress state produced by the applied forces on predefined points – i.e. cross-sections – of the panel, verifying its admissibility in the strength domain of the material (usually idealized with simple schematizations based on few mechanical parameters, i.e. the compressive strength of masonry, its diagonal tensile strength, the cohesion and friction of mortar joints). The failure of the panel is commonly defined through a maximum drift threshold, based on the prevailing failure mechanism that occurred in the panel.

Further theoretical details related to the piecewise constitutive laws governing the behaviour of piers and spandrels, the relationship between strength degradation and element damage level, the failure criteria implemented in TREMURI program and adopted for the execution of nonlinear dynamic analyses are discussed in the next paragraphs. Both Chapter 4 and Chapter 5 of the thesis exploit the EFM and its nonlinear capabilities in the simulation of the global seismic response of masonry buildings, with different purposes. Section 4.4 proposes to simulate the seismic-induced fundamental frequency variations in masonry buildings through a calibrated EFM, proposing a specific damage assessment framework to interpret the numerical results. The application of this procedure, reported in Section 4.5.2, allows building the EFM-based *frequency-decay control chart* of the Pizzoli town hall building, for its quick post-seismic damage assessment based on vibrations measurements. Section 5.2, finally, employs the same nonlinear dynamic analyses as *benchmark* results, to give some indications about the reliability of the simplified SMAV approach for the seismic serviceability assessment of masonry buildings.

Piecewise linear constitutive laws implemented in TREMURI program

The nonlinear dynamic analyses on the EFM of the Pizzoli town hall building carried out in this thesis (Sections 5.2) are performed with the research version of TREMURI program (Lagomarsino et al., 2013). The code adopts a three-dimensional EF idealization of the building and simulates its global seismic response by referring only to the in-plane response of walls. More in detail, the masonry panels are modelled as nonlinear beams with lumped plasticity, whose shear-drift behaviour is governed by piecewise-linear constitutive laws (Cattari & Lagomarsino, 2017; Cattari et al., 2018b). Furthermore, it is also possible to simulate a hysteretic response, formulated through a phenomenological approach. A detailed description of the adopted constitutive laws is provided in the following.

The nonlinear beam model with lumped inelasticity idealization and a piecewise-linear behaviour (Cattari & Lagomarsino, 2017) allows describing the nonlinear response of the masonry panels until very severe Damage Levels (DLs, from 1 to 5), which are associated with different performance conditions, through a progressive strength degradation in correspondence of determined values of drift (Figure 2.8a). In particular, it is possible to describe both the monotonic and, more importantly in this context, the cyclic behaviour of the masonry panels. Specifically, the hysteretic response is formulated through a phenomenological approach, to capture the differences in the possible failure modes (flexural, shear or hybrid failures) and the different response of piers and spandrels (Figure 2.9a,b).

The model requires the definition of a set of parameters aimed to describe the initial elastic stiffness of the panel and its progressive degradation as well as the decrease in the

34
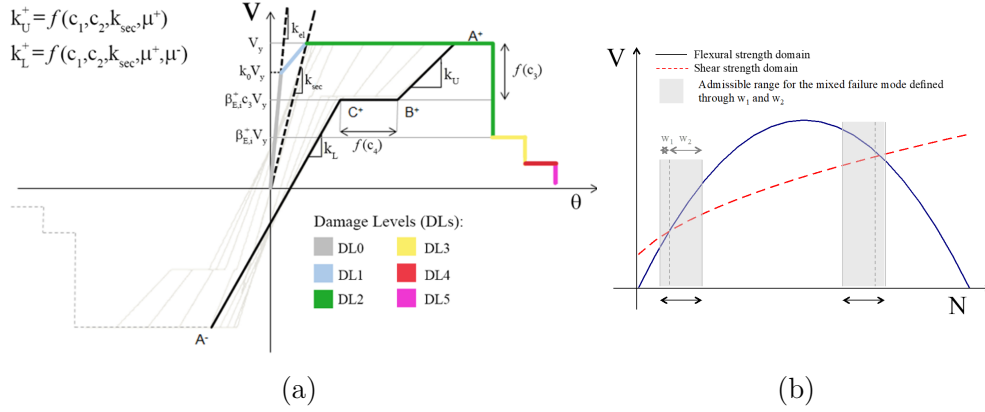
Figure 2.8: (a) Piecewise-linear constitutive law and hysteretic response in the shear-drift plane $V - \vartheta$ adopted for masonry panels and (b) schematic representation of the occurrence of a hybrid failure in the shear-axial force domain $V - N$.

maximum strength of the panel V_y for increasing damage conditions ($\theta_{E,i}$ as the i-th drift value corresponding to the i-th DL, $\beta_{E,i}$ as the i-th fraction of the residual shear strength with respect to V_y).

The elastic regime is described, according to the beam theory, by defining the elastic Young E_m and shear G_m moduli. The progressive stiffness degradation is computed approximately as the secant stiffness to the point of maximum strength, assigning a proper ratio k_r between the initial k_{el} and secant k_{sec} stiffness, and a coefficient k_0 lower than 1, which determines the strength at the end of the elastic branch with respect to the shear strength V_y.

The maximum strength of the panel is computed according to the simplified criteria proposed in the literature, considering the possible failure modes that may occur (crushing, bed joint sliding, shear diagonal cracking, see Figure 2.5) which are based on the choice of a reference point or section for calculation (Calderini et al., 2009). The strength V_y is estimated as the minimum among the predictions of the strength domains associated with the different failure criteria, based on the current axial stress acting on the element. This approach allows identifying as well the prevailing behaviour governing the hysteretic response of the element. In particular, among the several approaches available in the literature for the evaluation of the peak strength associated with the shear failure mode, the criterion proposed by Turnšek and Čačovič, 1971, describing the diagonal shear failure – with the modification introduced in Turnšek and Sheppard, 1980, left side of Table 2.1 – is assumed as a reference in the thesis, being compatible with the stone masonry typology of the buildings considered in the applications (Chapter 3). The strength associated with the flexural failure mode was evaluated with the same approach proposed in the Italian NTC 2018 and the European EN1998-3, neglecting the tensile strength of the material and assuming a stress-block normal distribution at the compressed toe (right side of Table 2.1). The final strength of the panel V_y and the mode of failure are predicted, for each value of the applied axial load, as the minimum between the shear strength associated with the shear failure mode and the one associated with the flexural failure mode. It should be remarked that all the parameters required by the adopted strength criteria are immediately

(a)   (b)
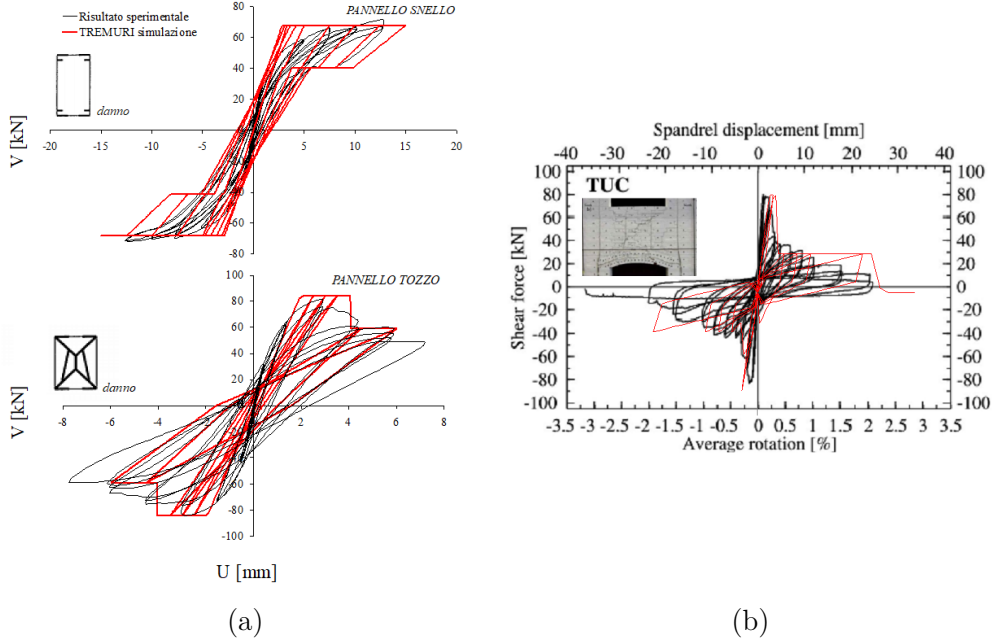
Figure 2.9: Comparison between the hysteretic responses simulated by the piecewise-linear constitutive laws (in red) and the experimental response of (a) slender and squat masonry piers (Anthoine et al., 1995), (b) spandrels (Beyer & Dazio, 2012).

derived from the mechanical parameters assumed as reference for the masonry – the initial stiffness moduli E_m, G_m, the compressive f_c and shear τ_0 strengths of the masonry and its density ρ_m – as well as from the geometry and the structural configuration characterizing each panel.

In the post-peak, the drift thresholds $\theta_{E,i}$ and corresponding strength decays $\beta_{E,i}$ are defined according to the dominant flexural or shear response of the panel, for each of the considered damage conditions. Moreover, they may be differentiated for spandrel and pier elements. In the case of a hybrid failure mode, average values are computed by the program starting from those previously assumed. The occurrence of a hybrid mode is established through a given admissible range in the shear-axial force $V - N$ domain in which the flexural and shear domains intersect each other (Figure 2.8b).

A further set of parameters describes the hysteretic response of the panel, defining the slope of loading and unloading branches of the hysteresis loops (Figure 2.8a). The unloading branch from A+ to C+ is ruled by the stiffness k_U, computed for the positive quadrant as

$$k_U^+ = k_{sec}(\mu^+)^{c_1} \left(1 - c_2(1 + \beta_{E,i}^+)\right)$$

where μ^+ the maximum ductility reached in the backbone of the positive quadrant, c_1 decreases the value of k_U with respect to the secant stiffness k_sec (assuming values ranging from 0 for the elastoplastic law to 1 for the secant stiffness), c_2 aims to further degrade the value of k_U considering the progressing strength decay on the backbone, described by the

Table 2.1: Strength criteria assumed for masonry panels in case of shear failure (diagonal cracking) and flexural failure modes.

Shear failure	Flexural failure
$V_s = \dfrac{\sigma B^2 t}{2}\left(1 - \dfrac{1}{0.85 f_c}\right)\dfrac{1}{H_0}$	$V_f = \dfrac{f_{ds} B t}{b}\sqrt{1 + \dfrac{\sigma}{f_{ds}}}$

B panel width, t panel thickness, σ mean normal stress on the cross-section, f_c masonry compressive strength, H_0 height of contra-flexure, $f_{ds} = 1.5\tau_0$, $1 \leq b = H/B \leq 1.5$

maximum damage level reached which corresponds to a specific value of strength decay $\beta_{E,i}$ (assuming values from 0 to 1). An analogous expression can be defined for the negative quadrant. After a first unloading branch A+B+ ruled by k_U, the hysteretic behaviour may also exhibit a horizontal branch B+-C+, where the point B+ is determined by the c_3 coefficient varying from 0 (A+B+ branch until zero shear) to 1 (for the elastic nonlinear condition). The extension of the B+C+ branch is determined by the c_4 coefficient. Finally, the loading branch from C+ to A- is ruled by the stiffness k_L, computed taking into account k_U and the maximum ductility value reached in both positive and negative quadrant (μ^-, μ^+). Some numerical validations of the model have been illustrated in the literature and national codes (such as the Italian CNR-DT 212/2013), both through the comparison with shaking table tests results (Cattari & Lagomarsino, 2013) and with the actual response of URM buildings hit by seismic events (Cattari et al., 2014a; Cattari et al., 2014c; Marino et al., 2016; Brunelli et al., 2020).

It is evident that the above parameters – the mechanical properties of the masonry, the parameters governing the monotonic and cyclic behaviour of the elements, the drift thresholds and strength decays associated with damage levels – can assume different values depending on the masonry typology under study. The parameters adopted in this work refers to the simple stone masonry typology of the Pizzoli town hall building (Section 3.3.1) and are reported in Section 4.5.2, as a result of a linear calibration and nonlinear validation based on the ambient and seismic response measured on the building, respectively.

2.1.2 Rigid polygons models

The in-plane dynamic behaviour of floor diaphragms has a relevant influence on the seismic response of existing buildings. Within seismic analyses, the assumption of rigid diaphragms is often adopted to simplify the structural model and reduce its computational burden (Kunnath et al., 1991). In this context, a recent proposal of the literature exploits the rigid-diaphragm assumption to assess the seismic serviceability of strategic buildings through ambient vibration testing (Acunzo et al., 2018; Spina et al., 2019).

If, on the one hand, output-only modal analysis presents several advantages compared to input-output techniques – first, the use of natural excitation sources, second, the ability to test large and massive structures in operational conditions with little invasiveness, last, the reduced cost in terms of money and time (Section 1.1) – on the other hand, this approach does not commonly allow the identification of a *complete modal model*, combining
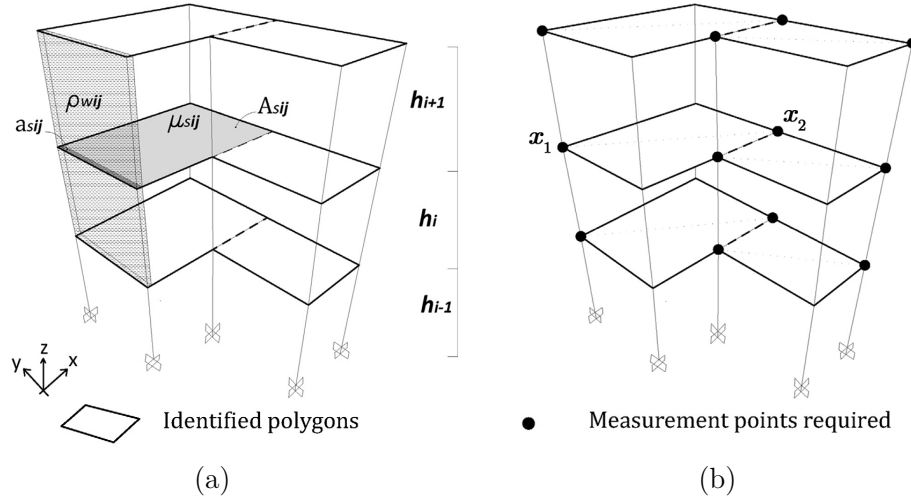
Figure 2.10: Schematic representation of the MRP model (adapted from Acunzo et al., 2018). (a) Inertial properties of the rigid-polygon and (b) required measurement points for the identification of modal masses.

natural frequencies, damping ratios and mode shapes with the knowledge of the modal mass properties of the structure. Since the excitation forces are not measured, indeed, the mode shapes cannot be scaled by the – unknown – modal mass matrix.

This drawback restricts the scope of several structural applications concerning damage detection (Bernal & Gunes, 2002), health monitoring (Doebling et al., 1996) and, not least, the seismic assessment (Mori et al., 2015). Different solutions to this problem have been proposed in the literature (López-Aenlle et al., 2012). Those exploiting output-only data and experimental techniques are commonly based on stiffness and/or mass perturbations, comparing the dynamic response of the modified structure with the reference configuration (Parloo et al., 2001; Khatibi et al., 2012). The mass-change techniques have been tested on laboratory structures (Parloo et al., 2002), bridges (Parloo et al., 2005) and even buildings (Brincker et al., 2004). However, the difficulties in transportation and positioning of the added masses – which should sum up to more than 5% of the total mass of the structure (López-Aenlle et al., 2010) – makes this method unfeasible to test existing buildings.

Other authors propose the use of a calibrated high-fidelity finite element model (FEM) of the structure (Ventura et al., 2005; Aenlle & Brincker, 2013). This choice, however, would require further efforts in the estimation of the mechanical parameters which govern the model dynamics. Such a calibration can be achieved either through specific experimental investigations – in situ destructive tests on the structural elements, laboratory tests on the building materials – or, as more often pursued, seeking the solution of an optimization problem. In this regard, the downside of *model updating* compared to *structural identification*, such as the risk of overfitting, is further discussed in Section 4.3.2.

To overcome these limitations, a more flexible and less computational-demanding model has been recently proposed in the literature (Acunzo et al., 2018). The *Multi Rigid Polygons* model (MRP) discretize the floor diaphragms through one or more rigid-behaving polygons, allowing the scaling of the experimental mode shapes through the reduced-order

mass matrix of the building. In this respect, only a rough knowledge regarding the building geometry, the inertial properties of the materials and the dynamic behaviour of the diaphragms is required (Figure 2.10a). A detailed theoretical description of the model, alongside numerical simulations and experimental validations, can be found in Acunzo et al., 2018. In the following paragraphs, the main aspects related to the rigid-polygon discretization are summarized.

Employing the rigid-polygon modelling technique, indeed, requires the fulfilment of the rigid-behaving diaphragm assumption, which depends on the actual behaviour of the real structure. As stated in Section 1.2, this possibility should not be given for granted for buildings with irregular plans (Kunnath et al., 1991) and, in particular, for historical masonry buildings with nonrigid diaphragms (timber floors, vaults) which could exhibit deformable dynamics. This issue is extensively addressed in Chapter 4, in which a specific procedure has been developed to validate the rigid diaphragm assumption exploiting ambient vibration measurements (Section 4.3.1).

The solution proposed by the MRP model, which makes it suitable for buildings with complex-shaped plans and nonrigid diaphragms, consists in increasing the number of rigid-polygons – and the number of sensors employed – to refine the discretization of the floor diaphragm. Following this perspective, such a strategy should be adopted preferably *a priori*, based on the engineering judgement on the expected dynamic behaviour of the structure, but also *a posteriori*, if a coarse discretization does not accurately reproduce the experimental results – which comes at the cost of a new and more elaborate test. Indeed, the identification of the rigid motion of a polygon (rigid translations in two orthogonal directions and rigid rotation) requires at least two bi-axial measurement points (Figure 2.10b).

Assuming to measure the in-plane ambient response (the acceleration, velocity or displacement field) of a rigid-behaving rectangular diaphragm in at least two physical points of coordinates $\boldsymbol{x}_1 = (x_1, y_1)$ and $\boldsymbol{x}_2 = (x_2, y_2)$ with respect to its centroid, the k-th experimental mode shape $\bar{\boldsymbol{\Psi}}_k = [\bar{u}_{1,k}, \bar{v}_{1,k}, \bar{u}_{2,k}, \bar{v}_{2,k}]^\top$ can be identified by means of output-only modal analysis techniques (Section 2.2.1). The linear algebraic system

$$\bar{\boldsymbol{\Psi}}_k = \boldsymbol{D}\bar{\boldsymbol{\Phi}}_k \tag{2.1}$$

expresses the k-th experimental mode shape $\bar{\boldsymbol{\Psi}}_k$ in terms of the rigid-motion components $\bar{\boldsymbol{\Phi}}_k = [u, v, \theta]^\top$ of the polygon (rigid translations u, v along the two directions x, y, rigid rotation θ) through the linear transformation $\boldsymbol{D}$. In such a case, the system matrix D has more rows than columns – there are at least four equations but only three unknown variables – and, thus, the system (2.1) is overdetermined. Even though a solution is not guaranteed to exist in the general case, the system can be solved in the least-squares sense. Assuming the matrix D to be full-rank and employing its pseudoinverse, the solution reads

$$\bar{\boldsymbol{\Phi}}_k^* = \boldsymbol{D}^\dagger \bar{\boldsymbol{\Psi}}_k \tag{2.2}$$

where $\boldsymbol{D}^\dagger = (\boldsymbol{D}^T \boldsymbol{D}^{-1})\boldsymbol{D}^\top$ is the Moore-Penrose inverse. This procedure, with little effort, can be theoretically extended to redundant measurement points and multiple rigid polygons. Considering now a multi-storey building, in which the diaphragm of each floor is ideally subdivided in a certain number of polygons which move rigidly in their plane, the mass matrix of a single polygon is determined by estimating its mass polar moment

of inertia, accounting for the inertial contribution of both the horizontal (slabs, vaults, beams) and vertical (columns, bearing walls, infill walls) elements. Thus, once the (global) mass matrix $\boldsymbol{M}$ of the model is known, the (global) mode shape is scaled as

$$\Gamma_{k,q} = \boldsymbol{\Phi}_k^\top \boldsymbol{M} \boldsymbol{b}_q, \quad \boldsymbol{\Phi}_k = \mu_k \bar{\boldsymbol{\Phi}}_k, \quad \mu_k = (\bar{\boldsymbol{\Phi}}_k^\top \boldsymbol{M} \bar{\boldsymbol{\Phi}}_k)^{\frac{1}{2}} \tag{2.3}$$

where $\boldsymbol{\Phi}_k$ are the mass-scaled rigid mode shapes of the $k-th$ mode and $\Gamma_{k,q}$ its modal participation factor – in which $\boldsymbol{b}_q$ takes into account the response along the q rigid component to a unitary base-input. Finally, the k-th ratio between the modal effective mass participating along the q-th component and the total dynamic mass is

$$\mathcal{M}_{k,q} = \Gamma_{k,q}^2 \tag{2.4}$$

which can be interpreted as a measure of the significance of a certain mode in the global – seismic – behaviour of the structure. Indeed, since the actual behaviour of the real building does not exactly match the one described by the MRP approximation, expression (2.1) holds only in an approximate way. In this sense, to a smaller diaphragm deformability corresponds a smaller approximation error. To evaluate the accuracy of the model, the authors propose to, first, validate the rigid-motion assumption (2.1) computing the Modal Assurance Criterion (MAC, Allemang & Brown, 1982) between the experimental mode shapes and the reconstructed rigid ones, second, to verify the consistency of the mass scaling (2.3) checking the orthogonality between the mass-scaled rigid mode shapes and, last, to accept only sets of modes whose total effective mass ratios (2.4), for each component, is less or equal than unity. Conversely, an adequate number of rigid-behaving experimental mode should be identified, to consider a relevant part (commonly equal or greater than 85 %) of the total dynamic mass in the assessment phase.

The ability of the MRP model to estimate the modal participation factors from AVTs is exploited by the SMAV methodology – which, for this reason, is explored among the *inverse methods*, Section 2.2.2 – to carry out the serviceability assessment of existing buildings. A procedure to qualitatively validate the rigid diaphragm assumption through ambient vibration testing is proposed in Chapter 4, Section 4.3.1. Moreover, through a low-fidelity mechanical model of a deformable diaphragm, some analytical closed-form expressions are derived to identify its mechanical shear stiffness (Section 4.3.2). Finally, the sensibility in the identification of the modal participation factors to different rigid-polygon approximations – and their potential influence on the seismic predictions – is addressed in Chapter 5, in the framework of the general validation of the SMAV assessment for masonry buildings.

2.2 Inverse methods

2.2.1 Output-only modal identification in the frequency domain: the *Frequency Domain Decomposition*

The *Frequency Domain Decomposition* (FFD) has been proposed in the literature in 2000 (Brincker et al., 2000), among the output-only modal identification techniques operating in the frequency domain. As mentioned in the Introduction to the thesis (Chapter 1), the statement "output-only" refers to the employment of measurements of the sole response

of a dynamic system to identify its modal properties (natural frequencies, mode shapes, damping ratios). This approach is commonly known as *operational modal analysis*, which derived as a novel but complementary field to the traditional input-output *experimental modal analysis*. The increasing popularity of this discipline is driven by the possibility to carry out cost and time-saving tests with little invasiveness for the structure, which does not interfere with its operational conditions (Rainieri & Fabbrocino, 2015). Exploiting the vibrations naturally induced by wind, traffic, seismic microtremors and human activities, this framework allows the identification of operational modal parameters without requiring any measurement of input excitation forces, which are assumed as random both in the time and space domains, broadband smooth and mutually uncorrelated.

Among the several output-only identification techniques available in the literature(Peeters & De Roeck, 2001; Reynders, 2012), for the class of nonparametrical approaches in the frequency domain, the FDD is the natural evolution of the spectral density peak-picking technique, overcoming some of its limitations regarding close modes. The fundamental idea – actually inherited from the older input-output complex mode indication function(Shih et al., 1988), Figure 2.11a – is to exploit the *singular value decomposition* of the output cross-spectral density matrix to extract the independent responses (modes) which, together, compose the system response. Such a decomposition provides exact results if the loading is white noise, the structure is lightly damped and the mode shapes of close modes are geometrically orthogonal. The main theoretical aspects of this straightforward technique, which has been employed to identify the modal properties of the case-study structures proposed in this thesis (Chapter 3), are summarized in the following.

The input-output relationship of a dynamic system can be expressed as

$$\boldsymbol{G}_{yy}(\omega) = \boldsymbol{H}(\omega)\boldsymbol{G}_{ff}(\omega)\boldsymbol{H}(\omega)^H \tag{2.5}$$

where ω is the circular frequency, $\boldsymbol{G}_{yy}, \boldsymbol{G}_{ff}$ are, respectively, the Power Spectral Density (PSD) matrices of the output response $\boldsymbol{y}$ and input forces $\boldsymbol{f}$, $\boldsymbol{H}$ is the frequency response function matrix of the system – such that $\boldsymbol{y}(\omega) = \boldsymbol{H}(\omega)\boldsymbol{f}(\omega)$ – and the superscript H denote the Hermitian. Assuming an independent white noise input, i.e. $\boldsymbol{G}_{ff}$ is constant in frequency and diagonal, from (2.5) follows that

$$\boldsymbol{G}_{yy}(\omega) \propto \boldsymbol{H}(\omega)\boldsymbol{I}\boldsymbol{H}(\omega)^H \tag{2.6}$$

where $\boldsymbol{I}$ is the identity matrix. Equation (2.6) explicitly shows that $\boldsymbol{G}_{yy}$, the cross-PSD matrix of the system response, is suited for modal parameter estimation. Employing the classical modal expansion of the response

$$\boldsymbol{y}(t) = \boldsymbol{\Phi}\boldsymbol{q}(t) \tag{2.7}$$

where $\boldsymbol{\Phi}$ collects column-wise the eigenvectors of the system, expressing the autocorrelation function of the response $\boldsymbol{R}_{qq}(\tau)$ with respect to the new modal coordinates $\boldsymbol{q}(t)$ as

$$\boldsymbol{R}_{yy}(\tau) = \mathbb{E}\{\boldsymbol{y}(t+\tau)\boldsymbol{y}^T\} = \boldsymbol{\Phi}\boldsymbol{R}_{qq}(\tau)\boldsymbol{\Phi}^H \tag{2.8}$$

and, finally, Fourier-transforming the right-hand side gives

$$\boldsymbol{G}_{yy}(\omega) = \boldsymbol{\Phi}\boldsymbol{G}_{qq}(\omega)\boldsymbol{\Phi}^H = \boldsymbol{U}(\omega)\boldsymbol{S}(\omega)\boldsymbol{V}(\omega)^H \tag{2.9}$$
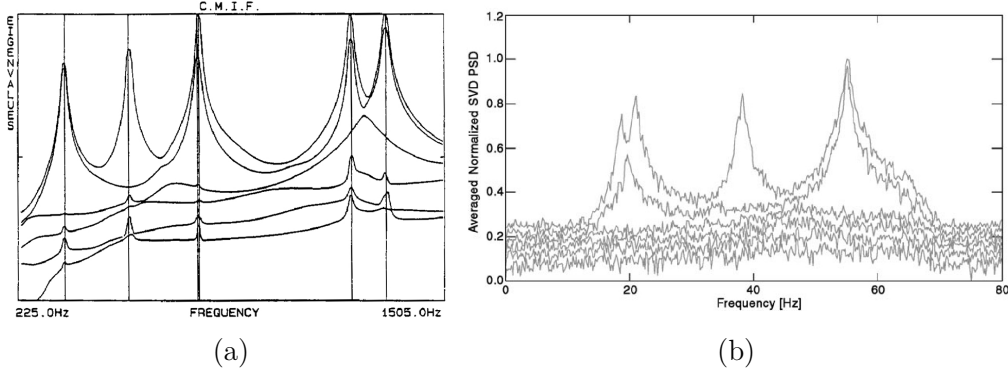
Figure 2.11: (a) Complex Mode Indication Function (CMIF) of the frequency response function matrix (from Shih et al., 1988) and (b) Frequency Domain Decomposition (FDD) of the response spectral matrix (adapted from Brincker et al., 2001b).

Thus, if the modal coordinates are uncorrelated and the mode shapes orthogonal, the PSD matrix of the modal coordinates $\boldsymbol{G}_{qq}$ is diagonal, and (2.9) is a singular value decomposition of the response spectral matrix $\boldsymbol{G}_{yy}$. For each frequency ω, the SVD $\boldsymbol{G}_{yy} = \boldsymbol{U}\boldsymbol{S}\boldsymbol{V}^H$ provides the singular vectors $\boldsymbol{U}, \boldsymbol{V}$ as estimates of the mode shapes $\boldsymbol{\Phi}$, whereas peaks in the singular values $\boldsymbol{S}$ are estimates of the modal frequencies (Figure 2.11b). In particular, if only the k-th mode is dominating a frequency band, at the resonance ω_k the first singular vector is an estimate of the k-th mode shape and the corresponding singular value is the k-th auto-PSD of the single degree-of-freedom system.

Further indications about the behaviour of singular values and vectors in presence of close modes can be found in Brincker et al., 2001b. Indeed, the technique allows identifying damping as well (Brincker et al., 2001a). More recent developments pursued the automation of the algorithm (Brincker et al., 2007), the enhancement of modal estimates (Zhang et al., 2010), the unbiased estimation of damping (Tamura et al., 2002; Rainieri et al., 2010), the application to nonstationary inputs(Pioldi & Rizzi, 2017).

It is understood, in this discussion, the concept of wide-sense stationary random process. In such a case – for example, dealing with measurements of structural response to ambient excitation – the formal definition of PSD is

$$S_{XX}(\omega) = \frac{1}{2\pi} \lim_{T \to \infty} \frac{1}{T} \mathbb{E}\left[|\tilde{\boldsymbol{X}}_T(\omega)|^2\right] \tag{2.10}$$

where ω is the angular frequency, $\mathbb{E}$ is the expected value operator and $\tilde{\mathbf{X}}_T(\omega)$ is the process collecting the Fourier transforms $\tilde{x}_T(\omega)$ of the windowed realizations $x_T(t)$ of the stochastic process. The function $S_{XX}(\omega)$ is related to the autocorrelation function $R_{XX}(\tau) = \mathbb{E}\left[X(t)X(t+\tau)\right]$ by the Fourier pair (Wiener-Kinchin theorem)

$$S_{XX}(\omega) = \frac{1}{2\pi} \int_{-\infty}^{+\infty} R_{XX}(\tau)e^{-j\omega\tau}d\tau, \qquad R_{XX}(\tau) = \int_{-\infty}^{+\infty} S_{XX}(\omega)e^{j\omega\tau}d\omega \tag{2.11}$$

The PSD can be efficiently estimated from a single realization of the physical process, i.e. a single test of finite time, employing the Welch method (Welch, 1967) as the average of several *periodograms* – discrete Fourier transform of overlapping and windowed segments

42

of the measured time history. Beyond the FDD technique, adopted to identify the modal properties of the case studies structures (Chapter 3), the Welch technique is adopted in the thesis as a general tool for the estimation of the spectral density of stationary processes, such as the vibrational ambient behaviour of floor diaphragms (Chapter 4).

2.2.2   *Seismic Model from Ambient Vibrations* (SMAV)

The *Seismic Model from Ambient Vibrations* (SMAV), originally developed in 2015 by the Italian Department of Civil Protection with the National Research Council of Italy (Mori et al., 2015; Spina et al., 2019), is a *speditive* (i.e. quick) procedure conceived to estimate the seismic serviceability of strategic buildings based on the modal parameter identified by AVTs (Section 2.2.1). As stated by the authors, the idea that led to the development of SMAV was to provide a tool that, based solely on the results of modal identification and on a rapid survey of the geometric characteristics of the structure, would be able to estimate the building seismic vulnerability referred to its operational state, i.e. up to low levels of damage.

Being naturally conceived for large-scale assessment, thus requiring time-saving evaluations, the first implementation of the procedure (Mori et al., 2015) initially relied on the simplifying assumption of in-plane perfectly rigid floors to estimate modal masses. With this assumption, however, the procedure was not suitable for buildings with non-rectangular plan (e.g. T-shape) or historical buildings with deformable floor diaphragms (masonry buildings with timber floors, vaults). A more recent and refined implementation (Spina et al., 2019) based on the MRP model (Acunzo et al., 2018), which relaxes the hypothesis of a single rigid diaphragm and subdivides each floor into several rigid polygons according to its geometry and mechanical features, allows a more reliable estimation of modal masses for irregularly shaped buildings. As previously discussed (Section 2.1.2), conversely, this requires an increased effort in planning and execution of AVTs, since every rigid-behaving polygon requires at least two bi-axial measurement points.

Once the set of modal parameters is known and the MRP model of the building is available, SMAV allows estimating the response of the building for an expected seismic input – assigned through a response spectrum or a time-history – through a linear procedure with modal superposition. Indeed, the modal parameters set of natural frequencies $\boldsymbol{f}$, damping ratios $\boldsymbol{\xi}$ (identified or assumed), mass-scaled mode shapes $\boldsymbol{\Phi}$ – as illustrated in Section 2.1.2, scaled through the coefficient μ_k, allowing the evaluation of the modal participation factor Γ_k for the k-th mode – constitute a so-called *complete* modal model of the building, limited to the identified natural modes. If the acceleration time-history of the earthquake is employed as a seismic input, a time-domain integration allows computing the k-th modal dynamic response $u_k(t)$ of the system to the input $\ddot{\boldsymbol{u}}_{f,q}(t)$ along the q component as

$$u_{k,q}(t) = -\frac{\Gamma_{k,q}}{\omega_k^d} \int_0^t \ddot{\boldsymbol{u}}_{f,q}(t) \sin(\omega_k^d t) e^{-\xi_k \omega_k (t-\tau)} d\tau \tag{2.12}$$

in which $\omega_k = 2\pi f_k$ stands for the k-th natural circular frequency of the structure and $\omega_k^d = \omega_k \sqrt{1 - \xi_k^2}$ accounts for the damping. Each mode contribution is finally combined

according to the modal superposition principle

$$\boldsymbol{u}_q(t) = \sum_k \boldsymbol{\Phi}_k u_{k,q}(t) \tag{2.13}$$

where $\boldsymbol{u}_q(t)$ holds the response of each polygon centroid along the q-th component. On the other hand, if the seismic analysis is carried out employing a response spectrum – such as a pseudo-acceleration spectrum $S_a(T,\xi)$, commonly estimated from a set of accelerograms (see Section 5.2.1) – the k-th modal response on the q component can be estimated as

$$\boldsymbol{u}_{k,q} = \boldsymbol{\Phi}_k S_{d,q}(T_k,\xi_k)\Gamma_{k,q} \tag{2.14}$$

with $S_d(T,\xi) = S_a(T,\xi)\omega^2$ as the pseudo-displacement response spectrum. The total response, taking into account the non-contemporaneity of the input and the maximum response in the two directions, is estimated through a complete quadratic combination (as suggested by the Italian NTC 2018).

It is further possible, potentially, to estimate the uncondensed displacements in every point of the floor with a simple linear transformation. This allows estimating the *maximum interstorey drift ratio* ϑ_i of the structure as

$$\vartheta_{i,q} = \frac{\max |\Delta u(t)|}{\Delta h} \tag{2.15}$$

where $\Delta u, \Delta h$ are the difference between the estimated displacements – along a fixed direction q – and the height of two vertically aligned points on the structure. Indeed, the time variable is dropped if the response is evaluated through the response spectrum approach. Indeed, the differences $\Delta u, \Delta h$ can be substituted by u_h, h – the roof displacement and the roof height – to estimate the roof drift ϑ_r with respect to the ground.

Linear-equivalent analysis with Frequency Shift Curves (FSCs)

As pointed out by several scientific contributions (Villaverde, 2007), the variation of the fundamental frequencies of structures during earthquakes raises serious concerns regarding simplified seismic assessment approaches based on modal parameters identified from AVTs. This is the case of the SMAV methodology which, to overcome this issue, employs the so-called *Frequency Shift Curves* (FSCs, Spina et al., 2019), which address the frequency variation exhibited by masonry buildings during seismic events.

The drop of fundamental frequencies of buildings due to earthquakes, observed both in presence and absence of structural damage, is a widely studied phenomenon that has been mainly investigated for reinforced concrete buildings. A more detailed list of references from the literature is reported in the Introduction (Chapter 1). Further insights are provided in Section 4.4.1, which explicitly address the numerical simulation of this phenomenon for damaged masonry buildings.

According to its simplified approach, the SMAV assessment takes into account the frequency variation phenomenon through the use of analytical curves, conceived to describe the frequency behaviour of masonry buildings as a function of its current seismic response – the roof drift ϑ_r, Equation (2.15). The curves have been built with a stochastic approach (Figure 2.12a), by least-squares fitting the results of Monte Carlo simulations on a single
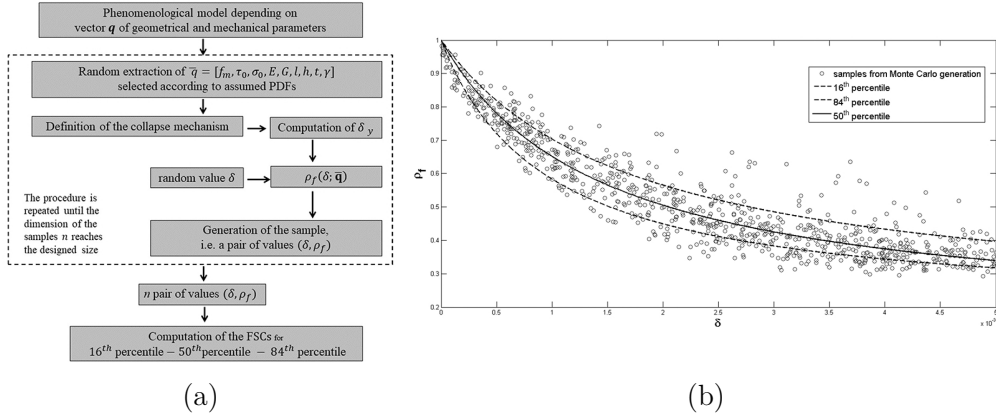
Figure 2.12: (a) Flowchart of the Monte Carlo simulation for the numerical generation of (b) the FSCs for masonry buildings (adapted from Spina et al., 2019).
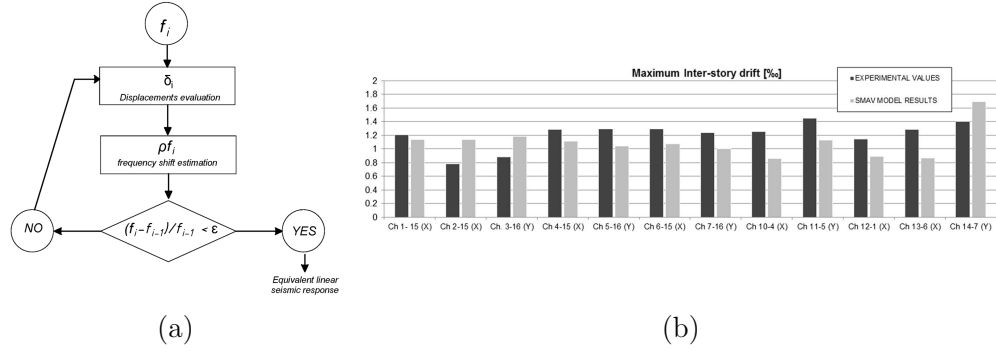
Figure 2.13: (a) Scheme of the iterative linear-equivalent analysis with frequency shifts and (b) comparison between the SMAV predictions and the experimental seismic response of the Pizzoli town hall building, monitored by OSS (adapted from Spina et al., 2019).

masonry panel varying its geometrical, material and mechanical properties. In particular, the variation of frequency is identified thanks to its proportionality with the secant stiffness of the masonry panel, assuming a nonlinear constitutive law describing its elastic and plastic behaviour according to different damaging modes (see also Section 2.1.1). In this sense, both transient and permanent effects are considered. Further details regarding the simulation framework and the constitutive laws assumed for masonry can be found in Spina et al., 2019. It should be pointed out the analytical model chosen as representative of the frequency shift, which is

$$f(\vartheta) = \frac{c_1\vartheta + c_2}{\vartheta + c_2}f_0, \quad \vartheta \geq 0 \tag{2.16}$$

where f_0 represents the initial fundamental frequency. The rational polynomial model 2.16 is able to capture the variable speed of the phenomenon – the velocity of the shift, i.e. its derivative, which decreases for increasing drift of the panel (Figure 2.12b).

Avoiding the computational burdening of a nonlinear solution, SMAV performs a linear

equivalent analysis along the frequency-shift curves, according to an iterative approach (Figure 2.13a). In particular, the FSCs are assumed to be representative of the dynamic behaviour of the whole building, supposing the frequency variations to depend only on the roof drift, that all the fundamental frequencies undergo the same shift and, finally, that the mode shapes are invariant during the analysis. The first iteration estimates the seismic response of the building – through Equations 2.12 or 2.14) – and decreases the experimental frequencies identified from ambient vibrations according to the estimated maximum roof drift. Each subsequent iteration updates the response estimation and the corresponding frequency shift, up to frequency convergence (less than 1 % of variation). The reliability of both the FSCs and the SMAV assessment procedure has been validated by the Authors through experimental measurements of the seismic response of a monitored building, the Pizzoli town hall (one of the case studies of this thesis, presented in Chapter 3), with good results in terms of distribution and amplitude of the predicted interstorey drifts (Figure 2.13b). A comparison with the co-seismic fundamental frequency shifts simulated for the same building – through an equivalent-frame idealization and nonlinear dynamic analyses – is reported in Section 5.2.2.

Chapter 3

Selected case studies

The Chapter presents synthetically the stock of real structures available to the research and experimentally tested through ambient vibrations. Among the others, two structures have been extensively employed to validate the proposals of the thesis. The first is a scaled steel frame built in a laboratory environment, conceived to study the efficiency of seismic isolation devices. The second is an existing masonry building permanently monitored by the Italian Structural Seismic Monitoring Network (OSS), which shared vibration data acquired on the structure – both ambient and seismic responses – during the earthquake sequence that hit Central Italy in 2016.

3.1   Available structures and vibration data

The objectives of the thesis build on the availability of vibration measurements, focusing those acquired on existing masonry buildings and characterizing their dynamic behaviour during ambient conditions. The contributions presented in the following Chapters mainly rely, for their applicative part, on experimental data acquired on real structures, which were directly tested or, conversely, made available to the present research from other scientific collaborations.

The first set of structures is composed of strategic buildings located in different provinces of Liguria, Northern Italy, mainly in seismic-prone areas belonging to the westernmost part of the region – which, being hit in the past by strong earthquakes, are today subject of several studies addressed at the probabilistic characterization of their seismic hazard (Barani et al., 2020). The candidate has been involved in the surveying, testing, modelling and analysis of such buildings within the *SMAV Liguria Project 2018-2019* (Sivori et al., 2018) funded by the Italian Department of Civil Protection (DPC), aimed at the quick assessment of the seismic serviceability of strategic buildings through the SMAV methodology (Section 2.2.2). The project is part of a more comprehensive national initiative (Dolce, 2012; Dolce et al., 2018) to test the reliability of emergency systems for the mitigation of the seismic risk in urbanized areas – which included, alongside, studies of site amplification and seismic microzonation. Of the total of eight structures tested through ambient vibration measurements, three are ordinary masonry buildings – the town halls of the Alassio,
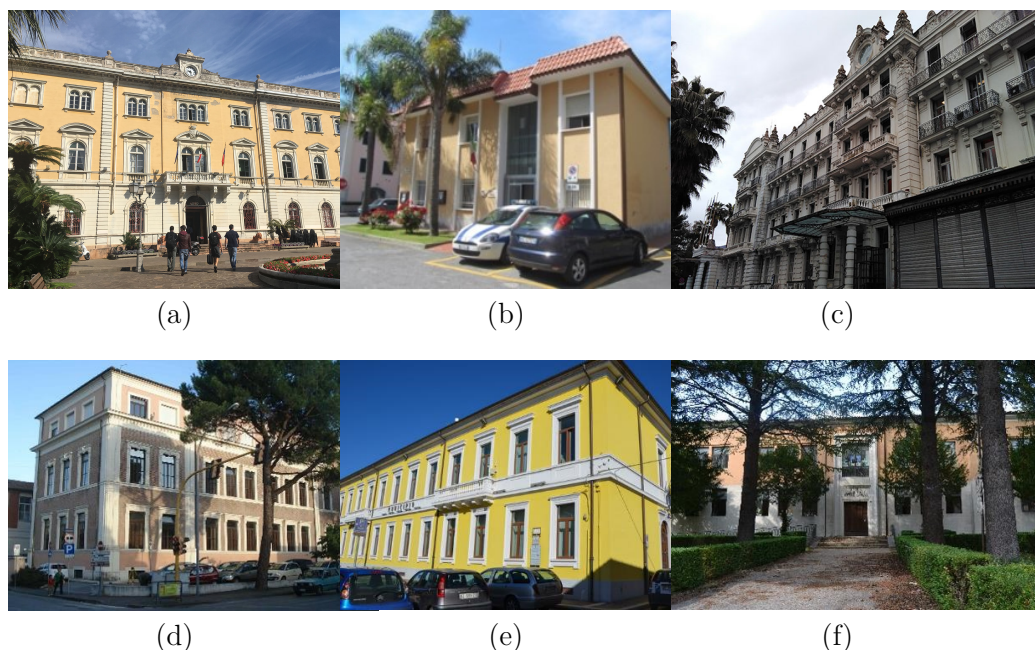
Figure 3.1: Existing masonry buildings tested in the framework of the *SMAV Liguria Project 2018-2019* – (a) Alassio town hall, (b) San Bartolomeo town hall, (c) Sanremo town hall – and permanently monitored by OSS in Central Italy – (d) Fabriano courthouse, (e) Pizzoli town hall, (f) Pietro Capuzi school in Visso.

San Bartolomeo and Sanremo municipalities, top of Figure 3.1. The project has been recently renewed for the years 2020-2021 and is involving the testing of five more buildings, granting a wider stock of real structures to test the practical implications of AVT-based methodologies.

The second set of structures involves three existing masonry buildings permanently monitored by the Italian Structural Seismic Monitoring Network (referred hereinafter as OSS, Dolce et al., 2017a) managed by DPC, whose monitoring data were shared with several Italian universities in the framework of the DPC-ReLUIS Project 2017-2018, Research Line "Masonry Structures", Task 4.1 - "Analysis of buildings monitored by Osservatorio Sismico delle Strutture (OSS)". All these structures were hit, with different severity, by the Central Italy earthquake sequence of 2016-2017. In particular, the candidate was involved in the surveying of the post-earthquake damage suffered by two buildings, the Pietro Capuzi School in Visso, Marche Region and the Pizzoli town hall in Abruzzo Region (bottom of Figure 3.1).

The main characteristics of the buildings aforementioned, including the structural typology, the building materials, the plan regularity and the geometric dimensions are summarized in Table 3.1. Some of them are further described – including the results of their modal identification – in Appendix, others can be found in Sivori et al., 2018; Cattari et al., 2019b. Among them, the case study presented in the thesis and extensively employed in the applications is the Pizzoli town hall. This choice is motivated, first, by (i) the common

structural characteristics – ordinary low-rise masonry building with reinforced concrete diaphragms, regular in plan and elevation, slight post-seismic damage – which simplify the analyses and are suited for a general example and, more importantly, by (ii) the availability of vibration data referred to both the ambient and seismic response of the building, fundamental for robust validation of the proposals related to seismic assessment.

Indeed, experimental vibration data acquired *in situ* have the advantage of being representative of examined structure in its operational conditions, nevertheless, their quality can be negatively affected by unwanted external factors which, often, are difficult to monitor – including noise, misorientation of sensors, signal desynchronization. From this perspective, vibration measurements carried in a controlled environment are usually more reliable. These reasons motivated the choice of an additional laboratory case study, the JetPACS (Joint Experimental Testing on Passive and semiActive Control Systems) steel frame (Dolce et al., 2008; Gattulli et al., 2009; Ponzo et al., 2012), built and tested in 2007 at the structural laboratory of the University of Basilicata. The employment of a simple scaled structure of well-known mechanical characteristic, as well as the availability of robust vibration data, allowed a first and straightforward validation of the thesis proposals. A detailed description of the JetPACS frame (Section 3.2.1) and the Pizzoli town hall building (Section 3.3.1), discussing as well their ambient dynamic behaviour, is reported in the following Sections.

3.2   Laboratory structures

3.2.1   JetPACS frame

In 2007, within a national project targeted at the mitigation of the dynamic response of structures to seismic actions promoted by the Italian Network of University Laboratories in Earthquake Engineering (DPC-ReLUIS Project 2005–2008, Research Line 7 - "Technologies for the isolation and control of structures and infrastructures") and funded by the Italian Department of Civil Protection, the experimental dynamic testing program JetPACS (Joint Experimental Testing on Passive and semiActive Control Systems) involved the design and construction of a 2:3 scaled steel building prototype aimed at testing active and passive energy dissipation devices for seismic protection (Dolce et al., 2008; Gattulli et al., 2009; Ponzo et al., 2012). The structural model is a three-dimensional single-bay steel frame representative of a residential housing steel building (Figure 3.2a). It is composed of two storeys with plan dimensions 4.2 m×3.2 m and an interstorey height of 2 m. The edge beams of each storey (IPE180) are supported by four columns (HEB140) and connected by HI-bond corrugated steel sheets bonded to the upper 100 mm-thick reinforced concrete slab. The beam-to-column joints are welded and, in correspondence with columns, stiffened by horizontal steel plates. The experimental frame has been realized in a laboratory environment employing Fe360 grade steel, which is characterized by a Young modulus equal to 206 000 MPa. The design gravity loads are represented by dead and live loads, equal to 3.25 kPa and 2 kPa respectively.

In addition to the bare frame configuration CB above described, whose total mass is around 7100 kg, additional concrete masses have been placed on each floor slab according to two different configurations. In the symmetric configuration CS, four additional masses have been placed at each level preserving the double symmetry of the structure. In such a

49

Table 3.1: Main structural, geometrical and material characteristics of the masonry buildings available to the present research.

Location	Typology	Material	Plan	a (m)	b (m)	a/b	A (m²)	n_l	h_i (m)	h (m)
Alassio (SV), Liguria	Town hall	Stone	Regular	40.5	15.7	2.6	635	3	6.25/4.45	15.9
San Bartolomeo (IM), Liguria	Town hall	Stone	Regular	13.5	8.2	1.7	110	2	3.3	6.6
Sanremo (IM), Liguria	Town hall	Stone	Regular	66	16.9	3.9	1115	4	4.75/4.1	17.3
Fabriano (AN), Marche	Courthouse	Brick	T-shaped	76.7	15.6	4.9	1220	3	5.3	16.8
Pizzoli (AQ), Abruzzo	Town hall	Stone	C-shaped	36.8	11.9	3.1	440	2	3.6/4.3	7.9
Visso (MC), Marche	School	Stone	T-shaped	39.6	11.4	3.47	600	2	4.3	9.4

a = plan length, b = plan width, a/b = plan length/width ratio, A = total plan area, n_l = number of storeys,
h_i = interstorey height, h = total height

(a)   (b)
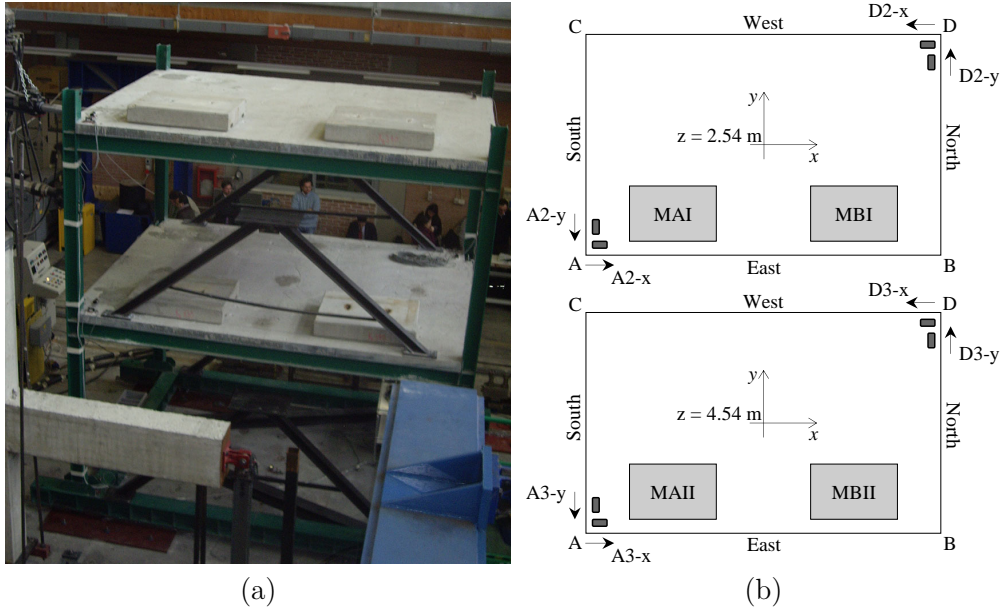
Figure 3.2: (a) Picture of the prototype steel frame in the nonsymmetric added-mass configuration CN. Plan view of each frame level, highlighting the location of the added masses and the measurement setup (b).

case, the masses (around 335 kg each) accounts for the non-structural dead loads and 30 % of live loads. In the non-symmetric configuration CN, conversely, only two masses have been added to each level, along the longest side of the frame in the x direction (Figure 3.2b). Analytical and computational models inspired by this structure, including some structural and parametric variations, are employed for simulation purposes in Section 4.5.1.

Measurement setup and modal identification

Several dynamic identification tests of the unbraced frame have been carried out at the Structural Laboratory of University of Basilicata (Gattulli et al., 2007; Ponzo et al., 2007) with a number of different excitation sources, such as ambient noise, instrumental hammer impact excitations and sine-sweep ground motion. The structural response has been recorded by a total of 16 unidirectional servo-accelerometers. Of the total, eight sensors are placed as pairs of two along the orthogonal directions x and y, at the opposite corners of each storey. The sensors are force-balance accelerometers SA-107LN from Columbia Research Laboratories, high sensitivity, low noise sensors specifically designed for use in seismic and low intensity, low-frequency motion studies. The accelerometers provide a high level and low impedance output, so that no signal conditioning is required in most applications. The sensor range is $\pm 0.1\,g$ with less than $0.1\,\%$ nonlinearity, noise lower than $2.5\,\mu\text{V}$ RMS from 0 to 50 Hz and a resolution of $1\,\mu g$. Signal's digitization, acquisition and synchronization are managed by a dedicated DAQ unit. In this thesis, only the response of the frame to environmental noise has been analysed by means of output-only modal techniques. In particular, ambient vibration measurements have been acquired for 1800 s

Table 3.2: Frequency and description of the modes experimentally identified on the Pizzoli town hall building from ambient vibration measurements, employing the FDD technique.

Mode	Frequency (Hz)			Shape	Type
	CB	CS	CN		
1	3.38	2.85	3.08	Translational along y	T_{y1}
2	4.23	3.58	3.84	Translational along x	T_{x1}
3	5.89	5.11	5.51	Torsional	R_1
4			8.90	Counter-phase translational along y	T_{y2}
5			12.96	Counter-phase translational along x	T_{x2}
6			17.64	Counter-phase torsional	R_2
7	15.60	13.15	14.08		S_1
8			15.28	Diaphragm shear deformation	S_2
9			16.55		S_3
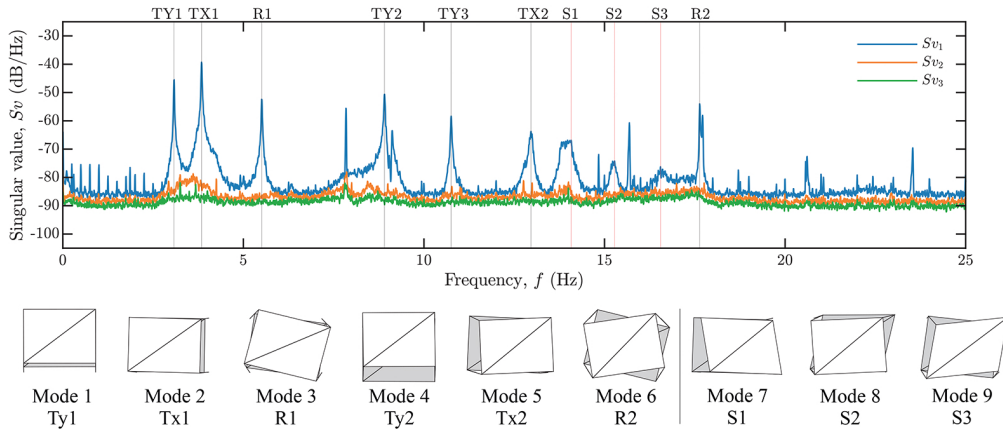
Figure 3.3: First three singular values of the response cross-spectral density matrix, obtained from FDD of the ambient response of the prototype frame in the CN configuration. Plan view of the identified mode shapes, rigid-behaving (left side) and nonrigid-behaving (right side).

at the sampling frequency of 200 Hz. In the following, the discussion of the experimental identification refers to the frame in the CN configuration, given the interesting dynamics caused by the nonsymmetric distribution of added masses.

The fundamental frequencies, the corresponding mode shapes and damping ratios are identified from the ambient response of the frame employing the Frequency Domain Decomposition (FDD, Section 2.2.1). The estimation involves the singular value decomposition of the cross-spectral density matrix, identifying the modes natural frequencies at the peaks of the first singular value and the mode shapes from the corresponding first singular vector. The auto- and cross-power spectral densities are estimated employing the Welch method, applying a Hamming window with 50 % overlap and fixing the frequency resolution to 0.01 Hz.

The first three singular values of the response cross-spectral density matrix in the range 0-25 Hz shows up to ten peaks of amplification (Figure 3.3). The mode identified at 10.75 Hz is almost identical, in terms of mode shapes, to the mode at 8.90 Hz and, thus, is neglected in the following considerations. The narrow peaks in the spectrum (i.e. 7.84 Hz and 15.78 Hz) can be attributed to unidentified harmonic components in the excitation. As shown by the experimental mode shapes (bottom side of Figure 3.3), the three modes at the lowest frequency – the translational modes T_{y1}, T_{x1} along the y, x directions, the rotational mode R_1 – exhibit in-phase displacements of the two storeys, whereas their high-frequency counterparts – modes T_{y2}, T_{x2}, R_2 – counter-phase displacements. It is to be noted that the translational modes T_{x1} and T_{x2} show a small but non-negligible torsional component due to the absence of symmetry with respect to the x direction. As a general observation, according to a qualitative analysis of the mode shapes, these modes seem to behave as rigid in the floor horizontal plane.

On the other hand, in the frequency band between 14 Hz and 18 Hz, the amplification peaks appear to be associated with nonrigid-diaphragms modes involving their shear deformation – type S. The experimental identification of the frame in the other two configurations – bare configuration CB and with additional symmetric masses CN – highlights significant variations in the frequencies of the identified modes, with a slight modification of the mode shapes. This effect, indeed, can be related to the change in the dynamic mass, confirming the structural nature of the identified modes (Table 3.2). The results of modal identification, as well as the acquired ambient vibration time-histories, are employed in 4.5.1 to calibrate computational models of the structure and to test the effectiveness of the AVTs-based inverse procedures theoretically developed in Section 4.3.

3.3 Monitored buildings

3.3.1 Pizzoli town hall

The Pizzoli town hall is a two-storey masonry building, built in 1920 in the same-named city (Figure 3.4a), province of L'Aquila, Abruzzo, Italy. Until 1974, the building housed a school. In the following years, the inner spaces were reorganized through the demolition of bearing walls and partition, ensuring a more functional distribution of the rooms to the city hall. The structure develops vertically with two floors above the ground and a non-habitable attic. Externally, the structure shows a certain regularity in the arrangement of the openings, which are evenly distributed along the walls and vertically aligned (Figure 3.4b). The building plan is composed of a main body of rectangular shape of length 36.75 m and width 11.9 m, with the longest side oriented in the EW direction. At the two extremities, two small projecting bodies give the C-shape. The interstorey height increases from 3.6 m at the ground level to 4.25 m at the first level. Three main bearing walls run along the whole length of the building and are crossed, in the front part, by three orthogonal secondary walls. The masonry piers are built with a cut local stone with courses of bricks – as revealed by the thermographic survey, Figure 3.5a – varying in thickness from 65 cm to 75 cm at the first level, from 30 cm to 65 cm at the second level and from 45 cm to 65 cm in the attic. The masonry shows good interlocking, good quality of mortar and firm transversal connection between wall facings.

The structural survey carried in situ by several university research groups – within the

(a)   (b)

Figure 3.4: (a) Orthophoto with reconstructed volumetry of the Pizzoli town hall building (from Google Earth) and (b) view of its front wall.

(a)   (b)
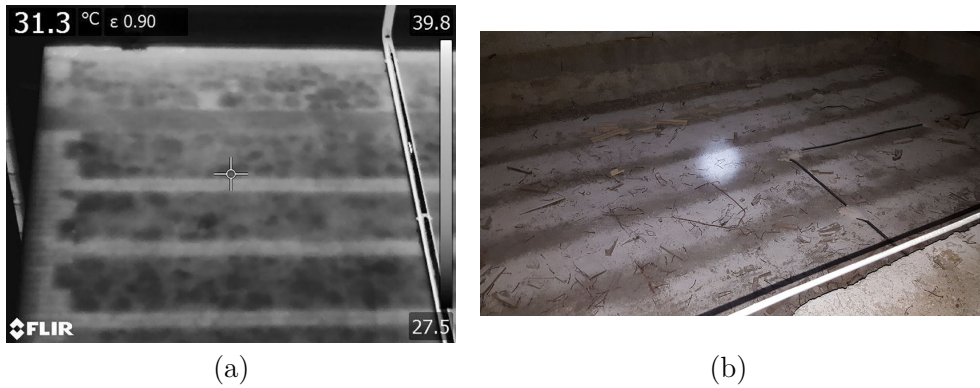
Figure 3.5: (a) Infra-red image highlighting the masonry typology, simple stone with brick courses. (b) Detail of the floor diaphragm at the top of the second level, showing the presence of iron beams drowned in the concrete slab.

ReLUIS Project 2017-2018, Task 4.1 (Cattari et al., 2019a) – together with the documentation provided by the Italian Department of Civil Protection provided, among the other, valuable information about the typology of the floor diaphragms (Figure 3.5b), which are composed of thin iron beams and hollow bricks capped by a concrete slab whose thickness is 16.5 cm and 12 cm at the first and the second level respectively. An equivalent frame model idealization of this structure will be employed, among other applications, to simulate the damaging of the structure to increasing-intensity seismic events, leading to the AV-based control chart of the building (Section 4.5.2).

Dynamic monitoring system and modal identification

The building is permanently monitored by the Italian Department of Civil Protection, within the national Structural Seismic Monitoring Network (OSS, Dolce et al., 2017a). In particular, the structural vibrations are measured by one mono-axial and three bi-axial accelerometers, placed at the top of each level of the building (Figure 3.6a). As reported in

Table 3.3: Frequency and description of the modes experimentally identified on the Pizzoli town hall building by employing the FDD technique.

Mode	Frequency (Hz)	Shape	Type
1	4.55	Translational along y	T_y
2	5.70	Torsional	R
3	6.55	Translational along x	T_x
4	9.05	Diaphragm bending	B
5	12.25	Diaphragm shear deformation	S
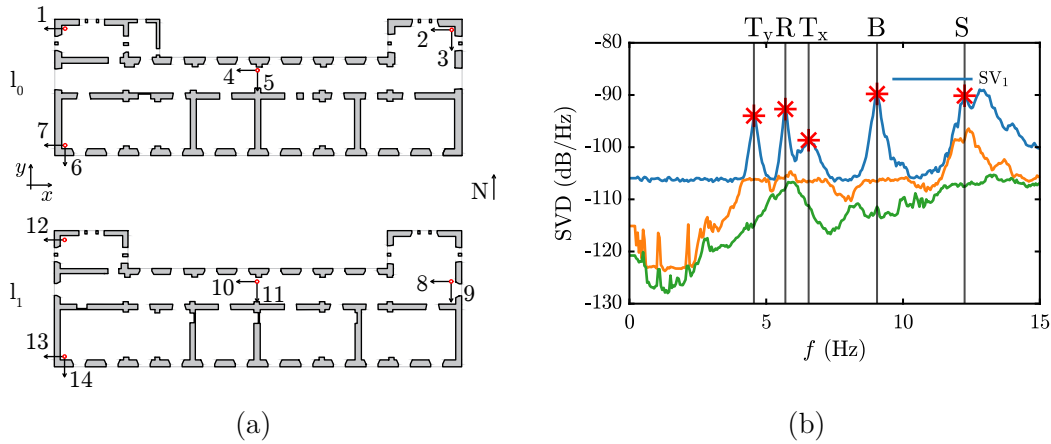
Figure 3.6: (a) Structural plan of the ground (l_0) and first floor (l_1) of the Pizzoli town hall building, highlighting the position of the sensors (at the top of each level). (b) Singular Value Decomposition (SVD) of the cross-spectral density matrix, highlighting the five identified modes in the frequency range 0-15 Hz.

Acunzo et al., 2018, the real-time monitoring system employs force-balance accelerometers, with high sensitivity and dynamic range, suitable for both strong-motion earthquake and low-intensity vibrations (with accelerations ranging from 10^{-4} to $2\,g$). The digitization is managed by a local unit through a 24 bit ADC converter, whereas channels synchronization is achieved by GPS receivers. The ambient vibration measurements employed in this thesis, as provided by OSS, have been acquired on the 1st of October 2016, after the first of the several seismic events that hit the structure in the following months (Spina et al., 2019). In this regard, the measurements are representative of a state of very slight damage – practically negligible – of the structure, which became more serious after the earthquake of January 2017 (Cattari et al., 2019a) as will be discussed in the following.

The ambient vibration data has been acquired with a sampling frequency of 250 Hz for one hour. The signals are decimated by a factor of 5 (Nyquist frequency of 25 Hz) and de-trended due to a linear increase of the mean value in some measurement channels. The natural frequencies and mode shapes of the building are experimentally identified employing the FDD technique, estimating the Welch periodograms with a frequency resolution of
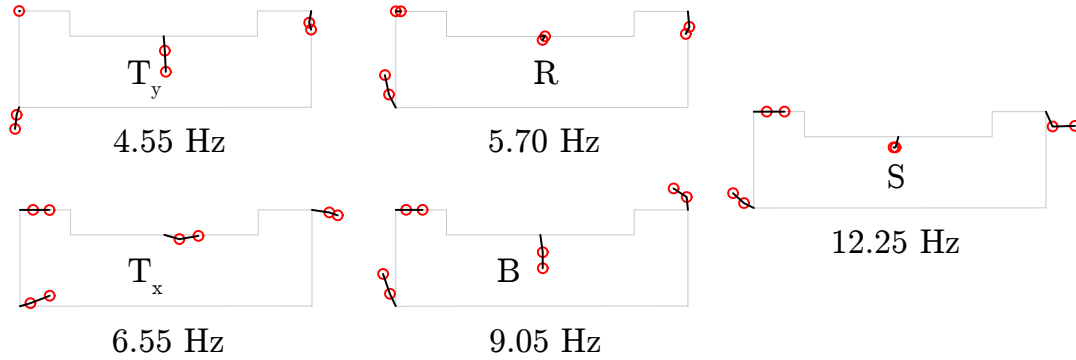
Figure 3.7: Graphical representation of the modes experimentally identified. The red circles represent the modal displacements measured at the two levels, whose magnitude linearly increases with height.

0.05 Hz.

Five modes are identified from the amplification peaks of the singular value plot in the range 0-15 Hz (Figure 3.6b). The results of the output-only identification employing FDD are synthetically reported in Table 3.3, whereas a simple representation of the mode shapes is reported in Figure 3.7. At the frequency of 4.55 Hz, the first identified mode involves the translation of the floors along the y direction (T_y), with modal displacements linearly increasing with the height of the building. The second identified mode at 5.7 Hz is a torsional mode (R), with the highest modal displacements located in the western part of the building. The third mode, identified at 6.55 Hz, clearly shows a translational behaviour of the floors, but along the x direction (T_x). The fourth identified mode at 9.05 Hz, as commonly found in elongated-plan buildings and later confirmed by the equivalent frame model of the structure, seems to involve the flexural bending of the floors in the horizontal plane (B). Finally, the fifth mode at 12.25 Hz is governed by the diaphragm in-plane shear behaviour (S). The results of modal identification from ambient vibrations, in particular the experimental frequencies of the rigid and shear-deformable modes, will be exploited for the structural identification of the in-plane shear stiffness of the floor diaphragms, later employed in model updating (Section 4.5.2).

Seismic response during the Central Italy earthquake sequence of 2016-2017

The Pizzoli town halls monitoring system was already operative in 2009, when a strong earthquake hit L'Aquila region. The building remained undamaged to the main shock and several aftershocks (Spina et al., 2011). Conversely, after the Central Italy earthquake sequence of 2016-2017 (Figure 3.8), the Pizzoli City Hall was declared closed for safety reasons. In particular, the building exhibited the effects of a global response without the activation of local mechanisms, producing slight levels of damage up to the event of 18 January 2017, in which the occurred damage – a mild cracking pattern concentrated in the masonry piers along the y direction – grow to a moderate level. The structural damage was surveyed in June 2017, from the outside of the structure on the perimeter walls and its inside, on the inner walls and floor diaphragms (Figure 3.10).

	Date and time UTC	PGA [g]	
		X	**Y**
Main shock	24/08/2016 01:36	0.082	**0.090**
	26/10/2016 17:10	**0.024**	0.023
	26/10/2016 19:18	0.022	**0.025**
	30/10/2016 06:40	**0.115**	0.111
	18/01/2017 10:14	**0.112**	0.100
Secondary event	25/07/2015 20:58	**0.000**	0.000
	21/06/2016 07:38	0.001	**0.001**
	07/09/2016 00:03	0.001	**0.001**
	03/11/2016 01:18	**0.001**	0.001
	28/11/2016 05:12	**0.001**	0.001
	19/02/2017 10:33	0.001	**0.001**
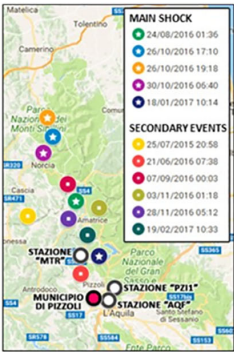
Figure 3.8: Main and secondary shocks recorded by the monitoring system of the Pizzoli town hall building during the Central Italy earthquake sequence of 2016-2017 (adapted from Cattari et al., 2019a). Values of the Peak Ground Acceleration (PGA) measured in the two main directions of the building.

(a)   (b)

Figure 3.9: (a) Superficial diagonal cracking of piers and (b) pseudo-vertical cracking at the interface with orthogonal walls, observed on the first floor of the Pizzoli town hall in June 2017.

The damage severity can be referred to as moderate, mainly located in the piers (Figure 3.9) and characterized by the presence of (i) at the ground level, both pseudo-horizontal cracks associated with a flexural mode and shear-failure diagonal cracks and (ii) at the first level, horizontal cracks at the top of extremities-piers and pseudo-vertical cracks in central piers. Some detachments and a general cracking pattern have been observed on the floor diaphragms, particularly at the top of the first floor (as reported in Figure 3.10). Further details regarding the observed and simulated damage on the Pizzoli town hall building can be found in Cattari et al., 2019a; Degli Abbati et al., 2021. The dynamic behaviour of the structure during the earthquake sequence, measured by the monitoring system and confirming the presence of moderate structural damage (Ceravolo et al., 2018; Spina et al., 2019; Miraglia et al., 2020), will be addressed in Section 4.5.2.

57

Figure 3.10: Pictures and schematic representation of the internal structural damage and external cracking pattern surveyed on the Pizzoli town hall building in June 2017, after the seismic sequence of earthquakes that hit Central Italy at the end of 2016.

Chapter 4

Methodological developments and applications

The thesis aims at the integration of ambient vibration measurements in seismic evaluations on existing buildings, with a twofold aim: firstly, addressing the analysis choices – related to the in-plane seismic behaviour of floor diaphragms – and, secondly, supporting the decisional processes on damaged buildings in the earthquake aftermath. With these purposes, the tools developed in this Chapter exploit experimental ambient vibration data to achieve the validation of modelling assumptions and the updating of structural models for the seismic assessment, employing state-of-the-art modal and structural identification techniques. In the wake of these developments, a procedure to develop the model-based frequency-damage control chart is finally proposed as an AV-support to decisional processes regarding the post-seismic safety of masonry buildings.

4.1   Overview

Several contributions of the literature support the employment of ambient vibration measurements to enhance the seismic analysis of buildings, highlighting their usefulness on multiple fronts of the research (Section 1.1). Among the others, the knowledge of experimental modal dynamics of structures is of crucial importance in the formulation, calibration and validation of mechanical models aimed at seismic predictions. This Chapter proposes some strategies to take advantage of operational modal data to improve the reliability of model-based seismic assessment.

In particular, as summarized in the next paragraphs, Section 4.2 and Section 4.3 state and solve direct and inverse problems regarding the in-plane behaviour of floor diaphragms, determining factor in the structural response of existing buildings to earthquakes (Section 1.2). The purpose is the validation of modelling hypotheses – such as the rigid diaphragm assumption – commonly adopted in seismic assessment procedures, as well as at the dynamic calibration of mechanical models, exploiting modal and structural identification techniques.

Starting from this knowledge, Section 4.4 proposes a general model-based methodology supporting the decisional processes on the structural performance of buildings damaged

by earthquakes, exploiting ambient measurements of their pre-seismic reference response for model calibration, of their post-seismic degraded response for damage assessment. The proposal will be particularized and exemplified in its application to masonry buildings. Finally, the experimental applications on laboratory prototypes and real buildings confirm, respectively, the validity and the relevance of the developed tools in the seismic assessment of existing buildings.

Modal identification of the in-plane behaviour of floor diaphragm

Within this framework, the thesis proposes a tool to validate the assumption of in-plane rigid behaviour of diaphragms using vibration data (Sivori et al., 2020b). A linear law suited to describe the displacement field of deformable diaphragms in the small displacement regime is briefly recalled (Section 4.2.1). The inverse kinematic problem to estimate in-plane rigid rotation and angular deformation from known vibration data is stated and solved, exploiting a perturbation approach in the case of problem under-determinacy due to minimum sensors availability. The assessment of the diaphragm rigid behaviour for the identifiable natural modes is then achieved qualitatively through a frequency domain representation of rotation and deformation (Section 4.3.1). The proposal is initially validated with simulations on a calibrated finite element model of a laboratory frame structure, taking into account the possible detrimental effects of unfavourable operational conditions, including position errors and misorientation of the sensors, measurement noise, desynchronization. More importantly, the reliability of the procedure is tested on an experimental ground using the vibration data acquired from a 2:3 scaled steel frame with steel-concrete slabs and eventually employed to investigate the diaphragms behaviour of a masonry building subjected to full-scale ambient vibration monitoring (Section 4.5).

Structural identification of the in-plane shear stiffness of floor diaphragm

Postulating the initial availability of synthetic spectral data resulting from modal experimental analyses (first-level modal identification problem), suited to identify and discriminate rigid-diaphragm modes from deformable ones (Section 4.3.1), the main objective of this contribution is to state and solve the inverse structural problem of identifying the diaphragm in-plane shear stiffness of existing buildings (second-level parametric or structural identification problem). Among the other possibilities, a low-dimension linear model of the diaphragm is formulated to describe the free undamped dynamics of the entire floor or one (or more) of its spans. An extra dynamically active degree-of-freedom is purposely introduced to account for the shear deformability of the diaphragm. The model mass and stiffness matrices are built analytically and the direct eigenproblem governing the modal properties is stated and solved (Section 4.2.2). The eigensolution is obtained in a suited analytic – although asymptotically approximate – fashion. In this respect, the multi-parameter perturbation technique employed can also be applied to larger dimension models, described by a generic number of mechanical parameters. The low-order approximate solution can be properly inverted to identify the unknown stiffness parameters (Section 4.3.2). Among the others, the parameter governing the in-plane shear stiffness of the diaphragm is derived analytically, as an explicit function only of the experimental frequencies of the rigid and deformability modes (Sivori et al., 2021b). This guarantees

the existence and uniqueness of a solution, within the class of mass and stiffness properties described by the low-dimension analytical model. Since the solution reliability, however, depends on how faithfully the analytical model can synthetically describe the real structure, the accuracy of the approximation and its range of validity are discussed. In this respect, the proposal is verified through pseudo-experimental data, numerically generated from the finite element model of a simple frame structure. Finally, the effectiveness of the procedure is tested experimentally, employing firstly experimental data from laboratory tests on scaled models and, lastly, vibration recordings from the full-scale monitoring of an existing masonry building (Section 4.5).

Pseudo-experimental identification of the fundamental frequency variations in masonry buildings induced by seismic damage

The proposal exploits the seismic-induced decay in fundamental frequencies of buildings deriving from structural damage, proposing a general model-based methodology relying on computational simulations aimed at damage assessment (Section 4.4.1). The general idea is to exploit ambient vibration data acquired in the pre-earthquake operational conditions, through vibration tests or thanks to a permanent monitoring system, to identify the reference modal parameters of the structure. This knowledge, obtained from output-only modal analysis (Section 2.2.1), can be employed to calibrate the elastic behaviour of a mechanical model, dynamically representative of the real structure. The employment of time-history analyses to predict the structural response to seismic inputs of increasing intensity – taking for granted the nonlinear capabilities of modern structural formulations, as well as the computational power today available – allows the simulation of different damage scenarios, forming a statistical base regarding the post-earthquake performance of the building (Section 4.4.2). The identification of the frequency decay induced by seismic damage – for example, simulating the post-seismic pseudo-experimental ambient response of the structure – allows building the *frequency-damage control chart* of the building, in which a measured variation of the fundamental frequencies is related, in a probabilistic form, to an expected level of global damage. The chart is conceived as an AV-based decisional tool, to quickly determine the performance and safety of structure after the seismic event without relying necessarily on in situ surveys. The evaluation of the global damage grade of the building is particularized in the case of masonry buildings through an equivalent frame model idealization (Section 4.4.3). Taking advantage of the tools developed for model validation and updating (respectively Sections 4.3.1 and 4.3.2), the methodology is finally applied to a monitored existing building, highlighting the agreement between frequency-assessed and occurred damage for the earthquakes that hit the structure in 2016 (Section 4.5).

4.2 Direct methods

4.2.1 Kinematic model of deformable floor diaphragm

During ambient vibration tests, the dynamic response of multi-storey buildings to an unknown environmental excitation usually satisfies the classic kinematic assumption of small amplitude displacements and displacement gradients. Within this framework, the issue

of experimentally determining whether the horizontal diaphragms of the building floors develop only rigid motion and remain undeformed in their plane (as usually assumed for modal identification purposes) can be formulated as a model-based identification problem. According to this standpoint, the identification process requires the statement of a direct problem based on a suited kinematic model, its mathematical inversion to treat the experimental measurements as known data and, finally, a proper discussion about the uniqueness of the inverse problem solution (Section 4.3.1).

If the *rigid body* assumption is adopted for a planar horizontal diaphragm, the small-amplitude (time-dependent) displacement vector $\mathbf{u} = (u, v)$ describing the in-plane motion of the diaphragm point at position $\mathbf{x}$ can be decomposed as $\mathbf{u}(\mathbf{x}) = \mathbf{u}_0 + \mathbf{u}_\theta$. Indeed, denoting $\mathbf{x}_0 = (x_0, y_0)$ the position of a suited reference point, the total displacement $\mathbf{u}(\mathbf{x})$ is the superposition of the displacement $\mathbf{u}_0 = \mathbf{u}(\mathbf{x}_0)$ and the extra displacement $\mathbf{u}_\theta = \mathbf{\Theta}\,\Delta\mathbf{x}$, linearly proportional to the position difference $\Delta\mathbf{x} = \mathbf{x} - \mathbf{x}_0$ through the skew-symmetric matrix $\mathbf{\Theta}$, depending on the rigid rotation θ. If the rigid body assumption is relaxed, the planar diaphragm is considered a *deformable body*, whose in-plane displacement field can be described – as first approximation – by the linear law

$$\mathbf{u}(\mathbf{x}) = \mathbf{u}_0 + \mathbf{G}\,\Delta\mathbf{x} \tag{4.1}$$

which actually admits (small) deformations of the diaphragm, but limits them to affine geometric transformations. Specifically, the deformable diaphragm can develop the rigid motions associated with the translation $\mathbf{u}_0$ and the rotation θ, which can be determined from the skew-symmetric part of the $\mathbf{G}$-matrix

$$\mathbf{\Theta} = \tfrac{1}{2}(\mathbf{G} - \mathbf{G}^\top) = \left[\begin{array}{cc} 0 & -\theta \\ \theta & 0 \end{array} \right] \tag{4.2}$$

but can also develop changes in shape and volume, properly described by the remaining symmetric part of the $\mathbf{G}$-matrix

$$\mathbf{E} = \tfrac{1}{2}(\mathbf{G} + \mathbf{G}^\top) = \left[\begin{array}{cc} E_{xx} & E_{xy} \\ E_{yx} & E_{yy} \end{array} \right] \tag{4.3}$$

where $E_{xy} = E_{yx}$ by construction. In analogy with the (infinitesimal) strain tensor in solid mechanics, the diagonal term E_{xx} and E_{yy} in the $\mathbf{E}$-matrix can be conventionally referred to as angular strains (or *normal strains*, adopting a common engineering-oriented notation). In particular, the nondimensional quantities E_{xx} or E_{yy} can be regarded as the ratios between the displacement difference $\Delta u = u - u_0$ and the undeformed (finite) length $|\Delta x|$, or between the displacement difference $\Delta v = v - v_0$ and the undeformed (finite) length $|\Delta y|$, respectively. Similarly, the quantity $\Gamma = 2E_{xy}$ can be conventionally referred to as *shear strain*, and can be regarded as the tangent of the angular loss of orthogonality between two perpendicular sides of the rectangular diaphragm portion with undeformed length $|\Delta x|$ and width $|\Delta y|$.

From the physical viewpoint, it is worth remarking that – although the hypothesis of small displacements does not exclude other deformed configurations – describing the displacement field of the deformable diaphragm through the linear law (4.1) is a simplifying assumption equivalent to admit all the possible (small amplitude) rigid motions, but also three independent deformation modes (Figure 4.1). In this respect, the normal and shear
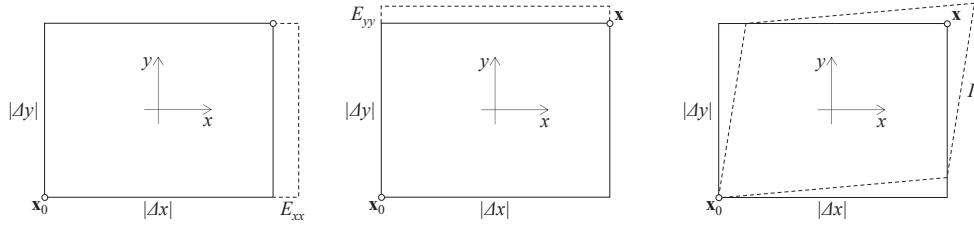
Figure 4.1: Deformation modes with amplitudes E_{xx},E_{yy} and Γ showing respectively the change in volume (modes I and II) and in shape (mode III).

strains play the role of modal amplitudes. Specifically, two deformation modes (modes I and II), with amplitudes E_{xx} or E_{yy}, describe the diaphragm change in volume, while the third mode (mode III), with amplitude Γ, describes the diaphragm change in shape.

4.2.2 Dynamic model of deformable floor diaphragm

In the mechanical formulation of analytical or computational models for building engineering, the generic building floor can be typically and efficiently described as a planar, horizontal and massive diaphragm connecting all the geometric vertices of the floor plan. From the structural viewpoint, the stiffness of the diaphragm in its own plane may strongly depend on many different technical aspects, including – among the others – the construction typology, the building materials and the efficiency of the connections among different resistant members (as discussed in NZSEE 2017 for timber floors and, more in general, in Solarino et al., 2019). Within this multifaceted scenario, introducing a priori the assumption of infinitely in-plane rigid diaphragms to reduce the computational effort of structural analyses can turn out to be an inaccurate simplification or, at least, an avoidable loss of generality.

To properly balance the opposite requirements of model synthesis and representativeness, the novel idea is to preserve a minimal description of the diaphragm deformability, without significantly increasing the complexity of the computational analyses. To this purpose, a single stationary displacement mode, kinematically compatible with a small deformation field, is admitted and superimposed to the rigid displacements of the diaphragm. To specify, the diaphragm is certainly allowed to move rigidly, as well as to develop small deformations according to an assigned geometric transformation of its initial configuration (referred to as *deformability mode* and assumed to preserve planarity). The amplitude of the deformability mode plays the role of an extra degree-of-freedom of the dynamic model, characterized by its own mass and stiffness. Even if – in principle – the deformability mode could be fixed arbitrarily, energetic criteria could be adopted to select – in practice – the transformation of the diaphragm configuration associated with the lowest possible elastic energy. It may be worth noting that, if necessary, more than one deformability mode could be taken into account.

For the purposes of the present work, a rectangular diaphragm with length $2A$, width $2B$ is considered (Figure 4.2a). The translational mass M and rotational inertia J are univocally determined by assuming uniform mass density for unit area. The planar rigid motion of the diaphragm is fully described by the in-plane time-dependent displacements
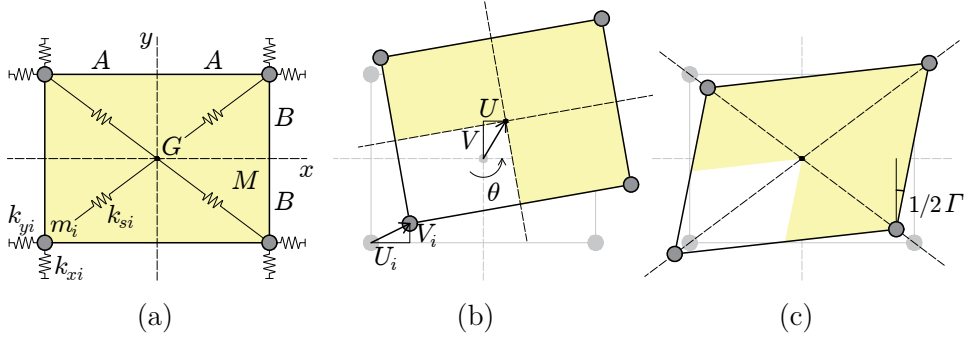
Figure 4.2: Deformable mass-spring model of the rectangular diaphragm: (a) reference configuration with geometric, inertial and elastic properties, (b) dynamic configuration generated by the rigid-body motions, (c) dynamic configuration generated by the *shear deformability mode*.

U and V and rotation θ of the configurational node (*central node G*), located at its centroid (Figure 4.2b). Among the other possibilities and on the basis of energetic considerations, the deformability mode selected to account for the diaphragm deformation is the *A shear mode* that transforms a rectangle into a parallelogram by stretching the rectangle diagonals (the transformation represented in Figure 4.2c). The angular defect of verticality assumed by the left and right sides of the rectangle, which can also be straightforwardly related to the loss of orthogonality between the rectangle sides, is chosen as modal amplitude. In analogy with the classic nomenclature of solid mechanics, it can also be conventionally referred to as *shear strain Γ*.

In order to accurately represent the mechanical behaviour of buildings, the diaphragm vertices must be considered configurational nodes (*peripheral nodes*) of the mechanical model. The masses and stiffnesses of these nodes may depend on a variety of technical aspects, starting from their connection degree with the structural members of the three-dimensional resistant structure of the building. For the purposes of the present work, it may be sufficient to consider four massive rotation-free peripheral nodes, located at the vertices of the rectangular diaphragm (Figure 4.2a) and provided with point mass m_i and linear elastic stiffnesses k_{xi} and k_{yi} along the rectangle sides ($i = 1, \ldots, 4$). The in-plane motion of the i-th node is fully described by the in-plane time-dependent displacements U_i and V_i.

According to the mechanical hypotheses, the forced dynamics of the deformable diaphragm is governed by a discrete elastic model, which can be considered linear as long as the displacement and modal amplitude are assumed sufficiently small. The model response can more conveniently be analysed by introducing nondimensional independent and dependent variables

$$\tau = \Omega_r t, \quad u = \frac{U}{L_r}, \quad v = \frac{V}{L_r}, \quad u_i = \frac{U_i}{L_r}, \quad v_i = \frac{V_i}{L_r} \tag{4.4}$$

where Ω_r and L_r are known frequency and length – for example, the first (circular) natural frequency of the rectangular diaphragm model and the length of its diagonal – suited to

serve as references for the time and space nondimensionalization, respectively. A minimal set $\boldsymbol{\mu}$ of nondimensional parameters sufficient to completely describe the structural properties of the dynamic model is

$$\beta = \frac{B}{A}, \quad \varrho_i^2 = \frac{m_i}{M}, \quad \chi^2 = \frac{J}{ML_r^2}, \quad \kappa_{xi} = \frac{k_{xi}}{M\Omega_r^2}, \quad \kappa_{yi} = \frac{k_{yi}}{M\Omega_r^2}, \quad \kappa_s = \frac{k_s}{M\Omega_r^2} \qquad (4.5)$$

where β is the *aspect ratio* of the rectangular diaphragm, ϱ_i^2 is the mass ratios between the mass attributed to the i-th peripheral node and the diaphragm mass, χ^2 is the rotational-to-translational mass of the diaphragm. Finally, the parameter κ_s synthetically accounts for the modal stiffness of the deformable diaphragm and can be interpreted as the equivalent nondimensional axial stiffness of a pair of identical diagonal bracings, elastically retaining the deformability mode.

Equations of motion

The linear equations of motions governing the forced dynamics of the mechanical model can be obtained by applying the Hamilton Principle for non-dissipative discrete systems excited by conservative external forces. Collecting the planar degrees-of-freedom of all the configuration nodes in the twelve-by-one column vector $\mathbf{u} = (u_1, v_1, u_2, v_2, u_3, v_3, u_4, v_4, u, v, \theta, \Gamma)$, the Hamilton action $\mathcal{H}$ can be expressed as

$$\mathcal{H} = \mathcal{K} - \mathcal{V} = \tfrac{1}{2}\dot{\mathbf{u}}^\top \mathbf{M}\dot{\mathbf{u}} - \left(\tfrac{1}{2}\mathbf{u}^\top \mathbf{K}\mathbf{u} - \mathbf{u}^\top \mathbf{b}\right) \qquad (4.6)$$

where $\mathcal{K}$ and $\mathcal{V}$ are the nondimensional kinetic and potential energies, respectively, depending on the symmetric twelve-by-twelve mass and stiffness matrices $\mathbf{M}$ and $\mathbf{K}$

$$\mathbf{M} = \begin{bmatrix} \mathbf{M}_{11} & \mathbf{M}_{12} & \mathbf{M}_{13} \\ \mathbf{M}_{21} & \mathbf{M}_{22} & \mathbf{M}_{23} \\ \mathbf{M}_{31} & \mathbf{M}_{32} & \mathbf{M}_{33} \end{bmatrix}, \qquad\qquad \mathbf{K} = \begin{bmatrix} \mathbf{K}_{11} & \mathbf{K}_{12} & \mathbf{K}_{13} \\ \mathbf{K}_{21} & \mathbf{K}_{22} & \mathbf{K}_{23} \\ \mathbf{K}_{31} & \mathbf{K}_{32} & \mathbf{K}_{33} \end{bmatrix} \qquad (4.7)$$

where the not-null mass submatrices are

$$\mathbf{M}_{11} = \begin{bmatrix} \varrho_1^2 & 0 & 0 & 0 \\ 0 & \varrho_1^2 & 0 & 0 \\ 0 & 0 & \varrho_2^2 & 0 \\ 0 & 0 & 0 & \varrho_2^2 \end{bmatrix}, \qquad \mathbf{M}_{22} = \begin{bmatrix} \varrho_3^2 & 0 & 0 & 0 \\ 0 & \varrho_3^2 & 0 & 0 \\ 0 & 0 & \varrho_4^2 & 0 \\ 0 & 0 & 0 & \varrho_4^2 \end{bmatrix},$$

$$\mathbf{M}_{33} = \begin{bmatrix} 1 & 0 & 0 & 0 \\ 0 & 1 & 0 & 0 \\ 0 & 0 & \chi^2 & 0 \\ 0 & 0 & 0 & \tfrac{1}{4}\beta^2\chi^2 \end{bmatrix} \qquad (4.8)$$

In particular, the term $\tfrac{1}{4}\beta^2\chi^2$ relates the shear deformation inertia to the rotational inertia χ^2 through the expression

$$J_\Gamma = \frac{1}{3}\frac{B^2}{A^2}M\left(A^2 + B^2\right) = \frac{1}{4}\frac{B^2}{A^2}J \qquad (4.9)$$

65

where M is the translational mass. The not-null stiffness submatrices are

$$\mathbf{K}_{11} = \begin{bmatrix} \frac{\kappa_s}{\beta^2+1} + \kappa_{x1} & \frac{\beta\kappa_s}{\beta^2+1} & 0 & 0 \\ \frac{\beta\kappa_s}{\beta^2+1} & \frac{\beta^2\kappa_s}{\beta^2+1} + \kappa_{y1} & 0 & 0 \\ 0 & 0 & \frac{\kappa_s}{\beta^2+1} + \kappa_{x2} & -\frac{\beta\kappa_s}{\beta^2+1} \\ 0 & 0 & -\frac{\beta\kappa_s}{\beta^2+1} & \frac{\beta^2\kappa_s}{\beta^2+1} + \kappa_{y2} \end{bmatrix},$$

$$\mathbf{K}_{12} = \begin{bmatrix} -\frac{\kappa_s}{\beta^2+1} & -\frac{\beta\kappa_s}{\beta^2+1} & 0 & 0 \\ -\frac{\beta\kappa_s}{\beta^2+1} & -\frac{\beta^2\kappa_s}{\beta^2+1} & 0 & 0 \\ 0 & 0 & -\frac{\kappa_s}{\beta^2+1} & \frac{\beta\kappa_s}{\beta^2+1} \\ 0 & 0 & \frac{\beta\kappa_s}{\beta^2+1} & -\frac{\beta^2\kappa_s}{\beta^2+1} \end{bmatrix}, \tag{4.10}$$

$$\mathbf{K}_{22} = \begin{bmatrix} \frac{\kappa_s}{\beta^2+1} + \kappa_{x3} & \frac{\beta\kappa_s}{\beta^2+1} & 0 & 0 \\ \frac{\beta\kappa_s}{\beta^2+1} & \frac{\beta^2\kappa_s}{\beta^2+1} + \kappa_{y3} & 0 & 0 \\ 0 & 0 & \frac{\kappa_s}{\beta^2+1} + \kappa_{x4} & -\frac{\beta\kappa_s}{\beta^2+1} \\ 0 & 0 & -\frac{\beta\kappa_s}{\beta^2+1} & \frac{\beta^2\kappa_s}{\beta^2+1} + \kappa_{y4} \end{bmatrix}$$

and, for the sake of symmetry, $\mathbf{K}_{21} = \mathbf{K}_{12}$. The twelve-by-one vector $\mathbf{b}$ collects column-wise the external forces acting on all the degrees-of-freedom.

Introducing a suited partition $\mathbf{u} = (\mathbf{q}, \mathbf{s})$ to distinguish the column subvector $\mathbf{q}$ collecting the free degrees-of-freedom (or Lagrangian coordinates) from the column subvector $\mathbf{s}$ collecting the slave degrees-of-freedom, the kinetic and potential energies can be expressed in partitioned form

$$\begin{aligned} \mathcal{K} &= \frac{1}{2} \begin{pmatrix} \dot{\mathbf{q}} \\ \dot{\mathbf{s}} \end{pmatrix}^\top \begin{bmatrix} \mathbf{M}_{qq} & \mathbf{M}_{qs} \\ \mathbf{M}_{sq} & \mathbf{M}_{ss} \end{bmatrix} \begin{pmatrix} \dot{\mathbf{q}} \\ \dot{\mathbf{s}} \end{pmatrix}, \\ \mathcal{V} &= \frac{1}{2} \begin{pmatrix} \mathbf{q} \\ \mathbf{s} \end{pmatrix}^\top \begin{bmatrix} \mathbf{K}_{qq} & \mathbf{K}_{qs} \\ \mathbf{K}_{sq} & \mathbf{K}_{ss} \end{bmatrix} \begin{pmatrix} \mathbf{q} \\ \mathbf{s} \end{pmatrix} - \begin{pmatrix} \mathbf{q} \\ \mathbf{s} \end{pmatrix}^\top \begin{pmatrix} \mathbf{b}_q \\ \mathbf{b}_s \end{pmatrix} \end{aligned} \tag{4.11}$$

where the relations $\mathbf{M}_{sq}^\top = \mathbf{M}_{qs}$ and $\mathbf{K}_{sq}^\top = \mathbf{K}_{qs}$ hold between the submatrices, for the sake of symmetry.

If the internal constraints between the slave and free degrees-of-freedom are linear holonomic, bilateral and time-independent, the constraining relations can conveniently be expressed in the matrix form $\mathbf{s} = \mathbf{V}\mathbf{q}$, where $\mathbf{V}$ is a rectangular constraint matrix. Consequently, the kinetic and potential energies of the constrained system can be expressed in the reduced space of the Lagrangian coordinates

$$\mathcal{K} = \tfrac{1}{2}\dot{\mathbf{q}}^\top \left(\mathbf{M}_{qq} + \mathbf{M}_{qs}\mathbf{V} + \mathbf{V}^\top\mathbf{M}_{sq} + \mathbf{V}^\top\mathbf{M}_{ss}\mathbf{V} \right) \dot{\mathbf{q}} \tag{4.12}$$

$$\mathcal{V} = \tfrac{1}{2}\mathbf{q}^\top \left(\mathbf{K}_{qq} + \mathbf{K}_{qs}\mathbf{V} + \mathbf{V}^\top\mathbf{K}_{sq} + \mathbf{V}^\top\mathbf{K}_{ss}\mathbf{V} \right) \mathbf{q} - \mathbf{q}^\top \left(\mathbf{b}_q + \mathbf{V}^\top\mathbf{b}_s \right) \tag{4.13}$$

and finally, imposing the action stationarity, the nondimensional equations of motion read

$$\mathbf{M}_q\ddot{\mathbf{q}} + \mathbf{K}_q\mathbf{q} = \mathbf{f} \tag{4.14}$$

where $\mathbf{M}_q = \mathbf{M}_{qq} + \mathbf{M}_{qs}\mathbf{V} + \mathbf{V}^\top \mathbf{M}_{sq} + \mathbf{V}^\top \mathbf{M}_{ss}\mathbf{V}$ and $\mathbf{K}_q = \mathbf{K}_{qq} + \mathbf{K}_{qs}\mathbf{V} + \mathbf{V}^\top \mathbf{K}_{sq} + \mathbf{V}^\top \mathbf{K}_{ss}\mathbf{V}$ are the symmetric mass and stiffness matrices of the constrained system, while $\mathbf{f} = \mathbf{b}_q + \mathbf{V}^\top \mathbf{b}_s$ is the column vector of the forces acting on the Lagrangian coordinates.

According to the motivations of the present work, two physical alternatives – following from the different definitions of the constraint matrix $\mathbf{V}$ – are analysed and discussed in the following. The first possibility consists in assuming the diaphragm extremely stiff in its own plane. Consequently, internal constraints of (ideally) perfect rigidity between the central node and the peripheral nodes can be imposed on the mechanical model. The corresponding twelve-by-three constraint matrix $\mathbf{V}_r$ is

$$\mathbf{V}_r = \begin{bmatrix} 1 & 0 & -\beta \\ 0 & 1 & 1 \\ 1 & 0 & -\beta \\ 0 & 1 & -1 \\ 1 & 0 & \beta \\ 0 & 1 & -1 \\ 1 & 0 & \beta \\ 0 & 1 & 1 \\ 0 & 0 & 0 \end{bmatrix} \tag{4.15}$$

The resulting constrained model, characterized by the three-by-one vector $\mathbf{q}_r = (u, v, \theta)$ of Lagrangian coordinates, can conventionally be referred to as *rigid model*. The three-by-three mass and stiffness matrices of the rigid model read

$$\mathbf{M}_r = \begin{bmatrix} 1 + \Sigma_\varrho^2 & 0 & -2\beta\Delta_{\varrho x}^2 \\ 0 & 1 + \Sigma_\varrho^2 & 2\Delta_{\varrho y}^2 \\ -2\beta\Delta_{\varrho x}^2 & 2\Delta_{\varrho y}^2 & \chi^2 + \Sigma_\theta^2 \end{bmatrix}, \qquad \mathbf{K}_r = \begin{bmatrix} \Sigma_{\kappa x} & 0 & -2\beta\Delta_{\kappa x} \\ 0 & \Sigma_{\kappa y} & 2\Delta_{\kappa y} \\ -2\beta\Delta_{\kappa x} & 2\Delta_{\kappa y} & \Sigma_{\kappa\theta} \end{bmatrix} \tag{4.16}$$

where the out-of-diagonal matrix terms account for the nondimensional mass and stiffness coupling between the translation and rotation $\mathbf{q}_r$-components.

The second possibility consists in assuming the diaphragm less stiff in its own plane so that the internal constraints of perfect rigidity between the central node and the peripheral nodes can be relaxed. Consequently, the shear-mode deformability is admitted in the mechanical model. The corresponding twelve-by-four constraint matrix $\mathbf{V}_d$ is

$$\mathbf{V}_d = \begin{bmatrix} 1 & 0 & -\beta & \frac{1}{2}\beta \\ 0 & 1 & 1 & \frac{1}{2}\beta^2 \\ 1 & 0 & -\beta & \frac{1}{2}\beta \\ 0 & 1 & -1 & -\frac{1}{2}\beta^2 \\ 1 & 0 & \beta & -\frac{1}{2}\beta \\ 0 & 1 & -1 & -\frac{1}{2}\beta^2 \\ 1 & 0 & \beta & -\frac{1}{2}\beta \\ 0 & 1 & 1 & \frac{1}{2}\beta^2 \end{bmatrix} \tag{4.17}$$

The resulting constrained model, characterized by the four-by-one vector $\mathbf{q}_d = (u, v, \theta, \Gamma)$ of Lagrangian coordinates, conventionally referred to as *deformable model*. The four-by-four mass and stiffness matrices of the deformable model read

$$\mathbf{M}_d = \begin{bmatrix} 1 + \Sigma_\varrho^2 & 0 & -2\beta\Delta_{\varrho x}^2 & \beta\Delta_{\varrho x}^2 \\ 0 & 1 + \Sigma_\varrho^2 & 2\Delta_{\varrho y}^2 & \beta^2\Delta_{\varrho y}^2 \\ -2\beta\Delta_{\varrho x}^2 & 2\Delta_{\varrho y}^2 & \chi^2 + \Sigma_\theta^2 & 0 \\ \beta\Delta_{\varrho x}^2 & \beta^2\Delta_{\varrho y}^2 & 0 & \frac{1}{4}\beta^2\left(\chi^2 + \Sigma_\theta^2\right) \end{bmatrix},$$

$$\mathbf{K}_d = \begin{bmatrix} \Sigma_{\kappa x} & 0 & -2\beta\Delta_{\kappa x} & \beta\Delta_{\kappa x} \\ 0 & \Sigma_{\kappa y} & 2\Delta_{\kappa y} & \beta^2\Delta_{\kappa y} \\ -2\beta\Delta_{kx} & 2\Delta_{\kappa y} & \Sigma_{\kappa\theta} & \beta^2\Delta_{\kappa xy} \\ \beta\Delta_{\kappa x} & \beta^2\Delta_{\kappa y} & \beta^2\Delta_{\kappa xy} & \beta_\Gamma\kappa_s + \Sigma_{\kappa\Gamma} \end{bmatrix}$$

(4.18)

where the out-of-diagonal matrix terms account for the nondimensional mass and stiffness coupling among the two translation, the rotation and the deformation $\mathbf{q}_r$-components. It may be worth remarking that the deformable model can be considered an extension of the rigid model, since the mass and stiffness matrices $\mathbf{M}_r$ and $\mathbf{M}_r$ can be recognized as submatrices of the matrices $\mathbf{M}_d$ and $\mathbf{M}_d$. The following auxiliary quantities have been introduced in the mass and stiffness matrices

$$\Sigma_\varrho^2 = \varrho_1^2 + \varrho_2^2 + \varrho_3^2 + \varrho_4^2, \qquad\qquad \Sigma_\theta^2 = (1 + \beta^2)\Sigma_\varrho^2, \qquad\qquad (4.19)$$
$$\Delta_{\varrho x}^2 = \tfrac{1}{2}(\varrho_1^2 + \varrho_2^2 - \varrho_3^2 - \varrho_4^2), \qquad\qquad \Delta_{\varrho y}^2 = \tfrac{1}{2}(\varrho_1^2 - \varrho_2^2 - \varrho_3^2 + \varrho_4^2),$$
$$\Sigma_{\kappa x} = \kappa_{x1} + \kappa_{x2} + \kappa_{x3} + \kappa_{x4}, \qquad\qquad \Sigma_{\kappa y} = \kappa_{y1} + \kappa_{y2} + \kappa_{y3} + \kappa_{y4},$$
$$\Delta_{\kappa x} = \tfrac{1}{2}(\kappa_{x1} + \kappa_{x2} - \kappa_{x3} - \kappa_{x4}), \qquad\qquad \Delta_{\kappa y} = \tfrac{1}{2}(\kappa_{y1} - \kappa_{y2} - \kappa_{y3} + \kappa_{y4}),$$
$$\Sigma_{\kappa\theta} = \Sigma_{\kappa y} + \beta^2\Sigma_{\kappa x}, \qquad\qquad \Sigma_{\kappa\Gamma} = \tfrac{1}{4}\beta^2\left(\Sigma_{\kappa x} + \beta^2\Sigma_{\kappa y}\right),$$
$$\beta_\Gamma = 2\beta^2(1 + \beta^2), \qquad\qquad \Delta_{\kappa xy} = \tfrac{1}{2}(\Sigma_{\kappa y} - \Sigma_{\kappa x})$$

where $(1 + \beta^2)$ can be recognized as the nondimensional semi-diagonal of the rectangular diaphragm.

Direct modal analysis

Denoting by Ω and $\omega = \Omega/\Omega_r$ the dimensional and nondimensional circular frequencies, the free dynamics of the diaphragm can be analysed by imposing a mono-harmonic solution $\mathbf{q} = \boldsymbol{\phi}\exp(\imath\omega\tau)$ in the homogeneous form of the equation of motion (4.14). Therefore, eliminating the ubiquitous time-dependence, a linear eigenproblem can be stated in the so-called *non-standard* form

$$\left(\mathbf{K}_q - \lambda\mathbf{M}_q\right)\boldsymbol{\phi} = \mathbf{0} \qquad\qquad (4.20)$$

where the eigensolutions are the real-valued eigenvalues $\lambda = \omega^2$ (or angular square frequencies) and the associated eigenvectors $\boldsymbol{\phi}$ (mode shapes or simply modes).

Depending on the model dimension n, the rigid and the deformable models of the diaphragm are characterized by $n = 3$ and $n = 4$ eigenpairs $(\lambda, \boldsymbol{\phi})$, respectively. The set of eigenvalues $\boldsymbol{\Lambda} = (\lambda_1, \ldots, \lambda_h, \ldots, \lambda_n)$, sorted in ascending order, constitutes the model spectrum. The matrix $\boldsymbol{\Phi} = [\boldsymbol{\phi}_1, \ldots, \boldsymbol{\phi}_h, \ldots, \boldsymbol{\phi}_n]$ collecting column-wise the associated modes is the modal matrix. Due to the low model dimension, a closed-form solution exists for all the eigenvalues $\lambda(\boldsymbol{\mu})$ of the spectrum $\boldsymbol{\Lambda}(\boldsymbol{\mu})$, and for all the eigenvectors $\boldsymbol{\phi}(\boldsymbol{\mu})$ of the matrix $\boldsymbol{\Phi}(\boldsymbol{\mu})$, as explicit – although non polynomial – function of the parameter vector $\boldsymbol{\mu}$.

From the qualitative viewpoint, if one of the eigencomponents dominates over the others, the eigenvector can be classified as *translation mode* (dominated by the components u and v), *rotation mode* (dominated by the component θ) and *shear mode* (dominated by the component Γ, only for the deformable model). Furthermore, particular parameter combinations can determine eigenvectors participated by two or more eigencomponents in a comparable manner, which can be referred to as *hybrid modes*. From the quantitative viewpoint, the assessment of the modal hybridization can be based on the energy-based asymptotically approximate definition of a modal localization factor (Lepidi & Gattulli, 2014).

4.3   Inverse methods

4.3.1   Modal identification of diaphragm rigid rotation and shear deformation

Data-driven identification of diaphragm deformation

Concerning the cinematic interpretation of the diaphragm motion (Section 4.2.1), the set of experimental vibration data – measured by two or more bi-axial sensors placed in different positions – can be employed to reconstruct its in-plane displacement field. Among the other possibilities, the reconstruction can be based on the tentative relationship

$$\mathbf{v}_j = \mathbf{v}_0 + \mathbf{H}\, \Delta \mathbf{x}_j \tag{4.21}$$

which states that the displacement $\mathbf{v}_j = (u_j, v_j)$ measured by the j-th sensor in the known position $\mathbf{x}_j$ linearly depends on the position difference $\Delta \mathbf{x}_j = \mathbf{x}_j - \mathbf{x}_0$ with respect to a reference sensor in the known position $\mathbf{x}_0$, measuring the displacement $\mathbf{v}_0$. As long as all the other variables are known or measured, the identification issue consists in determining the four independent $\mathbf{H}$-components H_{hk} (with $h, k = 1,2$). Equivalently, the physically meaning quantities

$$\theta = \tfrac{1}{2}\left(H_{21} - H_{12}\right), \quad \Gamma = H_{21} + H_{12}, \quad E_{xx} = H_{11}, \quad E_{yy} = H_{22} \tag{4.22}$$

can be determined, by recognizing the formal structural analogy between the linear equations (4.1) and (4.21). Therefore, introducing the 4-by-1 column vectors of unknowns $\mathbf{y} = (\theta, \Gamma, E_{xx}, E_{yy})$, the identification problem related to the j-th sensor can be stated in the linear algebraic form

$$\mathbf{A}_j \mathbf{y} = \mathbf{b}_j \tag{4.23}$$

where the 2-by-4 fully geometric matrix $\mathbf{A}_j$ and the 2-by-1 data vector $\mathbf{b}_j$ are

$$\mathbf{A}_j = \begin{bmatrix} -\Delta y_j & \tfrac{1}{2}\Delta y_j & \Delta x_j & 0 \\ \Delta x_j & \tfrac{1}{2}\Delta x_j & 0 & \Delta y_j \end{bmatrix}, \qquad \mathbf{b}_j = \begin{pmatrix} \Delta u_j \\ \Delta v_j \end{pmatrix} \tag{4.24}$$

where it is worth remarking that rank($\mathbf{A}_j$) = 2 in the general case corresponding to sensors *well-placement* (that is, if $\Delta y_j \neq 0$ and $\Delta x_j \neq 0$). *Well-placed* sensors will be considered in the following, assuming also $\Delta y_j > 0$ and $\Delta x_j > 0$ without loss of generality.

If vibration data from a generic number $N \geq 2$ of ideal (noise-free) biaxial sensors placed in different positions $\mathbf{x}_j$ are available, the identification problem can be stated in the linear algebraic form

$$\mathbf{A}\mathbf{y} = \mathbf{b} \tag{4.25}$$

which is equivalent to a linear regression problem, where the $2(N-1)$-by-4 matrix $\mathbf{A}$ has rank($\mathbf{A}_j$) ≤ 4 and the $2(N-1)$-by-1 vector $\mathbf{b}$ collect column-wise the submatrices $\mathbf{A}_j$ and subvectors $\mathbf{b}_j$, respectively.

Solving the linear equation (4.25) in the unknown vector $\mathbf{y}$ requires a discussion concerning the problem determinacy, depending on the amount of available data. First, it must be remarked that a mathematically valid solution that satisfies the equation (4.25) can always be found in the form

$$\mathbf{y} = \mathbf{A}^\dagger \, \mathbf{b} \tag{4.26}$$

where $\mathbf{A}^\dagger$ stands for the pseudo-inverse of the matrix $\mathbf{A}$. Three different situations corresponding to insufficient data ($N = 2$), sufficient data ($N = 3$) and redundant data ($N = 4$ or more) can be discussed as fundamental cases

- if vibration data from two sensors are available ($N = 2$), the linear identification problem is under-determined and the solution $\mathbf{y}$ is not unique. It can be demonstrated that the solution (4.26) returned by pseudoinverting the matrix $\mathbf{A}$ has minimum Euclidean norm $||\mathbf{y}||_2$ among all the others. Furthermore, since the governing matrix $\mathbf{A}$ is not full-ranked, the pseudoinverted matrix is $\mathbf{A}^\dagger = \mathbf{V}\mathbf{\Sigma}^\dagger\mathbf{U}^\top$, where $\mathbf{\Sigma}$ is the pseudoinvertible rectangular matrix satisfying the singular value decomposition $\mathbf{A} = \mathbf{U}\mathbf{\Sigma}\mathbf{V}^\top$. From the mechanical viewpoint, however, the minimum-norm solution is often discardable in favour of other solutions. Indeed, if no mathematical constraints are imposed on the relative smallness of the unknown variables, it tends to overestimate the strains with respect to the rigid rotation.

- if vibration data from three sensors are available ($N = 3$), the linear identification problem is determined and the solution $\mathbf{y}$ provided by the equation (4.26) is unique. As long as the governing matrix $\mathbf{A}$ is full-ranked, the pseudoinverted matrix is $\mathbf{A}^\dagger = \mathbf{A}^{-1}$. Of course, the problem determinacy does not allow to select a preferred set of unknown variables within an admissible set of solutions on the basis of mechanical considerations. Furthermore, the kinematic effects induced by unmodelled mechanisms of deformations cannot be recognized.

- if vibration data from four or more sensors are available ($N \geq 4$), the linear identification problem is over-determined and the solution $\mathbf{y}$ does not exist, in the general case. It can be demonstrated that the equation (4.26) returned by pseudoinverting the matrix $\mathbf{A}$ provides the least-squares solution $\mathbf{y}_*$ for the linear problem (4.25). As long as the governing matrix $\mathbf{A}$ is full-ranked, its pseudoinverse is $\mathbf{A}^\dagger = (\mathbf{A}^\top\mathbf{A})^{-1}\mathbf{A}^\top$ and the solution $\mathbf{y}_*$ is unique. Different solution criteria, other than the least-squares minimization of the Euclidean norm $||\mathbf{b}_*||_2$ of the residual vector $\mathbf{b}_* = \mathbf{b} - \mathbf{A}^\dagger\mathbf{y}_*$, can be determined based on mechanical considerations. Moreover, the residual vector $\mathbf{b}_*$ can be employed to quantify the importance of the unmodelled mechanisms of deformations.

It should be remarked that, in the general case, the unknowns θ and Γ (which involves the bending deformability of the edge beams) are expected to be dominant compared to the unknowns E_{xx}, E_{yy} (which involve the axial deformability of the edge beams). From the engineering viewpoint, it could be convenient to count on determined or over-determined solutions also in the typical operational case of minimal sensor availability ($N = 2$). To this purpose, perturbation methods can be employed, since these mathematical tools allow to introduce proper constraints of relative smallness among all the unknowns. According to a perturbation approach, a small auxiliary nondimensional parameter $\epsilon \ll 1$ can be introduced to conveniently order in ϵ-powers of smallness all the unknown variables

$$\theta = \epsilon\,\theta' + \epsilon^2\,\theta'', \qquad \Gamma = \epsilon^2\,\Gamma'', \qquad E_{xx} = \epsilon^3\,E_{xx}''', \qquad E_{yy} = \epsilon^3\,E_{yy}''' \qquad (4.27)$$

as well as all the known vibration data

$$\Delta u = \epsilon\,\Delta u' + \epsilon^2\,\Delta u'' + \epsilon^3\,\Delta u''', \qquad \Delta v = \epsilon\,\Delta v' + \epsilon^2\,\Delta v'' + \epsilon^3\,\Delta v''' \qquad (4.28)$$

71

where the unnecessary subscript j (for $N = 2$) is omitted for Δu and Δv, and the apices indicate the so-called (first, second, third) *sensitivities*. If all its sensitivities are determined, the ordered variable can be reconstructed and the auxiliary nondimensional parameter ϵ reabsorbed.

From the mechanical viewpoint, the variable ordering (4.27) accounts for the hypotheses that small (namely $\mathcal{O}(\epsilon)$) rigid rotations θ' can be associated with the dominant part $\Delta u'$, $\Delta v'$ of the small displacements. In parallel, the ordering introduces the complementary assumptions that very small (namely $\mathcal{O}(\epsilon^2)$) shear strains Γ'' can be associated with very small increments $\Delta u''$, $\Delta v''$ of the displacements. Finally, the ordering implies that extremely small (namely $\mathcal{O}(\epsilon^3)$) normal strains E'''_{xx}, E'''_{yy} can be associated with extremely small increments $\Delta u'''$, $\Delta v'''$ of the displacements. It is also understood that the relative positions Δx and Δy are one order of magnitude larger (namely $\mathcal{O}(1)$) than the rigid displacements. This mathematical assumption is largely acceptable if the two sensors are conveniently placed at two opposite corners of a rectangular diaphragm.

According to the proposed variable ordering, all the geometric terms of the matrix $\mathbf{A}$ turn out to be $\mathcal{O}(1)$. Therefore, the matrix $\mathbf{A}$ is not further orderable, while the two vectors $\mathbf{y}$ and $\mathbf{b}$ can be ordered in ϵ-powers

$$\mathbf{y} = \epsilon \mathbf{y}' + \epsilon^2 \, \mathbf{y}'' + \epsilon^3 \, \mathbf{y}''', \qquad \mathbf{b} = \epsilon \mathbf{b}' + \epsilon^2 \, \mathbf{b}'' + \epsilon^3 \, \mathbf{b}''' \tag{4.29}$$

where $\mathbf{y}' = (\theta', 0, 0, 0)$, $\mathbf{y}'' = (\theta'', \Gamma'', 0, 0)$, $\mathbf{y}''' = \left(0, 0, E'''_{xx}, E'''_{yy}\right)$, $\mathbf{b}' = (\Delta u', \Delta v')$, $\mathbf{b}'' = (\Delta u'', \Delta v'')$, $\mathbf{b}''' = (\Delta u''', \Delta v''')$. Therefore, substituting the ordering (4.29) in the equation (4.25), expanding and collecting terms of the same ϵ-power, an ordered hierarchy of algebraic equations yields

$$\epsilon^1 : \qquad\qquad \mathbf{A}\mathbf{y}' = \mathbf{b}' \tag{4.30}$$

$$\epsilon^2 : \qquad\qquad \mathbf{A}\mathbf{y}'' = \mathbf{b}'' \tag{4.31}$$

$$\epsilon^3 : \qquad\qquad \mathbf{A}\mathbf{y}''' = \mathbf{b}''' \tag{4.32}$$

where it is worth noting that the vector $\mathbf{b}$ is known from the available vibration measurements, but its contributions $\mathbf{b}'$, $\mathbf{b}''$, $\mathbf{b}'''$ are a priori unknown. However, the solution for all the unknowns can be obtained at each order by employing the following algorithmic strategy

i. the algebraic identification problem (4.30) governing the order ϵ^1 is overdetermined since two linear equations are available to assess only one unknown, given by the first sensitivity θ' of the rigid rotation. Therefore, the unknown vector $\mathbf{y}' = (\theta', 0, 0, 0)$ can be fully determined employing the known data vector $\mathbf{b}$ (since $\mathbf{b}'$ is unknown). Indeed, according to the least-squares criterion, the first sensitivity θ' of the rigid rotation reads

$$\theta' = \frac{\Delta v \Delta x - \Delta u \Delta y}{\Delta x^2 + \Delta y^2} \tag{4.33}$$

Therefore, the unknown displacement vector $\mathbf{b}'$ can be determined consistently with the least-squares solution $\mathbf{y}'$ as $\mathbf{b}' = \mathbf{A}\mathbf{y}'$. In the general case, a non-null second-order residual $\mathbf{b}'' = \mathbf{b} - \mathbf{b}'$ exists.

ii. the algebraic identification problem (4.31) governing the order ϵ^2 is determined since two equations are available to assess two unknowns, represented by the second sensitivities Γ'' and θ'' of the shear deformation and rigid rotation, respectively. Thus, inverting the equation to determine the unknown vector $\mathbf{y}'' = (\theta'', \Gamma'', 0, 0)$ from the known second-order residual $\mathbf{b}''$, the second-order sensitivities read

$$\theta'' = \frac{(\Delta y^2 - \Delta x^2)(\Delta u \Delta x + \Delta v \Delta y)}{2 \Delta x \Delta y \left(\Delta x^2 + \Delta y^2 \right)}, \qquad \Gamma'' = \frac{\Delta u}{\Delta y} + \frac{\Delta v}{\Delta x} \qquad (4.34)$$

It is to be noted that if the sensors are placed at two opposite corners of a square diaphragm ($|\Delta x| = |\Delta y|$), the second sensitivity θ'' is identically zero. Since the second-order solution is obtained from a determined linear problem, the third-order residual $\mathbf{b}''' = \mathbf{b} - \mathbf{b}' - \mathbf{b}''$ is certainly null.

iii. the algebraic identification problem (4.32) governing the order ϵ^3 is again determined since two equations are available to assess two unknowns, represented by the third sensitivities E'''_{xx} and E'''_{yy} of the two normal deformations. Thus, inverting the equation to determine the unknown vector $\mathbf{y}''' = (0, 0, E'''_{xx}, E'''_{yy})$ from the known second-order residual $\mathbf{b}'''$, the third-order sensitivities read

$$E'''_{xx} = 0, \qquad\qquad E'''_{yy} = 0 \qquad (4.35)$$

which is a plain mathematical result, since the third-order solution is obtained from a determined linear problem with null data ($\mathbf{b}''' = \mathbf{0}$).

Reconstructing the solution $\mathbf{y} = \epsilon \mathbf{y}' + \epsilon^2 \mathbf{y}'' + \epsilon^3 \mathbf{y}'''$ by summing all the sensitivities and then reabsorbing the auxiliary nondimensional parameter ϵ, the (unique) solution of the identification problem for the two-sensor case reads

$$\theta = \frac{1}{2} \left(\frac{\Delta v}{\Delta x} - \frac{\Delta u}{\Delta y} \right), \qquad \Gamma = \frac{\Delta u}{\Delta y} + \frac{\Delta v}{\Delta x}, \qquad E_{xx} = 0, \qquad E_{yy} = 0 \qquad (4.36)$$

which can also be verified to be one (but not the minimal one) of the infinite solutions satisfying the under-determined identification problem (4.25) related to two sensors. According to the assumed ordering for the unknown variables (4.27), the reconstructed solutions presented in the equation (4.36) actually state that $E_{xx} = \mathcal{O}(\epsilon^4), E_{yy} = \mathcal{O}(\epsilon^4)$ since the asymptotic analysis has been stopped at the third order of approximation. In this respect, it is worth noting that the analytical results *null normal deformations* and *normal deformations belonging to the fourth order* – although substantially equivalent from the engineering perspective – must be considered formally different from the mathematical viewpoint.

From the mechanical viewpoint, it may be worth remarking that the solution (4.36) can be somehow physically intuitive, but is not mathematically obvious. First, a different ordering of the variables – based on different engineering considerations – would result in a different analytical solution for the four unknowns. In this respect, alternative orderings could be suited for extra-deformable or extra-rigid diaphragms, for instance. Furthermore, the third-order solution (4.35) is a trivial result but not a tautology, since the normal strains E_{xx} and E_{yy} are not assumed null a priori. On the contrary, the normal strains

are found to identically vanish according to the perturbation-based solution of an algebraic problem that is mathematically consistent with the assumed variable ordering, stating only that the normal strains can be supposed smaller (by one order of magnitude) with respect to the rigid rotation and the shear strain.

Operational advice to validate the rigid diaphragms assumption from ambient vibration measurements

The engineering interpretation of the variables θ and Γ can be adopted to assess the in-plane rigidity or deformability for a rectangular-shaped diaphragm. Indeed, at least two measurement points of a generic planar displacement field are required to estimate the rigid rotation θ and the shear strain Γ. Similarly to what is commonly assumed for ambient response time histories, the time-dependent random variables $\theta(t)$ and $\Gamma(t)$ can be treated as wide-sense stationary random processes, described in the frequency domain by their Power Spectral Density (PSD, Section 2.2.1, Equation 2.10).

The rigid diaphragm assumption can be tested estimating the power spectral densities of θ and Γ processes and comparing rigid rotation and shear strain power spectral magnitudes, considering a small frequency band centred at the natural frequency of the identified natural modes. An ideal diaphragm behaving like a perfectly rigid body in its plane is expected to return exactly zero shear strain. This is unlikely to happen in the processing of vibration data from real experiments, for example as a result of measurement noise. However, due to the noise nature, no particular harmonic content in shear strain is expected. Deformability, instead, is expected to determine significant shear strain, quantitatively comparable with the rigid rotation in the limit case. Of course, high peaks in the spectrum of the shear strain – non-coincident to peaks of the other variables of motion – are expected to occur, corresponding to modes of pure deformability. Some operational issues that could disturb the identification of the rigid motion and shear deformation variables – such as sensors misalignment, measurement noise, desynchronization – are extensively discussed in Section 4.5.1 through numerical simulations. In particular, examples of the expected rigid rotation and shear strain spectra are provided for diaphragms of variable in-plane shear stiffness.

For what concerns an operational viewpoint, a few suggestions can be provided to overcome some practical issues in the execution of the vibration measurements. First, the deployment of the measurement network should be suitably designed to respect the criteria of minimum number, well-placement and same-orientation of sensors according to the hypotheses illustrated in the previous paragraphs. For what concerns their optimal location, some general suggestions can be provided. Considering a rectangular diaphragm, positioning the sensors at the opposing extremities of its diagonal is beneficial to the identification of both diaphragm rotations and shear strains. This precaution, in fact, prevents any singularity to appear in the derivative functions. In the case rotations, the amplitude of the measured displacements is expected to be higher the further away from the centre of rotation, which position – depending on the geometric and material properties of the walls causing stiffness asymmetries – can be evaluated a priori.

Second, the sensors should be properly placed to record the diaphragm motion, by fixing them preferably to the supporting walls (at the floor height) or the structural part of the floor. In the former case, the rigidity of the diaphragm – if experimentally verified – tends to also confirm the effectiveness of the wall-diaphragm connections. Otherwise, if

the estimation of the shear strain suggests the presence of a non-rigid diaphragm, additional sensors (for example, a third sensor placed in the diaphragm mid-span) could allow (i) avoiding phenomena of spatial aliasing from higher shear modes, for which the wavelength of the spatial deformation is expected to be shorter than the diaphragm diagonal length, and (ii) deepening the knowledge about possible diaphragm bending (Nakamura et al., 2017), which could still be relevant for the building seismic assessment. This choice, however, comes at the cost of a higher number of sensors employed and an increased effort in the design and setting of the measurements chain. Further experimental examples, addressing the testing of floor diaphragms in existing masonry buildings with a different number of sensors deployed, are reported in Appendix.

4.3.2 Structural identification of the diaphragm shear stiffness

Inverse modal analysis

Although undoubtedly valuable to carry out wide parametric analyses, the explicit functions $\mathbf{\Lambda}(\boldsymbol{\mu})$ and $\mathbf{\Phi}(\boldsymbol{\mu})$ presented in the forward modal problem (Section 4.2.2) are seldom employable in solving inverse spectral problems of parametric identification. Indeed, parametric identification typically consists in searching for an unknown parameter set $\boldsymbol{\mu}^*$ (output) describing a particular dynamic model characterized by a certain spectrum $\mathbf{\Lambda}^*$ and/or a certain modal matrix $\mathbf{\Phi}^*$, where all or part of the eigenvalues λ^* and eigenvectors $\boldsymbol{\phi}^*$ are known experimentally (input).

In this respect, it may be worth remarking that parametric identification is an advanced issue (second-level structural identification problem) that differs from modal identification. Specifically, parametric identification *starts from* the experimental knowledge of modal information, for instance as the outcome of ambient vibration tests and operational modal analyses (first-level modal identification problem). Assuming – for the sake of simplicity – that the experimental knowledge is limited to the spectrum $\mathbf{\Lambda}^*$, the exact analytical solution of the parametric identification problem would require the mathematical inversion of the function $\mathbf{\Lambda}(\boldsymbol{\mu})$, in order to solve the equation $\mathbf{\Lambda}(\boldsymbol{\mu}) = \mathbf{\Lambda}^*$. On the one hand, from the mathematical viewpoint, the frequent insufficiency or not-completeness of data tends to compromise the well-posedness of the problem, while the inherent nonlinearity of the governing equations does not guarantee the existence and uniqueness of the solution, in the general case. On the other hand, from the operative viewpoint, the non-polynomial nature of the functions $\mathbf{\Lambda}(\boldsymbol{\mu})$ and $\mathbf{\Phi}(\boldsymbol{\mu})$ reduces the possibility to achieve the analytical solution of the inverse eigenproblem, expressing the unknown $\boldsymbol{\mu}^*$ as an explicit function of the data $\mathbf{\Lambda}^*$.

Within this challenging scenario, it may be worth approaching the modal problem from a slightly different perspective. Specifically, building up uniformly valid and convergent series approximations of the eigenvalues and eigenvectors may allow a sufficiently accurate description of the exact spectrum $\mathbf{\Lambda}$ and modal matrix $\mathbf{\Phi}$, by virtue of polynomial functions of the parameters. Furthermore, low-order polynomial functions are more suitable to be analytically inverted. In general, a well-balanced equilibrium can be found between the competing requirements of (i) approximation accuracy in the direct modal problem, calling for high-order approximations, and (ii) availability of analytical solutions for the inverse identification problem, calling for low-order approximations. Multiparametric perturbation

methods are the proper mathematical tool to build up the necessary series approximations of the eigensolutions.

Multi-parameter perturbation method

Perturbation methods are asymptotic techniques that are widely used to perform eigensolution sensitivity analyses in a variety of scientific research fields, ranging from parametric design and spectral optimization to nonlinear modal identification, damping and damage detection, dynamic stability and bifurcation (Hajj et al., 2000; Kerschen et al., 2006; Lee et al., 2010; Lacarbonara et al., 2016; Lofrano et al., 2016; Lepidi & Bacigalupo, 2018). A general multiparametric perturbation technique for the eigensensitivity analysis of a discrete conservative dynamic system is presented in the following. Therefore, in the next paragraph, the technique is specifically applied to the deformable diaphragm model for the purpose of structural identification and model updating.

The preliminary requirement is that the structural matrices $\mathbf{K}_d(\mathbf{p})$ and $\mathbf{M}_d(\mathbf{p})$ governing the mechanical model are analytical functions of a finite set $\mathbf{p}$ of independent nondimensional parameters (which generally coincides with $\boldsymbol{\mu}$, but can also include suited combinations of the $\boldsymbol{\mu}$-components, if more convenient). In extreme synthesis, the methodological strategy consists in fixing a starting (known) set $\mathbf{p}^\circ$ of parameters, corresponding to an *unperturbed* (or *ideal*) mechanical model governed by the $\mathbf{p}^\circ$-dependent matrices $\mathbf{K}_d^\circ$ and $\mathbf{M}_d^\circ$ and characterized by a known spectrum $\boldsymbol{\Lambda}^\circ$ and known modal matrix $\boldsymbol{\Phi}^\circ$. The starting set $\mathbf{p}^\circ$ can be determined on the basis of an order of magnitude analysis or by solving an inverse spectral problem (Lepidi, 2013). Therefore, the generic *real* (non-ideal) mechanical models corresponding to the parameter set $\mathbf{p}$ is assumed as *perturbation* of the ideal mechanical model, originated by a small change in a generic direction $\mathbf{p}'$ of the parameter space (namely a *multi-parameter perturbation*). The smallness of the multi-parameter perturbation is regulated by a so-called *ordering* rule that – in the simplest case – can be introduced in the form

$$\mathbf{p} = \mathbf{p}^\circ + \epsilon \mathbf{p}' \tag{4.37}$$

where $\epsilon \ll 1$ is a small nondimensional parameter measuring the geometric distance between the ideal and the real mechanical models in the parameter space. Although not strictly necessary for pointing out the mathematical algorithm in the following, higher order perturbation schemes $\mathbf{p} = \mathbf{p}^\circ + \epsilon \mathbf{p}' + \epsilon^2 \mathbf{p}'' + \dots$ could be considered, without conceptual difficulties. Naturally, all and only the real mechanical models corresponding to the parameter set $\mathbf{p}$, encircled in a small-radius hypersphere of the parameter space centred at the starting set $\mathbf{p}^\circ$, can be described. Imposing the parameter ordering, the governing matrices $\mathbf{K}_d(\mathbf{p})$ and $\mathbf{M}_d(\mathbf{p})$ can be expanded in integer ϵ-power series

$$
\begin{aligned}
\mathbf{K}_d &= \mathbf{K}_d^\circ + \sum_n \epsilon^n \mathbf{K}_d^{(n)} = \mathbf{K}_d^\circ + \epsilon \mathbf{K}_d' + \epsilon^2 \mathbf{K}_d'' + \epsilon^3 \mathbf{K}_d''' + \epsilon^4 \mathbf{K}_d'''' + \dots \\
\mathbf{M}_d &= \mathbf{M}_d^\circ + \sum_n \epsilon^n \mathbf{M}_d^{(n)} = \mathbf{M}_d^\circ + \epsilon \mathbf{M}_d' + \epsilon^2 \mathbf{M}_d'' + \epsilon^3 \mathbf{M}_d''' + \epsilon^4 \mathbf{M}_d'''' + \dots
\end{aligned}
\tag{4.38}
$$

where the unperturbed matrices $\mathbf{K}_d^\circ$ and $\mathbf{M}_d^\circ$ tend to be sparse or even diagonal, if the set $\mathbf{p}^\circ$ is properly selected. The perturbation matrices $\mathbf{K}_d^{(n)}$ and $\mathbf{M}_d^{(n)}$ are symmetric at each ϵ-order and are known functions of the sets $\mathbf{p}^\circ$ and $\mathbf{p}'$ of mechanical parameters.

The symmetry of the stiffness and mass matrices $\mathbf{K}_d^\circ$ and $\mathbf{M}_d^\circ$ ensures that the spectrum $\mathbf{\Lambda}^\circ$ does not include defective eigenvalues. Therefore it is possible to postulate that the eigenvalues and eigenvectors can be expressed as integer ϵ-power series in the form

$$
\begin{aligned}
\lambda &= \lambda^\circ + \sum_n \epsilon^n \lambda^{(n)} = \lambda^\circ + \epsilon\lambda' + \epsilon^2\lambda'' + \epsilon^3\lambda''' + \epsilon^4\lambda'''' + \dots, \\
\boldsymbol{\phi} &= \boldsymbol{\phi}^\circ + \sum_n \epsilon^n \boldsymbol{\phi}^{(n)} = \boldsymbol{\phi}^\circ + \epsilon\boldsymbol{\phi}' + \epsilon^2\boldsymbol{\phi}'' + \epsilon^3\boldsymbol{\phi}''' + \epsilon^4\boldsymbol{\phi}'''' + \dots
\end{aligned}
\tag{4.39}
$$

where the coefficients $\lambda^{(n)}$ and $\boldsymbol{\phi}^{(n)}$ represent the n-th *sensitivities* of the eigenvalues and eigenvectors, respectively. The n-th sensitivities of the eigenvalues and eigenvectors are collected in the vector $\mathbf{\Lambda}^{(n)}$ and matrix $\mathbf{\Phi}^{(n)}$, which can also be referred to as *eigensensitivities*. According to the multi-parameter perturbation method, the eigensensitivities are the *unknowns* of the modal problem.

Imposing both the series expansions (4.38) of the data (governing matrices $\mathbf{K}_d^\circ$ and $\mathbf{M}_d^\circ$ and their perturbations) and the series expansions (4.39) of the unknowns (eigenvalues and eigenvectors *sensitivities*) in the eigenvalue problem, expanding and collecting terms of the same ϵ-power, an ϵ-ordered cascade of *perturbation equations* can be formulated

$$
\epsilon^0 : \left(\mathbf{K}_d^\circ - \lambda^\circ \mathbf{M}_d^\circ\right)\boldsymbol{\phi}^\circ = \mathbf{0}
\tag{4.40}
$$
$$
\epsilon^1 : \left(\mathbf{K}_d^\circ - \lambda^\circ \mathbf{M}_d^\circ\right)\boldsymbol{\phi}' = -\left(\mathbf{K}_d' - \lambda^\circ \mathbf{M}_d' - \lambda' \mathbf{M}_d^\circ\right)\boldsymbol{\phi}^\circ
$$
$$
\epsilon^2 : \left(\mathbf{K}_d^\circ - \lambda^\circ \mathbf{M}_d^\circ\right)\boldsymbol{\phi}'' = -\left(\mathbf{K}_d'' - \lambda^\circ \mathbf{M}_d'' - \lambda' \mathbf{M}_d' - \lambda'' \mathbf{M}_d^\circ\right)\boldsymbol{\phi}^\circ - \left(\mathbf{K}_d' - \lambda^\circ \mathbf{M}_d' - \lambda' \mathbf{M}_d^\circ\right)\boldsymbol{\phi}'
$$
$$
\dots : \dots
$$
$$
\epsilon^n : \left(\mathbf{K}_d^\circ - \lambda^\circ \mathbf{M}_d^\circ\right)\boldsymbol{\phi}^{(n)} = -\left(\mathbf{K}_d^{(n)} - \sum_{j=0}^n \lambda^{(j)}\mathbf{M}_d^{(n-j)}\right)\boldsymbol{\phi}^\circ - \sum_{k=1}^{n-1}\left[\left(\mathbf{K}_d^{(k)} - \sum_{j=0}^k \lambda^{(j)}\mathbf{M}_d^{(k-j)}\right)\boldsymbol{\phi}^{(n-k)}\right]
$$

where the equation at the ϵ^0-order can be recognized to govern the eigenproblem of the ideal mechanical model. The corresponding *generating* eigensolution is known by hypothesis and is composed of the generating eigenvalues λ_h° of the spectrum $\mathbf{\Lambda}^\circ$ and the associated generating eigenvectors $\boldsymbol{\phi}_h^\circ$ of the modal matrix $\mathbf{\Phi}^\circ$ (with $h = 1, \dots, n$). All the generating eigenvalues λ_h° are supposed to be simple (characterized by unitary algebraic multiplicity) and well separated (that is, the difference between any two eigenvalues is supposed to be at least one order of magnitude greater than ϵ).

The key assumption of simplicity and well-separation of the n-th generating eigenvalue determined at the lowest order (namely ϵ^0-order) ensures that each higher order (namely ϵ^n-order with $n \geq 1$) of the perturbation equations allows determining the n-th sensitivity $\lambda_h^{(n)}$ of the h-th eigenvalue and the n-th sensitivity $\boldsymbol{\phi}_h^{(n)}$ of the h-th eigenvector. Specifically, the n-th eigenvalue sensitivity $\lambda_h^{(n)}$ is determined by imposing the solvability condition of the ϵ^n-order Equation (4.40d), yielding

$$
\lambda_h^{(n)} = \alpha_h^\circ \boldsymbol{\phi}_h^{\circ\top}\left(\mathbf{K}_d^{(n)} - \sum_{j=0}^{n-1} \lambda_h^{(j)}\mathbf{M}_d^{(n-j)}\right)\boldsymbol{\phi}_h^\circ + \alpha_h^\circ \sum_{k=1}^{n-1}\left[\boldsymbol{\phi}_h^{\circ\top}\left(\mathbf{K}_d^{(k)} - \sum_{j=0}^k \lambda_h^{(j)}\mathbf{M}_d^{(k-j)}\right)\boldsymbol{\phi}_h^{(n-k)}\right]
\tag{4.41}
$$

where $\alpha^\circ = (\boldsymbol{\phi}^{\circ\top}\mathbf{M}_d^\circ \boldsymbol{\phi}^\circ)^{-1}$. From the technical viewpoint, the solvability has been imposed by requiring the orthogonality between the right-hand term of Equation (4.40d) and the

solution $\boldsymbol{\psi}_h$ of the auxiliary homogeneous problem $(\mathbf{K}_d^\circ - \lambda^\circ \mathbf{M}_d^\circ)^\top \boldsymbol{\psi} = \mathbf{0}$, according to the Fredholm Alternative for discrete linear systems. Furthermore, the identity $\boldsymbol{\psi}_h = \boldsymbol{\phi}_h^\circ$ has been employed, as long as the symmetry of the matrices $\mathbf{K}_d^\circ$ and $\mathbf{M}_d^\circ$ holds. Once the n-th eigenvalue sensitivity $\lambda_h^{(n)}$ is known, the n-th eigenvector sensitivity $\boldsymbol{\phi}_h^{(n)}$ is univocally determined

$$\boldsymbol{\phi}_h^{(n)} = -\mathbf{A}_h^\circ \left[\mathbf{A}_h^{\circ\top} \left(\mathbf{K}_d^\circ - \lambda_h^\circ \mathbf{M}_d^\circ \right) \mathbf{A}_h^\circ \right]^{-1} \sum_{k=1}^{n} \left[\mathbf{A}_h^{\circ\top} \left(\mathbf{K}_d^{(k)} - \sum_{j=0}^{k} \lambda_h^{(j)} \mathbf{M}_d^{(k-j)} \right) \boldsymbol{\phi}_h^{(n-k)} \right] \quad (4.42)$$

where the rectangular matrix $\mathbf{A}_h^\circ = [\boldsymbol{\phi}_1^\circ, \ldots, \boldsymbol{\phi}_{i \neq h}^\circ, \ldots, \boldsymbol{\phi}_N^\circ]$ is obtained by removing the h-th eigenvector from the modal matrix $\boldsymbol{\Phi}^\circ$. From the technical viewpoint, the n-th sensitivity of the h-th eigenvector has been expressed as a linear combination of all the i-th eigenvectors $\boldsymbol{\phi}_i^\circ$ (with $i \neq h$), with small (n-th order) combination coefficients (Lepidi, 2013).

From the mathematical viewpoint, determining the n-th sensitivities $\lambda_h^{(n)}$ and $\boldsymbol{\phi}_h^{(n)}$ allows the analytical assessment of all the coefficients of the power series (4.39) and, therefore, the asymptotic reconstruction of the eigenvalue and eigenvector up to the desired approximation order. The reconstruction procedure implies the complete reabsorption of the ϵ-parameter. From the mechanical viewpoint, Equations (4.41) and (4.42) allow to obtain closed-form expressions of the frequencies and modes of a discrete system as analytical – although asymptotically approximate – functions of the parameters. As a major remark, the multi-parameter perturbation method and the analytical formulas (4.41) and (4.42) are completely general, since they hold for any mechanical non-dissipative linear discrete system possessing a generic number of degrees-of-freedom and described by a generic number of parameters. It may be worth recalling that – coherently with the nature of perturbation techniques – the accuracy of the eigensolution approximations depends on the maximum order of the series, while its mathematical consistency holds within the limits of the parameter smallness assumptions and within the convergence radius of the power series.

Finally, it is worth to briefly address the advantages and potential drawbacks of the proposed perturbation approach in the field of model updating. If compared, for example, to the well-studied sensitivity method in finite element model updating (Jaishi & Ren, 2005; Reynders et al., 2010; Mottershead et al., 2011), the leading concept is quite similar. The linearization of the problem – being it an eigenvalue or an optimization problem – is exploited to formulate more simple and manageable inverse relationships. In this respect, the perturbative derivation has the benefit to identify a solution in a proper analytical form, within the space of the low-dimensional mass and stiffness matrices of the direct model. Indeed, the few parameters describing the model can be identified without recurring to numerical optimization schemes. On the downside, the flexibility of the approach relies on the possibility to describe the actual structural behaviour through a low-fidelity model, as discussed in the following with respect to the experimental applications.

Parameter identification and model updating

To the purpose of the parameter identification problem, the multi-parameter perturbation method allows determining the parametric relations $\boldsymbol{\Lambda}(\boldsymbol{\mu})$ and $\boldsymbol{\Phi}(\boldsymbol{\mu})$ (or equivalently $\boldsymbol{\Lambda}(\mathbf{p})$ and $\boldsymbol{\Phi}(\mathbf{p})$), required to state the inverse spectral problem. It is important to highlight that

– according to the multi-parameter perturbation method – the power series approximations of the eigenvalues and eigenvectors are polynomial functions of the ϵ-parameter regulating the amplitude of the multi-parameter perturbation $\mathbf{p}'$, whereas they remain non-polynomial functions of each $\mathbf{p}'$-component, in the general case. Therefore, the invertibility of the spectral problem must be discussed at each order of approximation.

In order to specify the multi-parameter perturbation method for the deformable model of the planar diaphragm, it is first necessary to select and order the parameter set $\mathbf{p}$. Its selection is a key technical point, because the perturbation-based inversion of the modal problem – if mathematically feasible – does not allow to identify unknown parameters other than those included in the set $\mathbf{p}$. For the deformable model, a suited set of independent parameters is $\mathbf{p} = (\beta, \chi^2, \kappa_s, \Sigma_\varrho^2, \Sigma_{\kappa x}, \Sigma_{\kappa y}, \Delta_{\varrho x}^2, \Delta_{\varrho y}^2, \Delta_{\kappa x}, \Delta_{\kappa y})$, sufficient to completely and univocally assess the mass and stiffness matrices (4.18). Relying on engineering considerations, a proper ϵ-power ordering of the $\mathbf{p}$-components is

$$\beta = \beta_0, \qquad \chi^2 = \chi_0^2 + \epsilon\chi_1^2, \qquad \Sigma_\varrho^2 = \Sigma_{\varrho 0}^2, \qquad \Delta_{\varrho x}^2 = \epsilon\Delta_{\varrho x 1}^2, \qquad \Delta_{\varrho y}^2 = \epsilon\Delta_{\varrho y 1}^2, \quad (4.43)$$
$$\kappa_s = \kappa_{s0} + \epsilon\kappa_{s1}, \qquad \Sigma_{\kappa x} = \Sigma_{\kappa x0}, \qquad \Sigma_{\kappa y} = \Sigma_{\kappa y0}, \qquad \Delta_{\kappa x} = \epsilon\Delta_{\kappa x1}, \qquad \Delta_{\kappa y} = \epsilon\Delta_{\kappa y1}$$

where the subscript indicates the ϵ-order of the parameter perturbation. Thus, it is consistent to assume the dependent parameter $\Delta_{\kappa xy}$ to be ordered as $\Delta_{\kappa xy} = \epsilon\Delta_{\kappa xy1}$. After substituting the parameter ordering (4.43) in the mass and stiffness matrices $\mathbf{M}_d$ and $\mathbf{K}_d$ reported in Equation (4.18), expanding and collecting terms of the same ϵ-power, the matrix expansions (4.38) can be specified for the deformable diaphragm. The unperturbed matrices $\mathbf{M}_d^\circ$ and $\mathbf{K}_d^\circ$ (depending on the zeroth-order parameters only) and the first perturbation matrices $\mathbf{M}_d'$ and $\mathbf{K}_d'$ are

$$\mathbf{M}_d^\circ = \begin{bmatrix} 1 + \Sigma_\varrho^2 & 0 & 0 & 0 \\ 0 & 1 + \Sigma_\varrho^2 & 0 & 0 \\ 0 & 0 & \chi_0^2 + \Sigma_\theta^2 & 0 \\ 0 & 0 & 0 & \frac{1}{4}\beta^2\left(\chi_0^2 + \Sigma_\theta^2\right) \end{bmatrix}, \qquad (4.44)$$

$$\mathbf{K}_d^\circ = \begin{bmatrix} \Sigma_{\kappa x} & 0 & 0 & 0 \\ 0 & \Sigma_{\kappa y} & 0 & 0 \\ 0 & 0 & \Sigma_{\kappa\theta} & 0 \\ 0 & 0 & 0 & \beta_\Gamma\kappa_{s0} + \Sigma_{\kappa\Gamma} \end{bmatrix}$$

$$\mathbf{M}_d' = \begin{bmatrix} 0 & 0 & -2\beta\Delta_{\varrho x1}^2 & \beta\Delta_{\varrho x1}^2 \\ 0 & 0 & 2\Delta_{\varrho y1}^2 & \beta^2\Delta_{\varrho y1}^2 \\ -2\beta\Delta_{\varrho x1}^2 & 2\Delta_{\varrho y1}^2 & \chi_1^2 & 0 \\ \beta\Delta_{\varrho x1}^2 & \beta^2\Delta_{\varrho y1}^2 & 0 & \frac{1}{4}\beta^2\chi_1^2 \end{bmatrix},$$

$$\mathbf{K}_d' = \begin{bmatrix} 0 & 0 & -2\beta\Delta_{\kappa x1} & \beta\Delta_{\kappa x1} \\ 0 & 0 & 2\Delta_{\kappa y1} & \beta^2\Delta_{\kappa y1} \\ -2\beta\Delta_{\kappa x1} & 2\Delta_{\kappa y1} & 0 & -\beta^2\Delta_{\kappa xy1} \\ \beta\Delta_{\kappa x1} & \beta^2\Delta_{\kappa y1} & -\beta^2\Delta_{\kappa xy1} & \beta_\Gamma\kappa_{s1} \end{bmatrix}$$

From the physical viewpoint, the matrices $\mathbf{M}_d^\circ$ and $\mathbf{K}_d^\circ$ collect the dominant contributions to the model mass and stiffness, whereas the perturbation matrices $\mathbf{M}_d'$ and $\mathbf{K}_d'$ collect

minor or minimal contributions to the model mass and stiffness, consistently with the perturbation approach.

Some brief remarks can be pointed out to specify the technical range of structural samples satisfying the particular order assignment (4.43). First, square and rectangular diaphragms are considered (namely, from the mathematical viewpoint, rectangles with aspect ratio $\beta = \mathcal{O}(1)$). Second, diaphragms with non-negligible rotational inertia are taken into account (rotational-to-translational mass ratio $\chi^2 = \mathcal{O}(1)$). Third, non-rigid but stiff diaphragms are assumed (shear stiffness $\kappa_s = \mathcal{O}(1)$). Finally, mass and stiffness eccentricities are certainly admitted, as long as they are not dominant (mass differences $\Delta_{\varrho x}^2 = \mathcal{O}(\epsilon)$, $\Delta_{\varrho y}^2 = \mathcal{O}(\epsilon)$ and stiffness differences $\Delta_{\kappa x} = \mathcal{O}(\epsilon)$, $\Delta_{\kappa y} = \mathcal{O}(\epsilon)$). It is worth remarking that different parameter orderings can equally be introduced, if necessary to describe other structural cases falling out of this parameter range (for instance, highly elongated rectangular diaphragms).

Following the general strategy outlined for the multi-parameter perturbation method, the zeroth-order analytical approximation of the model spectrum $\mathbf{\Lambda}^{\circ} = (\lambda_1^{\circ}, \lambda_2^{\circ}, \lambda_3^{\circ}, \lambda_4^{\circ})$ can be univocally determined. Specifically, the four generating eigenvalues and the corresponding eigenvectors are

$$\lambda_1^{\circ} = \frac{\Sigma_{\kappa x}}{1 + \Sigma_{\varrho}^2}, \qquad\qquad \boldsymbol{\phi}_1^{\circ} = (1,0,0,0) \qquad (4.45)$$

$$\lambda_2^{\circ} = \frac{\Sigma_{\kappa y}}{1 + \Sigma_{\varrho}^2}, \qquad\qquad \boldsymbol{\phi}_2^{\circ} = (0,1,0,0)$$

$$\lambda_3^{\circ} = \frac{\Sigma_{\kappa\theta}}{\chi_0^2 + \Sigma_{\theta}^2}, \qquad\qquad \boldsymbol{\phi}_3^{\circ} = (0,0,1,0)$$

$$\lambda_4^{\circ} = \frac{4(\beta_\Gamma \kappa_{s0} + \Sigma_{\kappa\Gamma})}{\beta^2 \left(\chi_0^2 + \Sigma_{\theta}^2\right)}, \qquad\qquad \boldsymbol{\phi}_4^{\circ} = (0,0,0,1)$$

where all the eigenvectors can be recognized to be canonical vectors with unitary-amplitude, meaning that zeroth order modes of the deformable system are perfectly localized on one or the other degrees-of-freedom. The first eigenvalue sensitivities are

$$\lambda_1' = 0 \qquad\qquad\qquad\qquad\qquad\qquad\qquad (4.46)$$

$$\lambda_2' = 0$$

$$\lambda_3' = -\frac{\chi_1^2 \Sigma_{\kappa\theta}}{\left(\chi_0^2 + \Sigma_{\theta}^2\right)^2}$$

$$\lambda_4' = \frac{4\beta_\Gamma \kappa_{s1} \left(\chi_0^2 + \Sigma_{\theta}^2\right) - 4\beta_\Gamma \kappa_{s0}\chi_1^2 - 4\Sigma_{\kappa\Gamma}\chi_1^2}{\beta^2 \left(\chi_0^2 + \Sigma_{\theta}^2\right)^2}$$

Higher (second, third) sensitivities could be determined up to the desired approximation order. It may be worth remarking that the lowest order significant perturbation of the eigenvalues λ_1 and λ_2 is given by the second sensitivities λ_1'' and λ_2'', because the first sensitivities λ_1' and λ_2' are identically null.

The accuracy of the power-series approximation (4.39), reconstructed up to the second order by employing the generating eigenvalues (4.45) and the sensitivities (4.46), must be discussed from a direct comparison with the exact eigenvalues. Particularly, the qualitative
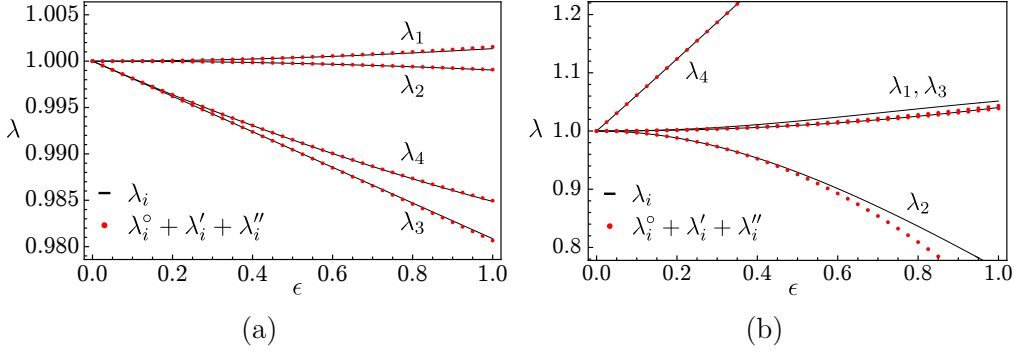
Figure 4.3: Comparison between the exact and approximate eigenvalue loci (normalized with respect to the unperturbed eigenvalue) versus ϵ-proportional perturbations of (a) the mass matrix, (b) the stiffness matrix of the deformable diaphragm (parameters $\beta = 2/3, \chi^2 = 1/4, \kappa_s = 1/3, \Sigma_\varrho^2 = 9, \Sigma_{\kappa x} = 2, \Sigma_{\kappa y} = 1, \Delta_{\varrho x}^2 = 1/4, \Delta_{\varrho y}^2 = 1/9, \Delta_{\kappa x} = 1/4, \Delta_{\kappa y} = 1/5$).

and quantitative agreement between the approximate and exact eigenvalues under variation of the perturbation parameter ϵ can be appreciated in Figure 4.3 for two different multiparameter perturbations. The multiparameter perturbations are purposely selected to introduce small (ϵ-proportional) variations of the mass and stiffness matrices, respectively. The approximate solution appears quite accurate with respect to mass perturbations (Figure 4.3a), since it closely matches the exact solution. Remarkably, the agreement between the approximate and exact solutions persists even beyond the expected range of accuracy (namely $\epsilon \ll 1$, according to the initial hypothesis of the perturbation method). The approximate solution turns out to be satisfyingly accurate for stiffness perturbations as well (Figure 4.3b), even if the larger sensitivity of some eigenvalues slightly reduces the approximation accuracy (for ϵ approaching unity).

Recalling the modal formulation outlined at the beginning of this Section, the parameter identification problem consists in inverting the analytical equation $\mathbf{\Lambda}(\boldsymbol{\mu}) = \mathbf{\Lambda}^*$ in order to determine the mechanical parameter set $\boldsymbol{\mu}$ (or $\mathbf{p}$) corresponding to the experimental spectrum $\mathbf{\Lambda}^*$. For the deformable diaphragm model, the problem can be solved straightforwardly by recognizing that the analytical expressions (4.45) of the generating eigenvalues linearly depend – with a direct or inverse relationship – on the unperturbed mass and stiffness parameters. Similarly, the analytical expressions (4.46) of the eigenvalue sensitivities depend on the mass and stiffness perturbations. Therefore, by virtue of the multiparameter perturbation method, Equations (4.45) and (4.46) are simple analytical relations in the form $\mathbf{\Lambda}(\mathbf{p})$, suited to be easily inverted to determine the diaphragm mass and stiffness $\mathbf{p}$-parameters that (approximately) correspond to a certain experimental spectrum $\mathbf{\Lambda}^* = (\lambda_1^*, \lambda_2^*, \lambda_3^*, \lambda_4^*)$.

Considering the availability of four zeroth-order equations for the generating eigenvalues and four higher-order equations for the lowest-order eigenvalue perturbations (given by the second sensitivities λ_1'' and λ_2'' for the eigenvalues λ_1 and λ_2 and by the first sensitivities λ_3' and λ_4' for the eigenvalues λ_3 and λ_4), the identification problem can be targeted at identifying no more than eight unknowns selected in the set of all the unperturbed parameters

and/or parameter perturbations. Consequently, the balance of data and unknowns states that some mechanical parameters must be considered known a priori. Among the other possibilities, engineering considerations suggest assuming – with all likelihood – the aspect ratio β and the masses $\Sigma_\rho^2, \Delta_{\rho x1}^2, \Delta_{\rho y1}^2$ as known information.

Based on the above conceptual framework and practical assumptions, the *parameter identification* consists in determining the unknown zeroth-order stiffnesses $\Sigma_{\kappa x}$ and $\Sigma_{\kappa y}$, rotational mass χ_0^2, and shear stiffness κ_{s0} of the deformable diaphragm model by (i) imposing the coincidence between the zeroth-order analytical approximation of the model spectrum $\boldsymbol{\Lambda}^\circ$ and the experimental spectrum $\boldsymbol{\Lambda}^*$ (namely $\lambda_i^\circ = \lambda_i^*$ for $i = 1, \ldots 4$), and (ii) analytically inverting Equations (4.45), yielding

$$\Sigma_{\kappa x} = \omega_1^{*2} \left(1 + \Sigma_\varrho^2\right) \tag{4.47}$$
$$\Sigma_{\kappa y} = \omega_2^{*2} \left(1 + \Sigma_\varrho^2\right)$$
$$\chi_0^2 = \frac{\left(\beta^2 \omega_1^{*2} + \omega_2^{*2}\right)\left(1 + \Sigma_\varrho^2\right) - \omega_3^{*2}\Sigma_\theta^2}{\omega_3^{*2}}$$
$$\kappa_{s0} = \frac{\beta^2\left(\omega_4^{*2}\left(\beta^2\omega_1^{*2} + \omega_2^{*2}\right) - \omega_3^{*2}\left(\omega_1^{*2} + \beta^2\omega_2^{*2}\right)\right)\left(1 + \Sigma_\varrho^2\right)}{4\beta_\Gamma \omega_3^{*2}}$$

where $\omega_1^*, \omega_2^*, \omega_3^*, \omega_4^*$ are the – adimensionalized, $\omega_i^* = \Omega_i^*/\Omega_r$ – experimental circular frequencies (square roots of the eigenvalues), coming out from operational modal analyses. It may be worth noting that the identified zero-order parameters do not depend on the first order (known) parameters accounting for the mass eccentricities $\Delta_{\rho x1}^2, \Delta_{\rho y1}^2$. The one-to-one association of the i-th experimental frequency ω_i^* with the i-th generating eigenvalue λ_i° can be governed by any assurance criterion suited to associate the generating eigenvectors with the corresponding experimental mode shapes.

The parameter identification suffices to assess a zeroth-order structural model of the deformable diaphragm, governed by the mass matrix $\mathbf{M}_d^\circ$ and stiffness matrix $\mathbf{K}_d^\circ$ generated by the identified parameters (4.47) and matching exactly the experimental spectrum $\boldsymbol{\Lambda}^*$. Clearly, the identified structural model cannot be expected to match exactly also the experimental modes $\boldsymbol{\Phi}^*$, because they have not been involved in the identification process. Once the zeroth-order structural model has been identified, the structural model can further be refined by determining higher order contributions to the mass and stiffness matrices. The model refinements can be required to not alter the coincidence between the analytical approximation of the model spectrum $\boldsymbol{\Lambda}^\circ + \boldsymbol{\Lambda}' + \boldsymbol{\Lambda}''$ and the experimental spectrum $\boldsymbol{\Lambda}^*$ (namely $\lambda_i^\circ + \lambda_i' + \lambda_i'' = \lambda_i^*$ for $i = 1, \ldots 4$).

Therefore, the *model updating* consists in determining the unknown higher-order perturbations (*updates*) of the model stiffnesses $\Delta_{\kappa x1}$ and $\Delta_{\kappa y1}$, rotational mass χ_1^2, and shear stiffness κ_{s1}. This is obtained by (i) imposing the coincidence between the second-order analytical approximation of the model spectrum $\boldsymbol{\Lambda}^\circ + \boldsymbol{\Lambda}' + \boldsymbol{\Lambda}''$ and the experimental spectrum $\boldsymbol{\Lambda}^*$, then (ii) analytically inverting the non-polynomial equations expressing the spectral coincidence (namely $\lambda_i' + \lambda_i'' = 0$ for $i = 1, \ldots 4$) to determine the unknown updates $\Delta_{\kappa x1}, \Delta_{\kappa y1}, \chi_1^2, \kappa_{s1}$ and finally, if the analytical inversion is impossible, (iii) approximate the unknown updates $\Delta_{\kappa x1}, \Delta_{\kappa y1}, \chi_1^2, \kappa_{s1}$ to the lowest order, consistently with the asymptotic

expansion. Following this strategy, the updating read

$$\Delta_{\kappa x1} = \frac{\Sigma_{\kappa x}\Delta_{\varrho x1}^2}{1 + \Sigma_\varrho^2} \tag{4.48}$$

$$\Delta_{\kappa y1} = \frac{\Sigma_{\kappa y}\Delta_{\varrho y1}^2}{1 + \Sigma_\varrho^2}$$

$$\chi_1^2 = 0 + \mathcal{O}(\epsilon)$$

$$\kappa_{s1} = \frac{\chi_1^2(\beta_\Gamma \kappa_{s0} + \Sigma_{\kappa\Gamma})}{\beta_\Gamma\left(\chi_0^2 + \Sigma_\theta^2\right)} + \mathcal{O}(\epsilon)$$

where it can be recognized that the first order parameters accounting for the stiffness eccentricities $\Delta_{\kappa x1}, \Delta_{\kappa y1}$ depend on the first order (known) parameters accounting for the mass eccentricities $\Delta_{\rho x1}^2, \Delta_{\rho y1}^2$, as expected. Finally, from the perspective of engineering applications, it is useful to relate the stiffness κ_s of the two cross bracings to the shear stiffness κ_G of a homogeneous plate with in-plane shear modulus G and thickness S. Based on a simple equivalence of elastic energy, this is achieved through the expression

$$\kappa_G = \frac{G_{eq}}{M\Omega_r^2} = \frac{2\beta\kappa_s}{1 + \beta^2} \tag{4.49}$$

where $G_{eq} = GS$ represents the (equivalent) physical stiffness of the diaphragm.

4.4 Development of model-based *frequency-damage control charts* for masonry buildings

4.4.1 Simulation and identification of fundamental frequency variations induced by earthquakes

As discussed in the introduction to the thesis and supported by several scientific contributions (Section 1.1), existing structures subjected to seismic events exhibit variations in the value of their fundamental frequencies. To briefly recall the main concepts highlighted by the current state of the research, the natural frequency shift can be observed both during the earthquake, as a temporary amplitude-dependent effect that vanishes in absence of structural damage, and after the earthquake, as a permanent effect of structural damage which can be partially and slowly recovered over time. Indeed, several other contributions can play a role in the identification of such variations, including varying environmental conditions, soil nonlinearities and soil-structure interactions, slow processes of stiffness recovery. In this discussion, in particular, the focus will be addressed to the post-seismic variations observed as a consequence of structural damage only, which can be considered among the dominant factors for moderate-intensity earthquakes. It is thus assumed that the influence of factors other than structural damage – to cite the most obvious example, the one caused by cyclic variations in temperature – is properly characterized and taken into account accordingly, if relevant. Investigating the effects of variable environmental conditions on the fundamental frequencies of structures, a widely studied field in the literature (Sohn, 2007; Kita et al., 2019), is outside the scope of this thesis. Nevertheless, as it will be shown, their proper treatment poses no issues to the following proposal.

For what concerns the *co-seismic shifts*, the fundamental frequency variations can happen even for very low excitation levels, in which case they pertain to the elastic regime of the structure and are dominated by the characteristic of the input. Indeed, if structural damage occurs, part of them becomes partially permanent. When employing experimental modal parameters identified from the ambient response of structures, for example in seismic assessment evaluations, these effects should be additionally considered to provide reliable seismic predictions. In the case of the SMAV simplified assessment approach, the nonlinear co-seismic behaviour of buildings is taken into account through the employment of *frequency-shift curves*, numerically generated from stochastic simulations on masonry panels (2.2.2). The topic of co-seismic fundamental frequency variations, in particular, is addressed in Chapter 5.

Conversely, the permanent or *post-seismic frequency decay* pertains to the plastic regime of the structure, thus is correlated with the presence of structural damage. This phenomenon, indeed, is at the base of structural health monitoring and damage assessment in seismic engineering applications. The strategy illustrated in the following paragraphs, exploiting the relationship between fundamental frequencies and structural integrity, propose a general model-driven approach based on vibration measurements supporting the decision processes on buildings in the post-earthquake scenario – regarding their usability, the forecast of the structural behaviour during aftershocks, etc. Related to these aspects, some recent contributions of the literature propose vibrational-based frameworks to assess the structural vulnerability of reinforced concrete structures after mainshock/aftershock

sequences. In particular, the evaluations are carried out through time-evolving fragility curves, as a function of the fundamental period elongation due to structural degradation (Trevlopoulos & Guéguen, 2016; Trevlopoulos et al., 2020). The peculiar aspects regarding damage simulation and identification, in particular, will be deepened in relation to masonry buildings, in accordance with the motivations and objectives of the thesis (Section 1.2). The proposed procedure follows the scheme

(a) pre-seismic experimental modal identification

(b) computational simulation

   (b.1) model formulation and calibration, selection of the analysis framework

   (b.2) pre-processing: definition (i) of the seismic input, ensuring a wide range of seismic intensities to induce increasing levels of structural damage and (ii) of the post-seismic ambient excitation, representative of a low-intensity bandpass white noise and addressed to identification purposes in (b.4)

   (b.3) analysis: simulation of the structural response to increasing-intensity seismic inputs, employing nonlinear dynamic analyses

   (b.4) post-processing: identification of the damage-induced *fundamental frequency decays* (through output-only modal identification), correlation with the global *damage grade*, probabilistic characterization of the *control chart*

(c) post-seismic experimental modal identification

(d) *control chart*-based assessment based on the measured frequency decay

The first step deals with the experimental identification of the modal parameters of the building (fundamental frequencies, mode shapes, damping ratios) from vibration measurements acquired in the pre-earthquake operational condition of the structure, fixing the undamaged reference state (a). The modal identification, indeed, can be achieved by exploiting any output-only technique (Section 2.2.1). The sources of aleatory uncertainties, in this case, can be traced back to the quality of measurements – depending on the sensors range and sensitivity, instrumental noise, signal digitization and synchronization, acquisition time, etc. – as well as to unaccounted ambient effects – frequency content of the input, variation in temperature, humidity, etc. Equally important, systematics – such as errors in sensor positioning and orientation, potentially leading to spatial aliasing – should be avoided or properly limited, not to compromise the reliability of the identified modal parameters. These and other operational issues are discussed, through simple numerical simulations, in Section 4.5.1.

The computational simulation (b) requires the selection of the proper structural modelling technique, as well as the corresponding analysis framework. A compromise between fidelity and simplification in structural modelling should be reached, so that the requirements of representativeness as wells as computational efficiency are satisfied (b.1).

The available techniques of modal and structural updating (such as those presented in Sections 4.3.1, 4.3.2 for what concerns the behaviour of floor diaphragms) can be employed to calibrate the mechanical properties of the model and to narrow other possible modelling uncertainties, ensuring that its linear dynamics is consistent with the experimental behaviour identified in (a) from the ambient response of the undamaged structure.
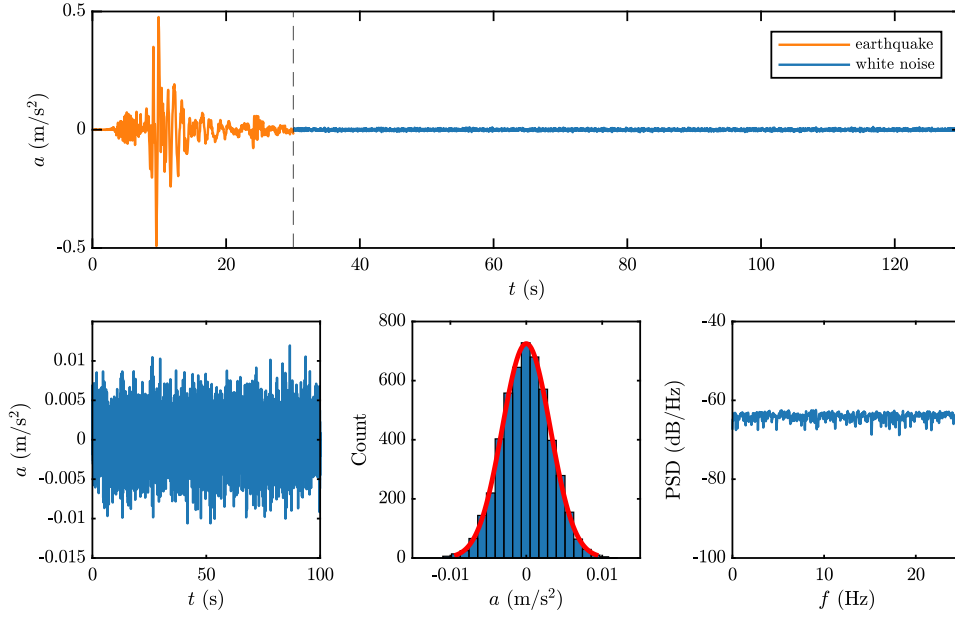
Figure 4.4: Low-intensity band-passed Gaussian white noise excitation, postponed to the earthquake to simulate the post-seismic ambient vibrations of the building.

Concerning the selection of the suitable analysis framework, the development of the *control chart* requires the execution of several nonlinear dynamic analyses for increasing intensities of the seismic excitation, with the purpose of exploring states of increasing structural damage. Their characterization can be achieved by interpreting the numerical results, establishing a statistical correlation between a measurable parameter – representative of the seismic response – and the simulated level of global damage. In this context, the common techniques employed for the probabilistic investigation of structural fragility can be employed for the task. There are several nonlinear dynamic analysis procedures available in the literature to statistically characterize the relationship between Engineering Demand Parameters (EDPs) and the Intensity Measures (IMs) of the recorded ground motions, such as the Incremental Dynamic Analysis (IDA, Vamvatsikos & Cornell, 2002), the Multiple-Stripe Analysis (MSA, Jalayer & Cornell, 2009), the Cloud Method (Bazzurro et al., 1998; Jalayer et al., 2015). Moreover, several scientific contributions address the choice of optimal intensity measures for probabilistic seismic demand analyses (Shome, 1999; Elenas & Meskouris, 2001; Luco & Cornell, 2007; Mollaioli et al., 2013; Ebrahimian et al., 2015; Minas & Galasso, 2019; Wang et al., 2019; Kita et al., 2020). It should be clarified that, in this context, the investigation should be aimed at the characterization of the statistical relationship between two structural response measures – frequency decay and structural damage – rather than between earthquake intensity and structural response. Nonetheless, the selection of the seismic input ground motion could benefit from specific site-related disaggregation studies.

The choice of the suited nonlinear dynamic analysis framework, indeed, determines the

criteria for the selection and processing of the seismic records (b.2i) – involving the postponement of a low-intensity ambient excitation source to the earthquake signal (b.2ii) – and the suitable solution algorithm (b.3). To guarantee a robust post-seismic identification, the input noise (Figure 4.4) should be (*) bandpass white in the range of fundamental frequencies to be excited and monitored, (**) low-amplitude such to avoid a nonlinear response, (***) long enough to guarantee a satisfying frequency resolution, (****) high- frequency sampled (i.e. in short time steps) to improve the accuracy of the solution algorithm. Less robust but more computationally efficient strategies – avoiding the addition of the ambient noise part – could be employed as well, such as those relying on the free-decay response to the ending part of the earthquake.

In the post-processing phase, the EDPs representative of the structural response are estimated. Among the others, the fundamental frequency decay arising from structural damage can be estimated by means of output-only modal identification of the post-seismic simulated ambient response of the structure (b.4). The correlation with the expected global level of damage on the structure can be pursued with reference to empirical definitions (such as those adopted in macroseismic post-earthquake assessment, Grünthal, 1998), comparing a proper EDP to defined thresholds or, with a more refined approach, interpreting the seriousness and extension of the damage exhibited by the structural model. This topic, in particular, will be further examined in the following Sections dealing with masonry buildings, addressing the interpretation of the results produced by nonlinear dynamic analyses (Section 4.4.2) and proposing a damage assessment framework relying on the equivalent-frame idealization (Section 4.4.3).

Finally, once the frequency decay-damage relationship is known in a probabilistic sense, any experimentally detected variation in the fundamental frequency of the actual structure (c) – related to seismic-induced structural damage – provides as well an expectation of the damage grade of the structure through the *control chart* (d). Further criteria can be employed to relate each damage grade to specific performance requirements (e.g. serviceability, life safety). It is understood that, if known, the effect of other external factors potentially affecting the frequency variation – such as ambient conditions – should be removed prior to the reference-damaged frequency comparison (a)-(c).

4.4.2 Damage assessment framework for masonry buildings

Undoubtedly, the permanent decay in the natural frequencies of a structure can be considered a global measure of its stiffness degradation – assuming the mass to be unchanged and ruling out the influence of other external (i.e. soil) and ambient factors – imputable, among the other possibilities, to the occurrence of structural damage. The detection of such a variation from dynamic measurements is a well-known and understood concept in the Structural Health Monitoring (SHM) field (Section 1.1). In particular, in the past two decades, several studies have been conducted regarding the identification of structural damage on civil infrastructures (C. R. Farrar et al., 2001; Carden & Fanning, 2004). For what concerns buildings, even though new non-contact technologies such as computer vision (Feng & Feng, 2018) and radar interferometry(Luzi et al., 2017) are becoming more common, most applications are still relying on the use of vibration measurements by physicals sensors.

Vast room for improvements is still present concerning damage quantification – to relate a measured variation in the modal properties of the structure to the expected level of occurred structural damage – which appears even a more challenging task than damage detection, at least for masonry buildings. Nevertheless, such knowledge could be extremely valuable for monitored buildings, constituting a quick experimentally based evaluation regarding the expected performance of damaged structures in the post-earthquake scenarios. This useful information could support the judgements on the structural integrity, commonly driven by on-site surveys – which could be planned, potentially, after a preliminary assessment carried through the *control chart*. A forward step in this direction can be pursued by numerical simulations. In the case of masonry buildings, in particular, due to the emerging nonlinear behaviour exhibited by masonry even for low-intensity seismic excitations, nonlinear models are essential for accurate and reliable damage assessments. Among the other possibilities, the equivalent-frame modelling approach (Section 2.1.1) seems a straightforward choice, allowing the execution of nonlinear analysis (static and dynamic) of quite complex models with a reasonable computational effort. Nevertheless, as highlighted by the several research contributions addressing this problem, is not straightforward nor simple to interpret the simulated response in terms of actual expected damage in a meaningful way.

For this purpose, it is useful to rely on the empirical definitions of observational Damage Grades (DG) commonly adopted in macroseismic post-earthquake assessment, such as those proposed in the European Macroseismic Scale (EMS-98, Grünthal, 1998). Among the other meaningful EDPs, which usually represent a measurable quantity – such as the roof drift, the interstorey drift ratio, the peak floor accelerations, etc. – but of conventional nature, the damage grades have an unmeasurable but empirical nature, which is more closely representative of the physical nature of structural damage. Moreover, the damage grades can be related to the Performance Level (PL) commonly adopted in the modern seismic performance-based design and, more importantly, in the decisional processes regarding the safety of structures in post-earthquake scenarios. Assuming the DG as the reference demand parameter appears, in this framework, a robust choice. The pursued correlation between seismic-induced fundamental frequency variations and corresponding level of global damage aims, thus, at providing an experimentally identifiable *metric* for the damage grade.

Establishing a robust correlation between the damage observed at a smaller scale (i.e. severity and diffusion in various components of the building, such as walls, floors and roofing systems, stairs, non-structural elements) and the global scale (understood, in this discussion, as the damage grades proposed by EMS-98) is problematic and, although employed in several applications, is still an open issue in the literature. Topics that testify that this problem is still widely debated and that there is currently no unanimously recognized scientific approach are (i) the several damage conversion metrics adopted in literature, for example, to characterize statistically the large number of data coming from post-earthquake observation surveys, employed for the calibration of *empirical fragility curves* and (ii) the various criteria developed to interpret the results of nonlinear dynamic analyses, aimed at associating specific damage levels to their numerical results. In the thesis, primarily, reference is made to the use of dynamic analyses, believing this to be the tool able to describe more accurately the actual physical phenomenon and given that, in this context, the pursued damage evaluation should not be mistaken as a seismic verification in the strict sense

| SECTION 4 | Damage to structural elements and existing short term countermeasures | | | | | | | | | | | | | | | |

Figure 4.5: AeDES form for the survey of structural damage observed on buildings after the earthquake.
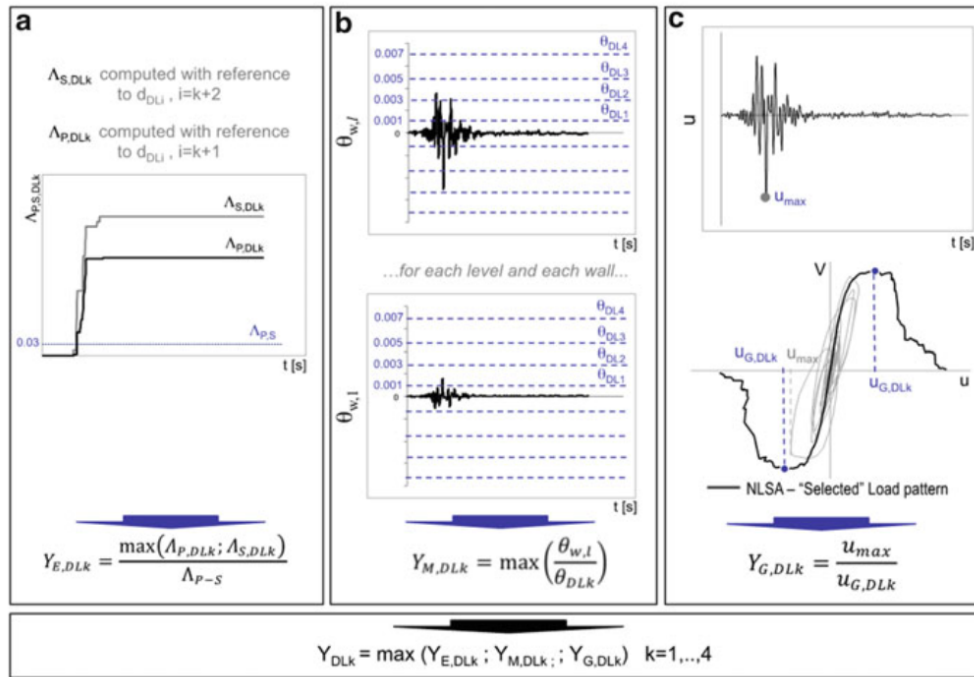
Figure 4.6: Multiscale approach for the definition of the damage levels (DLs) from nonlinear dynamic analyses (from Lagomarsino and Cattari, 2015b).

of regulatory approaches. Conversely, the aim is to achieve a realistic interpretation of the simulated seismic response to be correlated to physical parameters that can be measured experimentally, for example, through a monitoring system.

For what concerns (i) the analysis of the data collected after the earthquake and referred to the observed structural damage – in the case of buildings, carried out in Italy through the AeDES form (Baggio et al., 2007) – the conversion metrics have the purpose of translating

89

(a)   (b)
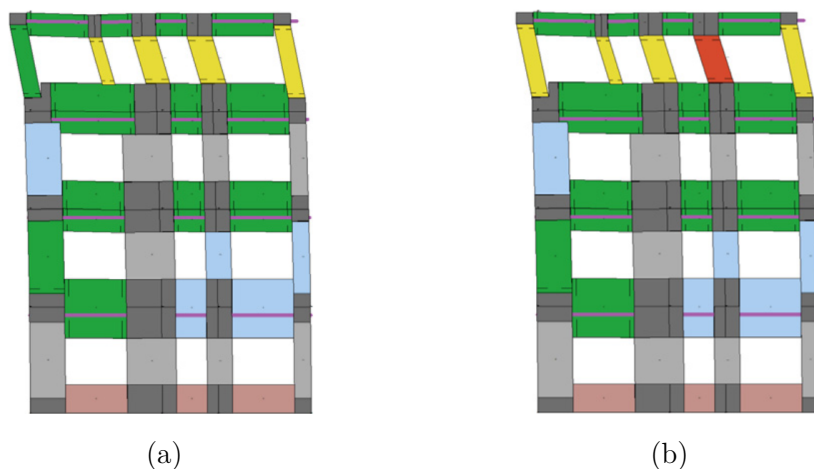
Figure 4.7: DL_{min} criterion for the damage level evaluation at macroelement scale. (a) Wall that did not reach DL3 (at the top storey one pier still is at DL2) and (b) wall that reached DL3 (at the top storey all the piers present DL3 or higher). Adapted from Marino et al., 2019.

the scattered information regarding damaged components (Figure 4.5 into a global and discrete damage level (according to EMS-98). Rules proposed in the literature to achieve this conversion are (related to masonry buildings)

- those employed by the D.a.DO platform (Dolce et al., 2017b; Dolce et al., 2019);

- those developed in Rota et al., 2008 and extended in Rosti et al., 2018;

- those recently proposed in Lagomarsino et al., 2021.

The first two proposals follow a similar approach, referring to the peak damage level observed in the bearing walls for the first, in walls and floor diaphragms for the second, assuming proper conversion rules based on damage extension. The third one, to overcome the typical overestimation of damage when referring to maxima, proposes a weighted average of the damage observed in structural and nonstructural elements, taking into account their relative importance in the global estimation through proper weights (differentiated based on the accuracy of the survey).

Concerning (ii) the interpretation of the results of nonlinear dynamic analyses, many alternative approaches have been proposed in the literature. Indeed, the amount of results produced by the analysis gives a comprehensive picture of the building response, but its proper processing – to determine the attainment of a given damage or performance level – is not straightforward. A state-of-the-art analysis of this topic is reported in Lagomarsino and Cattari, 2015b. Most of the research contributions address the formulation of a global damage index correlated to the DLs or, conversely, the definition of other physically meaningful criteria (such as those referred to the lateral strength evolution and expressed through drifts thresholds).

Generally, a limitation emerges in the adoption of a single criterion, which seems unreliable to detect all possible failure mechanisms – in particular when horizontal diaphragms

are flexible. To overcome this problem, a *multiscale approach* for defining DGs in the case of historical masonry building has been proposed in the framework of the PERPETU-ATE project (Lagomarsino & Cattari, 2015a), focused on the assessment of monumental architectural heritage. The leading idea is to combine different criteria and checks at various scales relevant for the seismic response of the building, i.e. structural elements scale (local damage), architectural elements scale (damage in macroelements), building global scale. Accordingly, a coherent approach is applied to define the DGs in case of both non-linear static analyses, where the EDP is represented by the displacement reached on the pushover curve, and nonlinear dynamic analyses (Figure 4.6), to which the method has been extended (Lagomarsino & Cattari, 2015b). The multiscale approach has been further developed recently (Marino et al., 2019), with the introduction of the concept of DL_{min}, replacing the adoption of interstorey drift thresholds at the wall scale. The proposal assigns a damage level to the wall based on the minimum damage level attained by all the elements of a certain floor (Figure 4.7). This allows overcoming the definition of conventional interfloor drift thresholds, which are not suited to take into account the different damage mechanism exhibited by structural elements of different slenderness (Section 2.1.1). A similar damage-assignment criterion has been recently pursued in Italian regulations (see NTC 2018, Circular 21/1/19 No. 7).

From this brief literature recap, different issues relevant to the purposes of this Section arise. Following other proposals of the literature for reinforced concrete – such as those based on damage indices (Williams & Sexsmith, 1995), such as the Park-Ang one – would be very problematic for masonry buildings, requiring the introduction of conventional threshold values which, currently, are lacking robust evidence from research. Some experiences of the literature (Mouyiannou et al., 2014; Lagomarsino & Cattari, 2015b) suggest, as a more robust approach, to combine different criteria and controls for different scales (at least global and macroelement scales). The introduction of the DL_{min} concept, overcoming some critical issues of the first multiscale proposal, is suitable for design and assessment in regulation codes, but appears too conservative for the scope of this research. The approach – if coherent with a regulatory framework, in which the adopted criteria referred to the *performance levels* should ensure a margin of safety – tends to overestimate the physically occurred damage, thus it seems inappropriate for the correlation with the EMS-98 *damage grades*. For these reasons, in the following proposal, the evaluation of the global damage level is derived from the average damage at the wall scale, making explicit the correlation between the controls implemented in the analysis and the physical significance of damage diffusion.

4.4.3 Identification of global damage grade from nonlinear dynamic analyses on equivalent frame models

The discussion focuses on the specific issues posed in the case of existing and historical masonry buildings characterized by a boxlike seismic behaviour, for which a three-dimensional equivalent frame model of the whole building is appropriate. In accordance with the common assumptions of this modelling approach, the identification of damage will refer to the global response of the building as the result of the in-plane behaviour of the bearing walls, ruling out the possible activation of local mechanisms. The assessment of damage to other structural elements (stairs, storey diaphragms, roof) is, in this phase, postponed to

future developments. Regarding the floor diaphragms, in particular, it should be clarified that most of the current equivalent-frame software implementations (such as TREMURI program employed in the thesis, Section 2.1.1) describe these structural elements as elastic-behaving. Actually, there are some contributions in the literature that could be followed to overcome this limitation. For example, the proposal of Ottonelli et al., 2020 suggests monitoring the maximum diaphragm shear deformation achieved during the analysis, to be compared with predefined damage thresholds. Nevertheless, at the current state of research and given the variety of diaphragm typologies, no universally recognized reference values exist. Furthermore, being this control carried out *ex-post*, it would be impossible to establish its relationship with the numerically identified variations in the fundamental frequencies or mode shapes, a fundamental task of this proposal.

The damaging of nonstructural elements (infill walls, false ceilings) is neglected as well, being understood that these elements can have a primary influence on the performance levels of some structural typologies (i.e. infills for the structural operativity of reinforced concrete buildings), even though that influence is still quite limited on the performance of masonry buildings (Ottonelli et al., 2020).

The piecewise linear constitutive laws adopted for masonry panels (Section 2.1.1), being empirically based, allow to naturally keep track of the Damage Level (DL) reached in each deformable structural element – piers and spandrels – during and after the seismic input. In particular, the shear-drift relationship governing the stiffness and strength deterioration of masonry panels to cyclic loading is based on the experimental observation. The reaching of a DL in a structural element – the exceeding of the corresponding drift threshold – is thus related to the actual physical evolution of damage, i.e. to the widening and propagation of cracks, for different failure modes. Nonetheless, the proposed approach could be equally adopted in other equivalent-frame implementations, for any assumed constitutive law. In such a case, indeed, the association of the DL to each structural element may not be software-driven, but still can be implemented by the analyst in the ex-post processing of the data (monitoring the element drift according to the same DL-threshold values).

Obviously, to provide a meaningful indicator of structural safety, there is the need to move from the local damage scale of the element to the global scale of the whole structure. The approach adopted in this thesis – already pursued in the literature for other purposes (Giovinazzi & Lagomarsino, 2004; Lagomarsino & Giovinazzi, 2006) – is to, first, provide a numerical interpretation of the linguistic description of the damage grades of buildings proposed by the European Macroseismic Scale (EMS98, Grünthal, 1998), second, to correlate the damage exhibited by the structural model at different scales to that interpretation. The EMS-98 supplies, with linguistic terms, the percentage of occurrence of five increasing damage grades on buildings for six different vulnerability classes, correlated in a fuzzy way to building typologies. The five damage grades for masonry buildings are defined – from a quantitative point of view – by a quite vague description of the expected damage and its extension on the building (left side of Table 4.1).

The first challenge, indeed, is to relate the DLs of the structural elements to the terms employed in the EMS-98 to describe the actual damage seriousness at the masonry panel scale. This point can be achieved by referring to the experimental response of masonry panels, on which the employed constitutive laws are based (Section 2.1.1). The proposal is to associate the terms characterizing the damage of masonry panel for each grade – *"hairline cracks", "cracks", "large and extensive cracks", "serious failure"* – with increasing
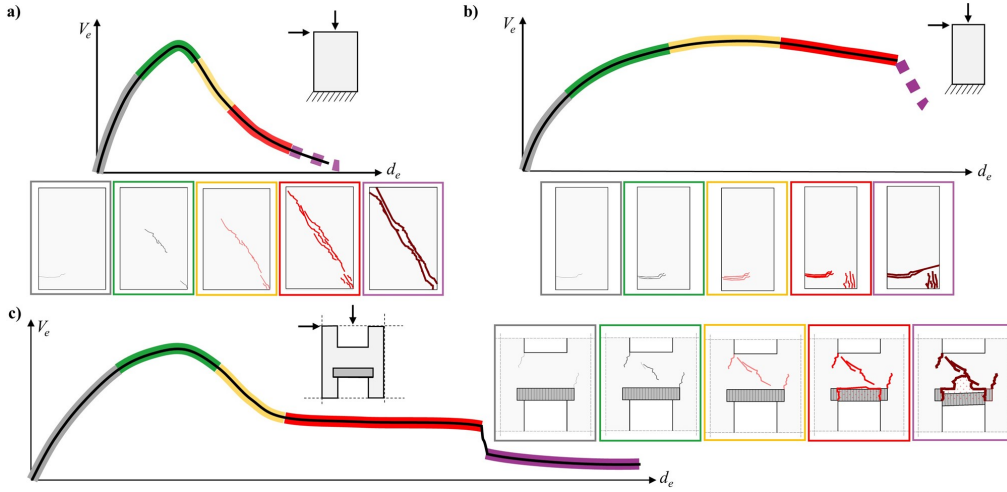
Figure 4.8: Interpretation of the observed damage at the wall scale for (a) squat pier elements under compressive-flexural action generating diagonal cracks, (b) slender pier elements under compressive-flexural action and (c) spandrel elements.

DLs at the element scale – respectively DL1, DL2, DL3, DL4 – starting from the absence of damage – DL0 – up to the complete *"collapse"* – DL5 – of the panel (Figure 4.8). This correspondence, relying on the definition of each observational DL in the constitutive law, is quite accurate for panels dominated by the shear response and is assumed valid also for the flexural case, given that the real behaviour exhibited in by seismic-damaged buildings is usually a mix of the two.

Moving up to the wall scale, a second issue regarding damage extension comes into play. The EMS-98 description, in this regard, is actually referred to the wall as an assemblage of masonry panels, potentially exhibiting different levels of damage. The same criteria, thus, should be followed to interpret the numerical simulations as well. A concrete possibility is to define an average damage level of the wall – DL_w – taking into account the damage contribution of each structural element – DL of piers and spandrels – as a function of its relative importance in the seismic response of the wall. In this respect, assuming a constant interstorey height with a regular distribution of windows, a quite accurate weight for piers can be based on the element horizontal cross-sectional resistant area, relative to the total resistant area of the piers pertaining to the wall. Based on the above considerations, the average damage of the wall DL_w can be estimated as

$$DL_w = \frac{\sum_p A_p DL_p}{\sum_p A_p} + c_{s,w} \frac{\sum_s DL_s}{n_s} \tag{4.50}$$

where the pedices p and s refer to *pier* and *spandrel* elements respectively, A is the cross-sectional area, DL is the element damage level, n_S is the total number of spandrel elements of the wall. The coefficient $c_{s,w}$ weight the general importance of spandrels in the w-th wall. It can be particularized based on an expert engineering judgement regarding the main seismic behaviour expected on building – in which the spandrels surely play a role, based on their stiffness, strength and coupling with other retaining elements. In presence

93
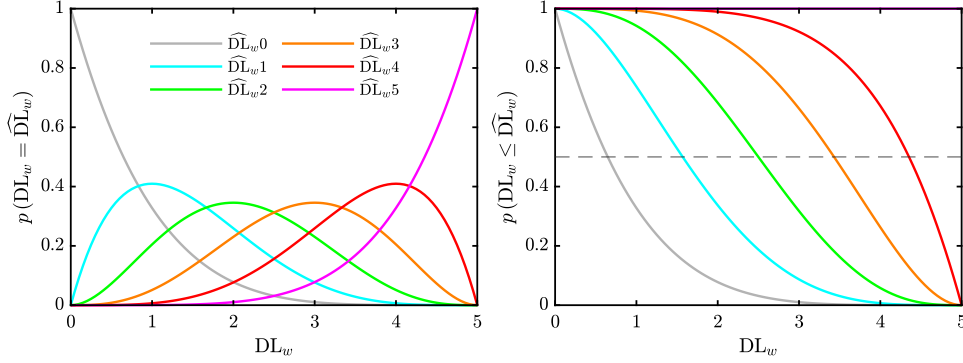
Figure 4.9: Probability mass function and cumulative distribution function for binomial distribution of the average damage level at the wall scale DL_w.

of co-seismic retaining elements (such as tie rods, reinforced concrete edge beams), when the spandrels are expected not to be significantly damage-prone, the second term can be neglected ($c_{p,w} = 0$). Finally, the discrete global damage grade of the building from wall scale $\widehat{\mathrm{DG}}_w$ can be quantitatively estimated interpreting the extension of damage on the walls – *"very few", "many", "most", "total (of)"* walls – provided by quantitative adjectives the EMS98 scale (Table 4.1). According to the fuzzy set theory, the qualitative definitions can be interpreted through a membership function (Giovinazzi & Lagomarsino, 2004), leading to the ranges

- *"few"* up to 10 %-20 %

- *"many"* up to 50 %-60 %

- *"most"* over 50 %

which, even though involving some overlapping, constitute a robust reference. To estimate the percentage of walls that reached a certain damage level, the continuous variable DL_w is firstly discretized employing the binomial distribution (Lagomarsino & Giovinazzi, 2006), assuming the upper bounds of each membership corresponding to a probability of 0.5 in the corresponding cumulative distribution function (Figure 4.9). This assumption leads to the discretization

$$
\widehat{\mathrm{DL}}_w =
\begin{cases}
0, & \mathrm{DL}_w \leq 0.7 \\
1, & 0.7 < \mathrm{DL}_w \leq 1.6 \\
2, & 1.6 < \mathrm{DL}_w \leq 2.5 \\
3, & 2.5 < \mathrm{DL}_w \leq 3.4 \\
4, & 3.4 < \mathrm{DL}_w \leq 4.3 \\
5, & 4.3 < \mathrm{DL}_w \leq 5
\end{cases}
\tag{4.51}
$$

where the hat symbol $\widehat{}$ indicates the integer-discretized version of the variable. It is now possible to compute the cumulative percentage of walls that attained a certain damage
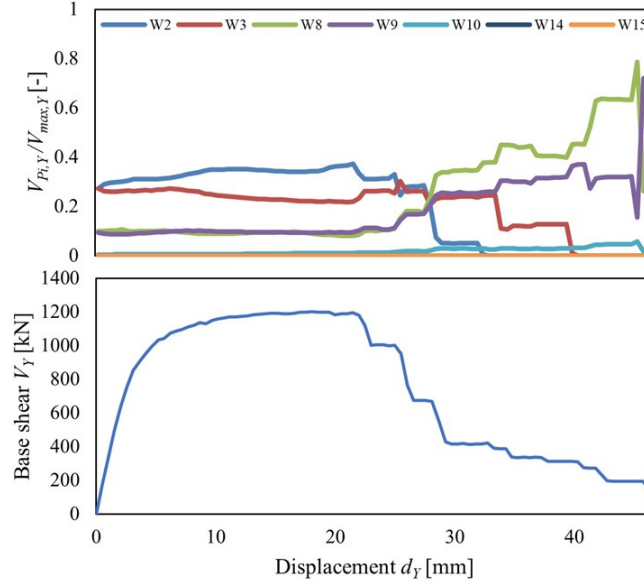
Figure 4.10: Example showing the relative contribution (top) of each wall in the total base reaction (bottom) of the building to a directional pushover field of horizontal forces.

level and establish the damage grade at the wall scale $\widehat{\mathrm{DG}}_w$, according to the thresholds proposed in Table 4.1. Indeed, the thresholds are understood as lower bounds, so that $\widehat{\mathrm{DG}}_w$ is determined by checking all the cumulative controls and choosing the highest resulting damage grade.

Further weights c_w can be employed to take into account the importance of a particular wall in the global response of building, for example, based on its relative reaction to a (unitary) pushover force field (Figure 4.10).

The followed criteria, based on the evaluation of damage severity and diffusion on walls, could not be able to detect the activation of possible soft-storey mechanisms which, from an engineering point of view, could be reasonably associated with the highest levels of damage. To overcome this drawback, a useful rule acting on walls' damage at the interstorey level can be considered, monitoring the mean damage of piers at the l-th level

$$\mathrm{DL}_{w,l} = \frac{\sum_p A_{p,l}\mathrm{DL}_p}{\sum_p A_{p,l}} \tag{4.52}$$

where the pedix l limits the sum to the piers of wall w belonging to the l-th level.

In the case of buildings with very large extensions, the wall-scale controls may not be sufficient to identify conditions in which the horizontal load-bearing capacity of the building (referring to high-severity damage levels) is already compromised. For these reasons, it is useful referring to heuristic criteria based on conventional controls at the global scale. The combination with a global-scale damage rule such as $\widehat{\mathrm{DG}}_\vartheta$, based on roof drift thresholds corresponding to conventional percentages of the total reacting base shear V relative to the maximum V_y on the *pushover curve*, right side of Table 4.1 – ensures a more robust evaluation.
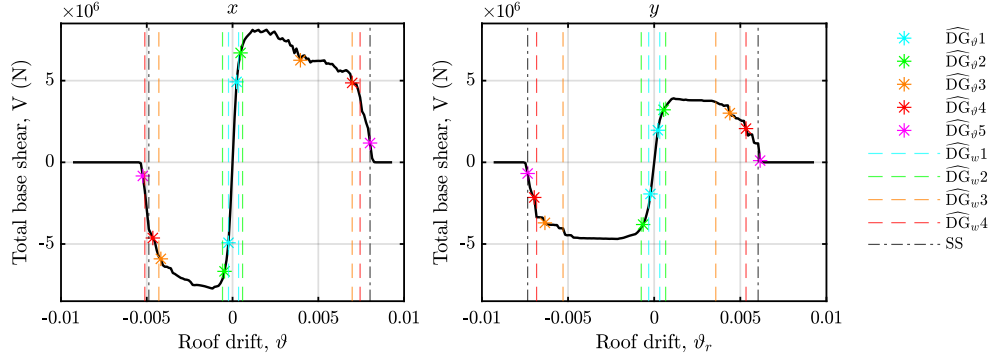
Figure 4.11: Damage grades identified by pushover analyses on the EFM of the Pizzoli town hall building, according to the wall-scale $\widehat{\mathrm{DG}}_w$ and global scale $\widehat{\mathrm{DG}}_\vartheta$ damage criteria. SS stands for soft-storey mechanism.

Finally, the global damage grade $\widehat{\mathrm{DG}}$ of the building is estimated as the maximum between the one estimated at the wall scale $\widehat{\mathrm{DG}}_w$ and the one estimated at the global scale $\widehat{\mathrm{DG}}_\vartheta$

$$\widehat{\mathrm{DG}} = \max\{\widehat{\mathrm{DG}}_\mathrm{w}, \widehat{\mathrm{DG}}_\vartheta\} \tag{4.53}$$

A preliminary result of the damage grade assessment for the Pizzoli town hall building (Section 4.5.2), tested through *pushover analyses* – a nonlinear static analysis in which a field of horizontal forces is applied along the height of the building, whose magnitude is proportional to its masses – is reported in Figure 4.11. In this specific case, for a meaningful comparison with the mono-directional forcing of the pushover analysis, the wall controls are referred to each direction, rather than to the global structure.

It should be finally remarked that, in principle, the described procedure – for what concerns the association of the global damage grade starting from the wall scale – should be applicable to interpret the real damage occurred on existing buildings, when accurate damage observations from field surveys are available. Obviously, this practical application is not straightforward nor quick and, thus, cannot replace the synthetic approaches usually adopted in damage survey forms (e.g. the AeDES form, Section 1.2). Nevertheless, when detailed data is available, it can be very useful for the validation of numerical-based damage assessments, as presented for the case of the Pizzoli town hall building (Section 4.5.2).

Table 4.1: Numerical interpretation of the EMS-98 damage grade classification for masonry buildings, referred to their equivalent-frame idealization.

EMS98 damage grade	Description	Wall scale $\widehat{DG}_w$	Global scale $\widehat{DG}_\vartheta$
Grade 1: Negligible to slight damage (no structural damage, slight non-structural damage)	Hair-line cracks in very few walls. Fall of small pieces of plaster only. Fall of loose stones from upper parts of buildings in very few cases.	$\displaystyle\sum_{\substack{w \\ \widehat{DL}_w \geq 1}} c_w \geq 0.2$	$\dfrac{V}{V_y} = 0.4, \quad \vartheta < \vartheta_y$
Grade 2: Moderate damage (slight structural damage, moderate non-structural damage)	Cracks in many walls. Fall of fairly large pieces of plaster. Partial collapse of chimneys.	$\displaystyle\sum_{\substack{w \\ \widehat{DL}_w \geq 2}} c_w \geq 0.35$	$\dfrac{V}{V_y} = 0.8, \quad \vartheta < \vartheta_y$
Grade 3: Substantial to heavy damage (moderate structural damage, heavy non-structural damage)	Large and extensive cracks in most walls. Roof tiles detach. Chimneys fracture at the roof line; failure of individual non-structural elements (partitions, gable walls).	$\displaystyle\sum_{\substack{w \\ \widehat{DL}_w \geq 3}} c_w \geq 0.5 \mid \sum_{\substack{w \\ \widehat{DL}_w \geq 4}} c_w \geq 0.1$	$\dfrac{V}{V_y} = 0.7, \quad \vartheta > \vartheta_y$
Grade 4: Very heavy damage (heavy structural damage, very heavy non-structural damage)	Serious failure of walls; partial structural failure of roofs and floors.	$\displaystyle\sum_{\substack{w \\ \widehat{DL}_w \geq 4}} c_w \geq 0.35 \mid \sum_{\substack{w \\ \widehat{DL}_w \geq 5}} c_w \geq 0.1$	$\dfrac{V}{V_y} = 0.4, \quad \vartheta > \vartheta_y$
Grade 5: Destruction (very heavy structural damage)	Total or near total collapse.	$\displaystyle\sum_{\substack{w \\ \widehat{DL}_w \geq 5}} c_w \geq 0.5 \mid \sum_{\substack{w \\ \widehat{DL}_{w,l} \geq 5}} c_w \geq 0.75$	$\dfrac{V}{V_y} = 0.2, \quad \vartheta > \vartheta_y$

4.5   Numerical simulations and experimental applications

4.5.1   JetPACS frame

Modal identification of diaphragm rigid rotation and shear deformation

According to the leading ideas presented and theoretically developed in Section 4.3.1, some numerical simulations are carried out to check the expectations through pseudo-experimental data, generated from a structural model defined by known physical parameters (mass and stiffness) and affected by controlled uncertainties. The simulations are based on the finite element model of a three-dimensional frame built with commercial software, representative of a laboratory prototype structure (Section 3.2.1) with a symmetric distribution of stiffness but a non-symmetric distribution of added masses (Figure 4.12a). The steel frame is composed of two rectangular storeys of steel-concrete slabs with plan dimensions 4.2 m × 3.2 m and an interstorey height of 2 m. All structural elements are modelled as linear Euler-Bernoulli beams with two nodes. The floor diaphragms are modelled with four-node shell elements following the Kirchhoff-Love formulation and their added masses have been lumped to the side nodes based on the Huygens-Steiner theorem.

In particular, three models are employed in the simulations to account for different in-plane stiffness contributions offered by the diaphragms. The *rigid-diaphragm model* (Model R) satisfies the assumption of rigid diaphragm behaviour since perfect rigidity constraints are imposed on the floor nodes. The *deformable-diaphragm model* (Model D), in which the diaphragms are not modelled and their mass is lumped to the side nodes, accounts for the limit case in which the slab does not contribute to the in-plane stiffness of the floor but only to its mass. Lastly, as an intermediate case, the *semideformable-diaphragm model* (Model S) is characterized by a shell of finite stiffness which provides a moderate in-plane rigidity contribution. The real-valued modal properties of the frame models (frequencies and periods, modal mass ratios, mode shapes) are obtained by solving the linear eigenvalues problem governing the free undamped oscillations in the small amplitude regime of vibration (Table 4.2).

Focusing first on the Model R, since an infinite axial stiffness is assumed for columns and due to the perfect rigidity constraints, the frame has effectively six degrees of freedom (rigid translations in the two main directions and in-plane rigid rotation for each diaphragm). Due to the non-symmetric mass distribution with respect to the horizontal barycentric axis, the eigenproblem solution is characterized by a non-negligible modal coupling of the translational and rotational degrees of freedom (Figure 4.12b). Looking at the mode shapes given by the eigenvectors, the modes dominated by *translational* motion of the diaphragms (according to the high value of the modal mass ratios $\mathcal{M}_x$ and $\mathcal{M}_y$) are labelled with a prefix T followed by their main displacement direction (horizontal x or vertical y), whereas modes dominated by *torsion* (associated with a high value of rotational mass ratio R_z) are labelled with a prefix R. Ascending numbers indicates modes of the same T or R nature and increasing frequencies. As shown in Figure 4.12b, the three modes at the lowest frequency involve an in-phase displacement of the two storeys while the three modes at the highest frequency a counter-phase displacement, as expected.

For the sake of representativeness, the nominal values (initial model) of the bending

Table 4.2: Natural frequencies, modal mass ratios (translational and rotational) and mode shape types of the three frame models with rigid (Model R), deformable (Model D) and semideformable (Model S) diaphragms.

	Model R						Model D						Model S					
	f (Hz)	T (s)	$\mathcal{M}_x$	$\mathcal{M}_y$	R_z	Type†	f (Hz)	T (s)	$\mathcal{M}_x$	$\mathcal{M}_y$	R_z	Type†	f (Hz)	T (s)	$\mathcal{M}_x$	$\mathcal{M}_y$	R_z	Type†
Mode 1	3.11	0.3215	0	0.91	0	T_{y1}	3.11	0.3215	0	0.91	0	T_{y1}	3.11	0.3215	0	0.91	0	T_{y1}
Mode 2	3.78	0.2646	0.87	0	0.01	T_{x1}	3.23	0.3096	0.03	0	0.77	R_1	3.33	0.3003	0.15	0	0.74	R_1
Mode 3	5.45	0.1835	0.01	0	0.88	R_1	3.64	0.2747	0.66	0	0	H1	3.90	0.2564	0.72	0	0.16	T_{x1}
Mode 4	9.26	0.1080	0	0.09	0	T_{y2}	4.41	0.2268	0.19	0	0.13	H2	9.26	0.1080	0	0.09	0	T_{y2}
Mode 5	13.03	0.0767	0.12	0	0	T_{x2}	9.26	0.1080	0	0.09	0	T_{y2}	10.56	0.0947	0	0	0.09	R_2
Mode 6	17.21	0.0581	0.1	0	0.1	R_2	9.33	0.1072	0	0	0.06	H3	13.24	0.0755	0.11	0	0	H1
Mode 7							12.16	0.0822	0.07	0	0.02	H4	20.96	0.0477	0	0	0	S_1
Mode 8							14.55	0.0687	0.05	0	0.03	H5	23.97	0.0417	0	0	0	S_2

† T = in-plane translation, R = in-plane rigid rotation, S = in-plane shear deformation,
H = in-plane rotation and shear deformation
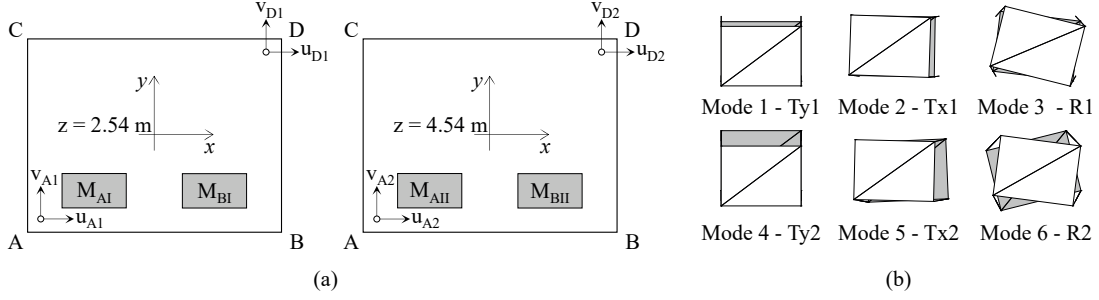
Figure 4.12: (a) Position of the measurement points and added masses at each level of the frame. (b) Plan view of the mode shapes of the rigid-diaphragm model (Model R).

stiffnesses of the columns are updated to better match the natural frequencies of the real prototype frame, experimentally identified from AVT (Section 3.2.1). In this regard, a simple manual calibration allowed to achieve a good agreement with the experimental results, as shown by a general decrease of the relative errors $\delta_f = |f_t - f|/f_t$ concerning the target frequencies f_t (Table 4.3). Moreover, as highlighted by the values of the Modal Assurance Criterion (MAC) (Allemang & Brown, 1982) close to unity (where the subscript *ii* stands for the diagonal term of the MAC matrix), the initial model already shows a high correlation with the identified mode shapes so that, in this respect, the improvement by the update procedure is negligible.

The one-sided power spectral density $G_{XX}(f) = 2S_{xx}(f)$ of the rigid rotation θ and shear strain Γ is estimated for positive frequencies according to the Welch method, simulating the dynamic response of the frame subjected to a zero-mean Gaussian white acceleration applied at the base. conventionally, all the modes are assigned a modal damping ratio equal to 10^{-3}, as the average of the values experimentally identified. The structural response is acquired at the second level of the frame by a pair of ideal (noise-free and perfectly synchronized) bi-axial accelerometers located at the two opposite corners of the diaphragm and whose axes are aligned with the horizontal and vertical directions (Figure 4.12a). The acquisition time is 1800 s with a sampling frequency of 50 Hz. The length of the periodograms, instead, is equal to 20 s and determines a frequency resolution of 0.05 Hz. The PSD of the rigid rotation θ (blue line) peaks at the natural frequencies of the four modes involving torsion, as expected (Figure 4.13a). Given the finite numerical precision of the computation, the spectral density of the shear strain Γ (orange line) can be regarded as negligible along the entire frequency band. These findings confirm the actual theoretical possibility to recognize the perfect rigidity of the diaphragms from the pseudo-experimental measurements of the frame response to white noise excitation.

To reproduce more realistic experimental conditions the uncertainty in the position and orientation assigned to the measurement points, the instrumental noise of the (non-ideal) sensors and lastly a possible desynchronization between records have to be considered in the simulations. Concerning position errors, the effect of a random error in the coordinates of the measurement points is modelled by a 4-dimensional multivariate normal distribution in which each independent random variable has zero mean and a variance $\sigma_x^2 = 2.5 \cdot 10^{-3}$ m^2. This means that in around 95% of the cases the absolute value of the error in each coordinate is lower than 10 cm, which in the worst-case scenario results in a 6% error

Table 4.3: Natural frequencies and periods, damping ratios and mode shapes type identified from FDD of the ambient response of the prototype frame in the CN configuration. On the right side relative errors in frequency δ_f and values of the MAC between the updated Model R and the experimental results.

		Experimental				Model R		
	f (Hz)	T (s)	ξ	Type		f (Hz)	δ_f (%)	$\mathrm{MAC_{ii}}$
Mode 1	3.08	0.32468	0.0011	T_{y1}		3.11	0.97	0.998
Mode 2	3.84	0.26042	0.0015	T_{x1}		3.78	1.56	0.998
Mode 3	5.51	0.18149	0.0012	R_1		5.45	1.09	0.995
Mode 4	8.90	0.11236	0.0010	T_{y2}		9.26	4.05	0.986
Mode 4b	10.75	0.09302	0.0010	T_{y3}				
Mode 5	12.96	0.07716	0.0028	T_{x2}		13.03	0.54	0.972
Mode 6	17.64	0.05669	0.0012	R_2		17.21	2.44	0.992
Mode 7	14.08	0.07101	0.0072	S_1				
Mode 8	15.28	0.06545	0.0045	S_2				
Mode 9	16.55	0.06043	0.0091	S_3				

in the estimation of the distance – equal to 5 m – between the two measurement points. The spectra show the rising of Γ-peaks at the same frequencies of θ-peaks with a power spectral density roughly two orders of magnitude lower (Figure 4.13b). Other simulations, here not reported for the sake of synthesis, highlight how Γ-peaks magnitude depends on the relevance of the position error and, in this case, tends to overcome θ-peaks one for an error with a hundred times higher variance ($\sigma_x^2 = 2.5 \cdot 10^{-1}$ m^2).

A simple example of orientation error is a 1-degree rotation with respect to the coordinate system of the diaphragm, which involves both the sensors but with opposite sign (one sensor with clockwise, the other with counter-clockwise misorientation). The existing θ-peaks are essentially unaffected, whereas new spurious (error-generated) rotational peaks arise for the pure translational modes along the y direction (Figure 4.13c). The shear strain Γ is the most influenced variable by this type of error. Nonphysical peaks arise corresponding to every resonant frequency, with a magnitude comparable with position error. However, in this case, the rotational modes seem to be the least affected. Greater misorientation angles (up to 10 degrees) and other combinations have been considered in the simulations as well. If on one hand, a fixed-angle rotation of the sensors in the same direction is mathematically equivalent to a position error, on the other hand, the misorientation of a single sensor seems to produce the worst possible scenario, in which the shear estimation becomes unreliable for a rotation close to 10 degrees (even for rotational modes).

Measurement noise can be simulated based on the sensor spectral noise curve provided by the manufacturer, which determines the maximum resolution achievable by the instrument. Such effect is modelled with a zero-mean Gaussian white noise process with variance $\sigma_u^2 = 1 \times 10^{-8}$ m^2/s^4, suitable for a piezoelectric accelerometer with an average spectral noise of 20×10^{-6} (m/s^2)/Hz$^{1/2}$ working in the 0-25 Hz range (bearing in mind that the white assumption is strongly simplifying). This results in the raising up of both the noise
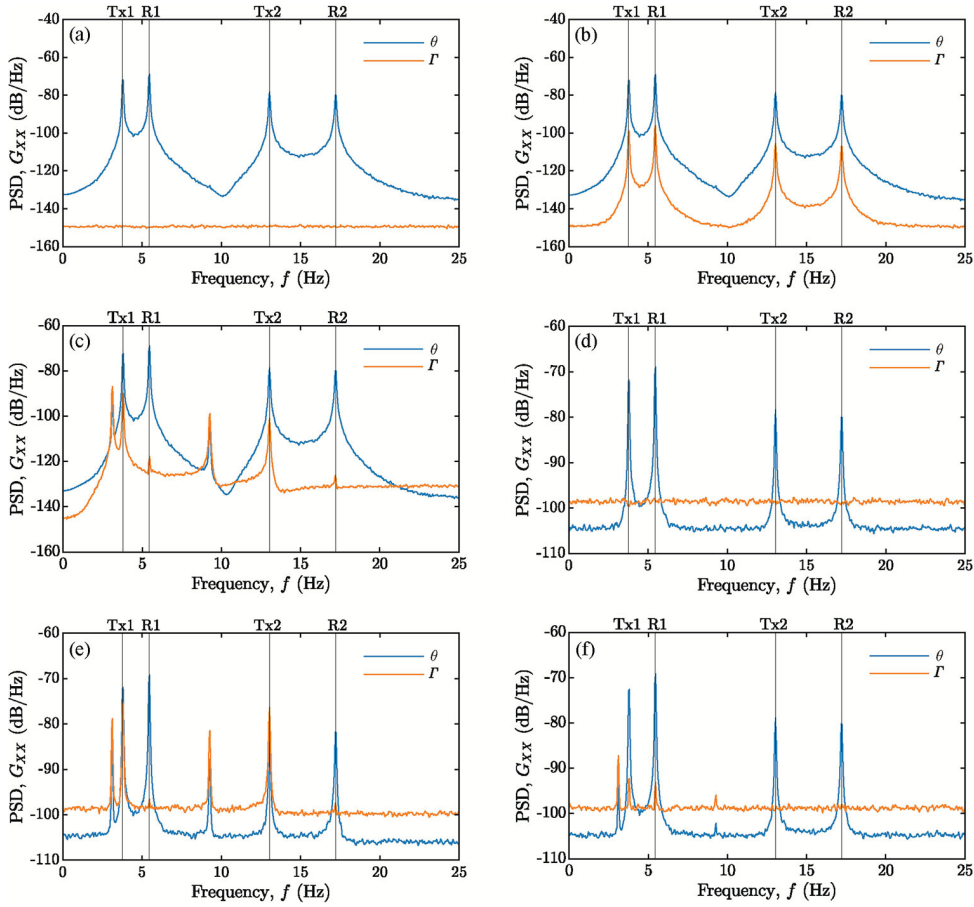
Figure 4.13: (a) Single-sided power spectral densities of the rigid rotation θ and shear strain Γ, estimated from the simulated ambient response of Model R. (b) Effect of position errors, (c) misorientation, (d) measurement noise, (e) desynchronization. (f) Concurrence of measurement noise, position and orientation errors.

floors understood as the constant part of spectra outside the peak bells. Even if the noise floor of Γ quickly exceeds the noise floor of θ (Figure 4.13d), due to the broadband nature of the measurement noise, no additional peaks are generated that affect the frequency content of Γ. In this respect, the possibility to identify modes involving θ and Γ still relies on a sufficiently high ratio between the (resonant) ambient response and the measurement noise powers.

Lastly, desynchronization can be a relevant issue when independent data acquisition systems are employed. In this regard, the samples acquired by one sensor are shifted by one-tenth of a sampling period (0.002 s) to simulate the drift between internal clocks of the acquisition units. This average value of the time shift is reasonable for a clock drifting by 20 μs/s and a GPS synchronization running every three minutes. The effects of desynchronization appear more disruptive than those caused by position errors since Γ-peaks rise at the frequencies of both translational-rotational modes and pure translational modes (Figure 4.13e). Moreover, the (spurious) shear strain Γ approaches the actual rigid
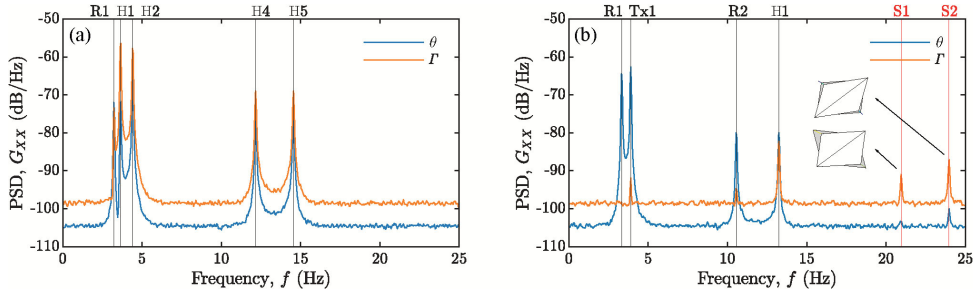
Figure 4.14: Single-sided power spectral densities of the rigid rotation θ and shear strain Γ, estimated from the simulated ambient response of (a) Model D and (b) Model S accounting for measurement noise.

rotation θ already for a low value of the time shift, slightly greater than the one considered (at around 0.004 s for the modes T_{x1} and T_{x2}), so that the rigid behaviour is no longer recoverable from the spectra. Torsional modes, instead, seem to be less affected regardless of the entity of the time shift. Of course, it has been verified that these effects are greatly reduced by increasing the synchronization frequency or by considering a smaller shift in time (which can be achieved in experiments employing reference high-precision clocks).

Even excluding desynchronization, the estimation of rotation and strain is likely affected by position errors, misorientation and measurement noise, already introduced as totally uncorrelated. As a closing remark, it is worth noting how different errors have different qualitative effects, clearly distinguishable from each other. In summary, a position or orientation error determines the rise of peaks in the PSD of the shear strain Γ whereas measurement noise determines an uplift of its noise floor (Figure 4.13f). Consequently, the effect of position and orientation errors could be far more compromising in the identification of a rigid diaphragm.

As a counterexample, the behaviour of deformable diaphragms is assessed considering different in-plane stiffness contributions (Table 4.2). Representative of the limit case in which the slabs do not contribute to the floor in-plane stiffness, Model D exhibits Γ-peaks already in the low-frequency band, with equal or higher spectral density compared to the peaks of θ (Figure 4.14a). Moreover, all the modes in the investigated frequency range appear as *hybrid* (label H), involving both in-plane rigid rotation and shear strain coupled at the same frequency. As long as desynchronization is avoided, it should be recalled how the rigid behaviour greatly differs from the deformable one. In the latter, indeed, the spectral density of the shear strain Γ can no longer be regarded as constant in frequency since it is showing several peaks paired with those of the rigid rotation θ with the same order of magnitude.

In the intermediate case represented by Model S, the floor stiffness contribution offered by the slab is artfully increased to decouple pure *shear* deformability modes (labelled with S) from rotational modes (Figure 4.14b). The model exhibits Γ-peaks of different magnitudes, some of which (e.g. mode T_{x1}) are comparable to those caused by errors in the position assigned to the sensors (Figure 4.13b). Nevertheless, modes with significant shear strain are still clearly identifiable, for example, the hybrid mode H_1 at 13.24 Hz. It should be noted how, if compared to the deformable case, some Γ-peaks occur at high
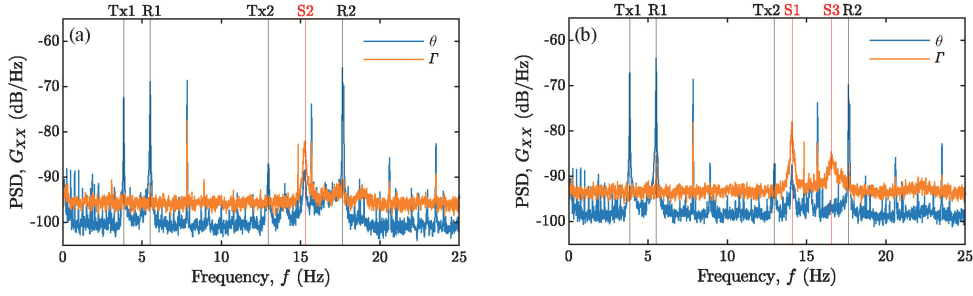
Figure 4.15: Single-sided power spectral densities of the rigid rotation θ and shear strain Γ, estimated from the ambient response of the prototype frame in the CN configuration (a) at the first level and (b) at the second level.
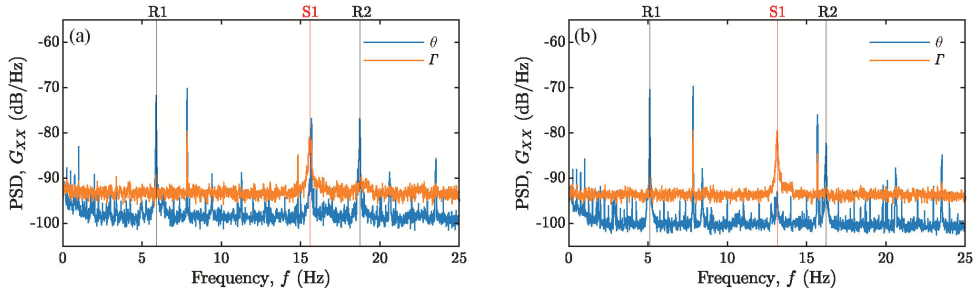
Figure 4.16: Single-sided power spectral densities of the rigid rotation θ and shear strain Γ, estimated from the ambient response at the second level of the prototype frame (a) in the bare CB and (b) in the symmetric CS configuration.

frequencies that are not coincident with θ-peaks. This is the case for the modes governed by deformability of the diaphragms, the pure shear modes S_1 and S_2 in the spectrum of Γ at 20.96 Hz and 23.97 Hz respectively. As a final remark, depending on the diaphragm stiffness, modes dominated by deformation could lay as well outside of the investigated frequency band. In this case, for example, the modes involving the in-plane bending of the diaphragms are found at much higher frequencies than those involving shear deformation, well above the Nyquist frequency and thus not appreciable in the previous analyses.

Experimental application

Moving to the analysis of experimental data acquired the actual JetPACS frame structure (Section 3.2.1), the comparison between the PSDs of the rigid rotation θ and shear strain Γ (Figure 4.15) suggests that both the levels are behaving as rigid bodies in their plane, at least up to 14 Hz. In this frequency band, indeed, the shear strain Γ shows an almost constant power spectral density at least two orders of magnitude lower than the one of θ-peaks. Furthermore, this statement is also supported by the good agreement with the simulated θ and Γ spectra of the finite element model with rigid diaphragm constraints (Figure 4.13d). In the frequency band between 14 Hz and 18 Hz, however, some peaks in the spectrum of Γ reveal the presence of deformation. Employing the FDD technique at the frequencies of Γ-peaks leads to the identification of three modes involving a relevant shear

104
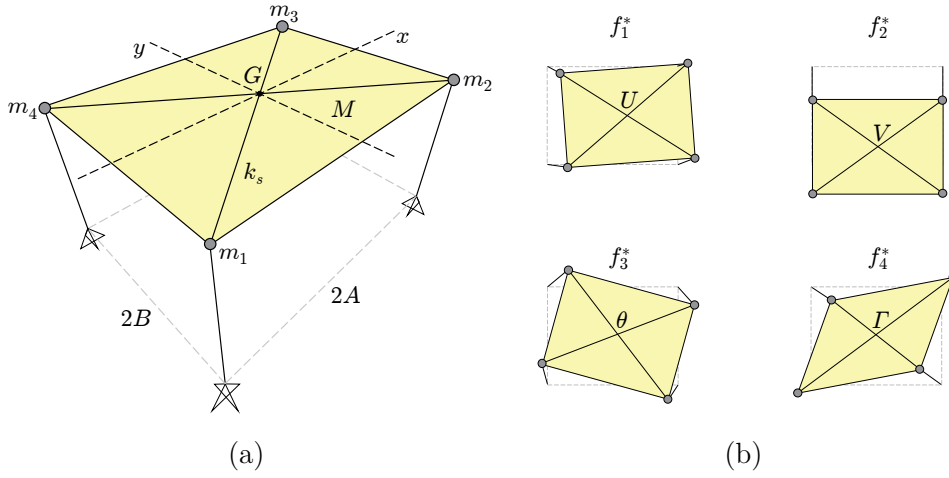
Figure 4.17: Scheme of (a) the one-storey finite element model 1S, developing (b) two modes dominated by the rigid translation U, V along the x and y directions at frequencies f_1^*, f_2^*, one mode dominated by the rigid rotation θ at frequency f_3^* and one mode dominated by the shear strain Γ at frequency f_4^*.

Table 4.4: Left side: values of the shear stiffness k_s assigned to the rigid, semi-rigid and deformable 1S frame model and corresponding natural frequencies of the rigid (f_1^*, f_2^*, f_3^*) and shear (f_4^*) modes. Right side: values of the zeroth-order k_{s0} shear stiffness approximation structurally identified from the pseudo-experimental frequencies.

1S model	k_s (N m^{-1})	f_1^* (Hz)	f_2^* (Hz)	f_3^* (Hz)	f_4^* (Hz)	k_{s0} (N m^{-1})
Rigid	1.00×10^8	24.56	14.16	18.03	156.00	1.09×10^8
Semi-rigid	1.00×10^7	24.12	14.16	17.83	55.46	1.21×10^7
Deformable	1.00×10^6	21.74	14.16	16.38	31.38	3.09×10^6

deformation of the diaphragms (highlighted in red in Figure 4.15), as shown by their mode shapes (on the right side of Figure 3.3. The estimation of the PSDs of rotation and strain in the bare CB and symmetric CS configurations shows how the change in mass is affecting the location of the Γ-peak corresponding to the mode S$_1$, supporting his structural nature (Figure 4.16).

Structural identification of the diaphragm shear stiffness

The actual effectiveness of the theoretical framework and the reliability of the inverse solutions obtained in Section 4.3.2, can be firstly verified by employing a structural model of known physical parameters. To this purpose, the pseudo-experimental data are generated by numerically simulating the free oscillations of a computational model describing the linear undamped dynamics of a prototypical simple structure. For the sake of simplicity, the finite element model (named 1S) of a three-dimensional one-storey, single-bay steel frame with an asymmetric distribution of mass and stiffness is employed (Figure 4.17a).

The dimensions of the rectangular frame plan are 2 m (along the x direction) by 1.5 m

(along the y direction) and the interstorey height is equal to $2\,\mathrm{m}$. The four steel columns (HEB 140), oriented with their maximum moment of inertia along the y directions, are rigidly connected at the top by four edge beams (IPE 180). Two additional point masses of $145\,\mathrm{kg}$ are added to the vertices of the edge along the x direction, breaking the mass symmetry of the structure. The floor in-plane shear stiffness k_s is provided by two diagonal bracings of varying axial stiffness. In particular, the *rigid*, *semi-rigid* and *deformable* models considered in the analyses conventionally correspond to the pseudo-experimental frequency f_4^* of the *shear mode* being close (same order of magnitude), far (up to one order larger) or very far (at least one order larger) with respect to the pseudo-experimental rigid modal frequencies f_1^*, f_2^*, f_3^* (Figure 4.17b). Lastly, concerning the modelling hypotheses, the two-nodes beam elements follow the Euler-Bernoulli theory and the peripheral nodes of the diaphragm are constrained to move in the plane.

Assuming thus the masses of the columns and of the floor beams to be lumped to the diaphragm peripheral nodes ($145\,\mathrm{kg}$ per node), the geometric and mass parameters read $A = 2\,\mathrm{m}$, $B = 1.5\,\mathrm{m}$, $M = 0\,\mathrm{kg}$, $m_1 = m_2 = 145 + 145\,\mathrm{kg}$, $m_3 = m_4 = 145\,\mathrm{kg}$. Employing the natural frequencies provided by the finite element solution of the eigenproblem as pseudo-experimental data, the inverse relationship (4.47d) allows identifying the zeroth-order approximation of the shear stiffness parameter k_{s0} (Table 4.4). The results highlight the effectiveness of the procedure in identifying the order of magnitude of k_s, committing – from an engineering point of view – an acceptable overestimation. The difference is at least one order of magnitude smaller than the shear stiffness value and tends to increase the higher the diaphragm deformability. This behaviour, however, should be expected and is consistent with the ϵ ordering previously assumed for the adimensional shear stiffness κ_s (see Equation 4.43), which is suitable for non-rigid but still stiff diaphragms.

Experimental application

In the following, the proposed procedure for the diaphragm shear stiffness identification is applied to the different mass configurations of the JetPACS frame, dynamically tested under ambient vibrations (CB, CS and CN, Section 3.2.1). For the sake of simplicity, the point masses added to the diaphragm ($335\,\mathrm{kg}$ each) are lumped to the nearest peripheral nodes, together with the column and beam masses (Table 4.5). Finally, a concrete slab with a mass of around $3000\,\mathrm{kg}$ provides an unknown in-plane equivalent shear stiffness $G_{eq} = GS$, where G is the shear modulus of the concrete and S is the diaphragm out-of-plane thickness. A possible energy-based equivalence between k_s and G_{eq} is reported at the end of Section 4.3.2.

Dealing with a multi-storey structure, different possibilities are available to carry out

Table 4.5: Geometrical and mass properties of the JetPACS frame in the bare (CB), symmetric (CS) and non-symmetric (CN) configurations.

JetPACS	A (m)	B (m)	M (kg)	m_1, m_2 (kg)	m_3, m_4 (kg)
CB				$2{\times}133$	$2{\times}133$
CS	2	1.5	$2{\times}3000$	$2{\times}(133{+}335)$	$2{\times}(133{+}335)$
CN				$2{\times}(133{+}335)$	$2{\times}133$

Table 4.6: Left side: natural frequencies f_1^*, f_2^*, f_3^* of the rigid modes and f_4^* of the shear mode as experimentally identified on the JetPACS frame. Right side: structural identification of the zeroth-order approximation G_{eq0} of the equivalent shear stiffness from experimental frequencies.

JetPACS	f_1^* (Hz)	f_2^* (Hz)	f_3^* (Hz)	f_4^* (Hz)	G_{eq0} (N m^{-1})
CB	4.23	3.38	5.89	15.60	2.71×10^6
CS	3.58	2.85	5.11	13.15	2.49×10^6
CN	3.84	3.08	5.51	14.08	2.45×10^6

the diaphragm stiffness identification. It should be possible, theoretically, to analyse the structure storey-by-storey, employing only the corresponding experimental measurements and assigning the mass parameters accordingly. However, this approach would face several difficulties in identifying the frequencies and local mode shapes of a particular storey. An alternative option, which has been followed in the proposed applications, is to consider the structure as a whole, without employing any additional information (i.e. higher-frequency modes). This choice can be justified both from a structural point of view, the stories of the analysed structures present the same mechanical characteristics, and from a conceptual point of view, in order to preserve the straightforwardness of the procedure. Indeed, a slight overestimation of the real diaphragm shear stiffness is expected as a trade-off.

The experimental modes of the frame in each mass configuration have been identified by means of output-only modal analysis, employing the well-known *frequency domain decomposition* technique, estimating the *Welch* periodograms with a frequency resolution of 0.01 Hz. Only the signals – 1800 s at a sampling frequency of 200 Hz – coming from two orthogonal pairs of mono-axial accelerometers placed at the opposite corners of each storey have been considered, supposing a minimum sensor availability situation that still allows discriminating rigid modes from shear-deformable ones. To this purpose, one of the possible approaches consists in identifying the frequencies of the two rigid translational modes f_1^*, f_2^* from the amplification peaks of the power spectral density (PSD) of the reconstructed rigid translations U, V of the diaphragm centroid. As an example, in the reference (bare) configuration CB, the rigid translation modes in the x and y can be identified at 4.23 Hz and 3.38 Hz respectively (top of Figure 4.18b). Similarly, for what concerns the torsional and the shear modes, they can be identified exploiting the experimental spectra of the rigid rotation θ and shear strain Γ (Sivori et al., 2020b). The Γ-peak at 15.60 Hz highlights the frequency f_4^* of the shear mode of the CB configuration (bottom of Figure 4.18b). Significant frequency shifts of the experimental modes can be observed in the CS and CN configurations due to the presence of added masses, as synthetically reported in Table 4.5. It should be remarked that any other output-only identification technique can be employed to identify the experimental modes, as wells as any correlation can serve for their association with the analytical model (see Section 4.3.2).

Based on known geometric and mass properties of the frame (Table 4.5), the zeroth-order approximation G_{eq0} of the equivalent shear stiffness parameter G_{eq} is structurally identified through expression 4.47d employing the outcome of the modal identification (Table 4.6). The results show a good agreement among the three different configurations (consistently with the unchanged stiffness properties of the diaphragm), confirming the
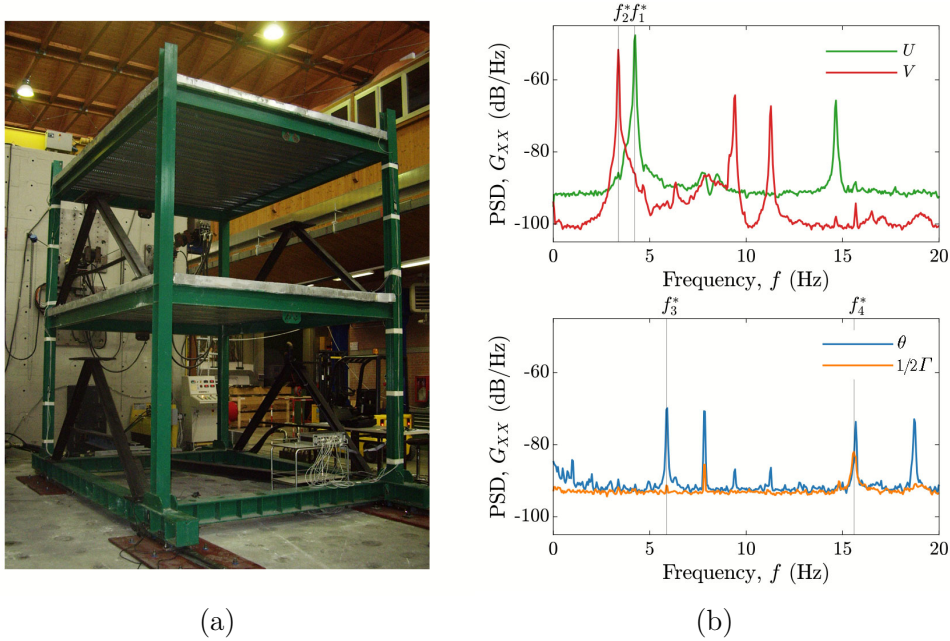
Figure 4.18: (a) Picture of the JetPACS frame in the bare configuration CB during the ambient vibration testing carried out in the DiSGG structural laboratory of the University of Basilicata. (b) Power spectral densities of the rigid translations U, V, the rigid rotation θ and shear strain Γ, estimated from ambient vibration data acquired at the second storey of the JetPACS frame (CB configuration).

effectiveness of the procedure in presence of mass perturbations (previously verified analytically, see Figure 4.3a).

On the one hand, from a physical point of view, the order of magnitude of the identified equivalent shear stiffness appears smaller than the one a 100 mm concrete slab (Ponzo et al., 2012) is expected to provide. On the other hand, it is not straightforward to evaluate the effectiveness of the diaphragm-to-beams connections, given the presence of a HI-bond corrugated steel sheet at the interface.

The finite element model of the JetPACS frame in the CN configuration (Table 4.5) has been employed to further investigate the reliability of the structural identification procedure for multi-storey frames with asymmetric distributions of mass and stiffness. The 2S model can be regarded as the two-storey extension of the one-storey structure previously modelled and analysed (in which the in-plane constraints are released). Similarly to the previous numerical simulations, the diaphragm shear stiffness identification is carried out assuming as known the geometry and the mass properties of the frame, employing the natural frequencies provided by the finite element solution as pseudo-experimental data. The known equivalent shear stiffness parameter G_{eq} assigned to the diaphragm is increased starting from a deformable diaphragm condition, which has been manually calibrated to be representative of the experimental results (CN modal identification of Table 4.6). Accordingly, the rigid modes and the shear mode share neighbouring frequencies of the spectrum. Increasing the shear stiffness of the diaphragm quickly moves the deformability

Table 4.7: Left side: values of the equivalent shear stiffness G_{eq} assigned to the rigid, semi-rigid and deformable 2S frame model and corresponding natural frequencies of the rigid (f_1^*, f_2^*, f_3^*) and shear (f_4^*) modes. Right side: values of the zeroth-order G_{eq0} approximation structurally identified from the pseudo-experimental frequencies.

2S model	G_{eq} (N m^{-1})	f_1^* (Hz)	f_2^* (Hz)	f_3^* (Hz)	f_4^* (Hz)	G_{eq0} (N m^{-1})
Rigid	1.75×10^8	4.15	3.30	5.41	122.13	2.67×10^8
Semi-rigid	1.75×10^7	4.14	3.29	5.39	40.6	2.82×10^7
Deformable	1.75×10^6	4.07	3.22	5.30	14.1	2.98×10^6

mode to higher frequencies, leaving the rigid mode frequencies practically unchanged.

The identification results, as expected, highlight a general worsening in the estimation of G_{eq} (Table 4.7) compared to the one-storey case. The identified shear stiffness of the diaphragm is generally overestimated, but still reasonably close (same order of magnitude) to the assigned value. The simulations, finally, shed some light on the experimental identification, suggesting an overestimation – compared to the value providing a good match between the numerical frequencies and the experimental ones – of the diaphragm shear stiffness characterizing the experimental model. It should be remarked that, however, this difference can be partially attributed to the conceptual differences between the computational and the analytical model.

4.5.2 Pizzoli town hall

Structural identification of the diaphragm shear stiffness

According to the AV-based tools developed in Section 4.3.1 and 4.3.2, the ambient vibration data acquired from the permanent monitoring system of the Pizzoli town hall building (Section 3.3.1) are employed, first, to investigate the rigid and shear-deformable contributions in the in-plane motion of floor diaphragms and, second, based on this knowledge, to identify the equivalent in-plane shear stiffness of diaphragms from their experimental dynamic behaviour. Regarding the first proposal, other applications to existing masonry buildings are reported in Sivori et al., 2019, 2020a; Sivori et al., 2020b and in Appendix.

The in-plane motion of the rectangular-shaped floor diaphragm is expressed in terms of its centroid rigid translations along the two main directions U, V, its rigid rotation θ and shear deformation Γ. The estimation is based on the exact solution 4.36 of the inverse kinematic problem for the case of minimum sensor availability (Section 4.2.1), i.e. $N = 2$ bi-directional sensors placed at the top of each floor (channels 2-3 and 6-7 for the ground floor, 8-9 and 13-14 for the first floor, see Section 3.3.1). The frequency content of such motion variables, in particular, can give valuable insights – in terms of rigid and shear-deformable modes – about the dynamic behaviour of the diaphragms, leading to the solution of the first-level identification problem (modal identification).

According to the spectral density of the centroid rigid displacements (Section 4.3.1), the rigid translation modes along the x and y directions can be identified at the frequencies f_1^* and f_2^* of 6.55 Hz and 4.55 Hz respectively (left of Figure 4.19). Conversely, the PSD spectrum of the rigid rotation θ suggests the torsional mode to be located at the frequency
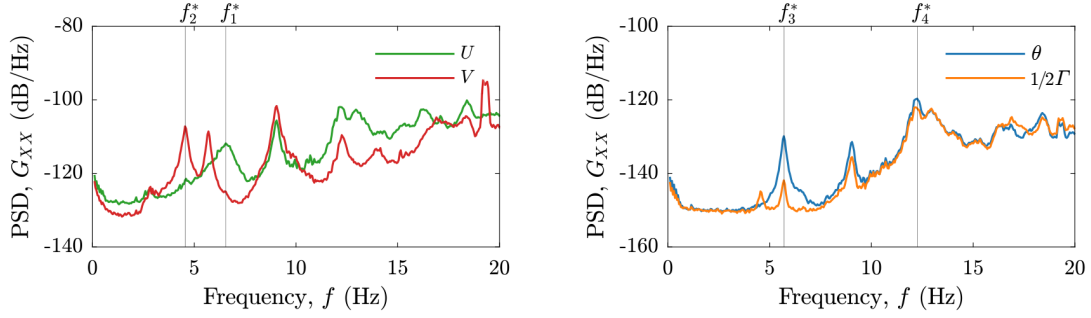
Figure 4.19: Power spectral density (PSD) spectrum of the reconstructed rigid displacements along the x, y directions U, V (left) and of the rigid rotation θ and shear deformation Γ (right).

Table 4.8: Frequencies f_1^*, f_2^*, f_3^* of the rigid modes and f_4^* of the shear mode as experimentally identified on the Pizzoli town hall building. Identified zeroth-order approximation G_{eq0} of the equivalent shear stiffness from experimental frequencies.

f_1^* (Hz)	f_2^* (Hz)	f_3^* (Hz)	f_4^* (Hz)	G_{eq0} $(\mathrm{N\,m^{-1}})$
6.55	4.55	5.70	12.25	2.74×10^8

f_3^* of 5.70 Hz, where the contribution of θ is significantly greater than the shear deformation one Γ (right of Figure 4.19). Finally, the frequency content of the shear deformation Γ shows a positive trend with frequency, reaching its highest magnitude at 12.25 Hz (right of Figure 4.19), which is assumed as the frequency f_4^* of the shear mode.

Being known the one-to-one association between the identified experimental and the analytical rigid and shear-deformable modes, the in-plane shear stiffness of the diaphragm can be directly identified from their experimental frequencies. The second-level identification problem (parameter identification) is pursued according to the zero-th order inverse approximation 4.47 proposed in this thesis (Section 4.3.2). To this purpose, the mass of the building is estimated assuming a masonry density of $2100\,\mathrm{kg\,m^{-3}}$ and an area density of $400\,\mathrm{kg\,m^{-2}}$ for the floor diaphragms. The mass of the perimeter walls is assumed to be evenly lumped to the diaphragm vertices, taking into account the additional presence of the two projecting bodies in the rear part of the building. The geometric and mass parameters are thus $A = 18.375\,\mathrm{m}$, $B = 4.2125\,\mathrm{m}$, $M = 1.10 \times 10^6\,\mathrm{kg}$, $m_1 = m_2 = 2.04 \times 10^5\,\mathrm{kg}$, $m_3 = m_4 = 2.04 \times 10^5 + 1.37 \times 10^5\,\mathrm{kg}$.

The identified value of G_{eq} should be representative of the equivalent shear stiffness provided at the floor level by a concrete slab of an average thickness of 0.14 m. If a concrete grade C20/25 with a Young modulus of elasticity of $3 \times 10^{10}\,\mathrm{Pa}$ and a Poisson ratio of 0.2 is assumed, the zeroth-order approximation of the shear stiffness (Table 4.8) is around one-sixth of the one ideally provided by the floor slabs. From the experimental point of view, however, it should be remarked that several factors could influence this contribution, including but not limited to the quality of the building materials, the compliance with the execution standards, the effectiveness of the diaphragm-to-masonry connections, the
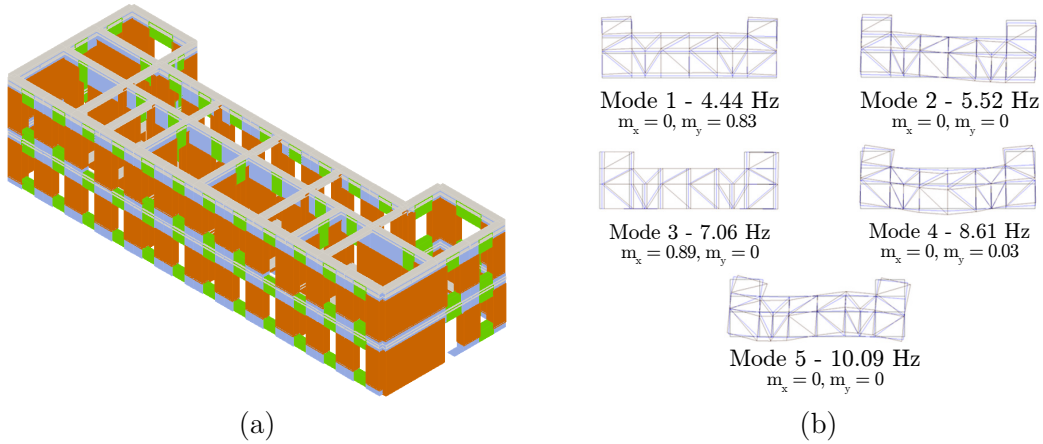
Figure 4.20: (a) Equivalent frame model of the Pizzoli town hall building and (b) frequencies and mode shapes after the linear calibration.

possible structural ageing, deterioration and damage. The last option appears the most probable explanation, since the ambient response provided by OSS has been acquired on the 1st of October 2016, after the first of the several seismic events that hit the structure in the following months (Cattari et al., 2019a; Spina et al., 2019). A slight overestimation of the in-plane shear stiffness parameter, indeed, is expected to result from the conceptual gap between the actual structure and the assumed analytical model which, according to its low-fidelity nature, is representative of a single-storey structure. Nevertheless, as it will be proposed in the following, the structural identification procedure can be useful to improve the calibration of more detailed computational models.

Equivalent frame model updating

In the following, the operational modal parameter – natural frequencies, mode shapes – as well as the structural parameters – the shear stiffness of floor diaphragms – previously identified from ambient vibration measurements, are employed to calibrate the equivalent frame model idealization (EFM, Section 2.2.1) of the building. The use of the EFM technique to investigate the seismic response of the building is supported, in this case, by the traditional structural configuration of the building, in particular by the opening arrangement following a regular pattern both in the horizontal and vertical development. In such a case, indeed, the discretization of the bearing walls as deformable masonry portions – piers and spandrels – and undeformable connections – rigid nodes – is closely representing the actual seismic behaviour of the physical structure. Thanks to the limited number of structural elements, the model has low computational requirements and, thus, can be easily employed in the nonlinear seismic analyses of masonry buildings. (Lagomarsino et al., 2013). An in-depth discussion about the equivalent-frame idealization is reported in Section 2.1.1.

The three-dimensional EFM of the building (Figure 4.20a) has been built using the commercial software version of the research program TREMURI (Lagomarsino et al., 2013) (named 3Muri and distributed by S.T.A. DATA), based on the geometrical, structural and

Table 4.9: Mechanical parameters assumed for the masonry panels.

E_m (Pa)	G_m (Pa)	f_c (Pa)	τ_0 (Pa)	ρ_m (kg m^{-3})
2.7×10^9	0.9×10^9	5.95×10^6	0.12×10^6	2100

mechanical characteristics acquired from the in situ survey (Section 3.3.1) and the available documentation (provided by the Italian Department of Civil Protection within the context of the DPC-ReLUIS Project 2017-2018, Task 4.1, Cattari et al., 2019a). In such a modelling approach, the vertical resistant elements – piers and spandrels, in which the deformation and the nonlinear response are concentrated and whose contribution is related to their in-plane stiffness and strength – are connected by rigid nodes and assembled through orthotropic elastic membranes representing the floor diaphragms.

The structural *mesh* is automatically generated based on empirical laws, which identify the deformable masonry portions starting from the geometry of the openings (according to the common occurrence of seismic damage, Section 2.1.1). Their reliability is supported by experimental evidence, through the observation of buildings heavily damaged by earthquakes in which the cracking pattern is clearly identifiable on the wall elements (see, for example, the example of the Visso school in Ottonelli et al., 2020). In this case, in particular, spandrel elements take into account the presence of reinforced concrete edge beams surrounding the diaphragms concrete slabs. Given its limited contribution to the floor horizontal stiffness, the roof has been modelled only through its proper weight. Further details about the elastic mechanical properties assumed for the vertical and horizontal elements and the assumed constitutive laws governing their nonlinear behaviour are provided in the following paragraphs, addressing the dynamic calibration of the model in the linear regime, and the validation o regime.

In order for the EFM to be representative of the actual building elastic behaviour, the model is dynamically calibrated in the linear regime, based on the ambient vibration response acquired by the permanent monitoring system (Section 3.3.1). In particular, assuming the estimation of the mass of the building to be enough accurate, only the stiffnesses of the vertical elements – piers and spandrels Young modulus of elasticity – and of the horizontal elements – the floor diaphragms in-plane shear stiffness – are updated based on experimental results.

For what concerns the stiffness properties of the vertical elements, in accordance with the values suggested by the Italian National Building Code for the simple-stone masonry typology of the building (proposed in the Italian NTC 2018, Circular 21/1/19 No. 7), the Young elastic modulus E_m is assumed to be equal to 2.7×10^9 Pa. This value is also compatible with the reference values proposed in the literature, derived from experimental data on similar masonry typologies (Kržan et al., 2015; Vanin et al., 2017). The shear modulus G_m is immediately derived, assuming the ratio between the elastic and shear moduli equal to three (as suggested in the Italian NTC 2018, Circular 21/1/19 No. 7). These assumptions (Table 4.9) make the free undamped dynamics of the model representative of experimental data, as shown – for the first three modes – by low values of the absolute

Table 4.10: Natural frequencies of the EF model of Pizzoli town hall building, varying the equivalent shear stiffness of the diaphragm starting from the identified value. Relative difference in frequency δf and MAC matrix between the numerical and the experimental mode shapes.

f (Hz)	G_{eq}= 9.1×10^7 N m^{-1}					G_{eq}= 2.74×10^8 N m^{-1}					G_{eq}= 8.22×10^8 N m^{-1}				
	4.08	4.77	6.61	6.76	7.56	4.44	5.52	7.06	8.61	10.09	4.55	5.75	7.07	10.39	11.54
$|\delta_f|$	0.10	0.16	0.01	0.25	0.38	0.02	0.03	0.08	0.05	0.18	0	0.01	0.08	0.15	0.06
4.55	0.95	0	0.01	0	0	0.97	0	0	0.01	0	0.96	0.01	0	0.02	0
5.70	0.02	0.89	0	0.02	0.60	0.03	0.94	0.01	0.02	0.43	0.04	0.91	0.01	0.01	0
6.55	0	0.02	0	0.95	0.22	0.01	0.08	0.95	0	0.28	0.01	0.11	0.95	0	0
9.05	0.01	0.01	0.77	0.01	0.15	0	0.02	0	0.93	0.03	0.02	0.02	0	0.86	0.17
12.25	0.03	0.15	0.01	0.14	0.70	0.01	0.35	0.08	0.05	0.76	0.01	0.42	0.07	0.04	0

relative difference in frequency $|\delta_f|$ (Table 4.10). No further updating techniques are employed in this context, given the general good accordance between the numerical model and the experimental results in terms of natural frequencies. Nevertheless, the influence of this parameter on the mode shapes is quite limited.

Conversely, further improvements in the model calibration are obtained updating the diaphragm mechanical properties, in particular for what concerns mode shape correlation. The equivalent in-plane shear stiffness of the floor membranes G_{eq} is updated from its initial value – representative of the ideal contribution of C20/25 concrete slabs of average thickness $14\,\mathrm{cm}$, $G_{eq}= 1.75 \times 10^9\,\mathrm{N\,m^{-1}}$ – to a lower value of $G_{eq}= 2.74 \times 10^9\,\mathrm{N\,m^{-1}}$, as structurally identified according to the proposal of this thesis. The calibrated model is able to reproduce, in the right order, the first five experimentally identified modes, with a good mode shape correlation expressed by the high values of the MAC (middle column of Table 4.10). It should be highlighted, in particular for the fourth bending mode B and the fifth shear mode S (Section 3.3.1), a high sensibility of the mode shapes to variations of the diaphragm shear stiffness, as shown by the sudden decrease in the MAC values for both more deformable and more stiff diaphragms (respectively one third and three times the identified shear stiffness, left and right side of Table 4.10). The frequency differences between experimental and numerical results are lower than $10\,\%$, except for the shear-deformability mode. This discrepancy could be attributed to the mass distribution of the EF frame which, at the floor level, is lumped to the perimeter nodes, increasing the floor rotational and shear inertia.

As already observed, in this specific case, the calibration of the shear stiffness of the floor diaphragms affects particularly the high-frequency natural modes (fourth and fifth modes). Although associated with a modest participating mass (Figure 4.20b) and, thus, to a minor influence on the seismic response of the structure, these modes can still be significant in the correct evaluation of local effects, such as the estimation of local deformations at the floor level. This indicator can be employed to estimate the expected damage and the related economic losses, as studied in recent developments of seismic engineering (Del Vecchio et al., 2018; Cardone et al., 2020; Del Vecchio et al., 2020; Ottonelli et al., 2020) and motivated by the heavy social impacts highlighted by Italian seismic events (Di Ludovico et al., 2017a, 2017b).

Simulation and identification of the seismic-induced variations in fundamental frequencies

As highlighted in the general overview of this Chapter (Section 4.1) and further discussed in Section 4.4.1 from the theoretical point of view, a general model-based methodology for the development of *frequency decay-damage control charts* of monitored masonry buildings, which is exemplified here in the case of the Pizzoli town hall. The present application employs the equivalent frame model of the building, which has been formulated and dynamically calibrated in the previous paragraphs, and relies on nonlinear dynamic analyses for the simulation of the building seismic response and damaging to increasing seismic intensities. In this regard, among the other possible solutions, the simulation framework selected to pursue a probabilistic investigation is the Multiple Stripe Analysis (MSA). The reasons supporting this choice, including the selection and treatment of the seismic input – which are referred to the comparison with the SMAV approach (Section 2.2.2 –
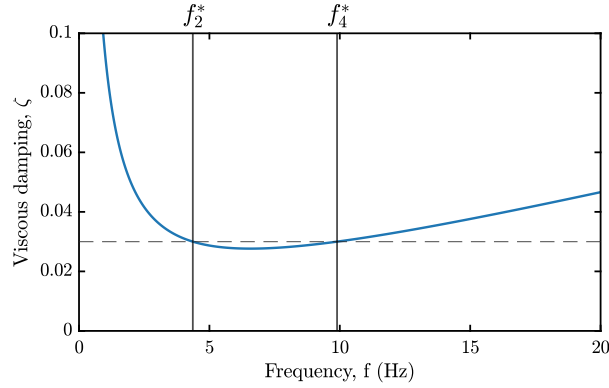
Figure 4.21: Rayleigh viscous damping model assumed in the nonlinear dynamic analyses.

Table 4.11: Parameters adopted for piers and spandrels, governing the piecewise-linear constitutive law.

p/s*	Shear behaviour				Flexural behaviour			
	Backbone		Hysteretic		Backbone		Hysteretic	
	$\theta_{S,i}$ (%)	$\beta_{S,i}$	c_1	0.8/0.2	$\theta_{F,i}$ (%)	$\beta_{F,i}$	c_1	0.9/0.2
DL3	0.45/†	0.6/0.7	c_2	0.8/0	0.6/0.6	1.0	c_2	0.8/0
DL4	0.7/0.4	0.1/0.7	c_3	0/0.3	0.8/0.8	0.8/0.7	c_3	0.6/0.3
DL5	0.9/0.7	0			1.1/1.2	0	c_4	0.5/0.8

* p stands for piers, s for spandrels.
† for spandrels, $\theta_{E,3}$ has been defined assuming a ductility factor equal to 4, similarly to what suggested in Beyer and Mangalathu, 2013.

are addressed in detail in Chapter 5. In particular, the analyses were performed with the TREMURI research program, whose modelling strategies, element strength criteria and nonlinear constitutive laws have been discussed in detail in Section 2.1.1. The solution of the time-history analysis is obtained through a Newmark integration method, assuming a Rayleigh viscous damping ζ equal to 0.03 for the first and fourth mode (Figure 4.21).

Before addressing the simulation results, some brief remarks are given regarding the assumed piecewise constitutive laws governing the hysteretic behaviour of the masonry elements. For what concerns the strength parameters of the masonry required by the adopted strength criteria (Section 2.1.1, Table 2.1), in absence of more specific experimental evidence, they are assumed – coherently with the masonry typology of the building – according to code suggestions and with proper corrective factors (such as those to take into account the presence of bricks courses, Section 3.3.1, Figure 3.5). Concerning the stiffness-related parameters, in order to describe the stiffness degradation in the nonlinear regime, the ratio between the initial and secant stiffness k_r is assumed to be equal to 1.75 – so that the cracked stiffness is around 57 % of the initial stiffness – whereas the ratio between the shear at the end of the elastic phase and the peak shear strength k_0 is assumed equal to 0.7.
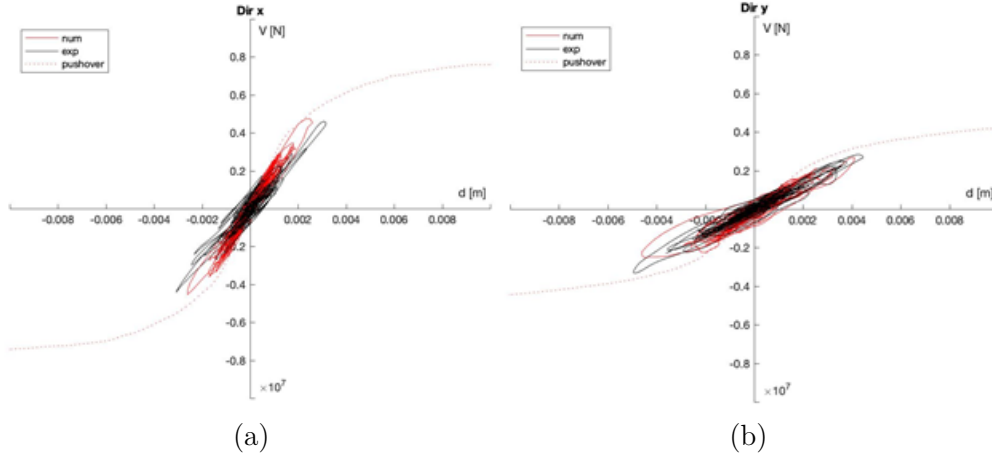
Figure 4.22: Shear-displacement $V - d$ curves as derived from experimental and numerical results, adopting an equivalent frame model idealization and the piecewise linear constitutive laws implemented in TREMURI program (from Degli Abbati et al., 2021).
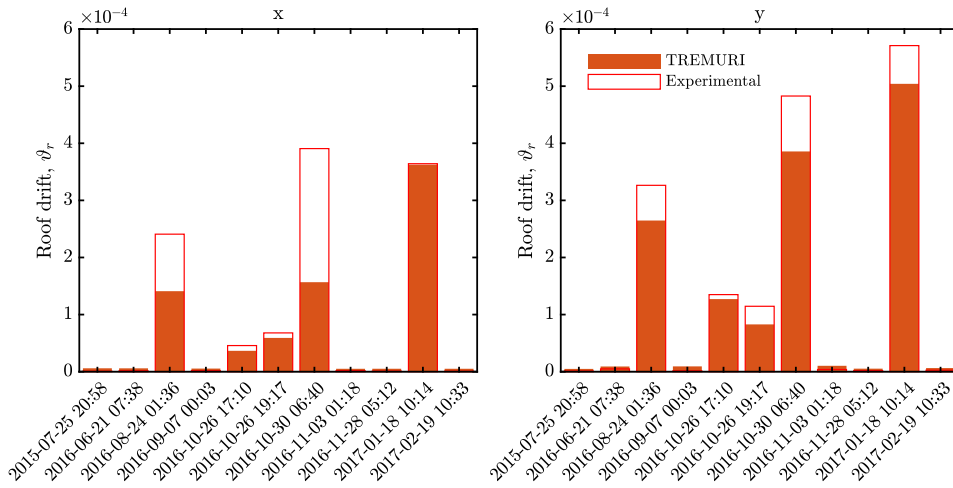
Figure 4.23: Comparison between the TREMURI prediction and the experimental response of the Pizzoli town hall building during minor and major seismic events in 2016/2017, reported in terms of maximum roof drift. The average roof displacement is estimated from frequency-domain integration of the measured acceleration response.

The drift thresholds θ_E and the corresponding strength decays β_E associated with different Damage Levels (DLs) and governing the post-peak behaviour of the masonry panels are reported in Table 4.11, differentiated depending on the failure mode (θ_s, β_s for shear, θ_f, β_f for flexural). They refer to the simple stone masonry typology and are consistent with the interval proposed in the literature (Kržan et al., 2015; Vanin et al., 2017). In particular, the drift thresholds and the shear strength degradation – which determine the shear-drift relationships described by the constitutive law – have been validated in the
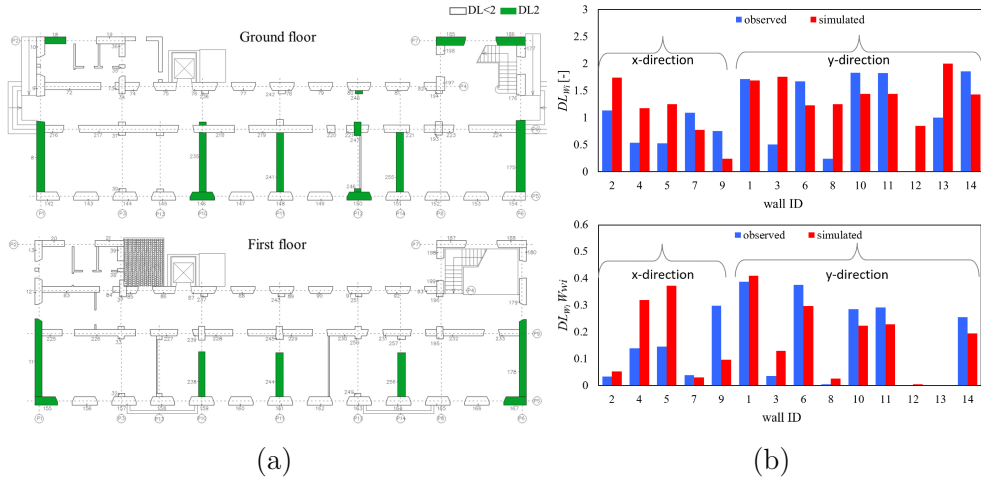
Figure 4.24: (a) Level of damage observed on the piers of the Pizzoli town hall building after the event of January 2017 and (b) comparison between the experimental and the EFM-simulated damage at the wall scale, according to the damage assessment procedure proposed in Section 4.4.3.

framework of other research activities. Their reliability has been discussed in Cattari et al., 2019a and in Degli Abbati et al., 2021 in the case of the EFM of the Pizzoli town hall building, referring to the good accordance between the simulated and experimental results on the seismic response and structural damage of the structure during the 2016/2017 Central Italy earthquake sequence (Figure 4.22), and in Brunelli et al., 2020 for other buildings of similar masonry typology. A further validation has been obtained – employing other records of minor and major seismic event provided by the OSS, Dolce et al., 2017a – in terms of maximum predicted roof drift with respect to the measured one (Figure 4.23), neglecting the effect of damage cumulation (in accordance with the in situ observations, Section 3.3.1). In particular, referring to the earthquake that hit the structure on the 18th of January 2017, the application of the damage assessment procedure proposed in Section 4.4.1 to (i) the damage surveyed on the structure in June 2017 (Figure 4.24a) and (ii) to the results of nonlinear dynamic analysis on the EFM shows a good agreement in terms of damage severity and distribution among the different walls (Figure 4.24b).

**Identification of the post-seismic fundamental frequency decay
due to structural damage**

In order to track the decay of the fundamental frequencies of the building due to seismic-induced structural damage, the EFM of the building has been excited with a base zero-mean Gaussian white noise of low intensity, postponed to the seismic input. This strategy allows simulating the pseudo-experimental ambient response of the structure, ruling out any possible influence of undesired frequency content of the seismic input. In particular, the identification algorithm involves the use of a common output-only identification technique, the Frequency Domain Decomposition (see Section 2.2.1), to keep track of the frequency decays of the first two translational modes of the building – T_x at $6.55\,\text{Hz}$ and T_y at
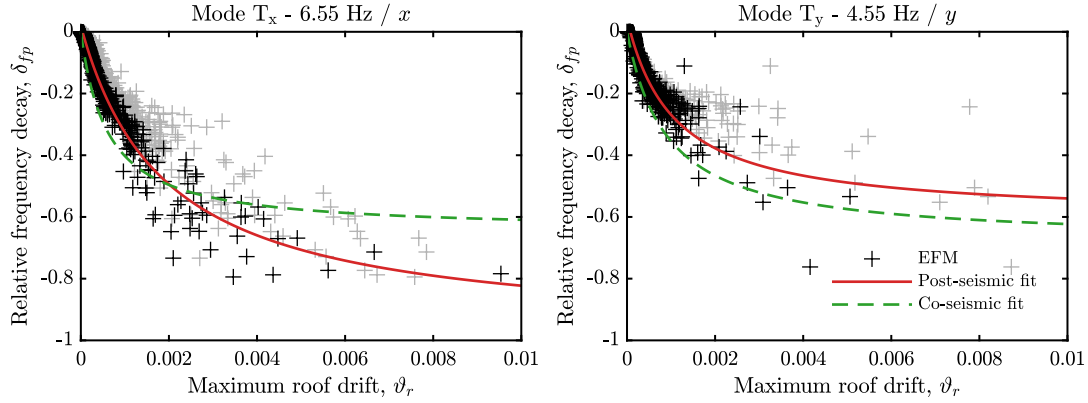
Figure 4.25: Post-seismic frequency decays δ_{fp} as a function of the maximum roof drift θ_r. Least-squares fitting of the rational polynomial 4.54. Grey crosses show the frequency behaviour with the interstorey drift ϑ_i.
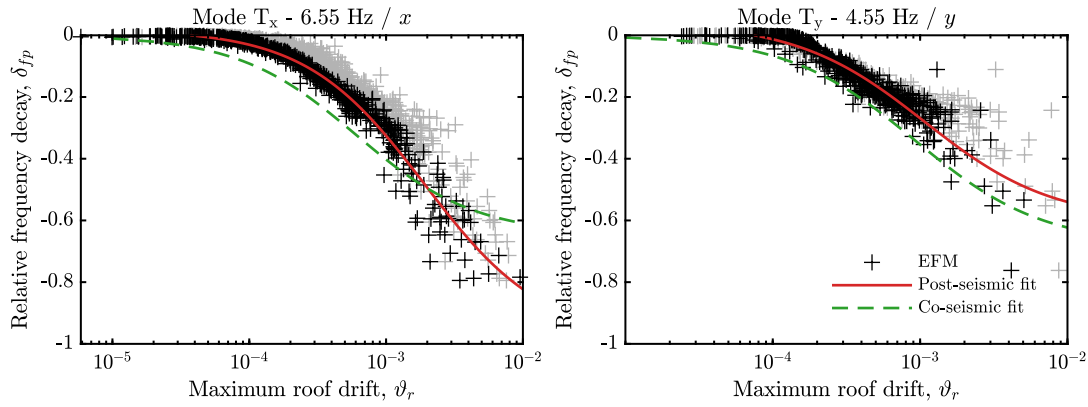
Figure 4.26: Log-lin magnification of the post-seismic frequency decays in the low-drift region, showing the initial absence of decay and the zero of the fitted polynomial (dashed red line). Grey crosses show the frequency behaviour with the interstorey drift ϑ_i.

$4.55\,\text{Hz}$ – at the end of the seismic event, checking the invariance of their mode shapes. This last and only requirement, on the one hand, allows the identified frequency decays to be associated with a particular mode and, on the other hand, ensure that only damage states that do not significantly alter the dynamic behaviour of the building are taken into account. In particular, this control is implemented verifying the correlation – MAC value – between the mode shapes of the undamaged and damaged state to be equal or greater than 0.8. The relative frequency decay of a mode is estimated according to Equation 5.1, where $\min(f_c(t))$ should be substituted by f_{post}, the decayed frequency of the mode identified post-seismic event.

A first representation of the frequency decay as a function of the maximum exhibited roof drift is reported in Figure 4.25. Indeed, the relative frequency variations are always

Table 4.12: Values of the parameters governing the *post-seismic frequency decay curves*, according to the EFM simulations on the Pizzoli town hall building.

| | Pizzoli EFM | |
	Mode T_x - $6.55\,\mathrm{Hz}$	Mode T_y - $4.55\,\mathrm{Hz}$
ϑ_0	3.754×10^{-5}	7.489e-05
c_1	0.0166	0.3975
c_2	19.45×10^{-4}	11.48×10^{-4}
$\frac{d\rho(\delta)}{d\delta}\big|_{\delta=0}$	-0.526×10^3	-0.600×10^3
RMSE	0.0291	0.0333

negative, as expected, according to a reduction in global stiffness due to structural damage, and their magnitude tends to increase nonlinearly with the maximum response. The identification procedure of the post-seismic decays is more robust than the time-frequency analyses employed to identify the co-seismic shifts (Section 5.2.2) – thanks to the time-averaging approach employed in the spectral density estimation – as confirmed by the lower variability of data. Moreover, as physically reasonable, the decays follow an initial horizontal slope such that, for very low drifts – thus for negligible damage – no frequency decay occurs (Figure 4.26). In this respect, a tentatively rational model to fit the data – as the shifted version of 5.3 employed for the co-seismic shifts, Section 5.2.2 – can be assumed to be

$$\delta_p(\vartheta) = \frac{(\vartheta - \vartheta_0)(c_1 - 1)}{\vartheta - \vartheta_0 + c_2}, \quad \vartheta, \vartheta_0 \geq 0 \tag{4.54}$$

in which ϑ_0 represents the zero of the function, i.e. the lower drift limit for appreciable frequency decays. Even though, along the y direction, the no-decay interval is wider in terms of achievable roof drifts, the stiffness decay appears much more rapid. The RMSE parameter, representing the goodness of the fit (Table 4.12), suggest the considered model be a good estimator of the frequency decay. Nevertheless, in this case, the behaviour in the two directions is quite different for mid-to-high drifts, as shown by the different asymptotic values of the fit (Table 4.12). In this range, the general lack of valid decays for the mode T_y comes as no surprise, given the lower resistance and less ductile behaviour of the structure already observed from the pushover curve in this direction (Figure 4.11) leading to fragile behaviours (with sudden changes in the corresponding mode shape). Indeed, higher-order polynomial functions could be employed to give a more accurate representation of the rapid change of curvature in the y-direction, with the drawback of being governed by a higher number of parameters.

A model-based *frequency-decay damage control chart* of the building exploiting ambient vibrations

Knowing an estimate of the post-seismic fundamental frequency decay δ_{fp} of the first two translational modes as a function of the maximum roof drift ϑ_r in the corresponding direction (Section 4.4.1), as well as having established the model-based damage assessment framework for the equivalent frame model idealization (Section 4.4), it is possible to build
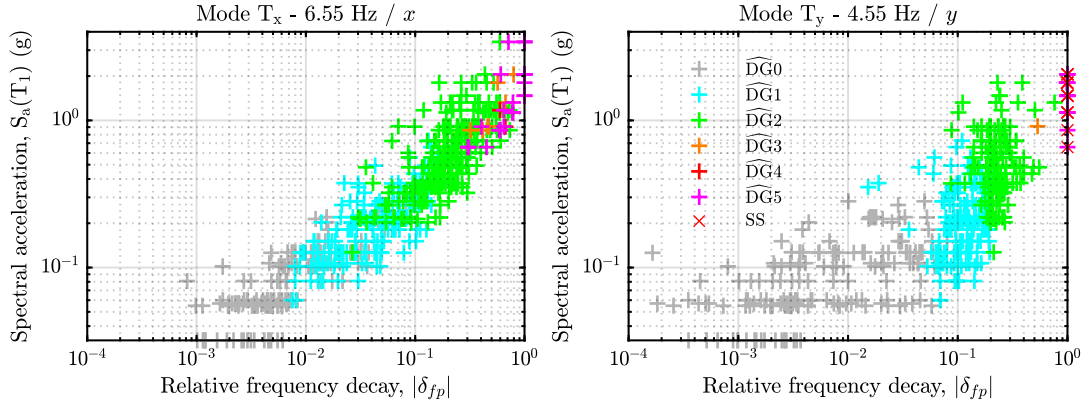
Figure 4.27: Post-seismic fundamental frequency decays δ_{fp} for stripes of seismic inputs with increasing spectral acceleration $S_a(T_1)$, as simulated by nonlinear dynamic analyses on the EFM of the Pizzoli town hall building.

the *frequency shift-damage control chart* of the building. This representation, conceived as a tool supporting the decisional process on the performance of the building in the post-earthquake scenario, associates the measured physical quantities coming from experimental data – in this case, frequency decays and/or maximum roof drifts – to the EDP represented by the model-driven grade of expected global damage. If the maximum roof drift exhibited during the earthquake can be measured – for example, in permanently monitored buildings – or, similarly, a permanent frequency decay is identified after the seismic event – again, exploiting SHM or repeated ambient vibrations tests – the control chart provides a rough but immediate probabilistic estimation of the structural damage to be expected on the structure, both in terms of seriousness and extension.

Before tackling the probabilistic interpretation of data, the one-to-one direct association of frequency decays with the corresponding grade of global damage highlights a first issue. Even though increasing intensities of the seismic event are able to produce increasing levels of damage and corresponding frequency decay (Figure 4.27), there are few samples characterized by moderate-to-heavy damage grades (i.e. higher than $\widehat{\mathrm{DG}}3$, Table 4.13). More importantly, some of them – i.e. $\widehat{\mathrm{DG}}5$, the one circled in purple on the left side of Figure 4.28 – seem to be not coherently described by the corresponding identified frequency decay. This drawback was somehow expected, since the identified decays – belonging to translational modes – should be considered representative of the dynamic behaviour of the structure in the corresponding direction, rather than globally. To be more specific, as already highlighted, these issues are related to a more fragile structural behaviour of the structure in the y direction – characterized by squat piers – leading rapidly to high levels of wall damage and/or to the activation of soft-storey mechanisms. Such conditions produce, respectively, very significant variations of the mode shape and/or uncontrolled drifts with complete frequency decays, so that the frequency-tracking of the representative mode loses its practical significance (Figure 4.29). Nevertheless, a frequency decay is still measurable in other modes which, however, cannot be considered representative of the occurred damage.
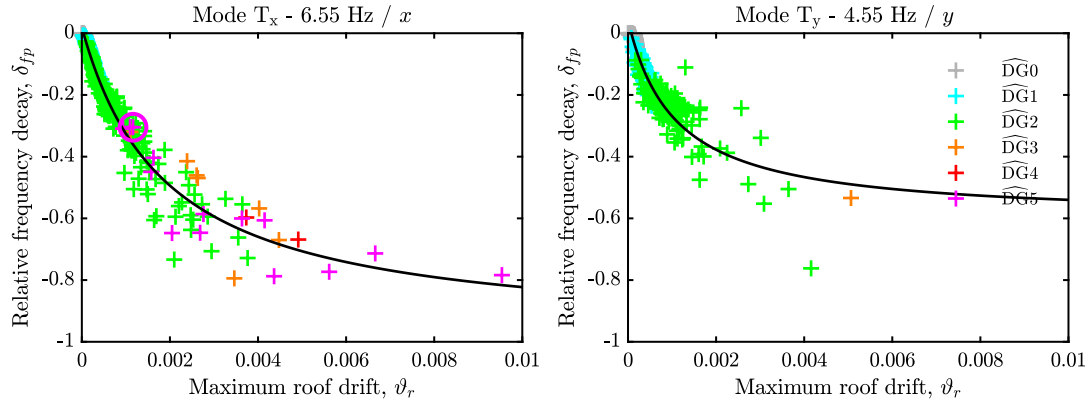
Figure 4.28: Post-seismic frequency decays of the first two translational modes δ_{fp} and associated grade of global damage $\widehat{\text{DG}}$ in the two main directions of the building, as estimated by nonlinear multiple stripe analysis on the calibrated equivalent frame model of the Pizzoli town hall. The circled mark on the left refers to the damage state shown in Figure 4.29.
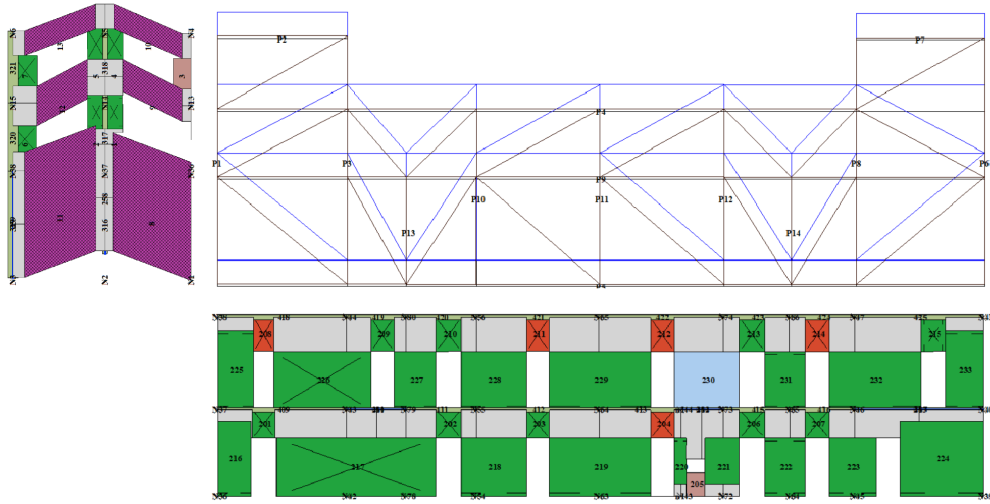
Figure 4.29: Seismic-induced damage state of the Pizzoli town hall building due to an earthquake with spectral acceleration $S_a(T_1)$ equal to 0.6580 g. The seismic excitation produces, in this case, a global damage grade $\widehat{\text{DG}}5$, a fundamental frequency decay of the translational mode in the x direction of around $-30\,\%$ (Figure 4.28), the activation of a storey mechanism in the y direction.

These drawbacks can be partially overcome considering only damage states which, at the same time, (i) respect the mode shape criterion and (ii) avoid the soft-storey mechanisms in both the modes and directions. This choice, which has been followed in the thesis, leads to very few samples exhibiting a damage grade $\widehat{\text{DG3}}$ and zero samples exhibiting higher damage grades, so that their probabilistic characterization becomes pointless. From a practical perspective, nevertheless, the employment of experimentally based control charts is more relevant to discriminate between states of low damage, rather than to identify the occurrence of high damage – which could be easily characterized by in situ observations as well. Furthermore, the cases of low-to-medium damage are those in which, following the building inspection, it may be more difficult to correctly judge the practicability of the structure and its response to aftershocks. In this respect, being known the residual load-bearing capacity of the building to horizontal actions as well as plausible damage scenarios, the proposed chart could provide useful support to the damage interpretation carried on the field.

Assuming the (absolute values of) frequency decays to be lognormally distributed (Table 4.14) – as commonly adopted in the elaboration of fragility curves, Simões et al., 2020 – the cumulative distribution functions can be interpreted as the probability that a certain damage state is reached or exceeded, given a measured frequency decay. This representation, together with the frequency-roof drift relationship, form the proposed *frequency decay-damage control chart* of the building (Figure 4.30). If the decay in the fundamental frequency of the translational modes is detected after the earthquake, the chart provides a probabilistic expectation of the global damage grade of the building. It is understood that, given the assumptions underlying the proposed AV-based control chart (Section 4.4.1, the frequency decay should be (i) resulting from structural damage only and (ii) identified checking the invariance of the corresponding mode shape (MAC ≥ 0.8). The first point implies that any other factor that could influence the frequency variation – such as ambient effects, phenomena of slow recovery etc. – is modelled or ruled out *a priori*. Otherwise, another unaffected EDP should be employed (for example, the maximum roof drift). Regarding the second point, further improvements could be addressed to the integration of MAC variations in the control chart, even though their identification from experimental measurements is commonly more sensitive to noise and, thus, less effective. The resulting relationship between roof drift and damage grade (Table 4.14 and Figure 4.30) appears to be comparable with previous scientific contributions related to masonry buildings (and referring to the interstorey drift as EDP, Calvi, 1999; Hazus, 1999). In particular, the serviceability limit, i.e. $\widehat{\text{DG3}}$, is expected to be reached for drifts between 2.5×10^{-4} and 5×10^{-4}, in accordance with the value of 3×10^{-4} suggested by these studies and code recommendations. On the other hand, the frequency decays seem to be overestimated along x in the high-drift range, based on the expectations from the corresponding drifts and damage grades. This outcome, requiring further investigations, could be influenced (i) in the first case, by the unbalance between roof drift and interstorey drifts (shown in Figures 4.25, 4.26), (ii) in the second case, by a general tendency of the EF formulation to overestimate the diffusion of damage (Brunelli et al., 2020) and (iii) finally and more in general, by aliasing phenomena in the numerical solution (depending, for example, on the time resolution assumed for the nonlinear dynamic analysis) and in the identification procedure. A further comparison with full-scale experimental tests and laboratory results – in terms of co-seismic shifts – is reported in Section 5.2.2.

A simple validation of the chart is pursued indirectly, exploiting the maximum drifts measured on the structure during the seismic event of 18 January 2017 (Figure 4.23). The chart provides a high probability expectation for slight damage, i.e. damage grade $\widehat{\mathrm{DG}}1$ and a more contained probability (less than $40\,\%$ in both directions) to reach a moderate damage state $\widehat{\mathrm{DG}}2$, in plausible accordance with the actual severity and extension of structural damage observed on the building (Section 3.3.1).
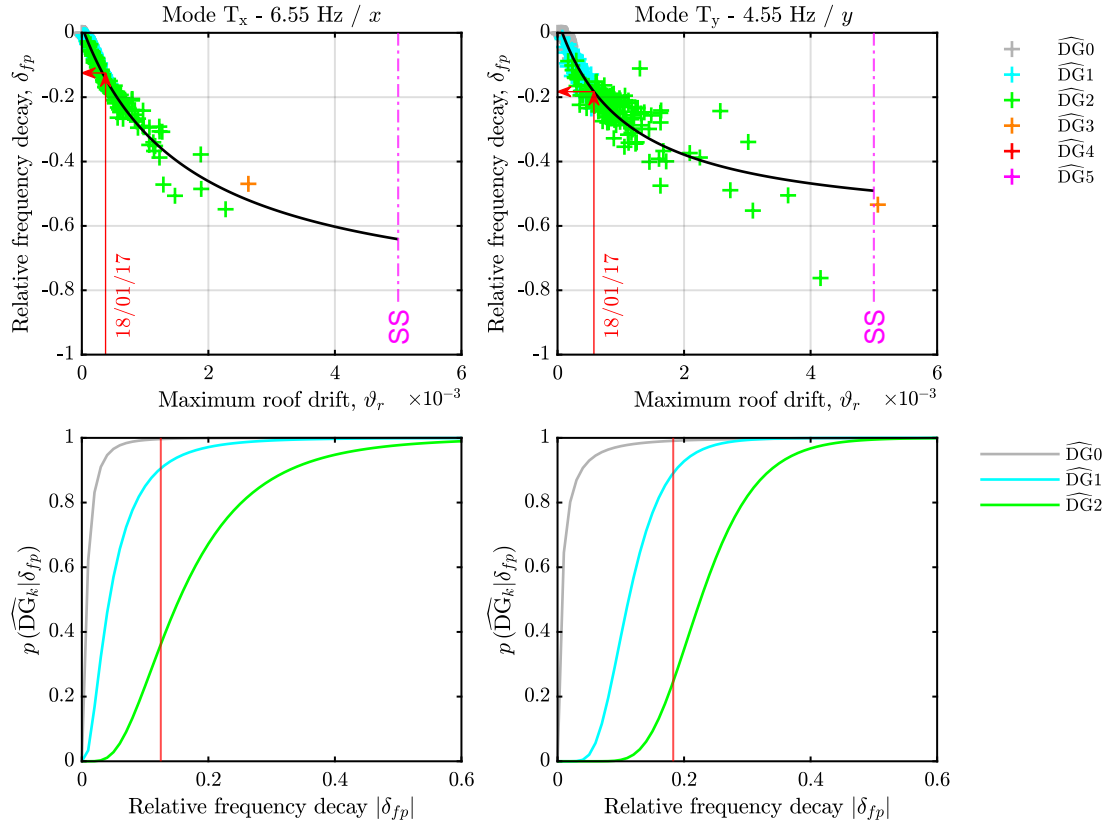
Figure 4.30: EFM-based *frequency decay-damage control chart* of the Pizzoli town hall building. The figure shows a simple roof-drift based assessment of the expected damage state, employing the maximum recorded response of the building during the seismic event of 18 January 2017.

Table 4.13: Mean m and variance ν of the lognormal distribution of the spectral acceleration $S_a(T_1)$ (with $T_1 = 0.15s$, see Section 5.2.1), for each of the global damage grades $\widehat{DG0}$. The samples considered, in this case, are those satisfying the MAC criterion for both the modes in the two directions.

	x $S_a(T_1)$ (g)			y $Sa(T_1)$ (g)		
	samples	m	ν	samples	m	ν
$\widehat{DG0}$	164	0.2383	0.1664	164	0.2539	0.1266
$\widehat{DG1}$	215	0.2821	0.0591	199	0.3155	0.0893
$\widehat{DG2}$	294	0.5631	0.1216	158	0.4330	0.1729
$\widehat{DG3}$	7	0.7732	0.0676	1	0.4800	
$\widehat{DG4}$	2	0.9070	0	0		
$\widehat{DG5}$	24	0.7047	0.0435	15	0.6353	0.1110

Table 4.14: Mean m and variance ν of the lognormal distribution of post-seismic fundamental frequency decay $|\delta_{fp}|$ and roof drift ϑ_r, for each of the global damage grade $\widehat{DG}$.

	samples	Mode T_x - 6.55 Hz / x $|\delta_{fp}|$		ϑ_r / x		Mode T_y - 4.55 Hz / y $|\delta_{fp}|$		ϑ_r / y	
		m	ν	m	ν	m	ν	m	ν
$\widehat{DG0}$	164	0.013	3.33×10^{-4}	6.53×10^{-5}	2.65×10^{-9}	0.017	2.11×10^{-3}	1.25×10^{-4}	4.17×10^{-9}
$\widehat{DG1}$	199	0.061	3.32×10^{-3}	1.79×10^{-4}	1.27×10^{-8}	0.122	2.52×10^{-3}	3.52×10^{-4}	1.56×10^{-8}
$\widehat{DG2}$	156	0.246	2.72×10^{-2}	7.67×10^{-4}	4.35×10^{-7}	0.237	5.62×10^{-3}	9.28×10^{-4}	2.72×10^{-7}

Chapter 5

AV-based seismic serviceability assessment of masonry buildings: application of the *Seismic Model from Ambient Vibrations* (SMAV) to the Pizzoli town hall

The Seismic Model from Ambient Vibrations (SMAV) is a valuable solution to assess the seismic behaviour of existing buildings, thanks to its cost, time and computational efficiency. Nevertheless, from the scientific point of view, its reliability has not been extensively verified yet, especially with regards to masonry buildings. The purpose of the Chapter is to provide a first contribution in filling this knowledge gap, employing a detailed comparison with the results of the state-of-the-art approach, nonlinear dynamic analyses carried out on the calibrated equivalent frame model of the Pizzoli town hall building. The results highlight how SMAV leads to generally conservative predictions of the maximum seismic response, confirming its reliability in guiding the serviceability assessment judgement for existing buildings.

5.1 Overview

The *Seismic Model from Ambient Vibrations* (SMAV, Mori et al., 2015; Spina et al., 2019), developed in 2015 by the collaboration between the Italian Department of Civil Protection and the Italian National Research Council, is a simplified methodology to assess the seismic serviceability of existing buildings based on the experimental modal parameters identified from ambient vibration tests (Figure 5.1). To briefly recall the main characteristics of SMAV (Section 2.2.2), it is worth remarking that this approach, according to its *speditive*
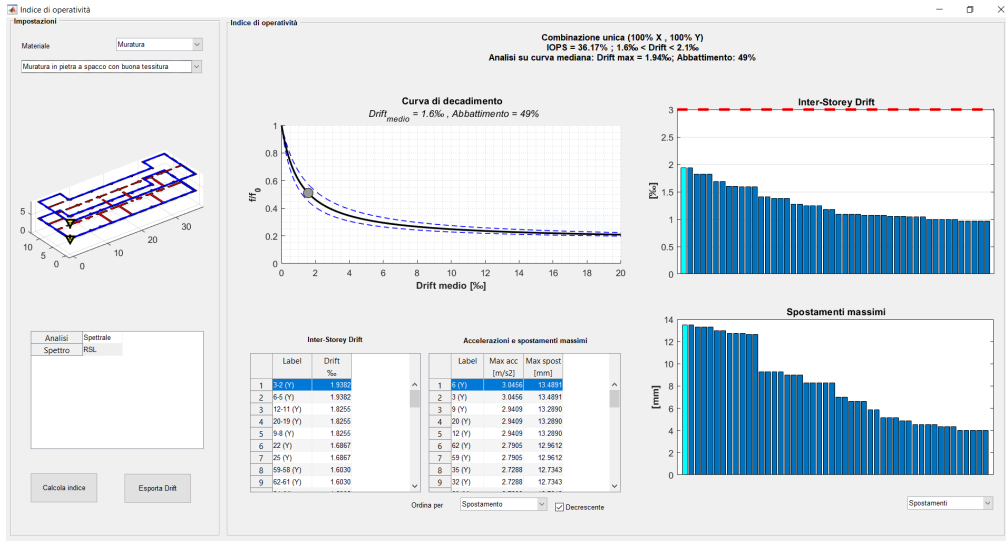
Figure 5.1: Example of the simplified SMAV serviceability assessment of the Pizzoli town hall building (stripe IM5 of Rome), provided by the VaSCO-smav program (Acunzo et al., 2015).

(efficient, rapid) nature, is based on the simplifying assumption of floor *rigid-diaphragms* (Section 2.1.2), which allows building a complete modal model of the building – in engineering terms, to recover the mass participation factors required for the seismic response estimation – referred to the experimental modes identified from ambient vibration data. The seismic assessment, limited to the serviceability limit state, is carried out through a linear-equivalent dynamic analysis with *frequency shift curves* (Spina et al., 2019), specifically developed to take into account the nonlinear behaviour of masonry structures during the earthquake (which have been briefly discussed in Section 2.2.2).

In this thesis, some tools have been developed, based on the experimental dynamic behaviour of deformable diaphragms, to verify qualitatively and quantitatively the compliance with the rigid-diaphragm assumption (in Sections 4.3.1,4.3.2). Conversely, from the seismic assessment point of view, the reliability of the linear technique adopted by SMAV – i.e. (operational) modal superposition with response spectrum and frequency shifts – requires further validations, in particular for masonry buildings. This structural typology, as discussed in Section 1.2, is characterized by the tendency to exhibit nonlinear behaviour for low intensities of the seismic event, so that the employment of a linear analysis technique could lead to inaccurate seismic predictions.

Due to the high vulnerability of masonry buildings, which was again remarked by the recent earthquakes (Oliveira, 2003; Lagomarsino, 2012; Cattari et al., 2014b; Sorrentino et al., 2014), nonlinear models are essential for accurate and reliable seismic assessments. Linear methods have been employed in the literature to study the seismic response of complex masonry buildings (Cattari & Lagomarsino, 2012; Lagomarsino et al., 2020) and historical monuments (Gattulli et al., 2013) although, in the last decades, the research field mainly directed his efforts towards nonlinear methods. Thanks to the scientific and technological advancements, the assessment procedures based on nonlinear static analyses

(Freeman, 1998; Krawinkler & Seneviratna, 1998; Fajfar, 1999; Magenes, 2000; Chopra & Goel, 2002; Galasco et al., 2004; Galasco et al., 2006) and nonlinear dynamic analyses (Vamvatsikos & Cornell, 2002; Lagomarsino et al., 2007; Baker, 2013; Mouyiannou et al., 2014; Lagomarsino & Cattari, 2015a; Lagomarsino & Cattari, 2015b) are more and more frequently employed, the second being considered the most reliable approach today available to simulate the seismic response of masonry buildings. It is undoubted that the employment of nonlinear dynamic analyses still presents some issues, in the proper definition of a representative seismic input, in the formulation of representative constitutive laws for masonry (Penna et al., 2013). On the other hand, exploiting the low computational requirements of the Equivalent Frame Model (EFM, Section 2.1.1), this analysis technique appears the right candidate for extensive validation of the SMAV methodology (Section 5.2).

In particular, among the other possibilities (Section 4.4.1), the multiple-stripe analysis (MSA, Jalayer, 2003) approach has been selected as the proper simulation framework. The MSA is a nonlinear dynamic analysis method involving *stripes* of response values, which are obtained subjecting a structural model to a set of ground motion records scaled to increasing levels of spectral acceleration. In particular, each stripe is representative – in an average spectral sense – of a seismic event of a fixed return period. This is the reason that motivated the choice of this analysis technique, given that each stripe intrinsically provides a suitable seismic input for the response spectrum approach adopted by SMAV. The analysis results allow estimating the distribution of one (or more) Engineering Demand Parameters (EDPs) for increasing seismic actions experienced by the structure. To this aim, the simulations employ the natural accelerograms selected in the RINTC (The Implicit Seismic Risk of Code-Conforming Structures) Project between 2015 and 2017 (Iervolino et al., 2018; Iervolino & Dolce, 2018; Workgroup, 2018), in which five Italian sites, ten return periods of the seismic event and two soil conditions were considered to span a wide range of seismic hazard levels within the country. This set of seismic inputs has been employed in the framework of other research studies addressing the solution of nonlinear dynamic analyses on equivalent frame models, confirming the reliability and computational efficiency of this modelling approach (Camilletti et al., 2017; Cattari et al., 2018b). In particular, only four sites (Milan, Rome, Naples and L'Aquila) and the rock soil condition were considered in the following analyses.

In the pre-processing phase, the earthquakes accelerograms have been cut, filtered and de-sampled for computational efficiency purposes (Section 5.2.1). The equivalent frame model of the Pizzoli town hall, a permanently monitored masonry building (Section 3.3.1), has been calibrated in the linear regime in terms of natural frequencies, mode shapes and diaphragm shear stiffness – based on the experimental ambient vibration data – and validated in the nonlinear regime – based on the measured structural seismic response and observed damage, Section 4.5.2. The model has been employed to deduce the time-history seismic response of the building. In the post-processing phase, besides extracting the proper EDPs for comparison purposes, the time-frequency analysis of the simulated seismic response allowed to identify the co-seismic frequency shifts of the building, validating those proposed by SMAV (Section 5.2.2).

According to the *speditive* nature of the SMAV methodology, the seismic input has been redefined in terms of the average pseudo-acceleration response spectra of each seismic stripe (Section 5.3.1). The Multi Rigid Polygons (MRP) model of the structure has

been built based on the observed experimental behaviour of floor diaphragms, assessing its sensibility to finer polygon discretization (Section 5.3.2). Employing the linear dynamic analysis with frequency shift curves, the expected maximum response of each stripe has been estimated according to SMAV. Finally, referring to a representative demand parameter – the maximum interstorey drift ratio – the results of the simplified SMAV methodology have been compared to the predictions of the nonlinear dynamic analyses carried out on the calibrated EFM, assumed as a reference (Section 5.4), discussing their reliability for increasing nonlinearity, i.e. for higher levels of structural damage.

5.2 Nonlinear dynamic analyses on the calibrated equivalent frame model

5.2.1 Definition of the seismic input

The analyses are performed considering all the available Intensity Measures (IMs), i.e. return periods of the bedrock seismic action (ranging from 10 to 100000 years, Table 5.1) in four – Milan, Rome, Naples and L'Aquila – of the five sites originally selected in the RINTC project. In particular, each return period corresponds to a so-called *stripe*, a set of 20 bi-directional natural accelerograms properly scaled to be compatible on average, at a fixed structural period T_1, with the spectral acceleration $S_a(T_1)$ resulting from the probabilistic seismic hazard study at the site. Further details about the accelerograms selection and the spectral compatibility requirements can be found in Iervolino et al., 2018. For the purposes of this study, the reference period T_1 is selected to be 0.15 s, consistently with the fundamental natural periods of the Pizzoli town hall buildings (around 0.22 s and 0.152 s for the first two translational modes respectively, see Section 3.3.1).

To optimize the computational efficiency of the simulations, the natural earthquake signals are pre-processed according to the following scheme

- removal of leading and trailing zeros, scaling;

- low-pass filtering and decimation (respectively from $200/125/100/80$ Hz to $50/62.5/50/40$ Hz, top of Figure 5.2);

- cutting:
    - start of the event: picking of the first arrival t_{fa} according to a short-time average/long-time average (STA/LTA) algorithm (as the mean contribution of the two components, middle of Figure 5.2);
    - end of the event: t_{99} corresponding to 99% of the earthquake Arias Intensity I_A (as the total contribution of two components, bottom of Figure 5.2);

- estimation of the acceleration response spectra from the raw and processed earthquake signals (Figure 5.3)

The first three points are mainly addressed to reduce the computational effort of the analyses. For what regards the seismic event detection, in particular, the starting trigger corresponds to STA/LTA ratio equal to or greater than 2, with a short time average of 1 s
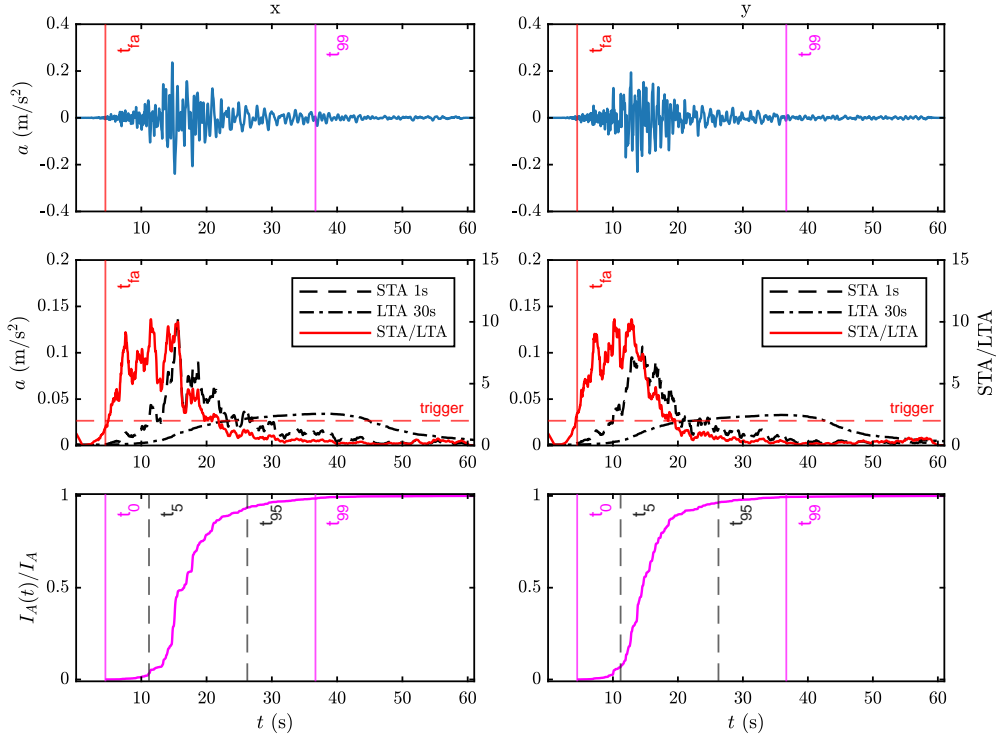
Figure 5.2: Example of application of the short-time average/long-time average (STA/LTA) algorithm and estimation of the Arias Intensity I_A for the event extraction. Each column represents one of the two orthogonal components of the earthquake, assumed to act (randomly) along the x and y direction of the building.
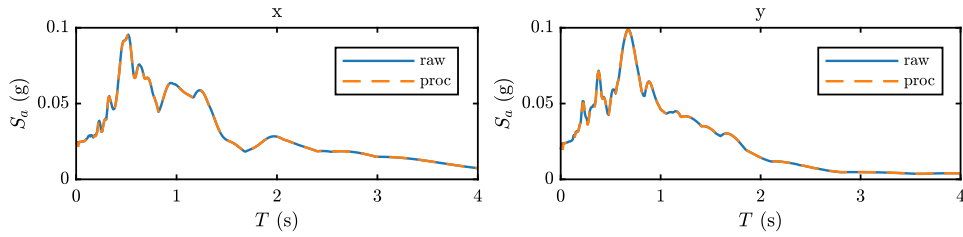
Figure 5.3: Example of the comparison between the acceleration response spectra (viscous damping $\zeta = 0.05$) obtained from the raw and processed earthquake signals.

over a long time average of 30 s. Defining the end of the event on the basis of a fraction of the total energy carried by the earthquake ensures most of its dynamic contribution to be taken into account. The last point, involving the comparison between the 5 %-damped acceleration response spectra – according to a maximum deviation criterion in the period interval 0.1 s-2 s – of the raw and processed earthquake signals, ensures the filtering, decimating and cutting operations are not substantially modifying the spectral content of the seismic event.

Table 5.1: Return period T_r and compatible spectral acceleration $S_a(T_1)$ at $T_1 = 0.15s$ of each IM-stripe considered in the Multiple Stripe Analysis (MSA) framework, for the four selected sites (bedrock soil condition).

	T_r	$S_a(T_1)$ (g)			
		Milan (MI)	Rome (RO)	Naples (NA)	L'Aquila (AQ)
IM1	10	0.032	0.060	0.055	0.0107
IM2	50	0.057	0.127	0.127	0.22
IM3	100	0.081	0.203	0.219	0.352
IM4	250	0.102	0.282	0.322	0.493
IM5	500	0.126	0.375	0.434	0.658
IM6	1000	0.151	0.480	0.560	0.858
IM7	2500	0.181	0.602	0.728	1.132
IM8	5000	0.214	0.725	0.907	1.471
IM9	10000	0.266	0.912	1.173	2.056
IM10	100000	0.373	1.323	1.806	3.417

Finally, the pre-processed signals are concatenated with a 100 s length zero-mean Gaussian white noise of low intensity (Figure 4.4), uncorrelated along the two components. This strategy, proposed in Section 4.4.1, allowed to evaluate – through a post-earthquake pseudo-experimental modal identification, Section 2.2.1 – the decay of the fundamental frequency of the building due to structural damage, leading to the development of the *frequency-decay damage control chart* of the building (Section 4.5.2).

5.2.2 Identification of the co-seismic fundamental frequency shifts

The nonlinear time-history analyses have been solved employing the research version of TREMURI program adopting a Newmark integration method, assuming a Rayleigh viscous damping ζ equal to 0.03 for the first and fourth mode (Figure 4.21). Besides extracting other relevant EDPs, such as the maximum drifts and the global damage grade $\widehat{DG}$, the *co-seismic fundamental frequency shifts* have been identified through a time-frequency analysis of the nonstationary response of the building to the forced input. For this purpose, the responses along the two main directions x and y of the building at the roof level – as the average acceleration of the nodes pertaining to this level – have been considered representative of the dynamic response of the building, being dominated by the two main translational modes T_x at 6.55 Hz and T_y at 4.55 Hz, respectively (Section 3.3.1). The roof response has been band-pass filtered, for each direction, in a suited frequency interval around the main frequency content of the corresponding structural mode, taking into account possible relative frequency shifts up to -90% of their initial value. This strategy ensures the removal of low-frequency components associable with the earthquake, as well as of unwanted high-frequency components. Adopting this strategy, the response in each direction can be substantially considered a monocomponent process, thus the Hilbert transform can be employed to identify the instantaneous frequencies of forced vibrations
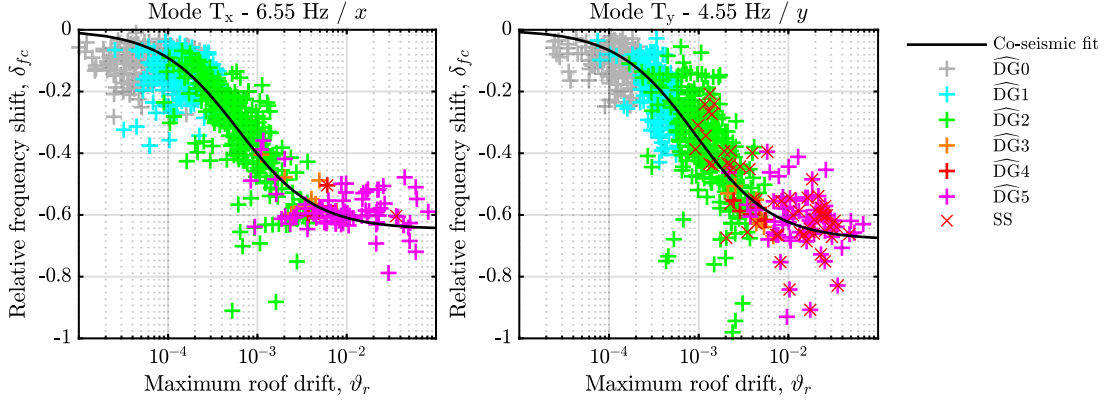
Figure 5.4: Co-seismic frequency shifts δ_{fc} of the translational modes in the two main directions and associated grade of global damage $\widehat{\mathrm{DG}}$, simulated by nonlinear dynamic analyses on the calibrated EFM of the Pizzoli town hall building. Least-squares fitting of the rational polynomial 5.3.

from the so-called *analytical representation* of the signal. Indeed, any other time-frequency technique – suited to follow the dominant frequency behaviour in time – could be employed for the task. The relative frequency shift δ_{fc} of each natural mode is estimated as

$$\delta_{fc} = \frac{\min\left(f_c(t)\right) - f_0}{f_0} \tag{5.1}$$

where f_0 and f_c represent respectively the natural frequency of the mode and the co-seismic instantaneous frequency – as the 5 s moving-average – identified during the earthquake. No particular restrictions are assumed for the possible values of δ_{fc}.

The identified frequency shifts have been related to a parameter representative of the global structural response of the building. Considering the amplitude dependence of the phenomenon, the EDP is selected as the maximum roof drift exhibited during the strong-motion phase. The maximum roof drift ϑ_r, along each of the main direction of the building, is simply estimated as

$$\vartheta_r = \frac{\max|d_r(t)|}{h} \tag{5.2}$$

as the ratio between the maximum (absolute value of the) average displacement of the roof nodes $u_r(t)$ and the total height of the building h, in each of the two main directions of the building. The results of the simulation (Figure 5.4) show how the frequency variation is always lower than unity, so that the minimum frequency of vibration reached during the earthquake is always lower than the natural frequency of the building, in accordance with the suggestions of the literature (Section 1.1). The data exhibit a nonlinear amplitude-dependent behaviour and seems to be affected by a significant dispersion, which appears more important for the translational mode T_y. Nevertheless, the response in the two directions shows an analogous trend (Figure 5.4), regardless of the more fragile nature of the structural system y direction (discussed in detail in Section 4.5.2). The shifts can be

131

Table 5.2: Values of the parameters governing the *co-seismic* frequency shift curves, according to SMAV for simple stone and to the EFM simulations on the Pizzoli town hall building.

| | SMAV | Pizzoli EFM | |
	simple stone	Mode T_x - 6.55 Hz	Mode T_y - 4.55 Hz
c_1	0.1655	0.3417	0.3576
c_2	11.00×10^{-4}	6.35×10^{-4}	8.19×10^{-4}
$\frac{d\rho(\delta)}{d\delta}\big|_{\delta=0}$	-0.755×10^3	-1.037×10^3	-0.784×10^3
RMSE		0.0944	0.0982
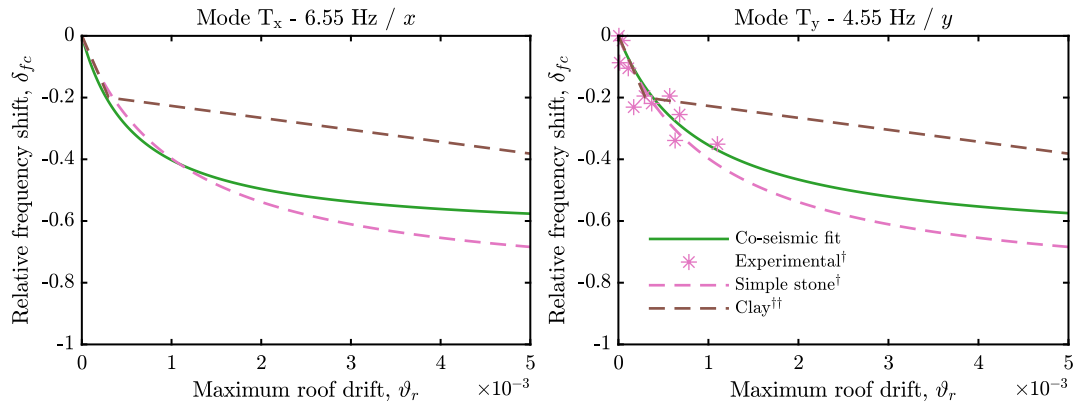
Figure 5.5: Comparison among the least-squares fitting of the EFM-simulated co-seismic frequency shifts of the Pizzoli town hall building, the actual experimental shifts identified during the Central Italy earthquake sequence of 2016, the median *frequency shift curve* for simple stone masonry employed by SMAV. † Reported in Spina et al., 2019.†† Reported in Michel et al., 2011 from the testing of a scaled building with clay masonry, as a function of the interstorey drift.

synthetically described – as proposed in Spina et al., 2019 – employing the linear/linear rational function model

$$\delta_c(\vartheta) = \frac{c_1\vartheta + c_2}{\vartheta + c_2} - 1 = \frac{\vartheta(c_1 - 1)}{\vartheta + c_2}, \quad \vartheta \geq 0 \tag{5.3}$$

where c_1, c_2 are the parameters to be fitted. It should be noted, in particular, that the model assumes a value of unity for $\vartheta = 0$, such that to zero drift corresponds zero frequency shift. Moreover, $c_1 - 1$ represents the horizontal asymptote of the function, such that $\lim_{\vartheta \to \infty} \delta_c(\vartheta) = c_1 - 1$.

The nonlinear estimator, fitted to data in a least-squares sense, shows a similar ability to explain the frequency shifts in the two directions, as shown by the comparable values of the Root Mean Square Error (RMSE, Table 5.2). The fitted models are in good accordance both with (i) the experimental results coming from the measured response of the building to the Central Italy earthquake sequence of 2016 and with (ii) the *frequency shift curves*

proposed by Spina et al., 2019 and employed by SMAV (Section 2.2.2), referring to the median curve for the simple stone masonry typology which characterizes the examined building (Figure 5.5). The two models, however, tend to slowly diverge for higher drifts, as highlighted by the different heights of the horizontal asymptote c_1-1 (Table 5.2). Referring to the results of the laboratory testing of a scaled building with clay masonry (Michel et al., 2011), the EFM frequency shifts appear comparable in the low-drift range (less than 5×10^{-4}), but generally higher in magnitude in the high-drift range. The discrepancy, calling for further explorations of this matter, is surely influenced by (i) the different masonry typologies (simple stone and clay), (ii) the assumed EDP (roof versus interstorey drift, similarly to the behaviour shown by post-seismic decays, see Figures 4.25, 4.26) and, finally, (iii) possible aliasing effects related to the numerical solution and dynamic identification.

5.3 Linear-equivalent dynamic analyses with frequency shift on the multi rigid polygons model

5.3.1 General assumptions

The high-fidelity simulation framework for the seismic assessment of the Pizzoli town hall masonry building – based on nonlinear dynamic analyses on the calibrated equivalent frame model – has been properly formulated (Section 5.2), whereas a simplified approach according to SMAV – based on linear-equivalent dynamic analysis with frequency shift curves on the rigid polygon model – will be pursued in the following Sections, comparing the predictions of the two methodologies with the purpose of providing indications on (i) the reliability of SMAV for masonry buildings and (ii) its limits of applicability.

The intrinsic difference in the nature and purpose of the two methodologies requires the adoption of proper measures, to make their application consistent. Firstly, the Multi Rigid Polygons (MRP) model, despite maintaining its peculiar simplifications (Section 2.1.2), should be dynamically coherent to the calibrated EFM model of the Pizzoli town hall (Section 4.5.2). The experimental nature of the MRP and the dynamic calibration of the EFM model implicitly satisfy this requirement, as long as the storey masses of the two models are the same. Indeed, few inconsistencies in the mass distributions still remain, which are tied to different modelling hypotheses. In accordance with the MRP assumption of in-plane rigid-behaving diaphragms, only the first three experimentally identified modes – in which the storey diaphragms are rigid-behaving, according to their rigid rotations and shear strains PSD spectra 4.5.2 – are considered. This choice allows employing a single rigid-polygon discretization for the storey diaphragms, still accounting for most of the dynamic mass of the building. Nevertheless, the sensibility of the MRP to more refined rigid-polygon discretization has been further investigated (Section 5.3.1).

For what concerns the description of the nonlinear regime, it has been shown that the *frequency shift curves* adopted by SMAV (Section 2.2.2) are consistent with the co-seismic dynamic behaviour shown by the EFM in the numerical simulations (Section 5.2.2). In this sense, the amplitude-dependent frequency shifts proposed in Spina et al., 2019 for simple-stone masonry are comparable to the one exhibited by the EFM and governed – at the scale of structural elements – by the piecewise linear constitutive laws adopted for piers

and spandrels (Section 2.1.1). This result was not a foregone conclusion, since the curves currently adopted in the SMAV procedure have been developed from parametric analyses on single masonry panels, whereas those obtained in this Section refer to the global dynamic response of a complex three-dimensional model of a real structure. In this sense, despite the significant differences between the models adopted – especially in the scale of analysis: single element and whole building – their good agreement can be explained considering that the seismic behaviour of the Pizzoli town hall building is dominated by the in-plane response of thick masonry piers, with a secondary role played by spandrels (according to the low number of openings).

Finally, careful consideration should be addressed towards the definition of a seismic input form suited for the SMAV assessment. An immediate choice, ideal for comparison purposes, would be to employ the direct integration of the equation of motion 2.1.2) to carry out each of the analyses already solved through EFM simulations. This approach, indeed, would allow the direct employment of each of the bi-directional seismic inputs previously elaborated (Section 5.2.1), and the one-by-one comparison of the response predictions would form the desired statistic. However, this possibility does not reflect the fundamental concept underlying the SMAV procedure (Section 2.2.2), to be a simplified tool – born from the research but, in several aspects, also addressed to the practice engineering field – for the *speditive* (i.e. quick) serviceability assessment of strategic buildings. In this regard, such evaluation is commonly carried out employing the average response spectrum of a set of natural accelerograms, more than the set itself (Section 2.2.2). The use of the average response spectrum, on the one hand, reduces the effects related to the variability of the seismic input and, on the other hand, is a more robust concept for professionally oriented users, which could lastly rely – in absence of more detailed evaluations – on information provided by national codes.

The second perspective, which has been pursued in the thesis, motivated the choice of the MSA framework, being each of the *stripes* representative – in an average sense – of the response spectrum at the site for increasing intensity of the seismic event. Accordingly, the SMAV seismic input is selected as the average 5 %-damped pseudo-displacement response spectrum of each stripe, which is composed of 20 bi-directional natural accelerograms related to an increasing Intensity Measure (IM). The average spectrum of the stripe is evaluated for each of the two orthogonal direction – maintaining the (randomized) orientation of horizontal components assumed for each event in the previous analyses – and applied accordingly. On the EFM side, following the same strategy, the maximum response predicted by each simulation has been averaged along each stripe, to allow a direct comparison between the two approaches.

5.3.2   Sensibility to the rigid-polygon discretization

It may be worth recalling that the SMAV procedure, adopting the so-called multi rigid polygon model (MRP, Section 2.1.2), is able to bypass the common impossibility to recover a complete modal model of the building from output-only measurements, i.e. to obtain mass-normalized mode shapes. To this purpose, the model assumes that each floor diaphragm – or portion of it – behaves in the plane as one or more rigid bodies of known mass, according to its experimental dynamics. This simplification, indeed, allows building
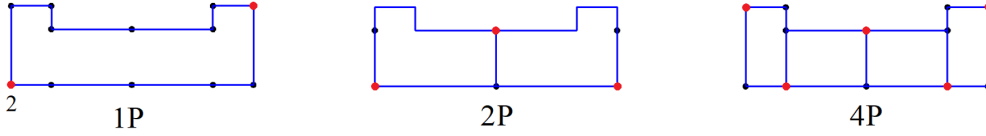
Figure 5.6: Simulated measurement configurations (red dots) for finer Multi Rigid Polygon (MRP) discretization of the Pizzoli town hall building, with one (1P), two (2P) and four (4P) rigid polygons.

a reduced-order mass matrix of the structure and to recover the modal participation factors of each mode, which are employed to estimate the seismic response in the assessment phase (Section 2.2.2). Indeed, in complex-shaped buildings or in presence of deformable diaphragms, finer discretization of the floors in rigid-behaving portions ensures more reliable estimations of the modal masses. On the other hand, since two bi-axial measurements for each polygon are required to recover its translational and rotational motion, this is reflected in a larger number of sensors required, raising considerably the efforts of vibrations tests. It is clear that errors in the identification of the modal participation factors directly reflects on the computation of the seismic response, thus on the reliability of the serviceability assessment.

Given these motivations, to better understand the effect of choosing different rigid-polygon discretization and the potential influence of the diaphragm deformability, different configurations of the MPR have been built, comparing the identified effective mass ratios with those estimated with the calibrated EFM of the building. In particular, due to the few sensors employed at each floor to monitor the dynamic behaviour of the structure (Section 3.3.1), the EFM has been employed to generate pseudo-experimental mode shapes, simulating three different measurement setups corresponding to as many rigid-polygon discretizations. The configurations named 1P, 2P, 4P account for one, two and four rigid polygons and require two, three and five bi-axial sensors respectively (Figure 5.6). As shown by the comparison with the EF model (Table 5.3), the rough 1P discretization generally tends to overestimate the mass ratios of about 10 %. Indeed, one rigid polygon is not sufficient to capture the behaviour of the fourth mode involving the bending deformations of the diaphragms (Section 3.3.1). The 2P and 4P models, on the other hand, seem to provide more reliable results, improving the estimation of the first mode mass ratio and succeeding in describing the fourth mode. Further results, related to the Sanremo town hall building tested in the framework of the SMAV Project in Liguria Region, Northern Italy (Section 3.1), are reported in Sivori et al., 2020a.

5.4 Results and comparisons

The outcomes of the simplified SMAV seismic analyses (Section 5.3), obtained through the VaSCO-smav program (Acunzo et al., 2015), are compared to the results obtained by the nonlinear dynamic analyses carried on the calibrated EFM of the building with TREMURI program 5.2. The Engineering Demand Parameter (EDP) chosen as representative of the seismic response, in accordance with the one assumed in the SMAV assessment (Section 2.2.2), is the maximum interstorey drift ratio ϑ_i. It should be remarked that the estimates

Table 5.3: Effective mass ratios estimated for the Pizzoli town hall building from the calibrated Equivalent Frame Model (EFM) and the Multi Rigid Polygon (MRP) model for finer rigid-polygon discretization.

| | | | EFM | | MRP | | | | | |
| | | | | | 1P | | 2P | | 4P | |
Modef (Hz)		Type	$\mathcal{M}_x$	$\mathcal{M}_y$	$\mathcal{M}_x$	$\mathcal{M}_y$	$\mathcal{M}_x$	$\mathcal{M}_y$	$\mathcal{M}_x$	$\mathcal{M}_y$
1	4.55	T_y	0	0.85	0.01	0.97	0	0.91	0	0.90
2	5.70	R	0	0	0	0	0	0.01	0	0.01
3	6.55	T_x	0.89	0	0.99	0	1.00	0	0.99	0
4	9.05	B	0	0.05			0	0.08	0	0.09
			0.89	0.9	1.00	0.97	1.00	1.00	0.99	1.00

of SMAV refer to the maximum response of the structure to the average seismic input – the average response spectrum – of the IM-th stripe. Conversely, in the case of the simulations carried out with the EFM (top of Figure 5.7), the parameter representative – in an average sense – of the response to the stripe is selected as the average of the maximum drifts caused by each seismic event belonging to a stripe (bottom of Figure 5.7). The results of the EFM simulations show a significant variability of the estimated maximum interstorey drift with respect to the spectral acceleration measure. Even though the choice of the most appropriate IM to reduce the variability of the EDP – relevant in the estimation of the average response spectra, Section 5.2.1 – has not been further investigated, a hint about the source of such variability comes from Figure 5.5. The reason could be linked to the nonstationarity of the modal parameters of the structures, such as the first fundamental period T_1 which co-vary during the analyses, not explicitly accounted for in the spectral response estimation.

To keep the discussion concise, the results obtained for both the main directions of the building are initially discussed regardless of their potential site dependence. The predictions of the SMAV simplified methodology – assuming the drifts resulting from the nonlinear dynamic analyses as reference results – shows (i) an overestimation of the maximum response in the x direction and (ii) a general intensity-dependent trend, more evident in the y direction (bottom of Figure 5.7). A linear-scale representation of the average IM-drifts predicted by the two methodologies, specified for each of the selected sites, further clarifies this statement (Figure 5.8). The simplified assessment seems to provide conservative estimations of the maximum response up to spectral accelerations of around 0.5 g, regardless of the site-variability of the seismic input. Such intensity is greater than the maximum considered for Milan and corresponds, roughly, to return periods of the seismic event of 500 years – IM5/6 – in Rome and Naples, of 250 years – IM4 – in L'Aquila (Table 5.1).

The trend is confirmed by the relative difference between the EFM and SMAV predictions, represented as a function of the recurrence intervals (Figure 5.9). The relationship with the IM-average global damage grade of the structure exhibited by the computational model (Section 4.4.3) highlights the potential source of such a difference. The predictions of SMAV appear in favour of safety when a slight-to-moderate level of global damage ($\widehat{DG2}$)
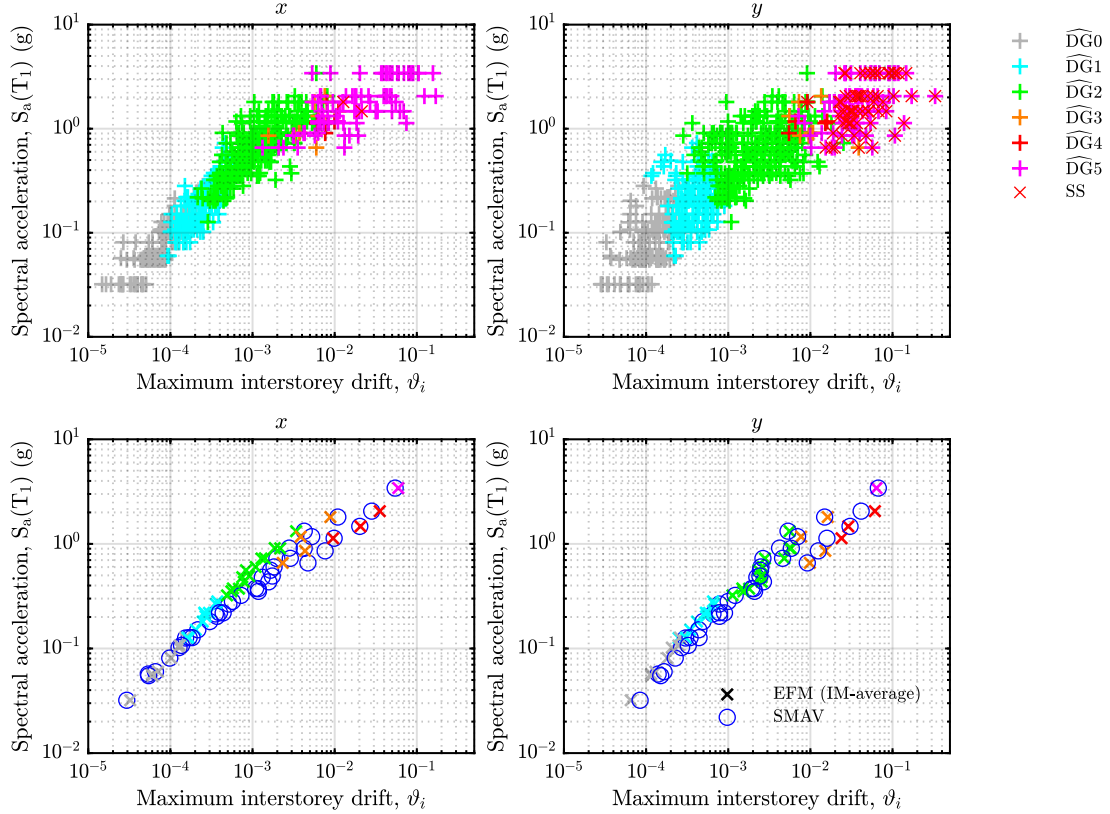
Figure 5.7: Top: maximum interstorey drift ratio ϑ_i in the two main directions estimated by nonlinear dynamic analyses on the EFM of the Pizzoli town hall building, related to the average spectral acceleration $S_a(0.15 \text{ s})$ of each stripe and the global damage grade $\widehat{\text{DG}}$. Bottom: averages of the maximum drift and damage grade achieved by each IM-stripe, compared with the response spectrum-based SMAV estimates.

is expected. For higher damage grades, conversely, the simplified assessment tends to lose its reliability, providing underestimated predictions of the maximum seismic response of the structure. This drawback can be interpreted as the decreasing ability in providing an accurate description of the structural behaviour in the nonlinear regime. This fact, indeed, is not surprising, considering the underlying linear-equivalent approach adopted by the methodology.

For what concerns the deterministic estimation of the maximum response, at least in this specific case, the SMAV methodology is expected to provide conservative predictions for intensities of the seismic event producing a linear elastic behaviour of the structure, up to those producing a slight-nonlinear anelastic behaviour, i.e. for moderate levels of structural damage. Nevertheless, this expectation seems in accordance with the scope of SMAV, which is primarily addressed to the serviceability assessment of existing buildings. According to the provisions of the Italian NTC 2018, the return periods commonly adopted in the SMAV framework are 100 years and 475 years, which correspond respectively to (i)
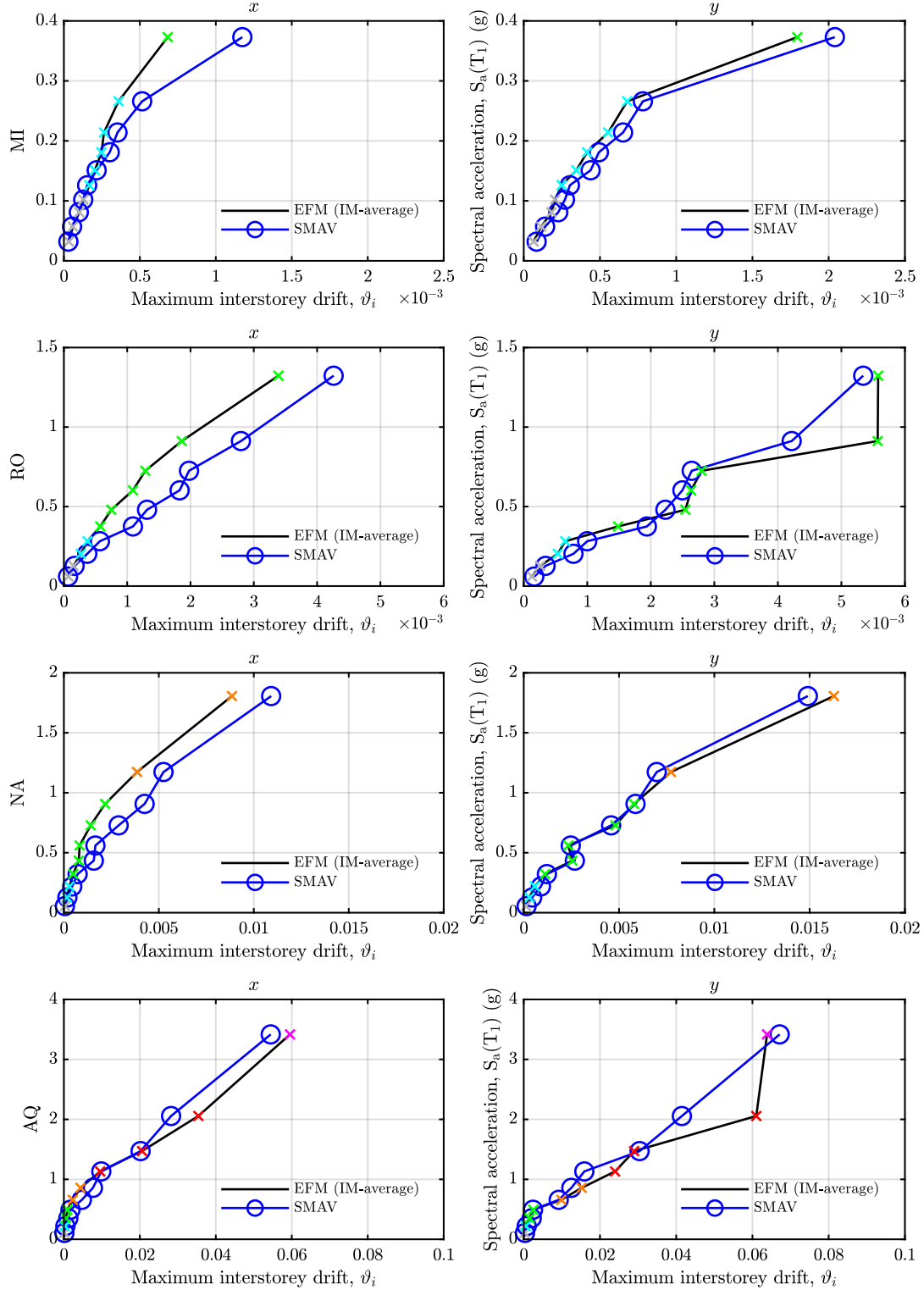
Figure 5.8: IM-average maximum interstorey drift ratio compared with the SMAV predictions for each considered site (Milan MI, Rome RO, Naples NA, L'Aquila AQ). The colours of the crosses represent the average global damage grade $\widehat{\mathrm{DG}}$ (see Figure 5.7) produced by the stripe.
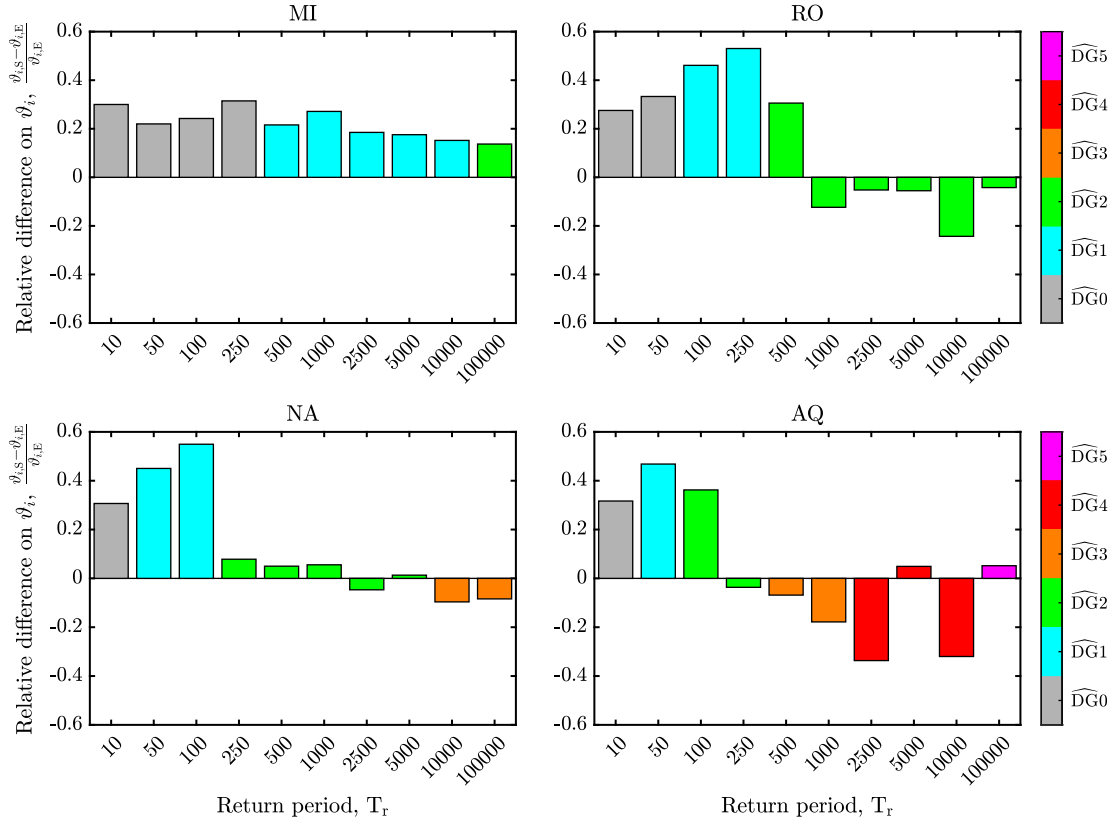
Figure 5.9: Relative difference in the maximum interstorey drift δ_i estimated by (E) non-linear dynamic analysis on the calibrated EFM of the Pizzoli town hall building and by (S) the SMAV linear-equivalent analysis with frequency shift, considering the average results over the IM-stripe for each of the four considered sites (Milan MI, Rome RO, Naples NA, L'Aquila AQ). Corresponding average global damage grade $\widehat{DG}$ of the stripe.

the damage limit state of strategic buildings and (ii) the life-safety limit state of residential buildings (in which strategic structures are supposed to maintain the serviceability). In this range of return periods, exception made for the L'Aquila site – partially justified by the very high seismic hazard characterizing this area – the results appear satisfying. Nonetheless, they cannot be considered conclusive, being referred to a single case study.

139

Chapter 6

Conclusions

The employment of dynamic measurements holds a prominent position in civil engineering, particularly for those applications relying on experimental testing. The efforts of the scientific community, in the last decades, have been increasingly directed towards the study of the *structural response* to ambient excitation, giving birth to the wide research field of *operational modal analysis*. In the wake of the recent technological advancements, the increasing accuracy of sensors and their cost-effectiveness makes nowadays *ambient vibration tests* (AVTs) an interesting solution to investigate the dynamics of existing structures. In this context, the thesis addresses the dissemination of ambient vibration measurements in the earthquake-engineering field, in particular for the seismic assessment of existing buildings.

The abundance of contributions from the literature highlights a fertile research ground for developments and the increasing number of monitored structures is favouring their large-scale diffusion in the close future. The usefulness of vibration measurements for earthquake engineering is unanimously recognized, spanning applications ranging from health monitoring to seismic assessment. The evaluations regarding the seismic vulnerability of existing buildings, in particular, saw the rise of mechanical-based approaches over empirical ones, allowing for accurate predictions at the cost of more sophisticated formulations. This advancement of the research remarked, at the same time, the need for physically representative structural models and the importance of experimental testing.

In this framework, the modal parameters identified from AVTs have been employed with great success to calibrate and validate structural formulations, mainly high-fidelity models for the analysis of individual structures. To some extents, they have been also employed directly, to build low-fidelity models for the seismic assessment at the territorial scale. However, few are the examples of the literature able to embed AVTs in a robust seismic assessment framework for buildings. Moreover, a general lack of applications involves the masonry building typology, although it constitutes a significant part of the built heritage which is remarkably susceptible to the seismic hazard. Some recent proposals of the literature, leveraging simplified approaches addressed to the *speditive* assessment of masonry building, are promising for their implications on seismic risk mitigation. On the other hand, from the theoretical point of view, further efforts in the research are required for their validation and systematic employment.

Based on these motivations, after clarifying the methodological framework underlying

the thesis developments and the experimental case studies available for their validation, the discussion approaches the use of AVTs to support the seismic assessment of buildings, starting from issues affecting masonry buildings to propose more general and far-reaching methodological solutions.

The assumption of in-plane rigid behaviour of floor diaphragms, in this context, is commonly adopted to simplify the formulation of structural models. Unreinforced masonry buildings, however, may present a large variability range of diaphragm stiffness, tied to their traditional construction techniques. The behaviour of floor diaphragms, nevertheless, plays a primary role in governing their seismic behaviour. For this purpose, a simple validation tool based on ambient vibration data is proposed in the thesis.

A model-based approach, relying on the kinematic model of a shear-deformable diaphragm, allows stating and solving the inverse problem of discriminating and estimating the in-plane rigid motion and the angular deformation of the diaphragm from dynamic measurements of its ambient response. In the recurring condition of problem indeterminacy, corresponding to the employment of two biaxial sensors, the solution is obtained exploiting a perturbation approach. The comparison between the spectral densities of *rigid motions* and *shear deformations* allows discussing the rigid behaviour of the diaphragms in the frequency band of the identifiable natural modes. The numerical simulations carried out on a calibrated frame model with rigid diaphragm constraints expose the adverse effects of measurement noise and desynchronization, highlighting how errors in the position and orientation of the sensors may prevent a correct estimation of the shear strain. The simulations involving deformable and semi-deformable diaphragms, on the other hand, reveal the possibility to identify the frequencies of pure deformability modes directly from the shear strain spectrum. The application to the JetPACS 2:3 scaled steel frame shows good agreement with the simulation results, confirming the rigid behaviour of its horizontal slabs at low frequencies. Lastly, employing data coming from the permanent monitoring system, the procedure has enabled the identification of the rigid-behaving diaphragm modes of the Pizzoli town hall building, a masonry building with reinforced concrete floors, pointing out as well the presence of shear-deformable diaphragm modes in the low-frequency band.

By leveraging the achievements of this proposal, providing spectral information from operational modal analyses (first-level modal identification problem) able to discriminate rigid-behaving diaphragm modes from nonrigid ones, a model-driven approach is pursued to analytically determine the diaphragm stiffness from vibration measurements. Starting from this spectral knowledge, the inverse problem of parametrically identifying the diaphragm in-plane shear stiffness (second-level structural identification problem) is tackled.

A low-fidelity discrete model of the diaphragm is formulated to describe its linear undamped dynamics, taking into account the shear deformability of the diaphragm through an extra dynamically active degree-of-freedom. The direct eigenproblem governing the modal properties is stated and solved in a suited analytic – although asymptotically approximate – fashion, employing a general multi-parameter perturbation strategy. This strategy provides analytical approximations of the eigenfrequencies as explicit functions of the mechanical parameters, up to the desired order of approximation. Their local validity is verified by numerical sensitivity analyses under small mass and stiffness perturbations. The low-order approximations are exploited to derive analytically invertible spectral relationships between the mechanical parameters and the experimental modal quantities. Specifically, explicit

formulas are determined to assess the main stiffness parameters, including the *shear stiffness* of the diaphragms, as functions of the experimental frequencies. Consistently with the asymptotic nature of the inverse solution, a minimal uncoupled structural model is identified at the lowest order, as well as a refined coupled structural model, including mass and stiffness eccentricities, is identified at higher orders (model updating). The accuracy of the structural identification is numerically verified through pseudo-experimental data, generated from the finite element model of a simple frame structure. Finally, the effectiveness of the procedure is successfully tested experimentally, by employing dynamic measurements from laboratory tests on the JetPACS frame, as well as vibration recordings from the full-scale monitoring of the Pizzoli town hall building.

Taking advantage of such vibration-based contributions to support, guide and validate structural formulations, the equivalent frame model of the Pizzoli town hall building is dynamically calibrated based on the experimentally identified modal and structural quantities. In particular, it is shown that the updating of the diaphragm shear stiffness, according to the proposed inverse expressions, gives accurate results in terms of mode shape reconstruction. The calibrated model of the building – whose reliability in the nonlinear regime is verified thanks to the actual observed damage and measured seismic response to the recent earthquakes that hit Central Italy in 2016 – is employed to investigate the statistical variations of its fundamental frequencies induced by seismic damage, in order to build the model-based *control chart* of the building for post-earthquake damage assessment through on AV measurements.

For this purpose, a general procedure – relying on the execution of several nonlinear dynamic analyses for seismic events of increasing intensity – is proposed. The frequency decays are identified through output-only techniques, simulating the pseudo-experimental ambient response of the building after the earthquake. The correlation with the expected level of structural damage is pursued relying on the descriptions provided by the European Macroseismic Scale. Their numerical interpretation, which is specified in the case of the equivalent frame idealization of masonry buildings, allows the estimation of the global damage grade exhibited by the computational model, starting from the damage level reached by the structural elements and taking into account its average extension and severity on the bearing walls. The *frequency decay-damage control chart* of the building associates with a measured decay in the fundamental frequencies of the building after the earthquake, the probability to reach a certain global grade of seismic-induced structural damage. This tool is proposed as AV-based support for decisional processes regarding the performance of damaged buildings in the post-earthquake scenario.

Finally, a critical review of a recently proposed ambient vibration-based methodology for the seismic serviceability assessment of masonry buildings – the *Seismic Model from Ambient Vibrations* (SMAV) – is pursued through the comparison with the state-of-the-art techniques for the seismic analysis of masonry buildings, nonlinear dynamic analyses on a calibrated equivalent frame model. The reliability of the rigid-diaphragm assumption and of the frequency-shift curves is validated employing the tools previously developed, and the SMAV predictions are tested within a multiple-stripe analysis framework. It is shown that the methodology, according to its simplified nature aimed at large-scale assessments, provides conservative results up to moderate levels of structural damage, confirming its reliability for the quick operational assessment of masonry buildings.

143

Future developments of the research

The contributions of the thesis illustrated in Chapter 4, relying on modal and structural identification techniques to extract valuable engineering information from ambient vibration measurements, offer promising perspectives to enhance the formulation and calibration of structural models for the seismic assessment of buildings.

The model-based inverse techniques proposed in Section 4.3, developed to investigate the dynamic behaviour of floor diaphragms from ambient vibration measurements, show their full potential when applied to traditional masonry buildings – where is challenging to assess the stiffness contribution offered by the different floor diaphragms typologies. Other potential fields of application, which have not been explored in the thesis, could involve the detection of damage induced on diaphragms by earthquakes, as well as the assessment of the efficacy of retrofitting interventions. Their natural development involves the handling of irregular complex-shaped diaphragms and multi-storey buildings, for which some limitations are present in the current proposal. To achieve these objectives, the employment of more refined models paired with widespread sensor networks seem essential requirements. In this perspective, the variety of building at disposal of the research constitutes a fruitful field for future developments.

The general model-driven procedure presented in Section 4.4, aimed at the development of frequency control charts for monitored buildings, appears an attractive choice to support the post-seismic operativity judgements. Further refinements of the proposal will be addressed to the introduction of ambient factors, soil-structure interactions, damaging of diaphragms and nonstructural elements, local mechanisms. Moreover, the tracking of mode shapes and damping variations appears a promising perspective to enhance the robustness of the proposal. The employment of parametric models, typologically representative of the variety and complexity of existing structures, could potentially lead to the generalization of the control chart for masonry buildings, accounting for wider ranges of structural characteristics and behaviours. Hopefully, in the close future, the advancements of the research currently pursued will be backed by the systematic employment of monitoring technologies even for ordinary structures, allowing the widespread diffusion of vibration-based methodologies for the mitigation of their seismic risk.

Bibliography

Acunzo, G., Fiorini, N., Mori, F., & Spina, D. (2015). VaSCO-smav: il software sviluppato per l'applicazione della metodologia SMAV. *Atti del XVI convegno ANIDIS*.

Acunzo, G., Fiorini, N., Mori, F., & Spina, D. (2018). Modal mass estimation from ambient vibrations measurement: A method for civil buildings. *Mechanical Systems and Signal Processing*, *98*, 580–593.

Aenlle, M., & Brincker, R. (2013). Modal scaling in operational modal analysis using a finite element model. *International Journal of Mechanical Sciences*, *76*, 86–101.

Allemang, R. J., & Brown, D. L. (1982). A correlation coefficient for modal vector analysis. *Proceedings of the 1st International Modal Analysis Conference*.

Amezquita-Sanchez, J. P., & Adeli, H. (2016). Signal processing techniques for vibration-based health monitoring of smart structures. *Archives of Computational Methods in Engineering*, *23*(1), 1–15.

Anthoine, A., Magonette, G., & Magenes, G. (1995). Shear-compression testing and analysis of brick masonry walls. *Proceedings of the 10th European Conference on Earthquake Engineering (ECEE)*.

Astorga, A., & Guéguen, P. (2020a). Influence of seismic strain rates on the co-and post-seismic response of civil engineering buildings. *Earthquake Engineering and Structural Dynamics*, *49*(15), 1758–1764.

Astorga, A., & Guéguen, P. (2020b). Structural health building response induced by earthquakes: Material softening and recovery. *Engineering Reports*, *2*(9), e12228.

Astorga, A., Guéguen, P., Ghimire, S., & Kashima, T. (2020). NDE1. 0: a new database of earthquake data recordings from buildings for engineering applications. *Bulletin of Earthquake Engineering*, *18*(4), 1321–1344.

Astorga, A., Guéguen, P., & Kashima, T. (2018). Nonlinear elasticity observed in buildings during a long sequence of earthquakes. *Bulletin of the Seismological Society of America*, *108*(3A), 1185–1198.

Astorga, A. L., Guéguen, P., Riviere, J., Kashima, T., & Johnson, P. A. (2019). Recovery of the resonance frequency of buildings following strong seismic deformation as a proxy for structural health. *Structural Health Monitoring*, *18*(5-6), 1966–1981.

Au, S.-K., Zhang, F.-L., & Ni, Y.-C. (2013). Bayesian operational modal analysis: theory, computation, practice. *Computers and Structures*, *126*, 3–14.

Baggio, C., Bernardini, A., Colozza, R., Corazza, L., Della Bella, M., Di Pasquale, G., Dolce, M., Goretti, A., Martinelli, A., Orsini, G., et al. (2007). Field manual for post-earthquake damage and safety assessment and short term countermeasures

(AeDES). *European Commission—Joint Research Centre—Institute for the Protection and Security of the Citizen, EUR, 22868.*

Baker, J. (2013). Trade-offs in ground motion selection techniques for collapse assessment of structures. *Vienna Congress on Recent Advances in Earthquake Engineering and Structural Dynamics.*

Barani, S., Ferretti, G., & De Ferrari, R. (2020). Incorporating results from seismic microzonation into probabilistic seismic hazard analysis: An example in western Liguria (Italy). *Engineering Geology, 267,* 105479.

Bazzurro, P., Cornell, C. A., Shome, N., & Carballo, J. E. (1998). Three proposals for characterizing MDOF nonlinear seismic response. *Journal of Structural Engineering, 124*(11), 1281–1289.

Bernal, D., & Gunes, B. (2002). Damage localization in output-only systems: A flexibility based approach. *Proceedings of the 20th International Modal Analysis Conference (IMAC).*

Beyer, K., & Dazio, A. (2012). Quasi-static cyclic tests on masonry spandrels. *Earthquake Spectra, 28*(3), 907–929.

Beyer, K., & Mangalathu, S. (2013). Review of strength models for masonry spandrels. *Bulletin of Earthquake Engineering, 11*(2), 521–542.

Bocca, M., Eriksson, L. M., Mahmood, A., Jäntti, R., & Kullaa, J. (2011). A synchronized wireless sensor network for experimental modal analysis in structural health monitoring. *Computer-Aided Civil and Infrastructure Engineering, 26*(7), 483–499.

Bodin, P., Vidale, J., Walsh, T., Çakir, R., & Çelebi, M. (2012). Transient and long-term changes in seismic response of the natural resources building, Olympia, Washington, due to earthquake shaking. *Journal of Earthquake Engineering, 16*(5), 607–622.

Boschi, S., Galano, L., & Vignoli, A. (2019). Mechanical characterisation of Tuscany masonry typologies by in situ tests. *Bulletin of Earthquake Engineering, 17*(1), 413–438.

Boutin, C., Hans, S., Ibraim, E., & Roussillon, P. (2005). In situ experiments and seismic analysis of existing buildings. Part II: Seismic integrity threshold. *Earthquake Engineering and Structural Dynamics, 34*(12), 1531–1546.

Brignola, A., Pampanin, S., & Podestà, S. (2012). Experimental evaluation of the in-plane stiffness of timber diaphragms. *Earthquake Spectra, 28*(4), 1687–1709.

Brincker, R., Rodrigues, J., & Andersen, P. (2004). Scaling the mode shapes of a building model by mass changes. *Proceedings of the 22nd International Modal Analysis Conference (IMAC),* 119–126.

Brincker, R., Andersen, P., & Jacobsen, N.-J. (2007). Automated frequency domain decomposition for operational modal analysis. *Proceedings of the 25th International Modal Analysis Conference (IMAC).*

Brincker, R., Ventura, C., & Andersen, P. (2001a). Damping estimation by frequency domain decomposition. *Proceedings of the 19th International Modal Analysis Conference (IMAC).*

Brincker, R., Zhang, L., & Andersen, P. (2000). Modal identification from ambient responses using frequency domain decomposition. *Proceedings of the 18th International Modal Analysis Conference (IMAC).*

Brincker, R., Zhang, L., & Andersen, P. (2001b). Modal identification of output-only systems using frequency domain decomposition. *Smart Materials and Structures*, *10*(3), 441.

Brownjohn, J. M. (2007). Structural health monitoring of civil infrastructure. *Philosophical Transactions of the Royal Society A: Mathematical, Physical and Engineering Sciences*, *365*(1851), 589–622.

Brownjohn, J. M., De Stefano, A., Xu, Y.-L., Wenzel, H., & Aktan, A. E. (2011). Vibration-based monitoring of civil infrastructure: challenges and successes. *Journal of Civil Structural Health Monitoring*, *1*(3), 79–95.

Brunelli, A., de Silva, F., Piro, A., Parisi, F., Sica, S., Silvestri, F., & Cattari, S. (2020). Numerical simulation of the seismic response and soil–structure interaction for a monitored masonry school building damaged by the 2016 Central Italy earthquake. *Bulletin of Earthquake Engineering*, 1–31.

Calderini, C., Cattari, S., Degli Abbati, S., Lagomarsino, S., Ottonelli, D., & Rossi, M. (2012). Modelling strategies for seismic global response of building and local mechanisms. *PERPETUATE (EU-FP7 Research Project), Deliverable D26*.

Calderini, C., Cattari, S., & Lagomarsino, S. (2009). In-plane strength of unreinforced masonry pier. *Earthquake Engineering and Structural Dynamics*, *38*, 243–267.

Calderini, C., Cattari, S., Lagomarsino, S., & Rossi, M. (2010). Review of existing models for global response and local mechanisms. *PERPETUATE (EU-FP7 Research Project), Deliverable D27*.

Calvi, G. M., Pinho, R., Magenes, G., Bommer, J. J., Restrepo-Vélez, L. F., & Crowley, H. (2006a). Development of seismic vulnerability assessment methodologies over the past 30 years. *ISET Journal of Earthquake Technology*, *43*(3), 75–104.

Calvi, G. M. (1999). A displacement-based approach for vulnerability evaluation of classes of buildings. *Journal of earthquake Engineering*, *3*(03), 411–438.

Calvi, G. M., Pinho, R., & Crowley, H. (2006b). State-of-the-knowledge on the period elongation of RC buildings during strong ground shaking. *Proceedings of the 1st European conference of Earthquake Engineering and Seismology (ECEES)*.

Camilletti, D. (2019). *Equivalent frame modelling of URM buildings: numerical validations and rules* (Doctoral dissertation). University of Genoa.

Camilletti, D., Cattari, S., Lagomarsino, S., Bonaldo, D., Guidi, G., Bracchi, S., Galasco, A., Magenes, G., Manzini, C., Penna, A., et al. (2017). RINTC project: Nonlinear dynamic analyses of Italian code-conforming URM buildings for collapse risk assessment. *Proceedings of the 6th International Conference on Computational Methods in Structural Dynamics and Earthquake Engineering (COMPDYN)*.

Capecchi, D., & Vestroni, F. (1993). Identification of finite element models in structural dynamics. *Engineering Structures*, *15*(1), 21–30.

Capecchi, D., & Vestroni, F. (1999). Monitoring of structural systems by using frequency data. *Earthquake Engineering and Structural Dynamics*, *28*(5), 447–461.

Caprili, S., Nardini, L., & Salvatore, W. (2012). Evaluation of seismic vulnerability of a complex RC existing building by linear and nonlinear modeling approaches. *Bulletin of Earthquake Engineering*, *10*(3), 913–954.

Carden, E. P., & Fanning, P. (2004). Vibration based condition monitoring: a review. *Structural Health Monitoring*, *3*(4), 355–377.

147

Carder, D. S. (1936). Observed vibration of buildings. *Bulletin of the Seismological Society of America, 26*(4), 245–277.

Cardone, D., Perrone, G., & Flora, A. (2020). Displacement-Based Simplified Seismic Loss Assessment of Pre-70S RC Buildings. *Journal of Earthquake Engineering, 24*(sup1), 82–113.

Casagrande, D., Giongo, I., Pederzolli, F., Franciosi, A., & Piazza, M. (2018). Analytical, numerical and experimental assessment of vibration performance in timber floors. *Engineering Structures, 168*, 748–758.

Cattari, S., Camilletti, D., Magenes, G., Manzini, C., Morandi, P., Spacone, E., Camata, G., Marano, C., Calio, I., Cannizzaro, F., et al. (2018a). A comparative study on a 2-storey benchmark case study through nonlinear seismic analysis. *Proceedings of the 16th European Conference on Earthquake Engineering (ECEE).*

Cattari, S., Chioccariello, A., Degée, H., Doneaux, C., & Lagomarsino, S. (2014a). Seismic assessment of masonry buildings from shaking table tests and nonlinear dynamic simulations by the Proper Orthogonal Decomposition (POD). *Proceedings of the 2nd European Conference on Earthquake Engineering and Seismology (ECEES).*

Cattari, S., Curti, E., Galasco, A., & Resemini, S. (2005). *Analisi sismica lineare e non lineare degli edifici in muratura. Teoria ed esempi di applicazione secondo OPCM 3274/2003 e 3431/2005* [In Italian]. Sitemi Editoriali.

Cattari, S., Degli Abbati, S., Ferretti, D., Lagomarsino, S., Ottonelli, D., & Tralli, A. (2014b). Damage assessment of fortresses after the 2012 Emilia earthquake (Italy). *Bulletin of earthquake engineering, 12*(5), 2333–2365.

Cattari, S., Degli Abbati, S., Ottonelli, D., Marano, C., Camata, G., Spacone, E., Da Porto, F., Modena, C., Lorenzoni, F., Magenes, G., Penna, A., Graziotti, F., Ceravolo, R., Miraglia, G., Lenticchia, E., Fiorini, N., & Spina, D. (2019a). Discussion on data recorded by the Italian structural seismic monitoring network on three masonry structures hit by the 2016-2017 Central Italy earthquake. *Proceedings of the 7th International Conference on Computational Methods in Structural Dynamics and Earthquake Engineering (COMPDYN).*

Cattari, S., & Lagomarsino, S. (2009). Modelling the seismic response of unreinforced existing masonry buildings: a critical review of some models proposed by codes. *Proceedings of the 11th Canadian Masonry Symposium.*

Cattari, S., & Lagomarsino, S. (2012). Definition of seismic safety verification procedures for historical buildings. *PERPETUATE (EU-FP7 Research Project), Deliverable D35.*

Cattari, S., & Lagomarsino, S. (2013). Analisi nonlineari per la simulazione del danno di un fabbricato in San Felice sul Panaro (Emilia, 2012) [In Italian]. *Atti del XV Convegno ANIDIS.*

Cattari, S., & Lagomarsino, S. (2017). Masonry structures. *Developments in the field of displacement based seismic assessment* (pp. 151–200). IUSS Press; EUCENTRE.

Cattari, S., Lagomarsino, S., Milani, G., Rossi, M., Simoni, M., & Tralli, A. (2014c). Non Linear Modelling of Fornasini Tower After the 2012 Emilia Earthquake (Italy). *Proceedings of the 9th International Conference on Structural Analysis of Historical Constructions.*

Cattari, S., Sivori, D., Brunelli, A., Sica, S., Piro, A., de Silva, F., Parisi, F., & Silvestri, F. (2019b). Soil-structure interaction effects on the dynamic behaviour of a masonry school damaged by the 2016–2017 Central Italy earthquake sequence. *Proceedings of the 7th International Conference on Earthquake Geotechnical Engineering (ICEGE)*.

Cattari, S., Camilletti, D., Lagomarsino, S., Bracchi, S., Rota, M., & Penna, A. (2018b). Masonry Italian code-conforming buildings. Part 2: nonlinear modelling and time-history analysis. *Journal of Earthquake Engineering*, *22*(sup2), 2010–2040.

Cattari, S., Camilletti, D., Magenes, G., Manzini, C. F., & Morandi, P. (2017). Comparative analysis of benchmark case studies for assessing the reliability of software packages targeted to the seismic assessment of URM buildings. [in Italian]. *Atti del XVII Convegno ANIDIS*.

Cattari, S., Degli Abbati, S., Ferretti, D., Lagomarsino, S., Ottonelli, D., Tralli, A. M., et al. (2012). The seismic behaviour of ancient masonry buildings after the earthquake in Emilia (Italy) on May 20 and 29. *Ingegneria Sismica*, *2*(29), 87–119.

Cattari, S., Resemini, S., & Lagomarsino, S. (2008). Modelling of vaults as equivalent diaphragms in 3D seismic analysis of masonry buildings. *Structural Analysis of Historic Construction: Preserving Safety and Significance, Two Volume Set* (pp. 537–544). CRC Press.

Ceci, A. M., Contento, A., Fanale, L., Galeota, D., Gattulli, V., Lepidi, M., & Potenza, F. (2010). Structural performance of the historic and modern buildings of the University of L'Aquila during the seismic events of April 2009. *Engineering Structures*, *32*(7), 1899–1924.

Çelebi, M. (2007). On the variation of fundamental frequency (period) of an undamaged building–a continuing discussion. *Proceedings of the International Conference on Experimental Vibration Analysis for Civil Engineering Structures*.

Ceravolo, R., Lenticchia, E., & Miraglia, G. (2018). Use of spectral entropy for damage detection in masonry buildings in the presence of mild seismicity. *Multidisciplinary Digital Publishing Institute Proceedings*, *2*(8), 432.

Ceravolo, R., Matta, E., Quattrone, A., & Zanotti Fragonara, L. (2017). Amplitude dependence of equivalent modal parameters in monitored buildings during earthquake swarms. *Earthquake Engineering and Structural Dynamics*, *46*(14), 2399–2417.

Chopra, A., & Goel, R. (2002). A modal pushover analysis procedure for estimating seismic demands for buildings. *Earthquake engineering and structural dynamics*, *31*(3), 561–582.

Clementi, F., Formisano, A., Milani, G., & Ubertini, F. (2021). Structural Health Monitoring of Architectural Heritage: From the past to the Future Advances.

Clinton, J. F., Bradford, S. C., Heaton, T. H., & Favela, J. (2006). The observed wander of the natural frequencies in a structure. *Bulletin of the Seismological Society of America*, *96*(1), 237–257.

Cunha, A., & Caetano, E. (2006). Experimental modal analysis of civil engineering structures. *Sound and Vibrations*, 12–20.

D'Altri, A. M., Sarhosis, V., Milani, G., Rots, J., Cattari, S., Lagomarsino, S., Sacco, E., Tralli, A., Castellazzi, G., & de Miranda, S. (2019). Modeling strategies for the computational analysis of unreinforced masonry structures: review and classification. *Archives of Computational Methods in Engineering*, 1–33.

D'Ayala, D., & Speranza, E. (2003). Definition of collapse mechanisms and seismic vulnerability of historic masonry buildings. *Earthquake Spectra*, *19*(3), 479–509.

De Falco, A., Guidetti, G., Mori, M., & Sevieri, G. (2017). Model uncertainties in seismic analysis of existing masonry buildings: the Equivalent-Frame Model within the Structural Element Models approach. *Atti del XVII Convegno ANIDIS*.

De Roeck, G., Peeters, B., & Maeck, J. (2000). Dynamic monitoring of civil engineering structures. *Proceedings of the 4th International Colloquium on Computation of Shell and Spatial Structures (IASS-IACM)*.

De Sortis, A., Antonacci, E., & Vestroni, F. (2005). Dynamic identification of a masonry building using forced vibration tests. *Engineering Structures*, *27*(2), 155–165.

Degli Abbati, S., Morandi, P., & Spacone, E. (2021). On the reliability of the equivalent frame models: the case study of the permanently monitored Pizzoli's town hall [Submitted for publication]. *Bulletin of Earthquake Engineering*.

Del Gaudio, C., De Martino, G., Di Ludovico, M., Manfredi, G., Prota, A., Ricci, P., & Verderame, G. M. (2019). Empirical fragility curves for masonry buildings after the 2009 L'Aquila, Italy, earthquake. *Bulletin of earthquake engineering*, *17*(11), 6301–6330.

Del Vecchio, C., Di Ludovico, M., Pampanin, S., & Prota, A. (2018). Repair costs of existing RC buildings damaged by the L'Aquila earthquake and comparison with FEMA P-58 predictions. *Earthquake Spectra*, *34*(1), 237–263.

Del Vecchio, C., Ludovico, M. D., & Prota, A. (2020). Repair costs of reinforced concrete building components: from actual data analysis to calibrated consequence functions. *Earthquake spectra*, *36*(1), 353–377.

Di Ludovico, M., Digrisolo, A., Moroni, C., Graziotti, F., Manfredi, V., Prota, A., Dolce, M., & Manfredi, G. (2019). Remarks on damage and response of school buildings after the Central Italy earthquake sequence. *Bulletin of Earthquake Engineering*, *17*(10), 5679–5700.

Di Ludovico, M., Prota, A., Moroni, C., Manfredi, G., & Dolce, M. (2017a). Reconstruction process of damaged residential buildings outside historical centres after the L'Aquila earthquake: part I—" light damage" reconstruction. *Bulletin of Earthquake Engineering*, *15*(2), 667–692.

Di Ludovico, M., Prota, A., Moroni, C., Manfredi, G., & Dolce, M. (2017b). Reconstruction process of damaged residential buildings outside historical centres after the L'Aquila earthquake: part II—"heavy damage" reconstruction. *Bulletin of Earthquake Engineering*, *15*(2), 693–729.

Dizhur, D., Wei, S., Giaretton, M., Schultz, A. E., Ingham, J. M., & Giongo, I. (2020). Testing of URM wall-to-diaphragm through-bolt plate anchor connections. *Earthquake Spectra*, 8755293020944187.

Doebling, S. W., Farrar, C. R., Prime, M. B., & Shevitz, D. W. (1996). *Damage identification and health monitoring of structural and mechanical systems from changes in their vibration characteristics: a literature review* (tech. rep.). Los Alamos National Lab., NM (United States).

Doebling, S. W., Farrar, C. R., & Prime, M. B. (1998). A summary review of vibration-based damage identification methods. *Shock and Vibration Digest*, *30*(2), 91–105.

Dolce, M., Nicoletti, M., De Sortis, A., Marchesini, S., Spina, D., & Talanas, F. (2017a). Osservatorio sismico delle strutture: the Italian structural seismic monitoring network. *Bulletin of Earthquake Engineering, 15*(2), 621–641.

Dolce, M., Ponzo, F. C., Di Cesare, A., Ditommaso, R., Moroni, C., Nigro, D., Serino, G., Sorace, S., Gattulli, V., Occhiuzzi, A., & Foti, D. (2008). Jet-pacs project: joint experimental testing on passive and semiactive control systems. *Proceedings of the 14th World Conference on Earthquake Engineering (WCEE)*.

Dolce, M., Speranza, E., Giordano, F., Borzi, B., Bocchi, F., Conte, C., Di Meo, A., Faravelli, M., & Pascale, V. (2019). Observed damage database of past Italian earthquakes: the Da. DO WebGIS. *Bollettino di Geofisica Teorica ed Applicata, 60*(2).

Dolce, M. (2012). The Italian national seismic prevention program. *Proceedings of the 15th World Conference on Earthquake Engineering (WCEE)*.

Dolce, M., & Di Bucci, D. (2017). Comparing recent Italian earthquakes. *Bulletin of Earthquake Engineering, 15*(2), 497–533.

Dolce, M., Speranza, E., Bocchi, F., & Conte, C. (2018). Probabilistic assessment of structural operational efficiency in emergency limit conditions: the I. OPà. CLE method. *Bulletin of Earthquake Engineering, 16*(9), 3791–3818.

Dolce, M., Speranza, E., Giordano, F., Borzi, B., & Bocchi, F. (2017b). Da. DO–A web-based tool for analyzing and comparing post-earthquake damage databaserelevant to national seismic events since 1976. *Atti del XVII Convegno ANIDIS*.

Ebrahimian, H., Jalayer, F., Lucchini, A., Mollaioli, F., & Manfredi, G. (2015). Preliminary ranking of alternative scalar and vector intensity measures of ground shaking. *Bulletin of Earthquake Engineering, 13*(10), 2805–2840.

Elenas, A., & Meskouris, K. (2001). Correlation study between seismic acceleration parameters and damage indices of structures. *Engineering Structures, 23*(6), 698–704.

European Committee for Standardization (CEN). (2004). Eurocode 8: Design of structures for earthquake resistance - Part 1: General rules, seismic actions and rules for buildings (EN1998-1).

European Committee for Standardization (CEN). (2005). Eurocode 8: Design of structures for earthquake resistance - Part 3: Assessment and retrofitting of buildings (EN1998-3).

Ewins, D. J. (2016). Exciting vibrations: the role of testing in an era of supercomputers and uncertainties. *Meccanica, 51*(12), 3241–3258.

Fajfar, P. (1999). Capacity spectrum method based on inelastic demand spectra. *Earthquake Engineering and Structural Dynamics, 28*(9), 979–993.

Farrar, C. R., Doebling, S. W., & Nix, D. A. (2001). Vibration–based structural damage identification. *Philosophical Transactions of the Royal Society of London A: Mathematical, Physical and Engineering Sciences, 359*(1778), 131–149.

Farrar, C. R., & Worden, K. (2007). An introduction to structural health monitoring. *Philosophical Transactions of the Royal Society A: Mathematical, Physical and Engineering Sciences, 365*(1851), 303–315.

Farrar, C., & James Iii, G. (1997). System identification from ambient vibration measurements on a bridge. *Journal of Sound and Vibration, 205*(1), 1–18.

Federici, F., Alesii, R., Colarieti, A., Faccio, M., Graziosi, F., & Gattulli, V. (2015). Analysis and Implementation of Distributed Data Processing in a Wireless Sensor Network for Structural Health Monitoring. *Sensors, 319*, 315–319.

Federici, F., Graziosi, F., Faccio, M., Colarieti, A., Gattulli, V., Lepidi, M., & Potenza, F. (2012). An integrated approach to the design of wireless sensor networks for structural health monitoring. *International Journal of Distributed Sensor Networks*, *8*(3).

Feng, D., & Feng, M. Q. (2018). Computer vision for SHM of civil infrastructure: From dynamic response measurement to damage detection–A review. *Engineering Structures*, *156*, 105–117.

Foti, D., Gattulli, V., & Potenza, F. (2014). Output-only identification and model updating by dynamic testing in unfavorable conditions of a seismically damaged building. *Computer-Aided Civil and Infrastructure Engineering*, *29*(9), 659–675.

Freeman, S. A. (1998). The capacity spectrum method. *Proceedings of the 11th European Conference on Earthquake Engineering (ECEE)*.

Friswell, M. I., Mottershead, J. E., & Ahmadian, H. (2001). Finite–element model updating using experimental test data: parametrization and regularization. *Philosophical Transactions of the Royal Society of London A: Mathematical, Physical and Engineering Sciences*, *359*(1778), 169–186.

Galasco, A., Lagomarsino, S., & Penna, A. (2006). On the use of pushover analysis for existing masonry buildings. *Proceedings of the 1st European Conference on Earthquake Engineering and Seismology (ECEES)*.

Galasco, A., Lagomarsino, S., Penna, A., & Resemini, S. (2004). Non-linear seismic analysis of masonry structures. *Proceedings of the 13th World Conference on Earthquake Engineering (WCEE)*.

Gallipoli, M. R., Mucciarelli, M., Šket-Motnikar, B., Zupančić, P., Gosar, A., Prevolnik, S., Herak, M., Stipčević, J., Herak, D., Milutinović, Z., et al. (2010). Empirical estimates of dynamic parameters on a large set of European buildings. *Bulletin of Earthquake Engineering*, *8*(3), 593–607.

García-Macías, E., Ierimonti, L., Venanzi, I., & Ubertini, F. (2019). An innovative methodology for online surrogate-based model updating of historic buildings using monitoring data. *International Journal of Architectural Heritage*, 1–21.

Gattulli, V., Antonacci, E., & Vestroni, F. (2013). Field observations and failure analysis of the Basilica S. Maria di Collemaggio after the 2009 L'Aquila earthquake. *Engineering failure analysis*, *34*, 715–734.

Gattulli, V., Lepidi, M., & Potenza, F. (2007). Identification of analytical and finite element models for the JETPACS three-dimensional frame. *DPC-RELUIS JETPACS Report*, (2).

Gattulli, V., Lepidi, M., Macdonald, J. H., & Taylor, C. A. (2005). One-to-two global-local interaction in a cable-stayed beam observed through analytical, finite element and experimental models. *International Journal of Non-Linear Mechanics*, *40*(4), 571–588.

Gattulli, V., Lepidi, M., & Potenza, F. (2009). Seismic protection of frame structures via semi-active control: modeling and implementation issues. *Earthquake Engineering and Engineering Vibration*, *8*(4), 627–645.

Gattulli, V., Lepidi, M., & Potenza, F. (2016). Dynamic testing and health monitoring of historic and modern civil structures in Italy. *Structural Monitoring and Maintenance*, *3*(1), 71–90.

152

Gentile, C., & Saisi, A. (2007). Ambient vibration testing of historic masonry towers for structural identification and damage assessment. *Construction and Building Materials*, *21*(6), 1311–1321.

Giongo, I., Dizhur, D., Tomasi, R., & Ingham, J. M. (2015). Field testing of flexible timber diaphragms in an existing vintage URM building. *Journal of Structural Engineering*, *141*(1), D4014009.

Giovinazzi, S., & Lagomarsino, S. (2004). A macroseismic method for the vulnerability assessment of buildings. *Proceedings of the 13th World Conference on Earthquake Engineering (WCEE)*.

Giraldo, D. F., Song, W., Dyke, S. J., & Caicedo, J. M. (2009). Modal identification through ambient vibration: comparative study. *Journal of Engineering Mechanics*, *135*(8), 759–770.

Greco, A., Fiore, I., Occhipinti, G., Caddemi, S., Spina, D., & Caliò, I. (2020). An Equivalent Non-Uniform Beam-Like Model for Dynamic Analysis of Multi-Storey Irregular Buildings. *Applied Sciences*, *10*(9), 3212.

Grünthal, G. (1998). *European macroseismic scale 1998* (tech. rep.). European Seismological Commission (ESC).

Gueguen, P. (2013). *Seismic vulnerability of structures*. John Wiley; Sons.

Guéguen, P., Brossault, M.-A., Roux, P., & Singaucho, J. C. (2020). Slow dynamics process observed in civil engineering structures to detect structural heterogeneities. *Engineering Structures*, *202*, 109833.

Guéguen, P., Gallipoli, M. R., Navarro, M., Masi, A., Michel, C., Guillier, B., Karakostas, C., Lekidis, V., Mucciarelli, M., Ponzo, F. C., et al. (2014). Testing buildings using ambient vibrations for earthquake engineering: a European review. *Proceedings of the 2nd European Conference on Earthquake Engineering and Seismology (ECEES)*.

Hajj, M., Fung, J., Nayfeh, A., & Fahey, S. (2000). Damping identification using perturbation techniques and higher-order spectra. *Nonlinear Dynamics*, *23*(2), 189–203.

Hans, S., Boutin, C., Ibraim, E., & Roussillon, P. (2005). In situ experiments and seismic analysis of existing buildings. Part I: Experimental investigations. *Earthquake Engineering and Structural Dynamics*, *34*(12), 1513–1529.

Hazus, M. (1999). Earthquake loss estimation methodology—technical and user manuals. *Federal Emergency Management Agency, Washington*.

Ierimonti, L., Venanzi, I., Cavalagli, N., Comodini, F., & Ubertini, F. (2020). An innovative continuous Bayesian model updating method for base-isolated RC buildings using vibration monitoring data. *Mechanical Systems and Signal Processing*, *139*, 106600.

Iervolino, I., Spillatura, A., & Bazzurro, P. (2018). Seismic reliability of code-conforming Italian buildings. *Journal of Earthquake Engineering*, *22*(sup2), 5–27.

Iervolino, I., & Dolce, M. (2018). Foreword to the Special Issue for the RINTC (The Implicit Seismic Risk of Code-Conforming Structures) Project.

Ivanovic, S. S., Trifunac, M. D., & Todorovska, M. (2000). Ambient vibration tests of structures-a review. *ISET Journal of Earthquake Technology*, *37*(4), 165–197.

Jaishi, B., & Ren, W.-X. (2005). Structural finite element model updating using ambient vibration test results. *Journal of Structural Engineering*, *131*(4), 617–628.

Jalayer, F. (2003). *Direct probabilistic seismic anaysis: implementing non-linear dynamic assessments* (Doctoral dissertation). Stanford University Stanford, CA.

Jalayer, F., & Cornell, C. (2009). Alternative non-linear demand estimation methods for probability-based seismic assessments. *Earthquake Engineering and Structural Dynamics*, *38*(8), 951–972.

Jalayer, F., De Risi, R., & Manfredi, G. (2015). Bayesian Cloud Analysis: efficient structural fragility assessment using linear regression. *Bulletin of Earthquake Engineering*, *13*(4), 1183–1203.

Katsanos, E., Sextos, A., & Elnashai, A. S. (2014). Prediction of inelastic response periods of buildings based on intensity measures and analytical model parameters. *Engineering structures*, *71*, 161–177.

Kerschen, G., Worden, K., Vakakis, A. F., & Golinval, J.-C. (2006). Past, present and future of nonlinear system identification in structural dynamics. *Mechanical Systems and Signal Processing*, *20*(3), 505–592.

Khatibi, M., Ashory, M., Malekjafarian, A., & Brincker, R. (2012). Mass–stiffness change method for scaling of operational mode shapes. *Mechanical Systems and Signal Processing*, *26*, 34–59.

Kita, A., Cavalagli, N., Masciotta, M. G., Lourenço, P. B., & Ubertini, F. (2020). Rapid post-earthquake damage localization and quantification in masonry structures through multidimensional non-linear seismic IDA. *Engineering Structures*, *219*, 110841.

Kita, A., Cavalagli, N., & Ubertini, F. (2019). Temperature effects on static and dynamic behavior of Consoli Palace in Gubbio, Italy. *Mechanical Systems and Signal Processing*, *120*, 180–202.

Krawinkler, H., & Seneviratna, G. (1998). Pros and cons of a pushover analysis of seismic performance evaluation. *Engineering structures*, *20*(4-6), 452–464.

Kržan, M., Gostič, S., Cattari, S., & Bosiljkov, V. (2015). Acquiring reference parameters of masonry for the structural performance analysis of historical buildings. *Bulletin of Earthquake Engineering*, *13*(1), 203–236.

Kunnath, S. K., Panahshahi, N., & Reinhorn, A. M. (1991). Seismic response of RC buildings with inelastic floor diaphragms. *Journal of Structural Engineering*, *117*(4), 1218–1237.

Lacarbonara, W., Carboni, B., & Quaranta, G. (2016). Nonlinear normal modes for damage detection. *Meccanica*, *51*(11), 2629–2645.

Lagomarsino, S. (2012). Damage assessment of churches after L'Aquila earthquake (2009). *Bulletin of Earthquake Engineering*, *10*(1), 73–92.

Lagomarsino, S., & Cattari, S. (2015a). PERPETUATE guidelines for seismic performance-based assessment of cultural heritage masonry structures. *Bulletin of Earthquake Engineering*, *13*(1), 13–47.

Lagomarsino, S., Galasco, A., & Penna, A. (2007). Non linear macro-element dynamic analysis of masonry buildings. *Proceedings of the ECCOMAS thematic conference on computational methods in structural dynamics and earthquake engineering, Rethymno, Crete*.

Lagomarsino, S., Penna, A., Galasco, A., & Cattari, S. (2013). TREMURI program: an equivalent frame model for the nonlinear seismic analysis of masonry buildings. *Engineering Structures*, *56*, 1787–1799.

Lagomarsino, S., & Cattari, S. (2015b). Seismic performance of historical masonry structures through pushover and nonlinear dynamic analyses. *Perspectives on European Earthquake Engineering and Seismology* (pp. 265–292). Springer, Cham.

Lagomarsino, S., & Giovinazzi, S. (2006). Macroseismic and mechanical models for the vulnerability and damage assessment of current buildings. *Bulletin of Earthquake Engineering, 4*(4), 415–443.

Lagomarsino, S., Marino, S., & Cattari, S. (2020). Linear static procedures for the seismic assessment of masonry buildings: Open issues in the new generation of European codes. *Structures, 26*, 427–440.

Lagomarsino, S., Ottonelli, D., & Cattari, S. (2021). The heuristic vulnerability model: fragility curves for masonry buildings [Under review]. *Bulletin of Earthquake Engineering.*

Lee, Y., Vakakis, A., McFarland, D., & Bergman, L. (2010). A global–local approach to nonlinear system identification: a review. *Structural Control and Health Monitoring, 17*(7), 742–760.

Lepidi, M. (2013). Multi-parameter perturbation methods for the eigensolution sensitivity analysis of nearly-resonant non-defective multi-degree-of-freedom systems. *Journal of Sound and Vibration, 332*(4), 1011–1032.

Lepidi, M., & Bacigalupo, A. (2018). Multi-parametric sensitivity analysis of the band structure for tetrachiral acoustic metamaterials. *International Journal of Solids and Structures, 136*, 186–202.

Lepidi, M., & Gattulli, V. (2014). A parametric multi-body section model for modal interactions of cable-supported bridges. *Journal of Sound and Vibration, 333*(19), 4579–4596.

Lepidi, M., Gattulli, V., & Foti, D. (2009). Swinging-bell resonances and their cancellation identified by dynamical testing in a modern bell tower. *Engineering Structures, 31*(7), 1486–1500.

Lofrano, E., Paolone, A., & Vasta, M. (2016). A perturbation approach for the identification of uncertain structures. *International Journal of Dynamics and Control, 4*(2), 204–212.

López-Aenlle, M., Fernández, P., Brincker, R., & Fernández-Canteli, A. (2010). Erratum to "Scaling-factor estimation using an optimized mass-change strategy"[Mech. Syst. Signal Process. 24 (5)(2010) 1260–1273]. *Mechanical Systems and Signal Processing, 24*(8), 3061–3074.

López-Aenlle, M., Brincker, R., Pelayo, F., & Canteli, A. F. (2012). On exact and approximated formulations for scaling-mode shapes in operational modal analysis by mass and stiffness change. *Journal of Sound and Vibration, 331*(3), 622–637.

Lorenzoni, F., Caldon, M., da Porto, F., Modena, C., & Aoki, T. (2018). Post-earthquake controls and damage detection through structural health monitoring: applications in l'Aquila. *Journal of Civil Structural Health Monitoring, 8*(2), 217–236.

Lourenço, P. (2002). Computations on historic masonry structures. *Progress in Structural Engineering and Materials, 4*(3), 301–319.

Luco, N., & Cornell, C. A. (2007). Structure-specific scalar intensity measures for near-source and ordinary earthquake ground motions. *Earthquake Spectra, 23*(2), 357–392.

Luzi, G., Crosetto, M., & Fernández, E. (2017). Radar interferometry for monitoring the vibration characteristics of buildings and civil structures: Recent case studies in Spain. *Sensors, 17*(4), 669.

Magenes, G. (2000). A method for pushover analysis in seismic assessment of masonry buildings. *Proceedings of the 12th World Conference on Earthquake Engineering (WCEE).*

Magenes, G. (2006). Masonry building design in seismic areas: recent experiences and prospects from a European standpoint. *Proceedings of the 1st European Conference on Earthquake Engineering and Seismology (ECEES).*

Marino, S. (2018). *Nonlinear Static Procedures for the seismic assessment of irregular URM buildings* (Doctoral dissertation). University of Genoa.

Marino, S., Cattari, S., Lagomarsino, S., Ingham, J., & Dizhur, D. (2016). Modelling of two damaged unreinforced masonry buildings following the Canterbury earthquakes. *Proceedings of the NZSEE Conference on Earthquake Engineering.*

Marino, S., Cattari, S., & Lagomarsino, S. (2019). Are the nonlinear static procedures feasible for the seismic assessment of irregular existing masonry buildings? *Engineering Structures, 200,* 109700.

Marques, R., & Lourenço, P. (2011). Possibilities and comparison of structural component models for the seismic assessment of modern unreinforced masonry buildings. *Computers and Structures, 89*(21-22), 2079–2091.

Masi, A., & Vona, M. (2010). Experimental and numerical evaluation of the fundamental period of undamaged and damaged RC framed buildings. *Bulletin of Earthquake Engineering, 8*(3), 643–656.

Michel, C., Guéguen, P., Lestuzzi, P., & Bard, P.-Y. (2010a). Comparison between seismic vulnerability models and experimental dynamic properties of existing buildings in France. *Bulletin of Earthquake Engineering, 8*(6), 1295–1307.

Michel, C., & Gueguen, P. (2010). Time-frequency analysis of small frequency variations in civil engineering structures under weak and strong motions using a reassignment method. *Structural health monitoring, 9*(2), 159–171.

Michel, C., Guéguen, P., & Bard, P.-Y. (2008). Dynamic parameters of structures extracted from ambient vibration measurements: An aid for the seismic vulnerability assessment of existing buildings in moderate seismic hazard regions. *Soil Dynamics and Earthquake Engineering, 28*(8), 593–604.

Michel, C., Guéguen, P., & Causse, M. (2012). Seismic vulnerability assessment to slight damage based on experimental modal parameters. *Earthquake Engineering and Structural Dynamics, 41*(1), 81–98.

Michel, C., Guéguen, P., El Arem, S., Mazars, J., & Kotronis, P. (2010b). Full-scale dynamic response of an RC building under weak seismic motions using earthquake recordings, ambient vibrations and modelling. *Earthquake Engineering and Structural Dynamics, 39*(4), 419–441.

Michel, C., Lattion, E., Oropeza, M., & Lestuzzi, P. (2009). Vulnerability assessment of existing masonry buildings in moderate seismicity areas using experimental techniques. *Proceedings of the 2009 Asian-Pacific Network of Centers for Earthquake Engineering Research (ANCER) Workshop.*

Michel, C., Zapico, B., Lestuzzi, P., Molina, F. J., & Weber, F. (2011). Quantification of fundamental frequency drop for unreinforced masonry buildings from dynamic tests. *Earthquake Engineering and Structural Dynamics, 40*(11), 1283–1296.

Minas, S., & Galasso, C. (2019). Accounting for spectral shape in simplified fragility analysis of case-study reinforced concrete frames. *Soil Dynamics and Earthquake Engineering*, *119*, 91–103.

Ministry of Infrastructures and Transportation. (2018a). Istruzioni per l'applicazione dell'aggiornamento delle norme tecniche per le costruzioni di cui al Decreto Ministeriale 17 Gennaio 2018 (NTC 2018, Circular 21/1/19 No. 7) [Rome, Italy (in Italian)].

Ministry of Infrastructures and Transportation. (2018b). Italian building code (NTC 2018) [Rome, Italy (in Italian)].

Miraglia, G., Lenticchia, E., Surace, C., & Ceravolo, R. (2020). Seismic damage identification by fitting the nonlinear and hysteretic dynamic response of monitored buildings. *Journal of Civil Structural Health Monitoring*, *10*(3), 457–469.

Mollaioli, F., Lucchini, A., Cheng, Y., & Monti, G. (2013). Intensity measures for the seismic response prediction of base-isolated buildings. *Bulletin of Earthquake Engineering*, *11*(5), 1841–1866.

Morassi, A., & Vestroni, F. (2008). *Dynamic methods for damage detection in structures.* Springer.

Mori, F., Acunzo, G., Fiorini, N., Pagliaroli, A., Spina, D., & Dolce, M. (2015). The SMAV (Seismic Model from Ambient Vibrations) methodology for the evaluation of the structural operativity of the buildings. *Atti del XVI Convegno ANIDIS*.

Mori, F., & Spina, D. (2015). Vulnerability assessment of strategic buildings based on ambient vibrations measurements. *Structural Monitoring and Maintenance*, *2*(2), 115–132.

Mottershead, J. E., Link, M., & Friswell, M. I. (2011). The sensitivity method in finite element model updating: A tutorial. *Mechanical Systems and Signal Processing*, *25*(7), 2275–2296.

Mouyiannou, A., Rota, M., Penna, A., & Magenes, G. (2014). Identification of suitable limit states from nonlinear dynamic analyses of masonry structures. *Journal of Earthquake Engineering*, *18*(2), 231–263.

Nagarajaiah, S., & Basu, B. (2009). Output only modal identification and structural damage detection using time frequency and wavelet techniques. *Earthquake Engineering and Engineering Vibration*, *8*(4), 583–605.

Nakamura, Y., Derakhshan, H., Magenes, G., & Griffith, M. C. (2017). Influence of diaphragm flexibility on seismic response of unreinforced masonry buildings. *Journal of Earthquake Engineering*, *21*(6), 935–960.

National Research Counsil. (2013). Istruzioni per la Valutazione Affidabilistica della Sicurezza Sismica di Edifici Esistenti (CNR-DT 212/2013) [Rome, Italy (in Italian)].

Navarro, M., & Oliveira, C. (2005). Dynamic properties of existing RC buildings using measurements of ambient vibrations. *Proceedings of the 6th European Conference on Structural Dynamics (EURODYN)*.

New Zealand Society for Earthquake Engineering. (2017). The Seismic Assessment of Existing Buildings (NZSEE 2017).

Oliveira, C. (2003). Seismic vulnerability of historical constructions: a contribution. *Bulletin of Earthquake Engineering*, *1*(1), 37–82.

Ottonelli, D., Cattari, S., & Lagomarsino, S. (2020). Displacement-Based Simplified Seismic Loss Assessment of Masonry Buildings. *Journal of Earthquake Engineering*, *24*(sup1), 23–59.

Parloo, E., Cauberghe, B., Benedettini, F., Alaggio, R., & Guillaume, P. (2005). Sensitivity-based operational mode shape normalisation: application to a bridge. *Mechanical Systems and Signal Processing, 19*(1), 43–55.

Parloo, E., Verboven, P., Cuillame, P., & Overmeire, M. V. (2001). Sensitivity-based mass normalization of mode shape estimates from output-only data. *Proceedings of the International Conference on Structural System Identification.*

Parloo, E., Verboven, P., Guillaume, P., & Van Overmeire, M. (2002). Sensitivity-based operational mode shape normalisation. *Mechanical Systems and Signal Processing, 16*(5), 757–767.

Peeters, B., & De Roeck, G. (2001). Stochastic system identification for operational modal analysis: a review. *Journal of Dynamic Systems, Measurement, and Control, 123*(4), 659–667.

Peeters, B., Maeck, J., & De Roeck, G. (2001). Vibration-based damage detection in civil engineering: excitation sources and temperature effects. *Smart Materials and Structures, 10*(3), 518.

Penna, A., Rota, M., Mouyiannou, A., & Magenes, G. (2013). Issues on the use of time-history analysis for the design and assessment of masonry structures. *Proceedings of the 4th International Conference on Computational Methods in Structural Dynamics and Earthquake Engineering (COMPDYN).*

Perrault, M., Gueguen, P., Aldea, A., & Demetriu, S. (2013). Using experimental data to reduce the single-building sigma of fragility curves: case study of the BRD tower in Bucharest, Romania. *Earthquake Engineering and Engineering Vibration, 12*(4), 643–658.

Piazza, M., Baldessari, C., & Tomasi, R. (2008). The role of in-plane floor stiffness in the seismic behaviour of traditional buildings. *Proceedings of the 14th World conference on Earthquake Engineering (WCEE).*

Picozzi, M., Ditommaso, R., Parolai, S., Mucciarelli, M., Milkereit, C., Sobiesiak, M., Di Giacomo, D., Gallipoli, M., Pilz, M., Vona, M., et al. (2010). Real time monitoring of structures in task force missions: the example of the Mw= 6.3 Central Italy Earthquake, April 6, 2009. *Natural Hazards, 52*(2), 253–256.

Pierdicca, A., Clementi, F., Isidori, D., Concettoni, E., Cristalli, C., & Lenci, S. (2016). Numerical model upgrading of a historical masonry palace monitored with a wireless sensor network. *International Journal of Masonry Research and Innovation, 1*(1), 74–98.

Pioldi, F., & Rizzi, E. (2017). A refined Frequency Domain Decomposition tool for structural modal monitoring in earthquake engineering. *Earthquake Engineering and Engineering Vibration, 16*(3), 627–648.

Ponzo, F. C., Cardone, D., Di Cesare, A., Moroni, C., Nigro, D., & Vigoriti, G. (2007). Dynamic tests on JETPACS steel frame: experimental model set up. *DPC-RELUIS JETPACS Report,* (3).

Ponzo, F. C., Ditommaso, R., Auletta, G., & Mossucca, A. (2010). A fast method for structural health monitoring of Italian reinforced concrete strategic buildings. *Bulletin of Earthquake Engineering, 8*(6), 1421–1434.

Ponzo, F. C., Di Cesare, A., Nigro, D., Vulcano, A., Mazza, F., Dolce, M., & Moroni, C. (2012). JET-PACS project: dynamic experimental tests and numerical results

obtained for a steel frame equipped with hysteretic damped chevron braces. *Journal of Earthquake Engineering*, *16*(5), 662–685.

Potenza, F., Federici, F., Lepidi, M., Gattulli, V., Graziosi, F., & Colarieti, A. (2015). Long-term structural monitoring of the damaged Basilica S. Maria di Collemaggio through a low-cost wireless sensor network. *Journal of Civil Structural Health Monitoring*, *5*(5), 655–676.

Quagliarini, E., Maracchini, G., & Clementi, F. (2017). Uses and limits of the Equivalent Frame Model on existing unreinforced masonry buildings for assessing their seismic risk: A review. *Journal of Building Engineering*, *10*, 166–182.

Rainieri, C., & Fabbrocino, G. (2010). Automated output-only dynamic identification of civil engineering structures. *Mechanical Systems and Signal Processing*, *24*(3), 678–695.

Rainieri, C., & Fabbrocino, G. (2014). *Operational modal analysis of civil engineering structures*. Springer.

Rainieri, C., & Fabbrocino, G. (2015). Learning operational modal analysis in four steps. *Proceedings of the 6th International Operational Modal Analysis Conference (IOMAC)*.

Rainieri, C., Fabbrocino, G., & Cosenza, E. (2010). On damping experimental estimation. *Proceedings of the 10th International Conference on Computational Structures Technology (CST)*.

Ren, W.-X., & Chen, H.-B. (2010). Finite element model updating in structural dynamics by using the response surface method. *Engineering Structures*, *32*(8), 2455–2465.

Reuland, Y., Lestuzzi, P., & Smith, I. F. (2019). Measurement-based support for post-earthquake assessment of buildings. *Structure and Infrastructure Engineering*, *15*(5), 647–662.

Reynders, E. (2012). System identification methods for (operational) modal analysis: review and comparison. *Archives of Computational Methods in Engineering*, *19*(1), 51–124.

Reynders, E., & De Roeck, G. (2008). Reference-based combined deterministic–stochastic subspace identification for experimental and operational modal analysis. *Mechanical Systems and Signal Processing*, *22*(3), 617–637.

Reynders, E., Teughels, A., & De Roeck, G. (2010). Finite element model updating and structural damage identification using OMAX data. *Mechanical Systems and Signal Processing*, *24*(5), 1306–1323.

Rizzi, E., Giongo, I., Ingham, J. M., & Dizhur, D. (2020). Testing and Modeling In-Plane Behavior of Retrofitted Timber Diaphragms. *Journal of Structural Engineering*, *146*(2), 04019191.

Roca, P., Cervera, M., Gariup, G., et al. (2010). Structural analysis of masonry historical constructions. Classical and advanced approaches. *Archives of Computational Methods in Engineering*, *17*(3), 299–325.

Rossi, M., Calderini, C., & Lagomarsino, S. (2016). Experimental testing of the seismic in-plane displacement capacity of masonry cross vaults through a scale model. *Bulletin of Earthquake Engineering*, *11*(1), 261–281.

Rossi, M., Barentin, C. C., Van Mele, T., & Block, P. (2017). Experimental study on the behaviour of masonry pavilion vaults on spreading supports. *Structures*, *11*, 110–120.

Rosti, A., Rota, M., & Penna, A. (2018). Damage classification and derivation of damage probability matrices from L'Aquila (2009) post-earthquake survey data. *Bulletin of Earthquake Engineering*, *16*(9), 3687–3720.

Rosti, A., Rota, M., & Penna, A. (2020). Empirical fragility curves for Italian URM buildings. *Bulletin of Earthquake Engineering*.

Rota, M., Penna, A., & Strobbia, C. (2008). Processing Italian damage data to derive typological fragility curves. *Soil Dynamics and Earthquake Engineering*, *28*(10-11), 933–947.

Salawu, O. S. (1997). Detection of structural damage through changes in frequency: a review. *Engineering structures*, *19*(9), 718–723.

Shih, C., Tsuei, Y., Allemang, R., & Brown, D. (1988). Complex mode indication function and its applications to spatial domain parameter estimation. *Mechanical Systems and Signal Processing*, *2*(4), 367–377.

Shome, N. (1999). *Probabilistic seismic demand analysis of nonlinear structures* (Doctoral dissertation). Stanford University.

Simões, A. G., Bento, R., Lagomarsino, S., Cattari, S., & Lourenço, P. B. (2020). Seismic assessment of nineteenth and twentieth centuries URM buildings in Lisbon: structural features and derivation of fragility curves. *Bulletin of Earthquake Engineering*, *18*(2), 645–672.

Sisti, R., Di Ludovico, M., Borri, A., & Prota, A. (2019). Damage assessment and the effectiveness of prevention: the response of ordinary unreinforced masonry buildings in Norcia during the Central Italy 2016–2017 seismic sequence. *Bulletin of Earthquake Engineering*, *17*(10), 5609–5629.

Sivori, D., Cattari, S., & Lepidi, M. (2019). Assessment of the rigid behaviour of diaphragms from ambient vibration measurements: application to masonry buildings in pre and post-earthquake conditions [In Italian]. *Atti del XVIII Convegno ANIDIS*.

Sivori, D., Cattari, S., & Lepidi, M. (2020a). Testing the dynamic behaviour of floor diaphragms for the seismic assessment of buildings. *Proceedings of the 17th World Conference on Earthquake Engineering (WCEE)*.

Sivori, D., Cattari, S., & Lepidi, M. (2021a). Development of frequency-variation curves for URM buildings accounting for the co-seismic shift and post-seismic decay effects. [In preparation]. *Bulletin of Earthquake Engineering*.

Sivori, D., Lepidi, M., & Cattari, S. (2020b). Ambient vibration tools to validate the rigid diaphragm assumption in the seismic assessment of buildings. *Earthquake Engineering and Structural Dynamics*, *49*(2), 194–211. https://doi.org/https://doi.org/10.1002/eqe.3235

Sivori, D., Lepidi, M., & Cattari, S. (2021b). Structural identification of the dynamic behavior of floor diaphragms in existing buildings. *Smart Structures and Systems*, *27*(2), 173–191. https://doi.org/https://doi.org/10.12989/sss.2021.27.2.17

Sivori, D., Cattari, S., De Ferrari, R., Lepidi, M., & Spina, D. (2018). Ambient vibration testing of existing buildings aimed to seismic assessment: experiences in Liguria (abstract). *International Conference on Computational Methods (ICCM)*. http://www.sci-en-tech.com/ICCM2018/PDFs/3366-10895-1-PB.pdf

Skolnik, D., Lei, Y., Yu, E., & Wallace, J. W. (2006). Identification, model updating, and response prediction of an instrumented 15-story steel-frame building. *Earthquake Spectra*, *22*(3), 781–802.

Snoj, J., Österreicher, M., & Dolšek, M. (2013). The importance of ambient and forced vibration measurements for the results of seismic performance assessment of buildings obtained by using a simplified non-linear procedure: case study of an old masonry building. *Bulletin of Earthquake Engineering*, *11*(6), 2105–2132.

Sohn, H. (2007). Effects of environmental and operational variability on structural health monitoring. *Philosophical Transactions of the Royal Society A: Mathematical, Physical and Engineering Sciences*, *365*(1851), 539–560.

Solarino, F., Oliveira, D. V., & Giresini, L. (2019). Wall-to-horizontal diaphragm connections in historical buildings: A state-of-the-art review. *Engineering Structures*, *199*, 109559.

Sorrentino, L., Liberatore, L., Decanini, L., & Liberatore, D. (2014). The performance of churches in the 2012 Emilia earthquakes. *Bulletin of Earthquake Engineering*, *12*(5), 2299–2331.

Sorrentino, L., Cattari, S., Da Porto, F., Magenes, G., & Penna, A. (2019). Seismic behaviour of ordinary masonry buildings during the 2016 central Italy earthquakes. *Bulletin of Earthquake Engineering*, *17*(10), 5583–5607.

Spina, D., Acunzo, G., Fiorini, N., Mori, F., & Dolce, M. (2018). A probabilistic simplified seismic model of masonry buildings based on ambient vibrations. *Bulletin of Earthquake Engineering*, 1–23.

Spina, D., Acunzo, G., Fiorini, N., Mori, F., & Dolce, M. (2019). A probabilistic simplified seismic model of masonry buildings based on ambient vibrations. *Bulletin of Earthquake Engineering*, *17*(2), 985–1007.

Spina, D., & Lamonaca, B. (1998). Strengthening assessment of building using ambient vibration tests. *Proceedings of the XI Conference on Earthquake Engineering*.

Spina, D., Lamonaca, B., Nicoletti, M., & Dolce, M. (2011). Structural monitoring by the Italian Department of Civil Protection and the case of 2009 Abruzzo seismic sequence. *Bulletin of Earthquake Engineering*, *9*(1), 325–346.

Sun, K., Zhou, Q., & Liu, Y. (2014). A phase locked loop-based approach to real-time modal analysis on synchrophasor measurements. *IEEE Transactions on Smart Grid*, *5*(1), 260–269.

Tamura, Y., Zhang, L., Yoshida, A., Nakata, S., & Itoh, T. (2002). Ambient vibration tests and modal identification of structures by FDD and 2DOF-RD technique. *Proceedings of the Structural Engineers World Congress*.

Todorovska, M. I. (2009). Seismic interferometry of a soil-structure interaction model with coupled horizontal and rocking response. *Bulletin of the Seismological Society of America*, *99*(2A), 611–625.

Tomaževič, M. (1999). *Earthquake-resistant design of masonry buildings*. World Scientific.

Trevlopoulos, K., & Guéguen, P. (2016). Period elongation-based framework for operative assessment of the variation of seismic vulnerability of reinforced concrete buildings during aftershock sequences. *Soil Dynamics and Earthquake Engineering*, *84*, 224–237.

Trevlopoulos, K., Guéguen, P., Helmstetter, A., & Cotton, F. (2020). Earthquake risk in reinforced concrete buildings during aftershock sequences based on period elongation and operational earthquake forecasting. *Structural Safety*, *84*, 101922.

Tsogka, C., Daskalakis, E., Comanducci, G., & Ubertini, F. (2017). The stretching method for vibration-based structural health monitoring of civil structures. *Computer-Aided Civil and Infrastructure Engineering*, *32*(4), 288–303.

Turnšek, V., & Čačovič, F. (1971). Some experimental results on the strength of brick masonry walls. *Proceedings of the 2nd International Brick Masonry Conference.*

Turnšek, V., & Sheppard, P. (1980). *The shear and flexural resistance of masonry walls.*

Ubertini, F., Comanducci, G., & Cavalagli, N. (2016). Vibration-based structural health monitoring of a historic bell-tower using output-only measurements and multivariate statistical analysis. *Structural Health Monitoring*, *15*(4), 438–457.

Vamvatsikos, D., & Cornell, C. (2002). Incremental dynamic analysis. *Earthquake engineering and structural dynamics*, *31*(3), 491–514.

Vanin, F., Zaganelli, D., Penna, A., & Beyer, K. (2017). Estimates for the stiffness, strength and drift capacity of stone masonry walls based on 123 quasi-static cyclic tests reported in the literature. *Bulletin of Earthquake Engineering*, *15*(12), 5435–5479.

Ventura, C., Lord, J., Turek, M., Brincker, R., Andersen, P., & Dascotte, E. (2005). FEM updating of tall buildings using ambient vibration data. *Proceedings of the 6th European Conference on Structural Dynamics (EURODYN).*

Vestroni, F., & Capecchi, D. (2000). Damage detection in beam structures based on frequency measurements. *Journal of Engineering Mechanics*, *126*(7), 761–768.

Vidal, F., Navarro, M., Aranda, C., & Enomoto, T. (2014). Changes in dynamic characteristics of Lorca RC buildings from pre-and post-earthquake ambient vibration data. *Bulletin of Earthquake Engineering*, *12*(5), 2095–2110.

Villaverde, R. (2007). Methods to assess the seismic collapse capacity of building structures: State of the art. *Journal of Structural Engineering*, *133*(1), 57–66.

Wang, X., Ye, A., Shafieezadeh, A., & Padgett, J. E. (2019). Fractional order optimal intensity measures for probabilistic seismic demand modeling of extended pile-shaft-supported bridges in liquefiable and laterally spreading ground. *Soil Dynamics and Earthquake Engineering*, *120*, 301–315.

Welch, P. (1967). The use of fast Fourier transform for the estimation of power spectra: a method based on time averaging over short, modified periodograms. *IEEE Transactions on Audio and Electroacoustics*, *15*(2), 70–73.

Williams, M. S., & Sexsmith, R. G. (1995). Seismic damage indices for concrete structures: a state-of-the-art review. *Earthquake Spectra*, *11*(2), 319–349.

Workgroup, R. (2018). Results of the 2015-2017 implicit seismic risk of code-conforming structures in Italy (RINTC) project. *ReLUIS report, Rete dei Laboratori Universitari di Ingegneria Sismica (ReLUIS), Naples, Italy.* http://www.reluis.it/images/stories/RINTC_2015-2017_FINAL_REPORT.pdf

Yi, F., Dyke, S. J., Caicedo, J. M., & Carlson, J. D. (2001). Experimental verification of multiinput seismic control strategies for smart dampers. *Journal of Engineering Mechanics*, *127*(11), 1152–1164.

Zhang, L., Wang, T., & Tamura, Y. (2010). A frequency–spatial domain decomposition (FSDD) method for operational modal analysis. *Mechanical Systems and Signal Processing*, *24*(5), 1227–1239.

Appendix: masonry buildings tested within the SMAV Liguria Project and monitored by OSS

The following paragraphs summarise the results of operational modal analysis of three masonry buildings, including some preliminary investigations regarding the in-plane dynamic behaviour of their floor diaphragms.

In particular, the town hall buildings of the Alassio and Sanremo municipalities have been tested through ambient vibration measurements in the framework of the *SMAV Liguria Project 2018-2019* (Sivori et al., 2018), funded by the Italian Department of Civil Protection (DPC) and aimed at the quick assessment of the seismic serviceability of strategic buildings through the SMAV methodology. This project belongs to a comprehensive national initiative (Dolce, 2012; Dolce et al., 2018) to assess the reliability of emergency systems for the mitigation of seismic risk in urbanized areas. The project has been recently renewed for the 2020-2021 biennium, involving the testing of five more buildings.

The Fabriano courthouse, conversely, is being permanently monitored by the Italian Structural Seismic Monitoring Network (OSS, Dolce et al., 2017a) managed by DPC, whose monitoring data were shared with several Italian universities in the framework of the ReLUIS 2017-2018 Project, Research Line "Masonry Structures", Task 4.1 - "Analysis of buildings monitored by the Osservatorio Sismico delle Strutture (OSS)".

Figure A1: (a) Bird's-eye view of Bellevue Palace (from Bing Maps). (b) Front view of the building, showing the regular distribution of openings on the façade.

Sanremo town hall building

Bellevue Palace was a luxury hotel built in Sanremo at the end of the 19th century. The building houses the city town hall, holding the strategic role to coordinate rescue operations in the municipality after the earthquake. The structure rises on a gentle slope with four floors above the ground and a habitable attic (Figure A1a). The openings are vertically aligned and evenly distributed both for internal and external walls, with the highest concentration in the front wall (Figure A1b). The rectangular plan develops smoothly in the x direction (EW), symmetrically with respect to the y direction (NS), with three main supporting walls running along the whole length of the building (Figure A2). Four orthogonal walls divide the plan into five parts of which the two outermost are slightly projecting. In particular, the east wing has undergone several structural interventions, including the removal of an internal bearing wall. The sides dimensions are $66\,\text{m} \times 16.90\,\text{m}$, for a total area of $1115\,\text{m}^2$. The interstorey height ranges from $4.75\,\text{m}$ on the ground floor to $4.10\,\text{m}$ on the top floor. The masonry walls, built with a cut local stone with good bonding, are $70\,\text{cm}$ thick at the ground and become thinner with height, to a minimum of $50\,\text{cm}$ at the topmost floor. The attic supports a timber pitched roof.
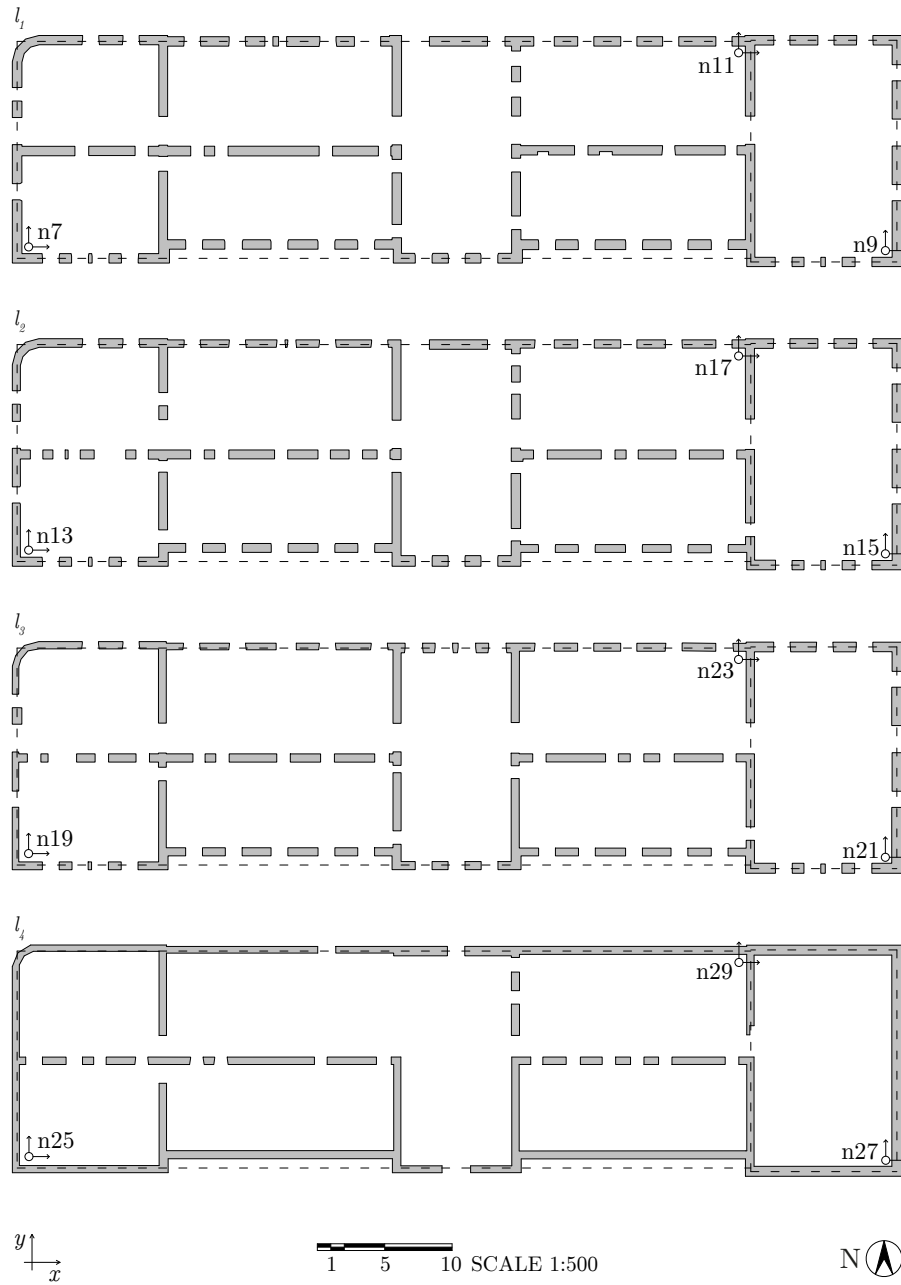
Figure A2: Structural plans of Bellevue palace, highlighting the position and orientation of the sensors.

Table A1: Measured nodes, sampling frequency f_s and length t_s of the acquired signals for each measurement configuration.

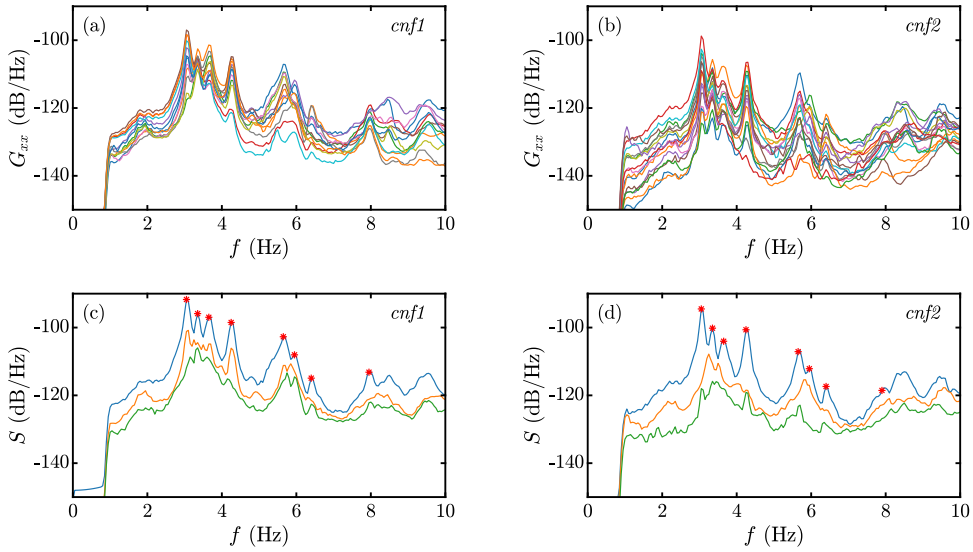| Config.	Level	Position	f_s (Hz)	t_s (s)
cnf1	l_4	n25,n27,n29	250	6300
	l_3	n19,n21,n23		
cnf2	l_4	n27,n29	250	3000
	l_2	n13,n15,n17		
	l_1	n7,n9,n11		

Figure A3: (a,b) Power spectral densities of the signals and (c,d) singular values of the spectral density matrix of each measurement configuration.

Ambient vibration tests

Ambient vibrations have been acquired employing eight seismometers *Lennartz 3D/5S*, each paired with an independent data acquisition recorder *MarsLite* equipped with a 20 bit A/D converter, an SD card for data storage and a GPS receiver for time synchronization. The measurement setup involved three sensors at each level of the building with two reference sensors on the rooftop, deployed in two partial configurations ($cnf1$ and $cnf2$, Figure A2). The ambient response of the building – in terms of velocity – has been measured with a sampling frequency f_s of 200 Hz for at least one hour for each measurement setup (Table A1).

The signals have been decimated by a factor of 5 and, according to the frequency response of the seismometers, high-pass filtered below 1 Hz. Therefore, the frequency band investigated goes from 1 Hz to 25 Hz. Natural frequencies, mode shapes and damping ratios are identified using the *Enhanced* Frequency Domain Decomposition (EFDD) technique (Section 2.2.1). The auto- and cross-power spectral densities are estimated employing the Welch method with 20 s Hamming windows and 50 % overlap (Figures A3a,b), resulting in a

Table A2: Natural frequencies, damping ratios and mode shape type identified on Bellevue Palace.

Mode	f_n (Hz)	ξ (%)	Type
1	3.05	1.5	R
2	3.35	1.1	T
3	3.65	0.9	R
4	4.25	1.2	B
5	5.65	1.8	S
6	5.95	1.5	
7	6.40	1.9	
8	7.95	1.6	
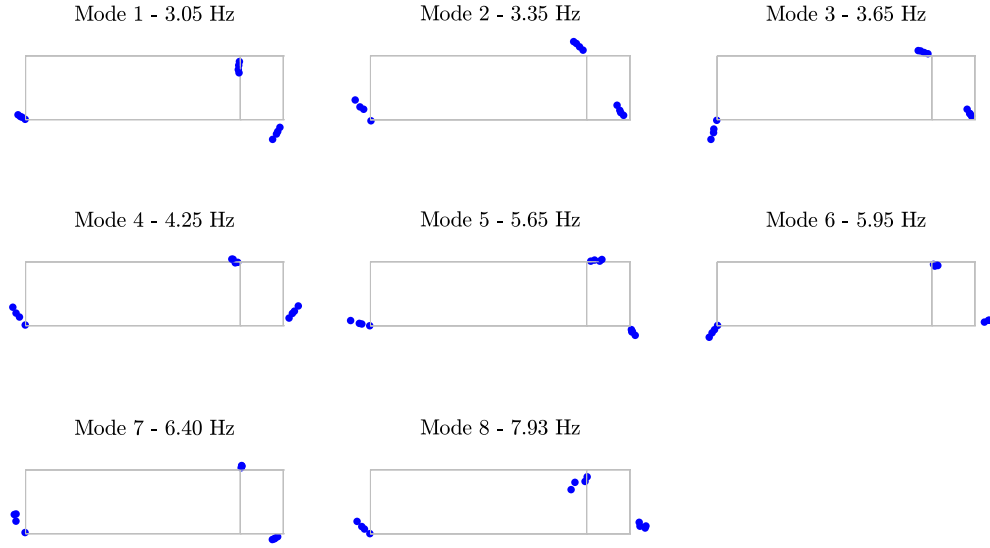
Figure A4: Identified modal displacements.

frequency resolution of 0.05 Hz. In both the measurement configurations, the first singular value of the spectral density matrix shows eight distinct resonance peaks below 10 Hz (Figures A3b,c). The global natural frequencies f_n and damping ratios ξ (Table A2) are estimated as the average of the corresponding quantities identified for each measurement configuration. The global modal amplitudes (Figures A4) are obtained by scaling and merging the partial mode shapes based on the modal amplitude identified for the reference sensor.

At 3.05 Hz and 3.65 Hz, the first and third identified modes show a torsional behaviour of the structure, in which the floor diaphragms rotate in their plane (R), around the leftmost and rightmost part of the building respectively. The second identified mode at 3.35 Hz, on the other hand, is dominated by the translation of the floors (T) – increasing linearly with the height of the building – along a diagonal direction. The remaining modes, laying at
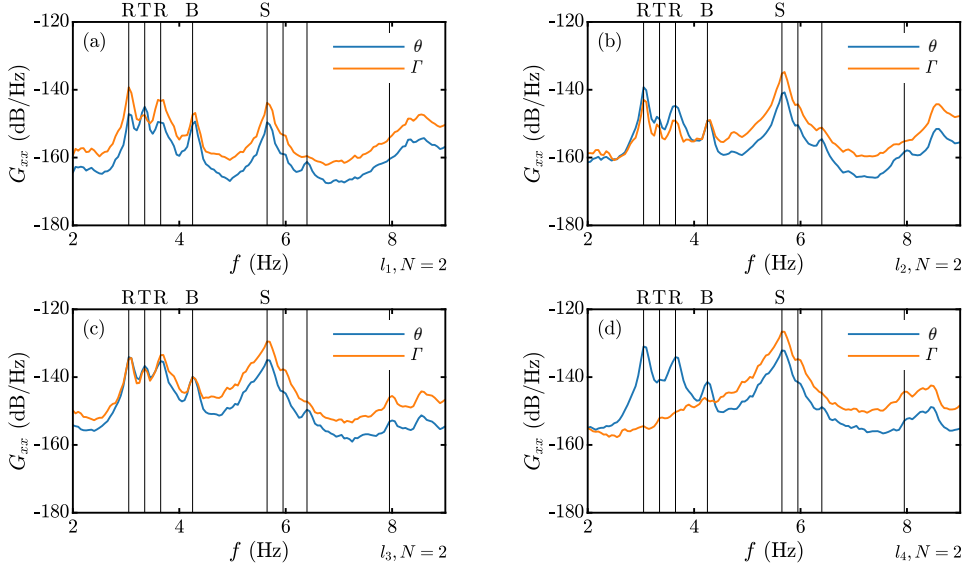
Figure A5: Power spectral densities (a,b,c,d) of the rigid rotation θ and shear strain Γ estimated at each level of the building (l_1, l_2, l_3, l_4) for $N = 2$.

higher frequencies, suffer from spatial aliasing due to the small number of sensors deployed. Nevertheless, several mode shapes show significant deformation components of the floors, as in the case of the bending deformation (B) of the fourth mode at $4.25\,\mathrm{Hz}$ and the shear deformation (S) of the fifth mode at $5.65\,\mathrm{Hz}$. The three modes at the highest frequency – at $5.95\,\mathrm{Hz}$, $6.4\,\mathrm{Hz}$ and $7.95\,\mathrm{Hz}$ – exhibit mode shapes of more complex geometry, with the concurring presence of rotation and deformation.

Experimental ambient behaviour of floor diaphragms

The rigid rotations θ and the shear strains Γ are estimated at each level of the building employing both the perturbation solution for $N = 2$ sensors (considering those placed on the opposite corners of the building, Figure A5) and the exact solution involving all the $N = 3$ sensors (Figure A6) – the second being sufficient to evaluate the axial strains E_x and E_y as well (Section 4.3.1). The spectra highlight how the first identified mode is rotating rigidly at the first two levels since, in terms of power spectral density, θ is two orders of magnitude greater than Γ (Figures A6a,c). For this mode, the spectral ratio G_θ/G_Γ is maximum at the second level. The rigid behaviour, however, vanishes at the upper floors. The second mode, given the absence of particular amplification peaks of θ and Γ, can be considered as a rigid translation of the diaphragms. Starting from the fourth mode, the deformation components become dominant with respect to the rigid ones. It is to be noted how this statement is valid for the axial strains as well, precluding any further analyses of the sub-diaphragms with the perturbation solution for $N = 2$ (due to the assumed smallness of E_x, E_y).
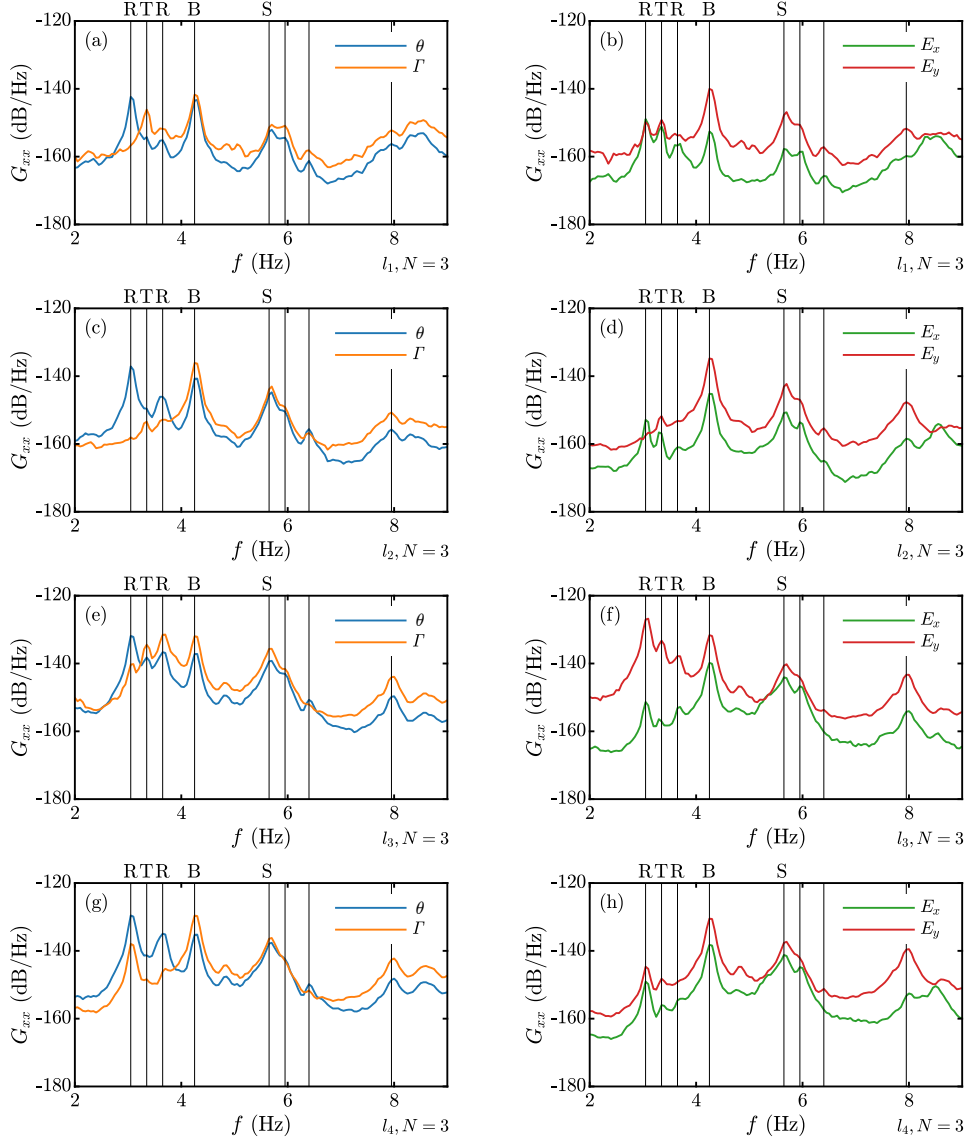
Figure A6: Power spectral densities (a,c,e,g) of the rigid rotation θ and shear strain Γ and (b,d,f,h) of the axial strains E_x, E_y estimated at each level of the building (l_1, l_2, l_3, l_4) for $N = 3$.

Alassio town hall building

The Alassio town hall is housed in a masonry building built in 1904 (Figure A7a). The structure rises isolated on a flat soil close to the seaside, with three floors above the ground and a habitable attic with a timber structure supporting the pitched roof. The building is characterized by a rectangular plan with dimensions of $40.5\,\text{m} \times 15.7\,\text{m}$, with the longest dimension aligned to the SE-NW direction. The bearing walls form a regular grid composed of three main walls crossed orthogonally by several secondary walls. The masonry piers are 70 cm thick at the ground and become thinner with height, down to a minimum of 50 cm at the topmost floor. As highlighted by the thermographic survey, masonry is made up of cut stones arranged in a regular fashion on courses of bricks (Figure A7b). The vertical layout is quite regular as well, with vertically aligned opening uniformly distributed over the external walls. The interstorey height, however, is not constant and decreases from 6.25 m on the ground floor to 4.25 m on the second floor.

Ambient vibration tests

The ambient response of the structure has been acquired employing a total of six *Lennartz 3D/5S* seismometers, deploying four sensors at each level of the building and two reference sensors on the rooftop in three partial configurations (Figure A8). The measurements have been acquired with a sampling frequency f_s of 125 Hz for half an hour for each measurement setup (Table A3).

The signals have been decimated by a factor of 2 and, due to the presence of measurement noise at low frequency, high-pass filtered below 3.5 Hz. Natural frequencies and mode shapes are identified employing the FDD technique, estimating the Welch periodograms with a frequency resolution of 0.05 Hz. Six modes have been identified from the amplification peaks of the singular value plot (Figure A9).

Figure A7: (a) Front view of the Alassio town hall building. (b) Thermographic image highlighting the presence of courses of bricks in the masonry texture.
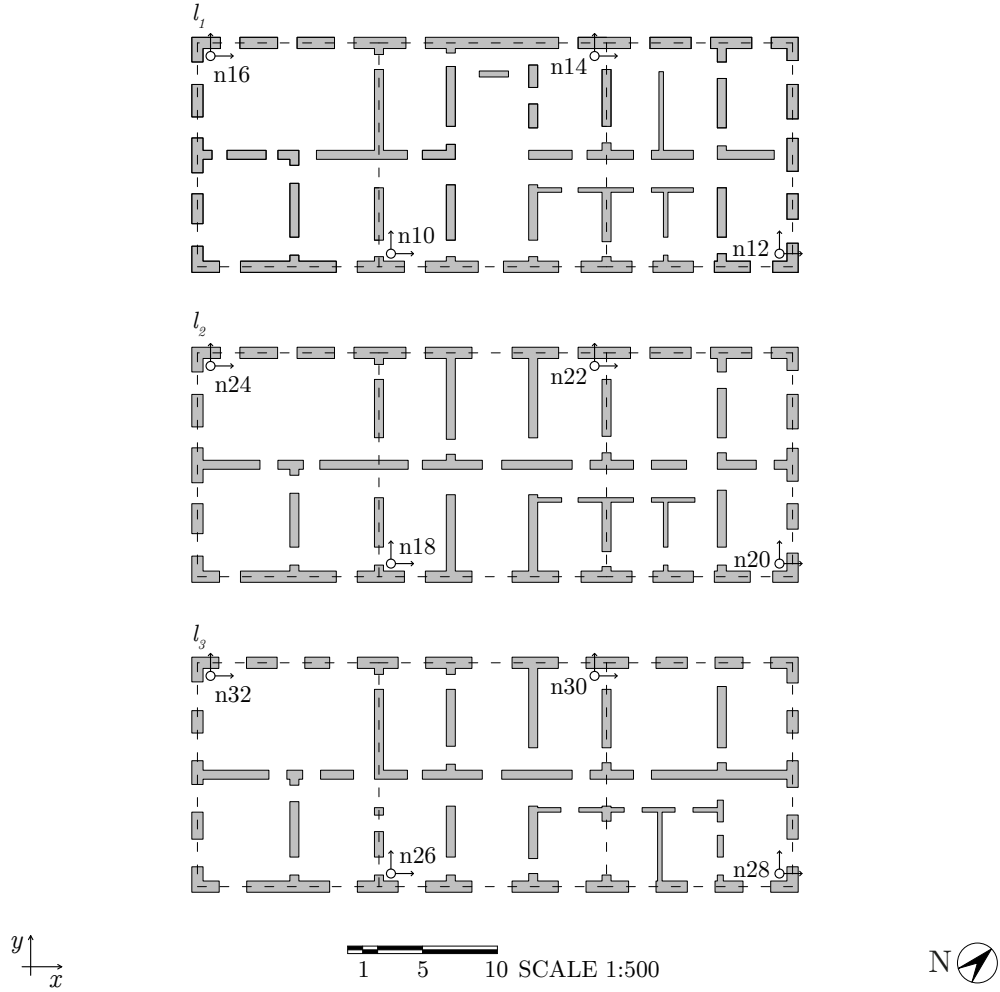
Figure A8: Structural plans of the Alassio town hall building, highlighting the position and orientation of the sensors.

Table A3: Measured nodes, sampling frequency f_s and length t_s of the acquired signals for each measurement configuration.

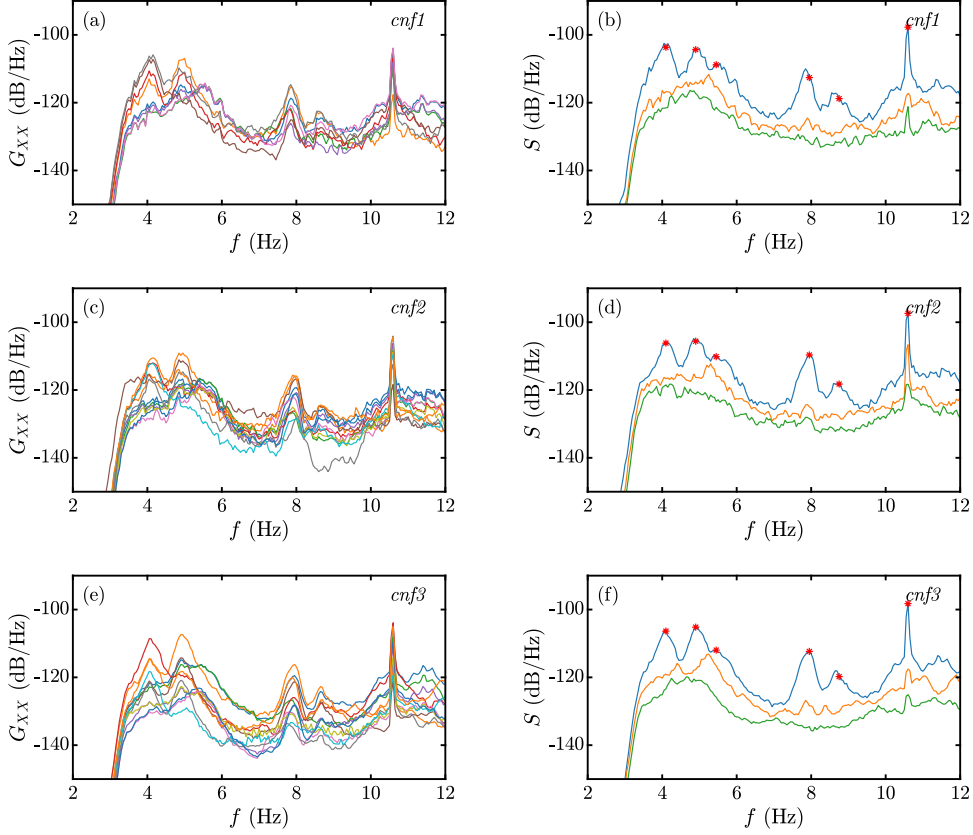| Configuration	Level	Position	f_s (Hz)	t_s (s)
cnf1	l_3	n26,n28,n30,n32	125	1800
cnf2	l_3	n26,n28	125	1800
	l_2	n18,n20,n22,n24		
cnf3	l_3	n26,n28	125	1800
	l_2	n10,n12,n14,n16		

171

Figure A9: (a,c,e) Power spectral densities of the signals and (b,d,f) singular values of the spectral density matrix for each measurement configuration.

The global natural frequencies f_n (Table A4) are estimated as the average of the corresponding quantities identified for each measurement configuration. The global modal amplitudes (Figure A10) are obtained by scaling and merging the partial mode shapes based on the modal amplitude identified for the reference sensor. The first identified mode at 4.10 Hz is a translational mode along the y direction (T_y) with modal amplitudes increasing with the height. The second identified mode at 4.90 Hz, on the other hand, is dominated by a torsional behaviour (R). The third mode identified at 5.45 Hz shows a translation along the x direction (T_x). The fourth and fifth identified modes, laying respectively at 7.90 Hz and 8.65 Hz, exhibit the in-plane bending deformation of the floor diaphragms (B), with a vertical shape that reaches its maximum displacement at the second floor. The amplification peak at 10.60 Hz, as shown by the unusual mode shape and given the high damping and the low phase collinearity, can be considered as a non-structural mode caused by a harmonic component of the input (Figure A10).

Table A4: Natural frequencies and mode shape type identified on the Alassio town hall building.

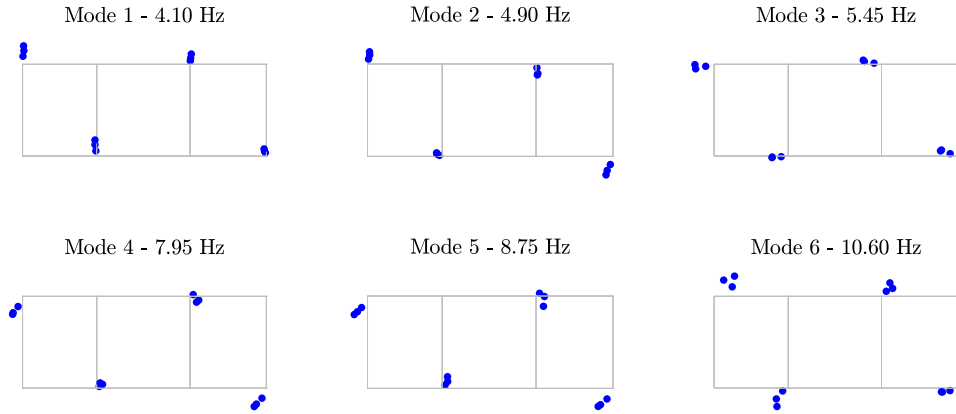| Mode	f_n (Hz)	Type
1	4.1	T_y
2	4.9	R
3	5.45	T_x
4	7.9	B
5	8.65	B

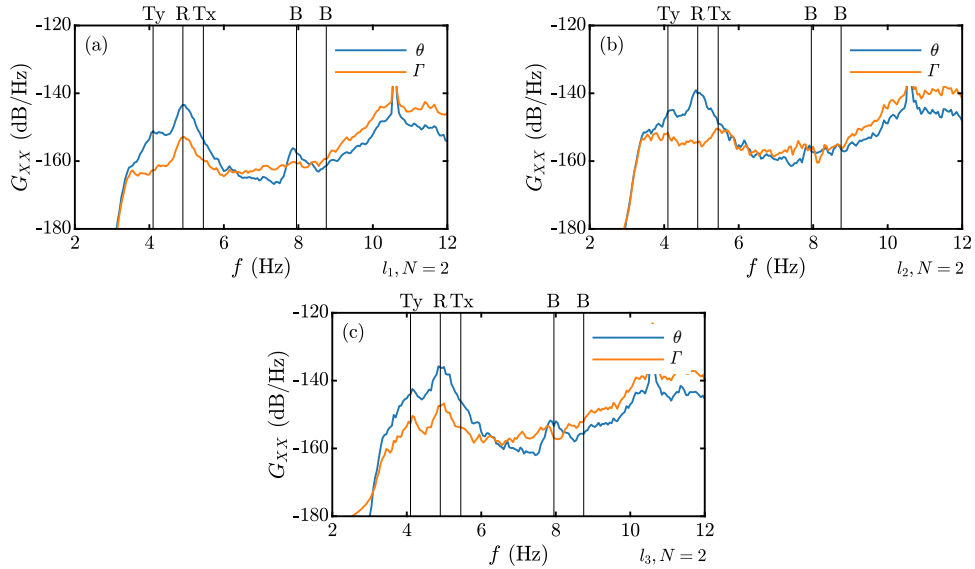Figure A10: Identified modal displacements.

Figure A11: Power spectral densities (a,b,c) of the rigid rotation θ and shear strain Γ estimated at each level of the building for $N = 2$.
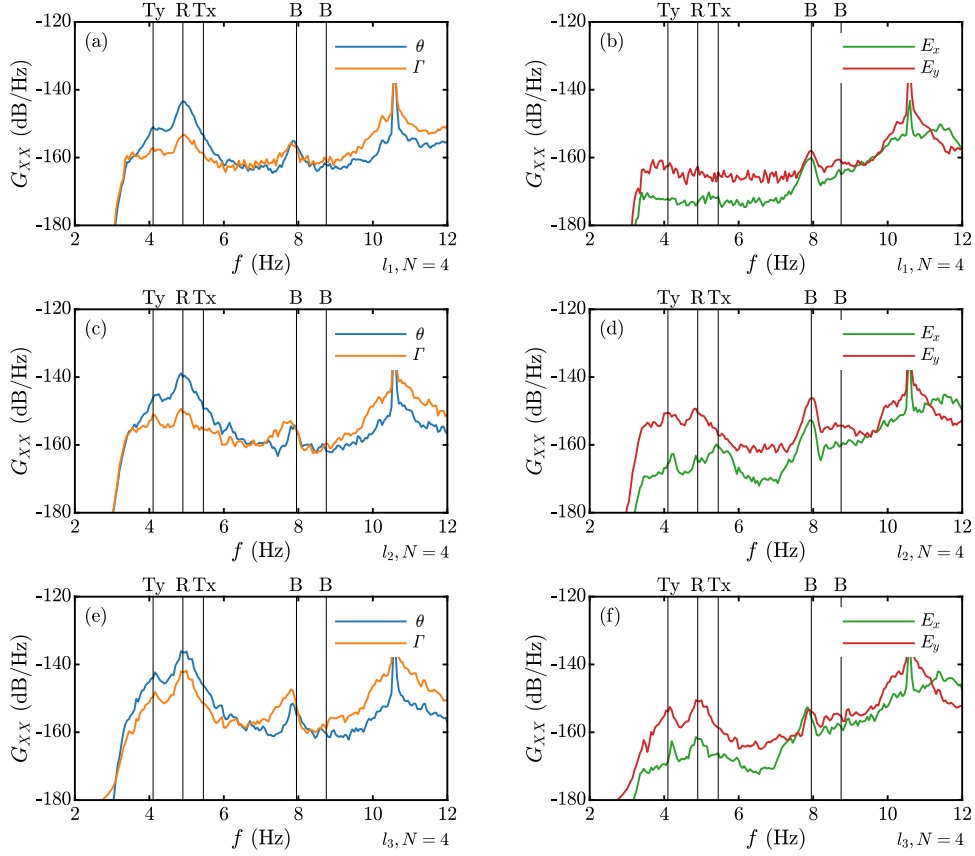
173

Figure A12: Power spectral densities (a,c,e) of the rigid rotation θ and shear strain Γ and (b,d,f) of the axial strains E_x, E_y estimated at each level of the building for $N = 4$.

Experimental ambient behaviour of floor diaphragms

The rigid rotations θ and the shear strains Γ are estimated at each level of the building employing the perturbation solution for $N = 2$ sensors (those of extremities at opposing corners, Figure A11), the least-squares solution for $N = 4$ sensors (Figure A12). The approximated solution for $N = 2$ shows quite good agreement with the least-squares results in the entire frequency band investigated. The spectra highlight a quasi-rigid behaviour for the first three identified modes (namely T_y, R and T_x) given the absence of amplification peaks of Γ. This statement, however, is valid only for the first two levels (Figure A12a,c). In particular, the third identified mode at 4.9 Hz is rotating quasi-rigidly and, in terms of power spectral density, θ is one order of magnitude greater than Γ with a ratio G_θ/G_Γ equal to 10. As already discussed, the rigid behaviour vanishes at the topmost floor, in which the axial deformations E_x and E_y play a primary role in the diaphragm dynamic behaviour (Figure A12f). Starting from the fourth identified mode, the deformation components become equal or greater than the rigid ones.

Fabriano courthouse building

The Fabriano courthouse is a massive masonry building permanently monitored by OSS. The structure rises isolated with one underground floor, three floors above the ground and an attic level covered by a pitched roof (Figure A13a). The vertical layout of the structure is quite regular since all the floors share the same interstorey height ($h_i = 5.3\,\text{m}$). The openings are mainly concentrated in the front and lateral walls of the building (Figure A13b), arranged along vertical alignments in a quite regular pattern. The T-shaped geometry of the plan of the building, on the other hand, is strongly irregular. The main body dimensions are $76.7\,\text{m} \times 15.6\,\text{m}$, whereas the smaller rear body extends for $15.9\,\text{m} \times 19.5\,\text{m}$. The masonry piers are made with cut stones arranged in a regular fashion, whose thickness ranges from $80\,\text{cm}$ to $110\,\text{cm}$ on the first floor, from $50\,\text{cm}$ to $60\,\text{cm}$ on the upper floors. The floor slabs have quite different structural typology from level to level. The ground floor is made of small iron beams and brick clay walls. The first floor is made of iron and hollow bricks. The second and the third-floor diaphragms are composed of Ω-shaped iron beams supporting wooden planks. The foundations are characterized by the continuation of the load-bearing walls for a depth of $1.9\,\text{m}$.

Ambient vibrations monitoring

The ambient response of the structure is monitored by three bi-axial and one mono-axial accelerometers at each level of the building (Figure A14), with a sampling frequency f_s of $250\,\text{Hz}$ for little less than one hour (Table A5).

Figure A13: (a) Orthophoto of the Fabriano courthouse (from Google Maps). (b) View of the left-wing, showing the regular pattern of openings on the perimeter walls.

Table A5: Measured nodes, sampling frequency f_s and length t_s of the acquired signals.

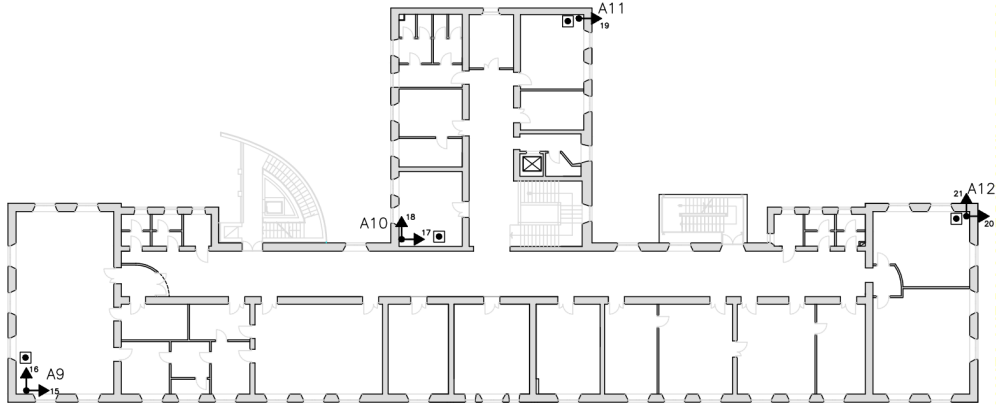| Level	Position	f_s (Hz)	t_s (s)
l_0	n1,n2,n3,n4		
l_1	n5,n6,n7,n8	250	3200
l_2	n9,n10,n11,n12		
l_3	n13,n14,n15,n16		

Figure A14: Structural plans (second level) of the Fabriano courthouse, highlighting the position and orientation of the monitoring system's sensors.
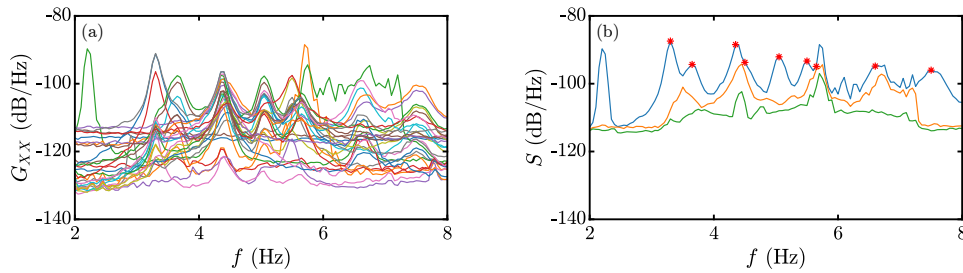

Figure A15: (a) Power spectral densities of the signals and (b) first three singular values of the spectral density matrix.

The signals have been decimated by a factor of 5 (Nyquist frequency $f_{ny} = 25\,\text{Hz}$) and de-trended to remove the linear increase of the mean value in some measurement channels. Natural frequencies, mode shapes and damping ratios are identified employing the FDD technique, estimating the Welch periodograms with a frequency resolution of $0.05\,\text{Hz}$. Up to nine modes have been identified from the amplification peaks of the singular value plot (Figure A15). As highlighted by their mode shapes (Figure A16), the first three identified mode (respectively at $3.3\,\text{Hz}$, $3.65\,\text{Hz}$ and $4.35\,\text{Hz}$) show the bending deformations of the floor in their plane (B). The fourth identified mode at $4.35\,\text{Hz}$ involves the translation of the floors along the y direction (T_y) with modal displacements increasing with the height of the building. The second identified mode at $5.7\,\text{Hz}$ is a torsional mode (R), with the maximum modal displacement located in the western part of the building. The third mode identified at $6.55\,\text{Hz}$ shows again a translational behaviour, this time along the x direction (T_x). The fourth identified mode at $9.05\,\text{Hz}$ shows the bending of the floors in the horizontal plane (B), whereas the fifth mode at $12.25\,\text{Hz}$ their shear deformation. The sixth mode appears as a quasi-symmetric mode with respect to y, involving the bending of the projecting bodies towards the centre of the building.

176

Table A6: Natural frequencies and mode shape type identified on the Fabriano courthouse.

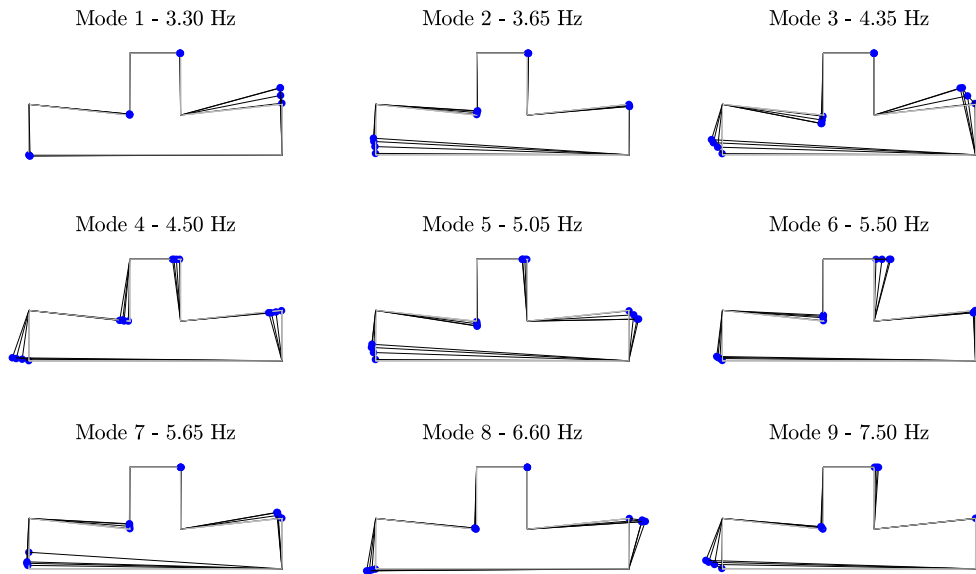| Mode	f_n (Hz)	Type
1	3.3	B
2	3.65	B
3	4.35	B
4	4.5	T_x
5	5.05	R
6	5.5	
7	5.65	
8	6.6	S
9	7.5	

Figure A16: Identified mode shapes.

Experimental ambient behaviour of floor diaphragm

The rigid rotation θ, the shear strain Γ and the axial strains E_x and E_y are estimated at each level of the building employing the exact solution for $N = 3$ sensors (those pertaining to the main body of the building, Figure A12). The spectra highlight a general deformable behaviour of diaphragms, dominated by the shear strain and axial deformation peaks in the entire investigated frequency band. This result is not surprising, considering the geometrical extension of the building which the activation of local modes in the wings, rather than global rigid-behaving modes.
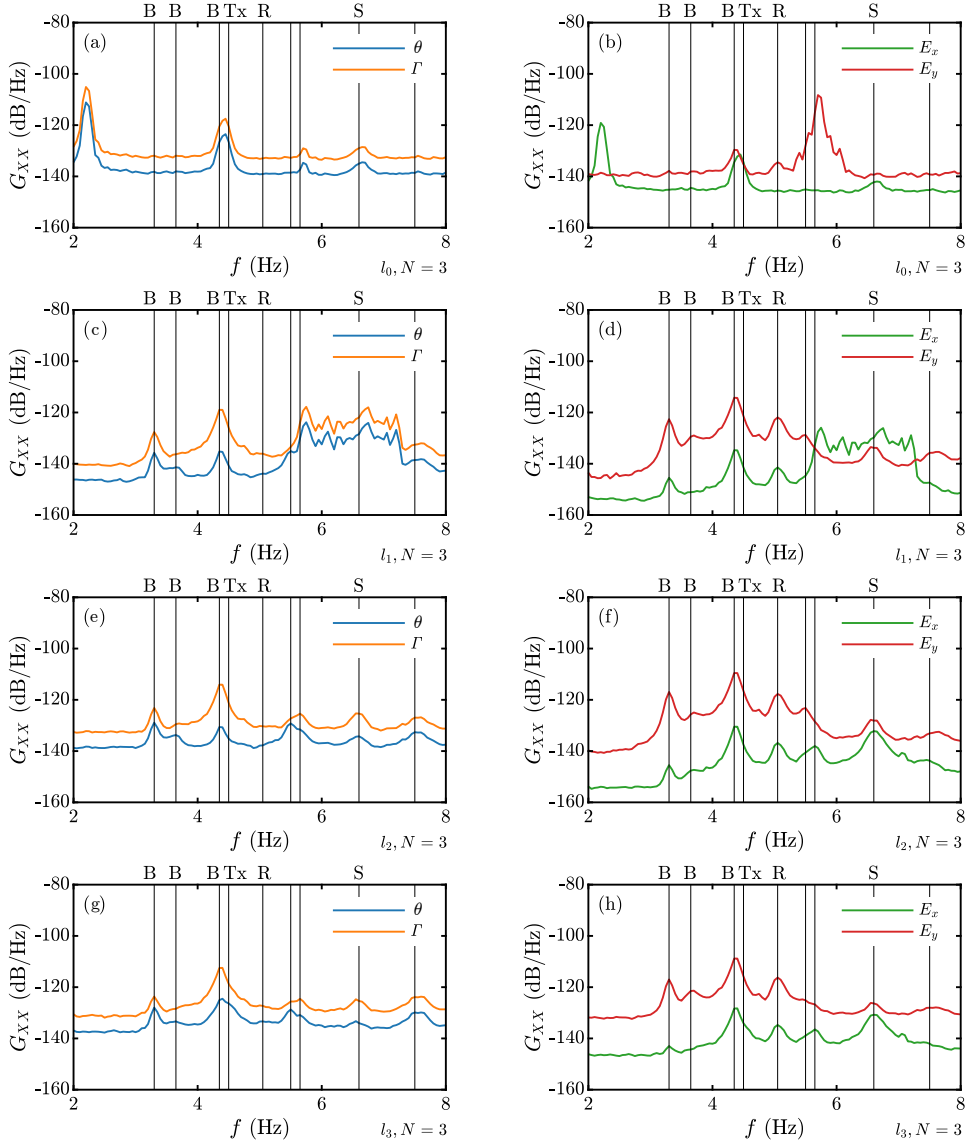
Figure A17: Power spectral densities (a,c,e,g) of the rigid rotation θ and shear strain Γ and (b,d,f,h) of the axial strains E_x, E_y estimated at each level of the building for $N = 3$.